論　文

Technical communication

Journal of the Ceramic Society of Japan 113 [2] 188-190 (2005)

Sintering and Mechanical Properties of $AlZrC_2$

U. LEELA-ADISORN, S.-M. CHOI, Nobuyuki TERA, Takeshi TAKEUCHI, Shinobu HASHIMOTO, Sawao HONDA, Hideo AWAJI, Kazuyuki HAYAKAWA* and Akira YAMAGUCHI**

Nagoya Institute of Technology, Gokiso-cho, Showa-ku, Nagoya-shi 466-8555
**Japan Fine Ceramics Center, Mutsuno, Atsuta-ku, Nagoya-shi 456-8587*
***Okayama Ceramics Center, Nishi-Katakami, Bizen-shi 705-0021*

$AlZrC_2$ の焼結と機械的特性

ウライワン・リーラアディソン・崔　成珉・寺　信行・竹内　健・橋本　忍・本多沢雄・淡路英夫・早川一幸*・山口明良**

名古屋工業大学，466-8555 名古屋市昭和区御器所町
*(財)ファインセラミックスセンター，456-8587 名古屋市熱田区六野
**岡山セラミックスセンター，705-0021 備前市西片上

$AlZrC_2$ powder prepared by solid-state reaction was sintered using a pulse electric current sintering technique in a temperature range from 1700 to 2000°C under the pressure of 40 MPa in vacuum for 5 min. The density and mechanical properties of the sintered $AlZrC_2$ monolith were estimated. As heating temperature increased, the density of the $AlZrC_2$ monolith increased and the mechanical properties were improved. The bulk density of the $AlZrC_2$ monolith sintered at 2000°C was 5.12 g/cm^3. The maximum values of the fracture strength and Vickers' hardness were 380 MPa and 11.1 GPa, respectively.

[Received December 6, 2004; Accepted December 10, 2004]

Key-words : *Complex carbide, $AlZrC_2$, PECS, Mechanical properties, Fracture strength, Vickers' hardness*

Introduction

In recent years, ternary compounds of complex carbide in Al-Ti-C system have attracted our interest because of their desirable mechanical properties,[1)-6)] i.e. their machinability and high strength. However, research on the complex carbides of the transition elements Zr of group IV is very rare. In previous work,[7)] we sintered dense $Zr_2Al_3C_5$ using a pulse electric current sintering (PECS) technique, and characterized the physical and mechanical properties of the $Zr_2Al_3C_5$ monolith. $AlZrC_2$, another phase of the Al-Zr-C system was crystallographically determined by Mikhalenko in 1979.[8),9)] Hashimoto et al.[10)] have prepared a composite material composed of aluminum and $AlZrC_2$, where $AlZrC_2$ powder was obtained by treatment of the composites with HCl. However, the properties of $AlZrC_2$ have not been studied so far.

In the present work, an $AlZrC_2$ powder compact was sintered by means of a PECS technique. This technique enables sintering of ceramic powders in a short time with rapid cooling. The technique can also sinter materials with poor sinterability. The mechanical properties of the sintered $AlZrC_2$ monolith prepared by the PECS technique are examined and discussed herein.

Experimental procedure

The starting material, $AlZrC_2$, was prepared from solid-state reaction using a technique described elsewhere,[11)] in which powders of Al, ZrC, and amorphous carbon from sugar were mixed at molar ratios of 21 : 14 : 15. The mixture was preformed as pellets and CIPed at 100 MPa. The pellets were then heated at 1600°C for 1 h in vacuum and ground into a fine powder. The obtained $AlZrC_2$ powder was heated using the PECS technique at a temperature range from 1700 to 2000°C under 40 MPa in vacuum for 5 min. After sintering, the phase of the sample was characterized by XRD. The density of the $AlZrC_2$ monolith was measured by Archimedes' method using kerosene as a medium. The sintered $AlZrC_2$ monolith was then cut into $2 \times 2 \times 10$ mm^3 test samples for estimating fracture strength and Vickers' hardness. The fracture strength was estimated using a three-point bending test with 8 mm span length and 0.5 mm/min cross-head speed. Vickers' hardness was measured under the condition of 98.07 N for 15 s according to the new Japanese Industrial Standard (JIS R1610: 2003). The fracture surfaces of each sample after bending tests were observed by scanning electron microscopy (SEM).

Results and discussion

The bulk density of the $AlZrC_2$ monolith increased with increasing heating temperature, as shown in **Table 1**. The calculated theoretical density shown in JCPDS[9)] is 5.282 g/cm^3 and the measured density specified in JCPDS[9)] is 5.000 g/cm^3. Table 1 indicates that the bulk density of the $AlZrC_2$ monolith sintered at 2000°C is higher than that of Mikhalenko's result.

The XRD patterns of the samples before and after heating are compared with the ideal XRD patterns of $AlZrC_2$ and

Table 1. Density of $AlZrC_2$ after Sintering by PECS at Various Temperatures under 40 MPa for 5 min

Sintered Temperatures	Bulk Density (g/cm^3)
1700℃	3.60
1800℃	3.92
1900℃	4.50
2000℃	5.12

Tanaka, H. (Contributing Editor)

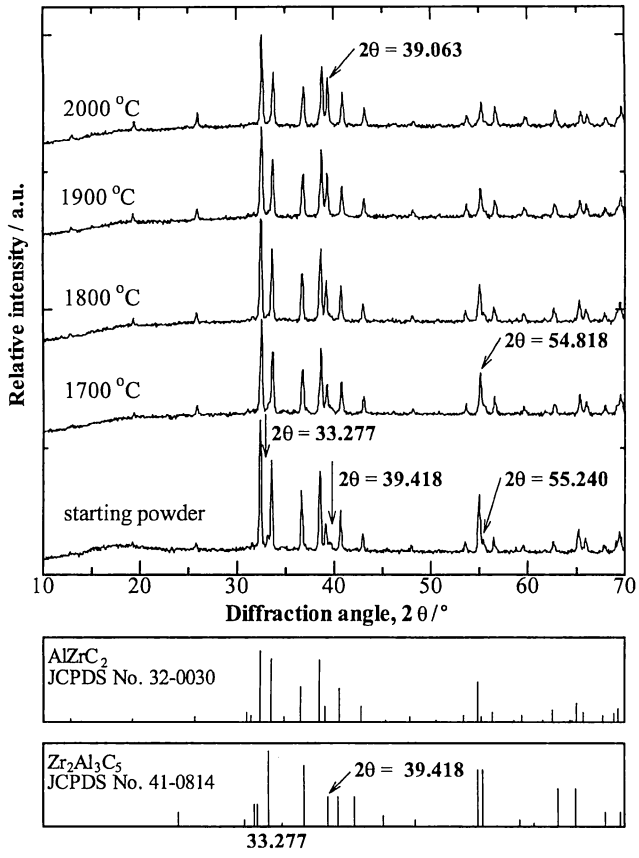

Fig. 1. XRD patterns of sintered $AlZrC_2$ by PECS at various temperatures under 40 MPa for 5 min, comparing with ideal XRD patterns.

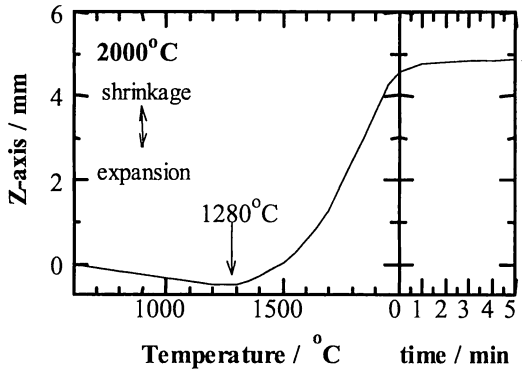

Fig. 2. Displacement of samples during sintering by PECS at 2000°C under 40 MPa for 5 min.

$Zr_2Al_3C_5$ in **Fig. 1**. The 2θ peaks at 33.277 and 39.418 for $Zr_2Al_3C_5$ (JCPDS No. 41-0814) found in the starting powder after synthesis[11] disappeared after sintering. From our previous work,[12] we can infer two reasons for this $Zr_2Al_3C_5$ loss; sublimation during sintering in vacuum or distortion of this phase under high pressure.

The displacement (*Z*-axis) of the $AlZrC_2$ compacts during sintering by the PECS technique is shown in **Fig. 2**. The sintering initiation was at around 1280°C. During the soaking duration at 2000°C, the *Z*-axis curve plateaus out at 1 min.

The mechanical properties of the sintered $AlZrC_2$ monolith at various temperatures are shown in **Figs. 3** and **4**. Both the

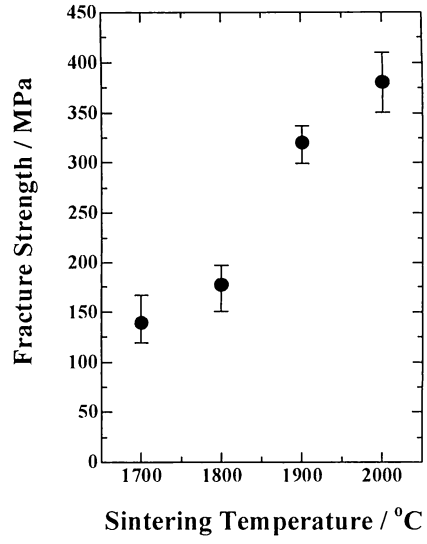

Fig. 3. Fracture strength of $AlZrC_2$ body sintered at various temperatures.

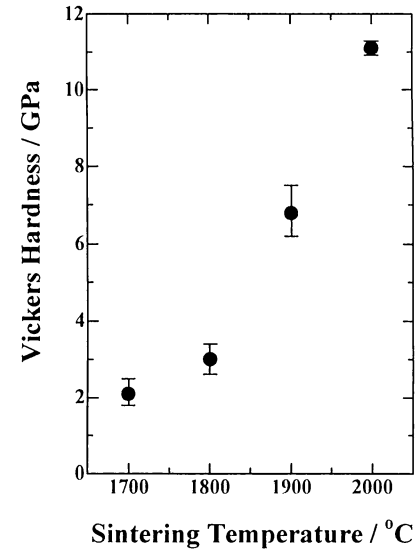

Fig. 4. Vickers' hardness of $AlZrC_2$ body sintered at various temperatures.

fracture strength and Vickers' hardness of the $AlZrC_2$ monolith showed the same tendency with heating temperature. At 2000°C, the $AlZrC_2$ monolith had maximum values of fracture strength and Vickers' hardness at 380 MPa and 11.1 GPa, respectively. The fracture strength and Vickers' hardness increased rapidly from 1800 to 2000°C, because the bulk density increased, as shown in Table 1.

SEM micrographs of the fracture surfaces are shown in **Fig. 5** for the sintered $AlZrC_2$ bodies at various temperatures. It was found that the sinterability of $AlZrC_2$ is low despite using the PECS technique. The samples sintered from 1700 to 1900°C showed porous structures. The sample sintered at 2000°C showed the densest structure with only a few small pores, and each grain was not distinguished. As a result, this sintering was thought to occur through a liquid phase reaction. However, this liquid phase component during heating is not yet to be clarified.

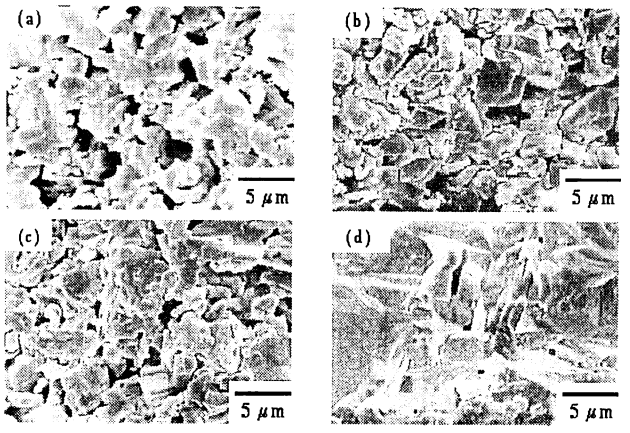

Fig. 5. Fracture surface of $AlZrC_2$ after sintering by the PECS technique under 40 MPa for 5 min. (a) 1700°C, (b) 1800°C, (c) 1900°C, and (d) 2000°C.

Conclusion

We fabricated a dense $AlZrC_2$ monolith using a pulse electric current sintering (PECS) technique. The second phase ($Zr_2Al_3C_5$) was not found in the sintered $AlZrC_2$ prepared by solid-state reaction. The density, fracture strength, and Vickers' hardness increased with increasing heating temperature. The $AlZrC_2$ monolith obtained at 2000°C and 40 MPa in vacuum for 5 min exhibited a bulk density of 5.12 g/cm^3, a fracture strength of 380 MPa, and a Vickers' hardness of 11.1 GPa.

Acknowledgement　The authors wish to thank the Royal Thai Government for providing a scholarship to the first author to pursue her Ph. D. studies at the Nagoya Institute of Technology under the TJTTP-OECF of Chulalongkorn University, Thailand.

References

1) Salama, I., El-Raghy, T. and Barsoum, M. W., *J. Alloys and Compounds*, Vol. 347, pp. 271-278 (2002).
2) Khoptiar, Y. and Gotman, I., *Mater. Lett.*, Vol. 57, pp. 72-76 (2002).
3) Wang, X. and Zhou, Y., *Z. Metallkd.*, Vol. 93, pp. 66-71 (2002).
4) Zhou, A., Wang, C. and Huang, Y., *Mater. Sci. Enging. A*, Vol. 352, pp. 333-339 (2003).
5) Ge, Z., Chen, K., Guo, J., Zhou, H. and Ferreira, J. M. F., *J. Eur. Ceram. Soc.*, Vol. 23, pp. 567-574 (2003).
6) Song, I.-H., Kim, D.K., Hahn, Y.-D. and Kim, H.-D., *Mater. Lett.*, Vol. 58, pp. 593-597 (2004).
7) Leela-adisorn, U., Choi, S.-M., Hashimoto, S., Honda, S. and Awaji, H., Proc. 21st Int. Korea-Japan Seminar on Ceramics, Nov. 4-6, Gwangju, Korea (2004) pp. 339-342.
8) Schuster, J. C. and Nowotny, H., *Z. Metallkd.*, Vol. 71, pp. 341-346 (1980).
9) JCPDS card No. 32-0030.
10) Hashimoto, S., Yamaguchi, A. and Yasuda, M., *J. Mater. Sci.*, Vol. 33, pp. 4835-4842 (1998).
11) Leela-adisorn, U. and Yamaguchi A., *Key Engineering Materials*, Vols. 280-283 (2005), Ed. by W. Pan, J. Gong, C. Ge, and J. Li, pp. 1379-1384, Trans. Tech. Publication, Switzerland.
12) Leela-adisorn, U., Choi, S.-M., Hashimoto, S., Honda, S., Awaji, H., Hayakawa, K. and Yamaguchi, A., Key Engineering Materials, to be submitted.

Available online at www.sciencedirect.com
SCIENCE DIRECT®
Materials Research Bulletin 40 (2005) 1577–1583
Materials Research Bulletin
www.elsevier.com/locate/matresbu

Low-temperature synthesis of leucite crystals using kaolin

Shinobu Hashimoto [a,*], Akira Yamaguchi [b], Koichiro Fukuda [a], Shaowei Zhang [c]

[a] *Department of Environmental and Materials Engineering, Nagoya Institute of Technology, Nagoya 466-8555, Japan*
[b] *Okayama Ceramics Research Foundation Research Laboratory, Bizen Okayama 705-0021, Japan*
[c] *Department of Engineering Materials, The University of Sheffield, Sheffield S1 3JD, UK*

Received 13 January 2005; received in revised form 26 March 2005; accepted 13 April 2005

Abstract

Synthesis of leucite crystals below 1000 °C using natural kaolin as the primary raw material was investigated. Spherical leucite crystals having a diameter of approximately 50 μm were prepared by heating a powder mixture of $Al_2(SO_4)_3$, kaolin and K_2SO_4 (in mass ratios of 3:3:15) at 900 °C for 3 h. Quartz, the main accessory phase in kaolin, and the amorphous metakaolin formed upon heating kaolin were found to be responsible for the decreased synthesis temperature.
© 2005 Elsevier Ltd. All rights reserved.

Keywords: A. Ceramics; A. Oxides; B. Crystal growth; C. Electron microscopy; C. X-ray diffraction

1. Introduction

Leucite ($KAlSi_2O_6$) has been used as an important crystal phase in dental porcelain/glass materials [1] because of its tone, color appeal and excellent biocompatibility. Furthermore, due to its high melting point (1693 °C) [2] and high thermal expansion coefficient (3.1×10^{-5} K^{-1}, to 600 °C) [3], leucite has potential application in preparing functional coatings on metal substrates or reinforcing metal-based composites.

Leucite is generally synthesized by heating the mixture of raw materials at a temperature above its melting point and then slowly cooling the mixture to room temperature [1,3]. Recently, spherical leucite crystals with a controlled size of between several micrometers to approximately 100 μm have been

* Corresponding author. Tel.: +81 52 735 5291; fax: +81 52 735 5291.
E-mail address: hashimoto.shinobu@nitech.ac.jp (S. Hashimoto).

0025-5408/$ – see front matter © 2005 Elsevier Ltd. All rights reserved.
doi:10.1016/j.materresbull.2005.04.013

synthesized at a much lower temperature (1000 °C) by the present authors [4,5] using reagent grade $Al_2(SO_4)_3$, SiO_2 and K_2SO_4 as starting raw materials. Because of their spherical morphology, the synthesized leucite crystals could be well distributed in dental materials, allowing the materials (e.g. artificial teeth) to be rendered with substantially enhanced mechanical strength. In addition, the synthesized leucite crystals could be used as a raw material in the fabrication of bulk leucite ceramics or as an additive to silica glass due to having a near reflection coefficient. However, the present study is the first report of synthesis at a temperature below 1000 °C using cheaper natural materials, such as kaolin.

2. Experimental

Reagent grade $Al_2(SO_4)_3 \cdot 14–18H_2O$ and K_2SO_4, and 2–10 μm Chinese kaolin (Fujian, China), the chemical composition of which is shown in Table 1, were used as starting materials. The XRD patterns shown in Fig. 1 reveal that, apart from the primary crystal phase, i.e. kaolinite ($Al_2O_3 \cdot 2SiO_2 \cdot 2H_2O$), SiO_2 (quartz) and muscovite are present in kaolin as accessory phases. The quartz content is estimated to be approximately 6.7 wt% based on the chemical compositions shown in Table 1.

$Al_2(SO_4)_3$ was prepared by heating $Al_2(SO_4)_3 \cdot 14–18H_2O$ for more than 12 h at 300 °C in air. The heated $Al_2(SO_4)_3$ was then mixed with kaolin and K_2SO_4 in mass ratios of 3:3:15 using a mortar in order to obtain a melted phase for the crystal growth of leucite during heating. A mass of this powder mixture (approximately 20 g) was heated in an alumina crucible (high: 75 mm, diameter: 55 mm) to 850–1100 °C at the rate of 10 °C/min and was maintained at temperature for 0–3 h. After heating, the furnace was allowed to cool naturally to room temperature. The reactant mass remaining at the bottom of the crucible was soaked in 3% hydrochloric acid at 70–80 °C for 1–2 h to dissolve the remaining K_2SO_4–$Al_2(SO_4)_3$ system components. Subsequently, the remaining sample was rinsed with distilled water, dried well at approximately 80 °C for 1 h and sifted with an 88-μm sieve to obtain pure reaction products. The resulting crystalline phases in the reaction products were examined by X-ray diffraction (XRD: Model XD-D1, Shimazu Co., Ltd., Kyoto, Japan) and their microstructures were examined using a scanning electron microscope (SEM: Model JEL 5200, Nihondensi Co., Ltd., Tokyo, Japan). In order to clarify the formation mechanism of leucite crystals, crystalline phases in the reactant masses before the hydrochloric acid treatment were also examined by XRD.

Table 1
Chmemical composition of kaolin (mass%)

SiO_2	49.35
Al_2O_3	36.03
Fe_2O_3	0.20
TiO_2	0.02
CaO	0.02
MgO	0.31
K_2O	2.29
Na_2O	0.04
Ig. loss	11.94
Total	100.20

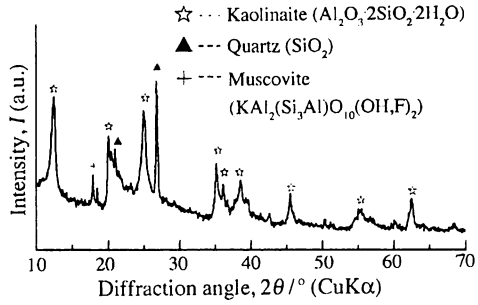

Fig. 1. XRD pattern of the Chinese kaolin used.

3. Results and discussion

3.1. Effect of temperature and time on the formation of leucite crystals

Figs. 2 and 3 show XRD patterns and SEM micrographs of the samples after heating the powder mixture at 850–1100 °C for 3 h and further treating with hydrochloric acid, respectively. At 850 °C, only quartz (but no leucite) was identified by XRD, and the microstructure reveals an extensive formation of grains of less than 10 μm in diameter. As the temperature increased to over 850 °C (900–1100 °C), the quartz disappeared and only leucite remained. Nevertheless, depending on the temperature, the formed leucite crystals showed different morphologies. At 900 °C, spherical leucite crystals having a diameter of approximately 50 μm were observed. However, at 1000 °C, the leucite crystals began to lose their spherical morphology. A further increase in temperature to 1100 °C led to the formation of leucite crystals of two different diameters, approximately 50 μm and 10–20 μm. At 900 °C, the number of leucite nuclei formed in the sample decreased. Therefore, a comparatively small number of leucite crystals appeared to be responsible for the increase in the size of leucite crystals, which is thought to cause the formation of large monocrystals. In contrast, upon increasing the temperature to 1100 °C, a large number of leucite nuclei formed, so that each of the leucite crystals became smaller and showed a tendency to form crystal agglomerations. Thus, these results indicated that when kaolin was used as the primary raw material, spherical leucite crystals of homogeneous size could be synthesized by heating the

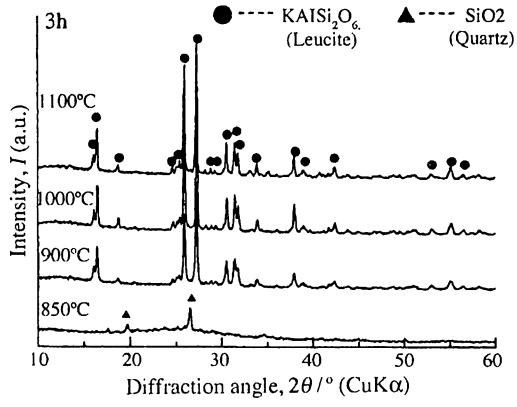

Fig. 2. XRD patterns of the samples after heating the mixture kaolin and K_2SO_4 (in mass ratios of 3:3:15) at 850–1100 °C for 3 h and further treating with hot hydrochloric acid.

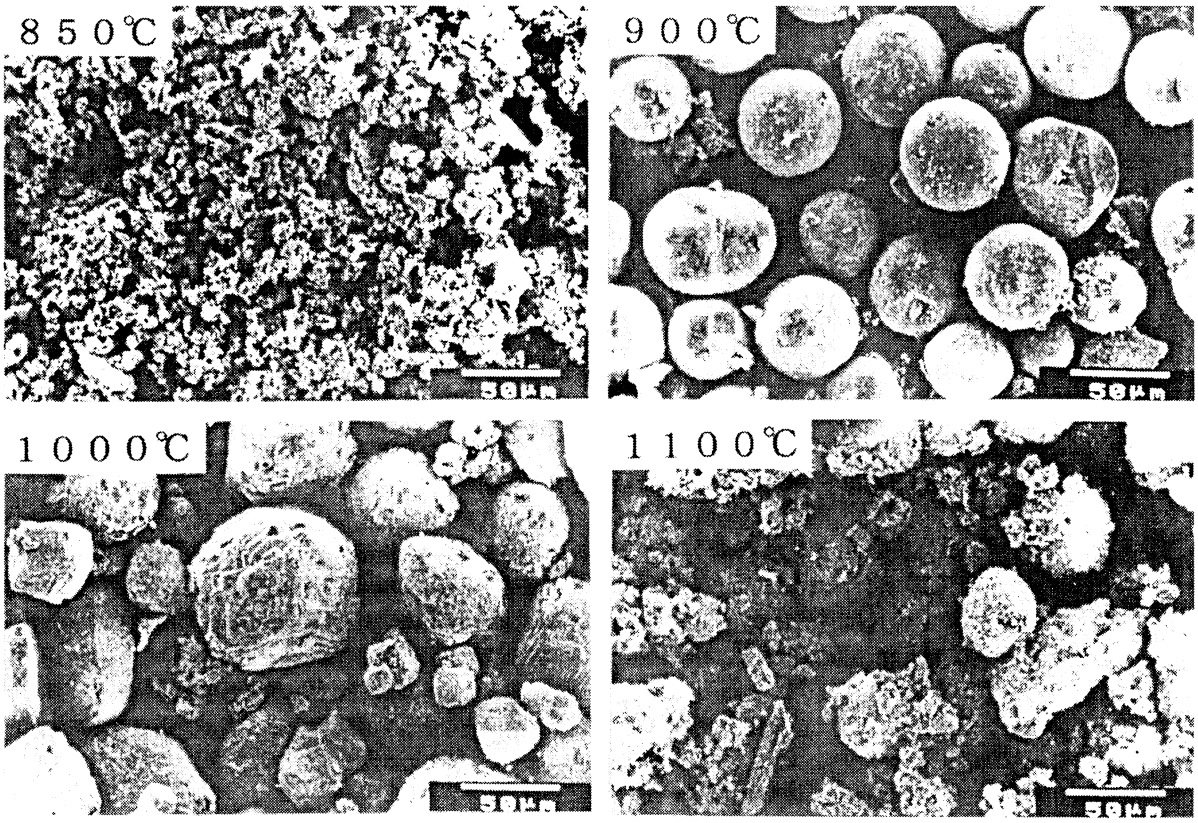

Fig. 3. SEM micrographs of the samples for which the XRD patterns are shown in Fig. 2.

powder mixture at 900 °C, which is lower than that (1000°C) reported in previous studies using reagent grade SiO_2 as a starting raw material [4,5].

Fig. 4 presents XRD patterns and SEM micrographs of the samples after heating the powder mixture at 900 °C for various time periods and further treating with hot hydrochloric acid. SiO_2 quartz and muscovite (but no leucite) were detected by XRD in the sample that was heated at 900 °C for 0 h. That is, the sample was heated to 900 °C but was not maintained at this temperature. No spherical grains were seen in the corresponding microstructure. After 1 h at 900 °C, leucite was observed to form, but SiO_2 quartz and muscovite were still present, and spherical grains were still not formed in the microstructure. However, after heating at 900 °C for 2 h, quartz and muscovite had almost disappeared and only leucite was identified by XRD, and the microstructure reveals the formation of spherical grains having a diameter of approximately 30 μm.

3.2. Formation mechanism of leucite crystals

The processes that occur upon firing natural kaolin have been well documented. Upon heating at approximately 550 °C, kaolin loses structural water to form dehydrated amorphous metakaolin. In a ^{27}Al and ^{29}Si magic-angle spinning nuclear magnetic resonance (MAS-NMR) study of the kaolinite–mullite transformation [6], Sanz et al. reported that the tetrahedral sheet of kaolinite begins to break down at

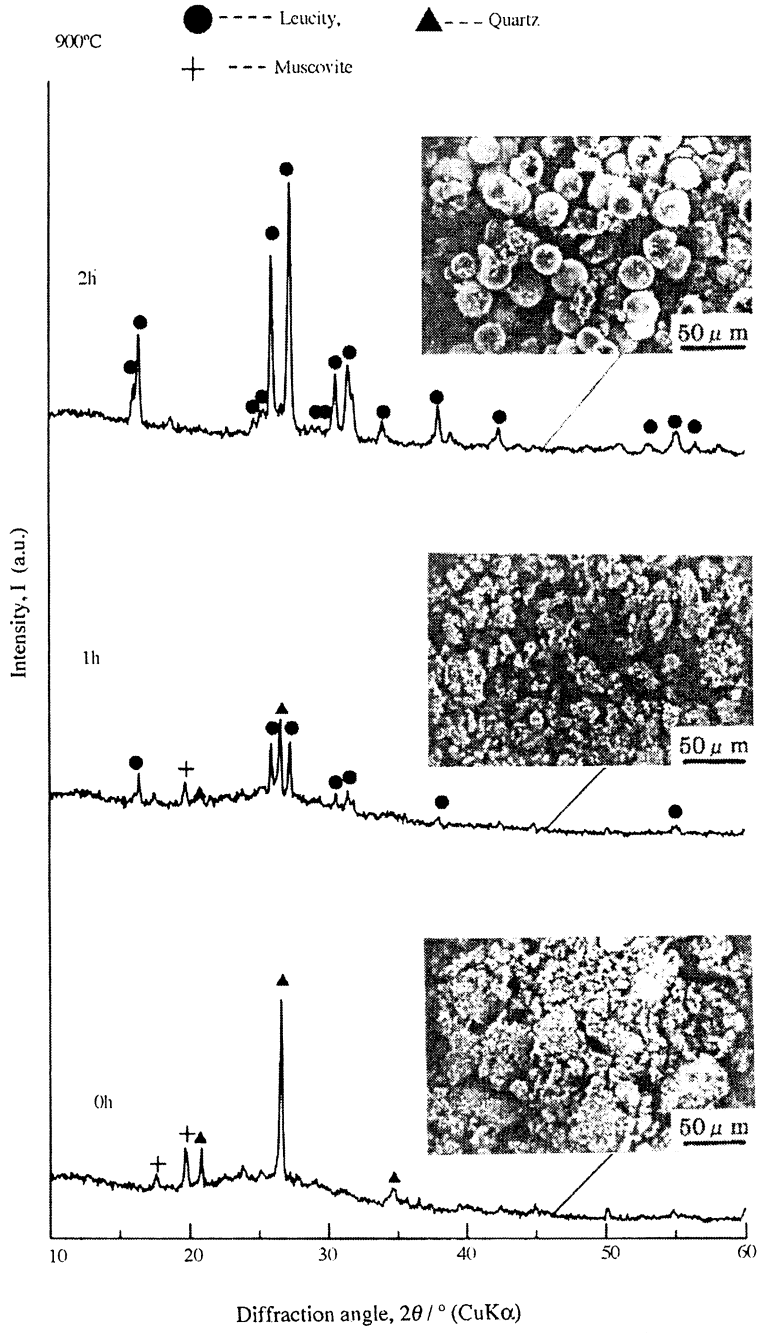

Fig. 4. XRD patterns and SEM micrographs of the samples after heating the mixture of $Al_2(SO_4)_3$, kaolin and K_2SO_4 (in mass ratios of 3:3:15) at 900 °C for 0–2 h and further treating with hot hydrochloric acid.

approximately 600 °C and continues to break down until reaching 900 °C. The formed metakaolin then becomes very active. Madani et al. have also studied zeolite formation from alkali-leached kaolinite using the MAS-NMR technique [7]. They found that the formed metakaolin further decomposes to form γ-Al_2O_3 and amorphous SiO_2 by increasing the heating temperature to approximately 980 °C [6,8].

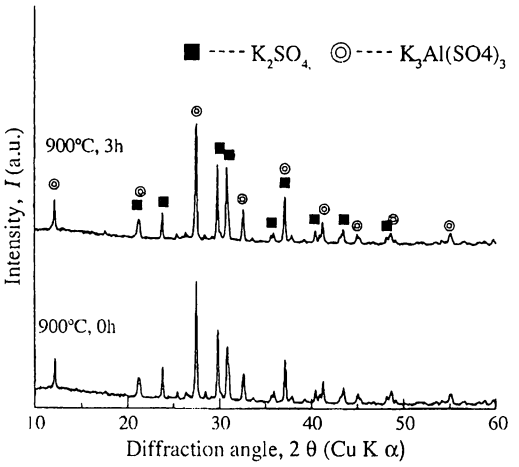

Fig. 5. XRD patterns of the samples after heating the mixture kaolin and K_2SO_4 (in mass ratios of 3:3:15) at 900 °C for 0 and 3 h without acid treatment.

Based on these findings, the XRD peaks of SiO_2 (quartz) detected in the samples heated for 3 h at 850 °C (Fig. 2) and for 0 h at 900 °C (Fig. 4) should be attributed to the original SiO_2 (quartz) present in the as-received kaolin (Fig. 1). As revealed in a previous study [5], SiO_2 (either in crystalline or amorphous form) in starting materials accelerates the nucleation of leucite crystals. Therefore, the SiO_2 quartz from kaolin should play a similar role in the present experiment. Fig. 5 shows XRD patterns of samples of the powder mixture that were heated to 900 °C and maintained for 0 or 3 h without acid treatment. K_2SO_4 and $K_3Al(SO_4)$ were detected in both samples. Although the phase diagram of the K_2SO_4–$Al_2(SO_4)_3$ system is not available, the low melting point of $K_3Al(SO_4)_3$ (690 °C) [9] means that a K_2SO_4–$Al_2(SO_4)_3$ liquid should form in the sample heated at 900 °C. As a result, the leucite crystals, upon forming via nucleation and subsequent growth, would become spherical so as to decrease the high surface energy (Figs. 3 and 4). The accelerated nucleation (due to the SiO_2 quartz) and crystallization (due to the reactive amorphous metakaolin) in this process are believed to be responsible for the decrease in the synthesis temperature from 1000 °C [4,5] to 900 °C (see Section 3.1).

4. Summary

Low-temperature synthesis of leucite crystals using natural kaolin was investigated. After a powder mixture of $Al_2(SO_4)_3$, kaolin and K_2SO_4 (in mass ratios of 3:3:15) was heated at 900 °C for 3 h, spherical leucite crystals having a diameter of approximately 50 μm were obtained. SiO_2 (quartz), the accessary phase in kaolin, and the amorphous metakaolin formed upon heating kaolin contributed to the decreased synthesis temperature of leucite crystals.

References

[1] S. Ban, K. Matuo, N. Muzutani, H. Iwase, J. Hasegawa, Dent. Mater. J. 17 (1998) 264–274.
[2] E.M. Levin, C.R. Robin, H.F. McMurdie, in: M.K. Reser (Ed.), Phase Diagram for Ceramist, American Ceramic Society, Columbus, OH, USA, 1964 (Fig. 407).

[3] S. Ban, K. Matuo, N. Mizutani, K. Kaikawa, J. Hasegawa, J. Jpn. Soc. Dent. Mater. Dev. 19 (2000) 318–325.
[4] S. Hashimoto, A. Yamaguchi, J. Ceram. Soc. Jpn. 108 (2000) 40–44.
[5] S. Hashimoto, A. Yamaguchi, J. Ceram. Soc. Jpn. 110 (2002) 27–31.
[6] J. Sanz, A. Madani, J.M. Serratosa, J.S. Moya, S. Aza, J. Am. Ceram. Soc. 71 (1988) C-418–C-421.
[7] A. Madani, A. Aznar, J. Sanz, J.M. Serratosa, J. Phys. Chem. 94 (1990) 760–765.
[8] A. Djemai, E. Balan, G. Morin, G. Hernandez, J.C. Labbe, J.P. Muller, J. Am. Ceram. Soc. 84 (2001) 1017–1024.
[9] JCPDS card, No. 27-1337.

Journal of the Ceramic Society of Japan 113 [4] 312-316 (2005)

Technical report

アスベストの機械的粉砕とその焼結性

橋本　忍・山口明良*

名古屋工業大学環境材料工学科，466-8555 名古屋市昭和区御器所町
*岡山セラミックス技術振興財団研究所，705-0021 備前市西片上 1406-18

Comminution of Asbestos by a Mechanical Grinding and its Sinterability

Shinobu HASHIMOTO and Akira YAMAGUCHI*

Department of Environmental and Materials Engineering, Nagoya Institute of Technology, Gokiso-cho, Showa-ku, Nagoya-shi 466-8555
**Okayama Ceramics Research Foundation Research Laboratory, 1406-18, Nishi Katakami, Bizen-shi 705-0021*

When asbestos (chrysotile: $Mg_3Si_2O_5(OH)_4$) was heated at 600°C for 3 h, dehydration reaction of it had been almost finished, changing to an amorphous phase in crystallography. Then the remaining fiber became brittle, because the structure of fiber could be easily ground till < 1 μm diameter in grain size using a mortar. When the compact body made by pressing the ground asbestos fiber at 80 MPa was heated at 1300°C for 1 h, the relative density of the compact reached 90%. Then the crystal phase of the compact was mainly forsterite (Mg_2SiO_4), but a small amount of chrinoenstatite ($MgSiO_3$) was also detected.

[Received December 27, 2004; Accepted January 20, 2005]

Key-words : *Asbestos, Chrysotile, Heat treatment, Amorphous phase, Mechanical grinding, Sinterability*

1. 緒　言

アスベストは天然に産する繊維状ケイ酸塩鉱物の総称で，一般には綿のようにほぐれることから石綿と呼ばれている．大別してジャモン石系とカクセン石系とがあるが，現在ではカンラン石が熱水変質を受けたときに生成するジャモン石系鉱物のクリソタイル ($Mg_3Si_2O_5(OH)_4$) のみが輸入利用されている[1]．それゆえクリソタイルを指してアスベストと称していることが多く，本論でもクリソタイルをアスベストとして扱う．このアスベストは，一般に0.02 μm から0.2 μm の径をもつ繊維状結晶が束状になった構造をしており，融点が高く（1521°C)[2]，高い抗張力を持ち，柔軟性があり，加工しやすく，耐熱性・断熱性に優れ，耐食性を有するなどの特性を持つ[1]．そのため主にセメントと複合化され，屋根材や壁材などの建築材として1950年ごろから戦後の経済復興に合わせて利用され始め，特に1960年代の高度経済成長期に急速にその需要が伸びた．1970年代の最盛期には，年間35万トンもの量が使用された[1),3]．欧米では，早くから発がん性などアスベストに起因する健康障害[1),3),4]が指摘され，使用規制・禁止の措置がとられてきた．わが国では1975年に，労働者保護の立場からアスベストの吹き付け工事は原則禁止された．しかしその後もアスベストの使用は続けられ，近年でも年間5～10万トンの使用量がある．最近になって，大手建材メーカーがアスベストを自主的に使用禁止にすると発表し，今後その使用量は大幅に減少するものとみられる．しかしながら，アスベストを含んだ建築建材の量は累積して数千万トンに達し，2010年から2020年にかけてその廃棄のピークを迎えるといわれている．アスベスト含有廃棄物は現在特定管理物質に指定され，撤去や埋め立て廃棄も厳重な管理下で行われている．

アスベスト含有建築廃材の無害化，さらにはその有効利用に関する研究は急務であり，現在多くの民間企業や公的研究機関で取り組まれている．溶融する高温まで加熱することによるアスベストの形態変質[5]，酸処理によるアスベストの組成変質[6]，アルミナ[7]，都市ごみ焼却灰[8]，アルミニウム精製時の副生精錬灰[9]，ケイ酸ソーダやケイ酸カリウム[10]など種々の添加物を加えて加熱することで，新たな低融点物質を形成させる無害化など，その多くは特許として公開されているが，いまだ低コストで安全に大量処理できる画期的な処理技術といわれているものはない．

本研究では，基礎的にまずアスベスト単体について着目し，その毒性の主原因と言われる繊維状形骸[1),4]を機械的に破壊することで，それを無害化できないか考えた．アスベストを単純に加熱しても，その繊維状形骸は融点近くまで保持される[5]．アスベストは室温では抗張力性に優れた材料であるが，加熱による脱水に伴い引っ張り強度は低下する[2]．しかしながらそれ以外には，アスベストの組成変化と機械的特性変化を関連付けた報告は少ない．そこで，アスベストの加熱に伴う組成変化と機械的磨砕による被粉砕性，特に繊維状形骸の消滅との関連性について検討した．加えて，アスベスト粉砕物の有効利用法を開発する基礎研究として，粉砕粉末から成形体を作製し，その焼結性について調べた．アスベスト単体は，高温で加熱すると主な結晶相としてはフォルステライト（Mg_2SiO_4）となるため[1)]，高周波用磁器の原料としての利用も期待される．また本基礎研究は，アスベストを含むセメント複合建築廃材の無害化において，熱処理と機械的破砕の同時処理が有効である可能性を示唆し，加えてその有効利用法の開発にも新しい方向性を示すものになると考えられる．

2. 実験方法

用いたアスベストはカナダ・ケベック州産クリソタイルで，その化学組成を表1に，走査型電子顕微鏡（SEM）によりその微細組織を観察した結果を図1に示す．主に径約0.2 μm の繊維質が束状に集まっているのが観察される．アルミナるつぼ（高さ75 mm，幅60 mm，容積150 cm^3）にクリソタイル約3 g を入れ，それを電気炉に入れて加熱した．電気炉の昇温速度は10°C/min とし，550°Cから1000°Cの温度で所定時間加熱した．加熱後，炉の電源を切り，るつぼは炉内で自然放冷させた．加熱処理によるアスベストの組成変化を粉末X線回折（XRD）分析により調べた．

Table 1. Chemical Composition of Chrysotile (mass%)

SiO_2	40.40
MgO	40.52
Fe_2O_3	2.08
Al_2O_3	1.40
CaO	0.48
H_2O	1.88
SO_3	0.10
Ig.loss	13.84
Total	100.70

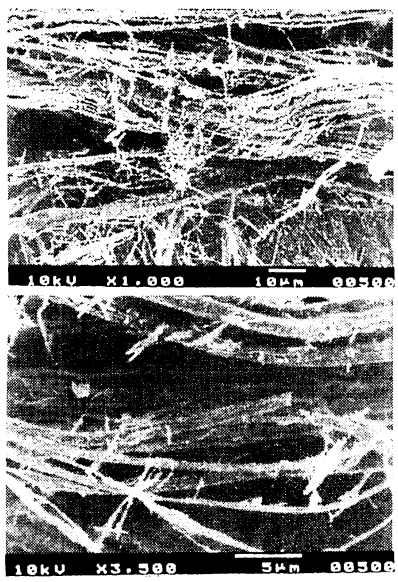

Fig. 1. SEM micrographs of original asbestos used.

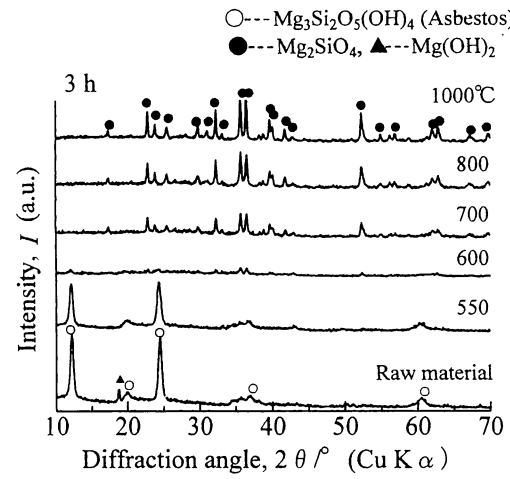

Fig. 2. XRD patterns of asbestos after heating at 550–1000°C for 3 h.

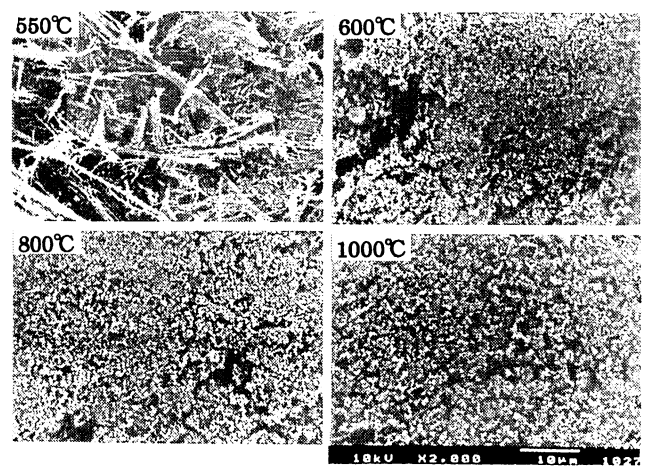

Fig. 3. SEM microphotographs of asbestos after heating at 550–1000°C for 3 h.

アスベストの粉砕実験は，未処理及び加熱処理後のアスベストをおのおの約0.5 g 秤量し，直径10 cm の Si_3N_4 製の乳鉢と乳棒を使って人手により粉砕（すりつぶす磨砕）した．同一作業者により毎秒1回転，そして乳棒と乳鉢の接点には常に2～3 kg の荷重が加わる条件で行った．粉砕処理されたアスベストの微細組織を，SEM により観察した．

次に，加熱処理後に粉砕したアスベスト粉末の焼結性について検討した．粉砕されたアスベスト粉末を20×20 mm の正方金型に入れ，80 MPa の一軸加圧成形を行い，得られた粉末成形体を電気炉にて1000°C～1400°Cの所定温度で1 h 焼成した．昇温速度は10°C/min とし，加熱保持後に炉の電源を切り，試料は炉内で自然冷却させた．得られた試料のかさ密度及び真密度を含水法及びアルキメデス法によりそれぞれ測定し，両者から相対密度を算出した．XRD 分析により加熱試料の構成結晶相を同定した．比較のために，未加熱処理アスベストを出発原料に用いて同様の成形体を作製し，これも1000°C～1400°Cの温度で焼成した．加熱後の試料の微細組織を観察し，熱処理後粉砕したアスベスト粉末の焼結性について検討した．

3. 結果と考察

3.1 アスベストの被粉砕性

図2は，アスベストを550°Cから1000°Cまでの各温度で3 h 加熱した試料の XRD 分析結果を示す．550°Cで加熱した試料からは，クリソタイルが同定された．600°Cの場合，クリソタイルの回折線はほぼ消滅し，わずかにフォルステライトの回折線が検出されるものの，その回折線強度は低く非晶質に近い状態であるとみられた．700°Cから1000°Cまで加熱温度が上昇するのに伴い，フォルステライトの回折線強度は大きくなる傾向を示したが，それ以外の新たな結晶相は同定されなかった．この加熱に伴う構成結晶相の変化は，以前の報告結果と一致する[10]．図3に，550°C, 600°C, 800°C及び1000°Cで3 h 加熱した各試料を乳鉢で5 min 粉砕した後，SEM でそれらの微細組織を観察した結果を示す．550°Cの場合，繊維長は短くなっているものの，繊維状形態は失われていなかった．一方600°Cの試料では，繊維状組織は破壊され，ほとんどが1 μm 以下の微細な粒にまで粉砕されていた．800°C及び1000°Cの加熱の場合も600°Cでの加熱の場合と同様で，いずれも繊維状形骸は破壊され，1 μm 以下の粒にまで粉砕されていた．次に，600°Cで3 h 加熱し，その後乳鉢による粉砕時間を10 s から120 s まで種々変えた場合の，試料の SEM 観察結果を図4に示す．600°Cで加熱された試料は脆く，10 s 間の粉砕では繊維状組織は残存しているが，20 s 間の粉砕後には繊維長は20～30 μm 以下に破壊さ

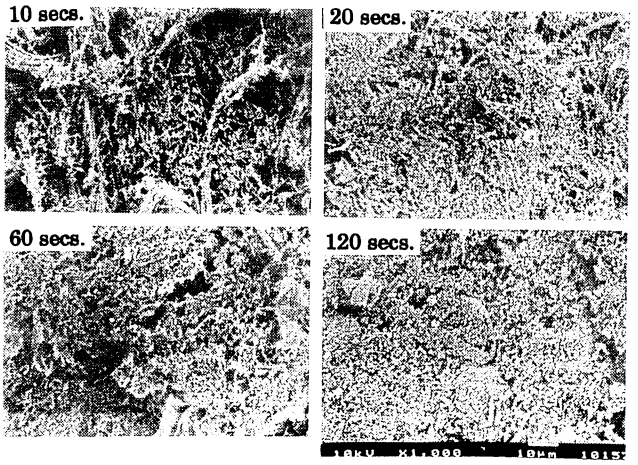

Fig. 4. SEM microphotographs of asbestos ground for various seconds using a mortar after heating at 600°C for 3 h.

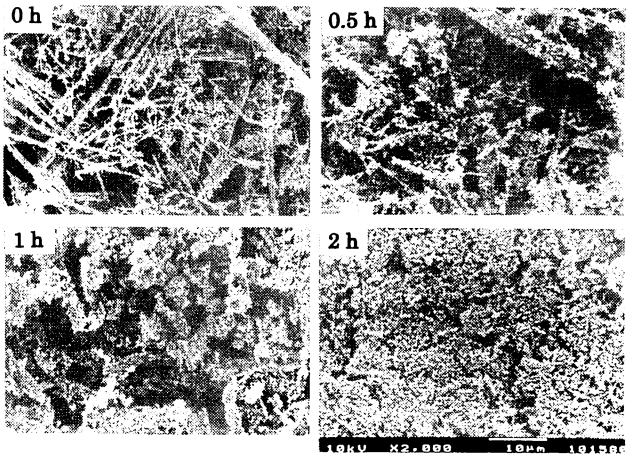

Fig. 6. SEM micrographs of asbestos ground for 5 min using a mortar after heating at 600°C for various hours.

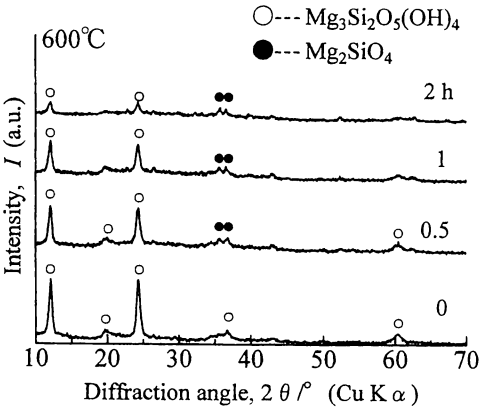

Fig. 5. XRD patterns of asbestos ground for 5 min using a mortar after heating at 600°C for various hours.

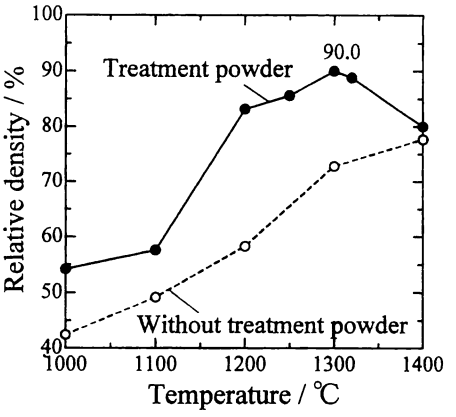

Fig. 7. Relative densities of the compacts made by asbestos with grinding for 5 min after heating 600°C for 3 h and raw asbestos without heat treatment, which were heated at 1000-1400°C for 1 h.

れた．60 s 間の粉砕後にはほとんど繊維状組織はみられなくなり，さらに120 s 間の粉砕後の試料には，図 3 に示した600°Cで5 min 粉砕した試料とほぼ同程度の 1 μm 以下の微細な粒のみになった．本実験条件では，120 s 間の粉砕処理で，加熱処理したアスベストの針状組織はほとんど破壊されることが分かった．しかしながら以後の実験では，十分な破壊を行う目的から，粉砕時間は 5 min とした．図 5 及び図 6 には，600°Cでアスベストを加熱し，その温度での保持時間別の試料の XRD 分析結果，及びそれらの試料をおのおの 5 min 粉砕処理した後，SEM によりその微細組織を観察した結果を示す．600°Cまで加熱し 0 h 保持した，すなわちすぐに冷却した試料にはクリソタイルが検出され，同試料の微細組織観察からは試料中には繊維状組織が多く残存しており，繊維状組織は破壊されにくいことが分かった．0.5 h 保持した試料は，クリソタイルの回折線強度は小さくなり，またその場合の試料の繊維長は短く寸断され，そのほとんどが長さ10 μm 以下になった．1 h 保持した試料は，さらにクリソタイルの回折線強度は小さくなり，また粉砕により繊維長も数 μm となり，一見して繊維とは判別できないまでの状態になった．2 h 保持した試料の XRD 回折線強度は弱く，粒はさらに細かく粉砕されて 1 μm 以下となり，図 2，図 3 に示された600°Cで 3 h 加熱保持した場合の XRD 図形，及びそれを 5 min 粉砕した試料の SEM 観察結果の粒形態とほぼ同じとなった．以上の結果より，アスベストは600°Cで 2 h 加熱された場合に構造水の脱水反応が大部分進行し，結晶学的に非晶質に近い状態になる．この状態になると繊維状組織は脆くなり，粉砕により容易に破壊できるようになる．アスベストのさらなる高温加熱により結晶相としてはフォルステライトが析出するようになるが，その繊維状組織の粉砕されやすい脆い状態は持続するものとみられる．以後の実験において，アスベストの脱水反応を十分に行わせ，脆弱化させる理由から，600°Cでの保持時間は 3 h とした．

3.2　焼結体の作製

次に，アスベストを600°Cで 3 h 加熱処理した試料を 5 min 粉砕して得た粉末から成形体を作製し，その焼結性について調べた．図 7 は，1000°Cから1400°Cの各温度で 1 h 加熱保持した場合の試料の相対密度変化を示している．比較のために，未処理アスベストから成形体を作製して，それを加熱した場合の相対密度変化も示した．未処理アスベストから成形体を作製した場合には，すべての加熱温度で熱処理・粉砕した試料成形体から得られた焼成体に比べ，相対密度は低下した．熱処理・粉砕した試料成形体を1300°Cで加熱した場合，相対密度は90%の最高値を示した．図 8 は熱処理・粉砕試料成形体を種々の温度で焼成して得た試料体，及び図 9 は未処理アスベスト成形体試料

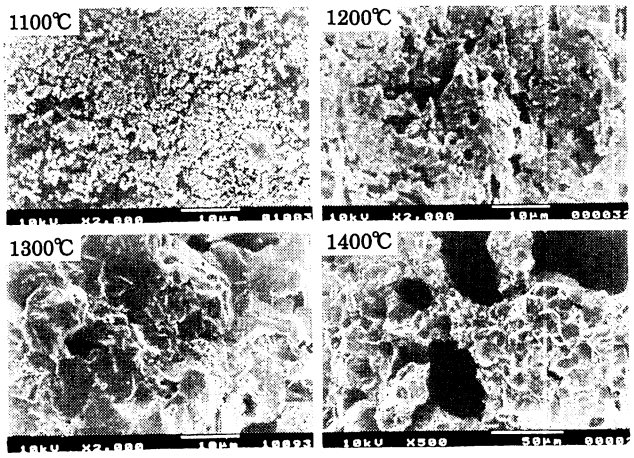

Fig. 8. SEM microphotographs of the fractured surfaces of the compacts made by asbestos with grinding after heating at 600°C for 3 h, which were heated at 1100–1400°C for 1 h.

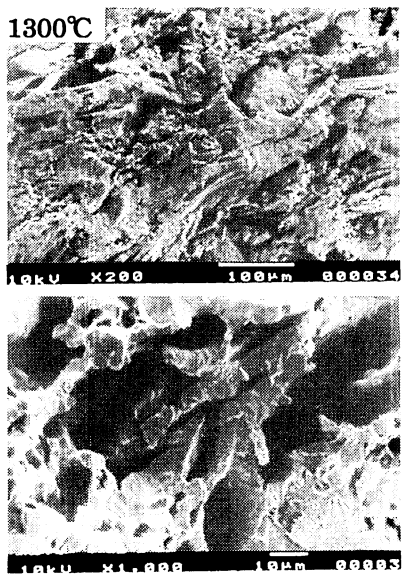

Fig. 9. SEM microphotograhs of the fractured surface of the compact made by raw asbestos after heating 1300°C for 1 h.

を1300°Cで焼成して得た試料体の，破断面のSEM観察写真を示す．図9の未処理アスベストを焼成した場合には，加熱中の脱水反応により試料内に多くの気泡を形成すること，及び繊維状の形骸を高温まで保持するため，繊維状粒子間の焼結反応が進行し難いため相対密度は上がらなかったものと考えられる．一方，図8中の熱処理・粉砕試料成形体を加熱した場合，温度の上昇とともに気孔は少なくなり，1300°Cで最も気孔は少なくなった．しかし1400°Cで加熱した場合には，数十 μm から大きいものでは数 mm に及ぶ径をもつ球形に近い空孔が多く観察されるようになり，図7で示されたように相対密度は低下した．図10には，熱処理・粉砕試料成形体を1100°C及び1400°Cで加熱した場合の，試料の粉末X線回折分析の結果を示す．加熱温度による違いはみられず，主な結晶相はともにフォルステライトであったが，クリノエンスタタイト（$MgO \cdot SiO_2$）もわずかだが検出された．最後に，熱処理・粉砕試料成形体を1400°Cで加熱した場合に気孔を多く形成し，相対密度が低下した理由につ

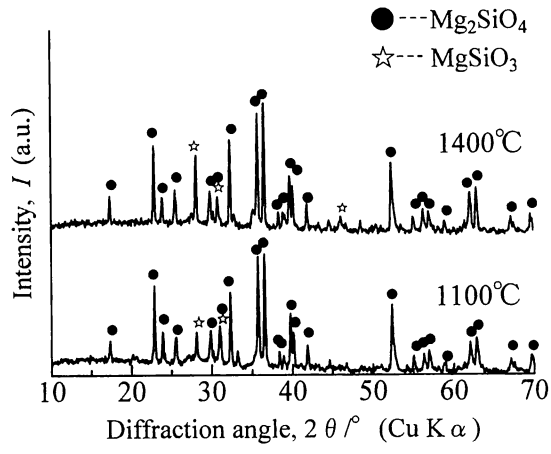

Fig. 10. XRD patterns of the compacts made by asbestos with heat treatment and grinding after heating at 1100°C and 1400°C for 1 h.

いて考える．$MgO-SiO_2$ 系2成分状態図[11]によれば，この系では1543°C以下の温度では融液は生成しない．ここで，表1に示されているアスベストの化学組成において，主成分である MgO 及び SiO_2 以外で，Al_2O_3 の共存が注目される．$MgO-SiO_2-Al_2O_3$ 系3成分状態図[12]によれば，組成比によっては1400°C以下の温度でも融液の生成が可能である．本試料体も1400°Cでの加熱において，Al_2O_3 が存在するところで $MgO-SiO_2-Al_2O_3$ 系融液が生成したとみられる．さらに Fe_2O_3 や CaO の共存が試料体内の部分的な融点をさらに下げている可能性もある．このような融液の生成の後，引き続いて蒸気圧値の高い気相種が生成し，例えば表1から不純物として微量存在すると示唆される硫酸塩の脱硫反応によって $SO_3(g)$ が放出され，試料体内に球形に近い気孔を多く形成するようになったと考えられる．その結果，試料体の相対密度は低下した．

4. まとめ

アスベストの繊維状形骸を消滅させる基礎研究を行った．空気中600°Cで3 h 加熱することにより，ほぼアスベストの構造水の脱水反応は完了し，さらにアスベストは非晶質化する．その非晶質化に伴ってアスベストは機械的に脆くなり，乳鉢による粉砕で容易に繊維状組織は破壊できるようになり，1 μm 以下の微細な粉末にすることができる．得られた粉末を80 MPa で一軸加圧して成形体を作製し，1300°Cで1 h 加熱することで相対密度90%の焼結体を得ることができる．その場合の主な結晶相はフォルステライトであるが，若干のクリノエンスタタイトも含まれる．

付　記　この研究は，(株)アイジー技術研究所(山形県東根市)の資金協力により行われたものである．

References

1) Hiraoka, M., "Haikibutsu, Handbook," Ohmsha (1996) pp. 999-1005 [in Japanese].
2) Winson, R. W., "Asbestos," 4th ed., Ed. by Lefond, S. J., Industrial Minerals and Rocks (1975) pp. 384-385.
3) Yokoyama, K., "Sekimen·Zeoraito no Subete," Nihon Kankyo Eisei Center (1987) [in Japanese].
4) Huziki, Y. and Mitomo, M., "Whisker," Sangyo Tosho (1993) pp. 167-172 [in Japanese].
5) Sakai, S., Takatsuki, H. and, Hiraoka, M., *Kankyo Gijutsu*, Vol. 18, pp. 397-405 (1989) [in Japanese].

6) Yasue, T., Kojima, Y., Obata, H., Ogura, T. and Arai, Y., *Gypsum & Lime*, No. 234 pp. 280–290 (1991) [in Japanese].
7) Yashima, I. and Ito, A., Kokai-Tokkyo-Koho, Hei5–138147 [in Japanese].
8) Moriyoshi, Y., Urano, T. and Miyaji, H., Kokai-Tokkyo-Koho, Hei9–206726 [in Japanese].
9) Yashima, I. and Ito, A., Kokai-Tokkyo-Koho, Hei6–134438 [in Japanese].
10) Inoue, M. and Oda, K., Kokai-Tokkyo-Koho, Hei9–110514 [in Japanese].
11) Levin, E. M., Robbins, C. R. and McMurdie, H. F., "Phase Diagrams for Ceramists," Am. Ceram. Soc., Columbus, Ohio (1964) p. 112, Fig. 266.
12) Levin, E. M., Robbins, C. R. and McMurdie, H. F., "Phase Diagrams for Ceramists," Am. Ceram. Soc., Columbus, Ohio (1964) p. 246, Fig. 712.

Technical report

Journal of the Ceramic Society of Japan 113 [12] 804-807 (2005)

アスベスト含有セメント板中のアスベストの機械的粉砕

橋本　忍・山口明良*・本多沢雄・淡路英夫・福田功一郎

名古屋工業大学環境材料工学科，466-8555 名古屋市昭和区御器所町
*岡山セラミックス技術振興財団研究所，705-0021 備前市西片上 1406-18

Comminution of Asbestos by a Mechanical Grinding in Asbestos-Containing Cement Board

Shinobu HASHIMOTO, Akira YAMAGUCHI,* Sawao HONDA, Hideo AWAJI and Koichiro FUKUDA

Department of Invironmental and Materials Engineering, Nagoya Institute of Technology, Gokiso-cho, Showa-ku, Nagoya-shi 466-8555
**Okayama Ceramics Research Foundation Research Laboratory, 1406-18, Nishi Katakami, Bizen-shi 705-0021*

When 10-20 mass% of asbestos (chrysotile: $Mg_3Si_2O_5(OH)_4$)-containing cement board of 5 mm thickness was heated at 600°C for 2 h, the asbestos lost the crystal structure due to its dehydration reaction in the cement board, changing to an amorphous phase. Further, the heated cement board could be easily ground to grains with several μm size using a mortar. Then the asbestos seemed to be ground to below the size at the same time, because the fiber shape of original asbestos was not found in the sample.

[Received August 22, 2005; Accepted October 20, 2005]

Key-words : *Asbestos, Chrysotile, Mechanical grinding, Heat treatment, Cement board*

1. 緒　言

これまでにわが国に輸入されたアスベスト（石綿）の総量は，白石綿（クリソタイル），青石綿（クロシドライト），茶石綿（アモサイト）などの種類を区別しないで財務省輸入統計を単純積算した場合，およそ1千万トンに達する．そのうち90%を超える量が鉄骨に対する吹き付けやセメント板など建築材として使用されてきた．労働安全衛生法関係政省令等の改正により1995年に毒性の高い青石綿，茶石綿の使用が禁止とされてからは，白石綿（クリソタイル：$Mg_3Si_2O_5(OH)_4$）のみがカナダから主に輸入され，2000年で10万トン弱，ここ数年でも毎年2～5万トン，2004年には8000トンの輸入があった．2004年は大手建材メーカーのアスベスト使用禁止の自主規制により輸入量が大幅に減った．その労働安全衛生法施行令の一部改正により2004年10月には，アスベストの原則禁止が打ち出された．しかしそれはこれまでにアスベスト含有量の特に高かった「繊維強化セメント板」や「ブレーキパッド」など特定10品目に対し，1 mass%以上含有してはならないというもので，それ以外の品目は除外されており，何よりクリソタイルの輸入そのものが禁止されたわけではなかった．しかしながら今後，厚生労働省の方針により2008年あるいは前倒してアスベストは全面使用禁止になるものとみられる．

アスベストに関する規制として作業者保護の立場から，1975年の労働安全衛生法令でいち早く「吹き付けアスベスト」の原則禁止が打ち出された．1987年には，学校教育施設にその「吹き付けアスベスト」が使われていることが分かり，いわゆる「学校パニック」とよばれて社会問題化したが，その調査と撤去という行政指導による対応により，アスベスト問題は一旦沈静化したかにみえた．しかし2005年，肺や，心筋，腹膜などの粘膜のがんの一種である「悪性中皮種」の原因が，作業現場などで数十年前のアスベストの吸入による[1]という労災認定問題が大きく取り上げられ，あらたな「公害」認定を視野に入れながら，再び社会の関心がアスベスト問題に向けられるようになった．この飛散性の高い「吹き付けアスベスト」の撤去及びその処理に関しては，1988年の旧厚生省のガイドラインにより撤去作業はマニュアル化され，特別管理産業廃棄物として管理型廃棄物最終処分場で埋め立て処理されている．しかしながら非飛散性のアスベスト含有セメント板に関しては，撤去の際にアスベストを飛散させないことや，またその運搬や保管に際し囲いや表示の義務がある程度である．廃棄物として処理する場合には，セメントで固定化されており安全であるという理由から，ほとんど一般廃棄物と同じ扱いとなっている．今後はセメントの風化や破砕によるアスベストの露出や飛散など，アスベスト含有セメント板も廃棄物としての安全性の問題が指摘され，管理型の廃棄処分が要求されるものとみられる．

これから先の2020年前後には，セメント板など国内に数千万トンあるアスベスト含有建築材の廃棄量がピークとなるといわれている．埋め立て処理をするにも，あるいは有効活用するためにも，セメント板を始めとする「非飛散性」とされるアスベスト含有建築材の安全な処理技術を確立することは急務なことであると考える．

著者らは最近，クリソタイルのみに対する簡便な熱処理と粉砕処理により，健康障害の原因であるクリソタイルの繊維状形態を，Stantonらの提唱した健康を害する危険サイズ：長さ8 μm以上，径0.25 μm以下[2]より小さくできることを見いだし報告した[3]．本研究では，実際にセメント板に強化材として加えられているアスベスト（クリソタイル）が，同様な熱処理と粉砕により，安全な大きさまでに破壊されるのかを，また化学組成の変化と併せて，それを検証することを目的とした．

2. 実験方法

実験に使用したアスベスト含有セメント板はJIS A5423適合品で，アスベスト（クリソタイル）含有量は質量比で10～20%，厚さ5 mmの民間家屋の屋根に用いられていたスレートと呼ばれる製品で，アスベスト製品であることを示す「a」の表示がある．以後，アスベストはクリソタイル自身を指すので，本論文中ではクリソタイルと記す．はじめにクリソタイルの微細形態を知っておくために，図1には代表的なカナダケベック州産のクリソタイルの走査型電子顕微鏡（SEM；JSM5200, JEOL

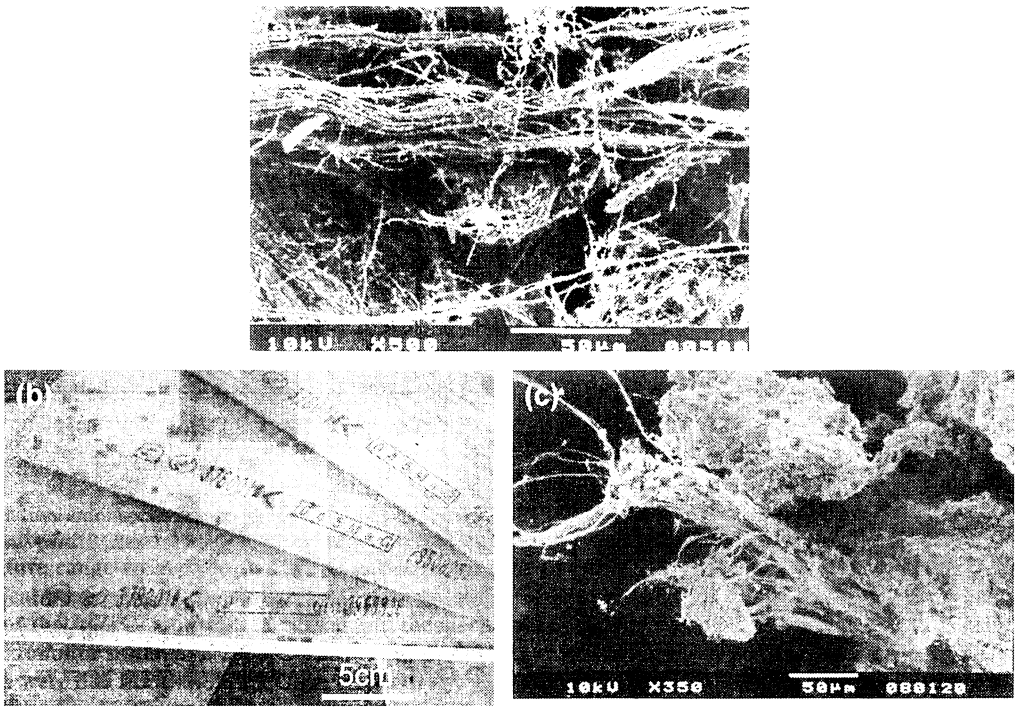

Fig. 1. SEM micrograph of Canadian chrysotile (a), appearance of chrysotile-containing cement board (b), and SEM micrograph of the fractured surface of the cement board (c).

製）観察写真，本実験で使用したクリソタイル含有セメント板の概観，及びそのセメント板の破断面における SEM 観察写真を示す．この写真のようにセメント板の破断面には，クリソタイルの繊維状結晶がむき出しになった状態が多く観察された．セメント板が繊維強化されている様子が伺えるとともに，破断すれば簡単にクリソタイルが露出してしまうことを示している．

そのセメント板から10×10 mm（厚さ 5 mm）の大きさに切り出し，実験に供する試料とした．試料を電気炉に入れ，600°C の温度で 0～3 h 加熱保持した．この600°Cという温度はクリソタイルのみの場合に効果のあった温度である[3]．昇温速度は600 °C/h とし，加熱後電源を OFF にして試料は室温まで自然放冷した．加熱後各試料の表面及び内部に分けて，X 線分析装置（XRD；島津製作所製，XD-D1）で構成結晶相の分析を行った．表面の分析では試料表面に X 線を直接入射して回折パターンを測定し，内部の分析では粉砕処理した粉末試料に対して回折パターンを測定した．比較のために非加熱処理試料についても表面及びその内部について XRD 分析を行った．

粉砕処理は，試料を熱処理した後，アルミナ製乳鉢に入れて粉砕した．軽く数秒叩いて粗砕し，その後クリソタイルのみを粉砕処理した場合と同様に，乳鉢と乳棒には常時 2～3 kg の荷重を掛けながら毎秒 1～2 回転の速度で 2～3 min，セメント成分もろとも粉砕した．粉砕された試料を SEM で観察することにより，その試料内部に繊維状粒子（残存クリソタイル）が存在するかを確認した．

3. 結果と考察

図 2 には，図 1 のカナダ産クリソタイル及び本実験で用いたセメント板の熱処理を施していない試料の粉末 X 線回折結果を示す．結果より，セメント板試料にクリソタイルが含まれていることが確認できた．また結晶相としては他に，SiO_2（quartz）と $CaCO_3$（calcite）が検出されたが，セメントの水和硬化体としての結晶相は結晶性が低いため回折線強度が小さく，ほとんど同定できなかった．これはセメント板が長年に中性化（炭酸化）の作用を受けたことによると考えられる[4]．このクリソタイル結晶の回折線の有無が，化学組成としてクリソタイルの存在の有無の指標として捉えることができる．

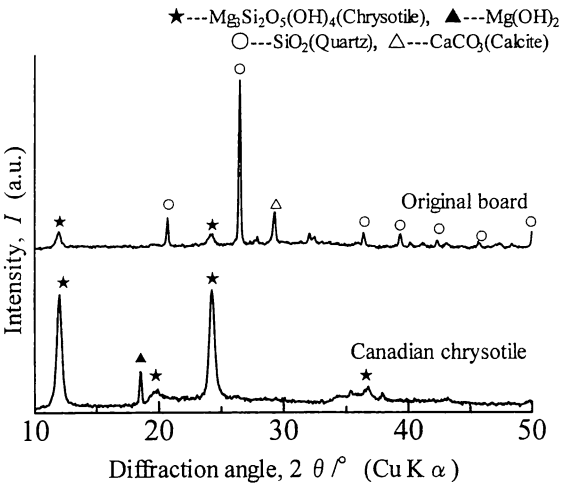

Fig. 2. XRD patterns of Canadian chrysotile and the chrysotile-containing cement board.

図 3 に，600°C での保持時間を変えた試料を，粉砕せずその表面をそのまま XRD 分析した結果を示す．0 h 保持した場合とは，600°C に到達後，その温度で保持せずすぐに冷却した試料であるが，その試料表面からはクリソタイルが検出された．一方，保持時間が 1 h の試料表面からは，クリソタイルを示す回折線は検出されなかった．図 4 には，600°C での保持時間を変えた試料内部の XRD 分析結果を示す．試料内部の場合，図

3の試料表面の場合には検出されなかった1h保持の試料からも，クリソタイルを示す回折線は検出された．しかしながら保持時間が2hになると，クリソタイルを示す回折線は検出されなくなった．この600°Cにおけるクリソタイルの結晶相の消滅は，クリソタイルの脱水反応による非晶質化に伴うものであると考えられる[3),5)]．

図5には，粉砕した非加熱処理試料と600°Cで0h，1h及び2h加熱保持し，その後粉砕処理した試料のSEM観察結果を示す．セメント硬化体（C-S-H）の比重は結晶相の種類によっても違うが，おおよそ2.2～2.8 g/cm^{3}の範囲にあり[6)]，これはクリソタイルの比重2.4～2.6 g/cm^3[7)]とほとんど同じ値である．しかしクリソタイルは内部構造が中空を呈し[8)]，また図1(a)のように径が0.2～数 μm の柔軟性をもった繊維状結晶でそれが束なった形態をしている．そのため繊維間にはある程度の空間（空気）を含むためにかさ比重は小さくなり，クリソタイルの実際のセメント板に占める体積割合は，重量に対する割合より大きくなることが考えられる．したがって重量比で10～20%含まれる場合，クリソタイルが均一に分散していれば，セメント板の微細組織のどこを観察してもクリソタイルが発見できる量であるといえる．実際に観察した図5の非加熱処理の試料の場合では，多くの繊維状クリソタイル粒子が観察された．保持時間を0hとした試料からは，ややその量は少なくなっているものの，繊維状の粒子は観察された．1h保持した試料からは，繊維状の粒子はほとんどみられなくなり，ところどころに写真のような比較的径の大きい繊維状粒子が観察された．図4の回

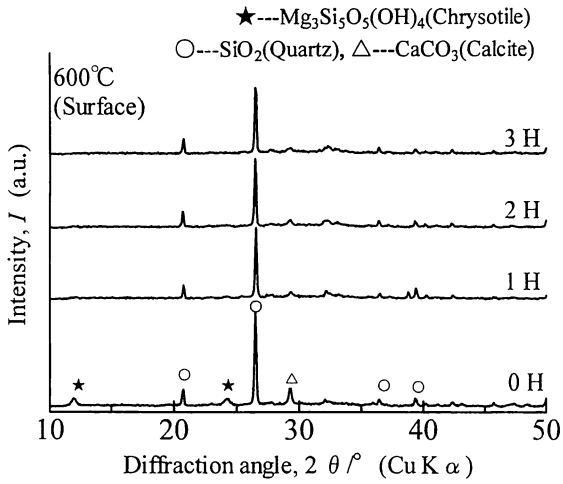

Fig. 3. XRD patterns of the surfaces of the chrysotile-containing cement board after heating at 600°C for 0-3 h.

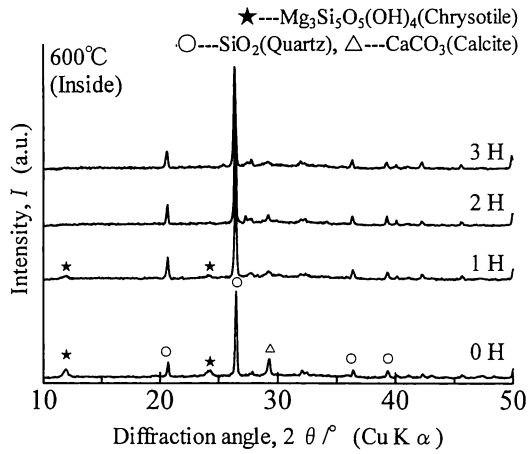

Fig. 4. XRD patterns of the inside of the chrysotile-containing cement board after heating at 600°C for 0-3 h.

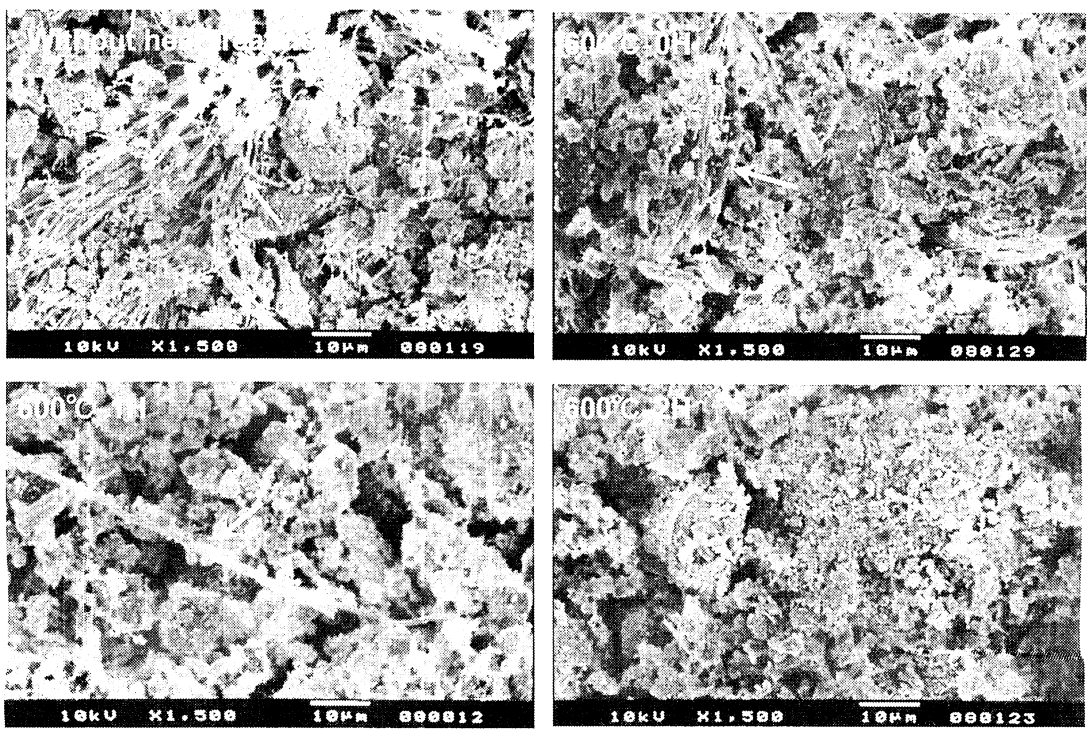

Fig. 5. SEM micrographs of the ground powder of the chrysotile-containing cement board with and without heating at 600°C for 0-2 h. (Arrow indicates asbestos.)

折パターンからも，1 h保持の条件ではクリソタイルの回折線がわずかに検出されており，この繊維状粒子がクリソタイルであるとみられた．一方，2 h保持した試料からは，径の比較的大きなものまで含めてほとんど繊維状の粒子はみられなくなった．また，図4の回折パターンでも2 h保持した条件ではクリソタイルの結晶相は検出されなくなっており，上記の観察結果と矛盾しない．以上の結果は，クリソタイル単体を対象とした前報告[3]の結論，すなわち，クリソタイルは600°C, 2 hの加熱処理によりほぼ脱水反応が完了し非晶質化すること，及びその場合に繊維状の形態を呈しているもののその粒子は非常に脆くなり，乳鉢粉砕により容易に1 μm以下に破壊できる，という結果と一致する．加えて，クリソタイルがセメントなど他成分と共存すると，クリソタイル自身の反応性が活性化し，脱水反応の促進，反応に伴う形態の消滅や，残った針状を有する粒子の脆化が促進した可能性も考えられる．

以上の結果から，クリソタイルを含有するセメント板を600°Cで2 h加熱し，その後粉砕処理することで，内包されたクリソタイルを組成的にも構造的にも破壊できることを明らかとし，クリソタイルを無害化できる有効な技術となり得ることを確認した．

4. まとめ

アスベスト単体での繊維状形骸を消滅させる研究結果を踏まえ，本研究では，セメント板中に含まれるアスベストの無害化への応用展開を図った．クリソタイル（白石綿）を質量比で10～20%含有する厚さ5 mmのセメント板を600°Cで2 h加熱保持することにより，セメント板中に内包された状態でもクリソタイルの化学組成は失われた．更にその後セメント成分もろとも粉砕することで，1 μm以下という針状粒子が確認できないまでに元のクリソタイルの繊維状の形態は破壊された．

付　記　この研究は，(株)アイジー技術研究所(山形県東根市)の資金協力により行われたものである．

References

1) Yokoyama, K., "Sekimen·Zeoraito no Subete," Ed. by Miyake, H., Nippon Kankyo Eisei Center (1987) [in Japanese].
2) Stanton, M. F., Layard, M., Tegeris, A., Miller, E., May, M., Morgan, E. and Smith, A., *J. Nat. Canc. Inst.*, Vol. 67, pp. 965-975 (1981).
3) Hashimoto, S. and Yamaguchi, A., *J. Ceram. Soc. Japan*, Vol. 113, pp. 312-316 (2005) [in Japanese].
4) Kobayashi, K., "Concrete Kozobutsu no Soki Rekka to Taikyusei Shindan," Ed. by Morikita, H., Morikita Shuppan (1991) pp. 132-134.
5) Kokai-Tokkyo-Koho, Hei 5-293457 [in Japanese].
6) Arai, Y., "Semento no Zairyo Kagaku," 2nd ed., Ed. by Sakuma, Y., Dainippon Tosho (1991) pp. 140-148.
7) Winson, R. W., "Asbestos," 4th ed., Ed. by Lefond, S. J., Industrial Minerals and Rocks, American Institute of Mining, Metallurgical and Petroleum Engineers (1975) pp. 384-385.
8) Yada, K., *Acta Cryst.*, Vol. 23, pp. 704-707 (1967).

CERAMICS INTERNATIONAL

Ceramics International 32 (2006) 431–439

www.elsevier.com/locate/ceramint

$AlZrC_2$ synthesis

U. Leela-adisorn [a,1,*], S.M. Choi [a], T. Matsunaga [a], S. Hashimoto [a], S. Honda [a], K. Hayakawa [b], H. Awaji [a], A. Yamaguchi [c]

[a] *Nagoya Institute of Technology, Department of Materials Science and Engineering, Gokiso-cho, Showa-ku, Nagoya-shi 466-8555, Japan*

[b] *Japan Fine Ceramics Center, Mutsuno, Atsuta-ku, Nagoya-shi 456-8587, Japan*

[c] *Okayama Ceramics Center, Nishi-Katakami, Bizen-shi 705-0021, Japan*

Received 7 February 2005; received in revised form 21 February 2005; accepted 14 March 2005
Available online 8 June 2005

Abstract

$AlZrC_2$ was synthesized using a direct solid-state method. Various types of carbon were used as starting materials together with aluminum zirconium carbide powders. The effect of different carbon on the formation of Al–Zr–C compounds formation were investigated. The atomic arrangement of carbon affects the Al–Zr–C compounds formation, i.e., crystalline carbon facilitates $Zr_2Al_3C_5$ formation while glassy carbon facilitates $AlZrC_2$ formation. High purity $AlZrC_2$ was prepared from the appropriate mol ratio of Al:ZrC:glassy carbon by heating in vacuum at 1600 °C for 1 h. However, a little amount of $Zr_2Al_3C_5$ still formed due to graphitization of glassy carbon at high temperature. Glassy carbon from sugar showed a lower degree of crystallization (graphitization) than glassy carbon from phenolic resin. Finally, the obtained two phase specimen was ground and heat treated again using pulse electric current sintering to produce single $AlZrC_2$.
© 2005 Elsevier Ltd and Techna Group S.r.l. All rights reserved.

Keywords: D. Carbide; D. Carbon; $AlZrC_2$; Graphitization

1. Introduction

Carbides are extensively used in various fields due to their excellent properties. For instance, SiC [1] is widely used as an engineering material because of its high-temperature fracture strength and creep resistance. The remarkable thermal stability and chemical inertness of B_4C make it well suited for applications requiring high stiffness or good wear resistance [2]. ZrC is an important structural material owing to its high strength and good corrosion resistance [3].

Several complex carbides have recently been synthesized and studied. For example, $Al_8B_4C_7$ [4] has remarkable antioxidant properties in carbon-containing refractory materials. Michalenko et al. found the $AlZrC_2$ phase in 1978 [5], but little has been reported about this material. Hashimoto et al. [6] produced a composite material of $AlZrC_2$ and Al, and characterized its mechanical properties. They prepared the $AlZrC_2$ by heating a mixture of Al and ZrC, followed by leaching with HCl. After synthesizing, however, ZrC still remained in the sample.

We synthesized high purity $AlZrC_2$ using a direct solid-state method.

2. Experimental procedure

2.1. Starting materials

The starting materials we used were

(1) Al, 99.9% pure; 10-μm mean particle size (High Purity Chemicals Co., Ltd.).
(2) ZrC, 95% pure (High Purity Chemicals Co., Ltd.).
(3) Graphite, 99.7% pure; 5-μm mean particle size (High Purity Chemicals Co., Ltd.).

* Corresponding author at: Department of Materials Science, Faculty of Science, Chulalongkorn University, Bangkok 10330, Thailand.
Tel.: +66 2 218 5544–6; fax: +66 2 218 5561.
E-mail address: luraiwan@yahoo.com (U. Leela-adisorn).
[1] Tel.: +81 52 735 5276; fax: +81 52 735 5276.

0272-8842/$30.00 © 2005 Elsevier Ltd and Techna Group S.r.l. All rights reserved.
doi:10.1016/j.ceramint.2005.03.019

Table 1
Al–ZrC–C mixtures with graphite as source of carbon

Composition	Mol ratio of starting materials (Al:ZrC:C)	Mol ratio of elements (Al:Zr:C)
A	1:1:1	1:1:2
B	3.5:3.5:3	3.5:3.5:6.5
C	4:4:2	4:4:6
D	4.5:4.5:1	4.5:4.5:5.5
E	3.5:3:3.5	3.5:3:6.5
F	4:2:4	4:2:6
G	4.5:1:4.5	4.5:1:5.5

(4) Amorphous carbon. In this work, we used three kinds of amorphous carbon, i.e.,
   (a) Prepared by heating phenolic resin in a muffle furnace at 400 °C for 30 min and grinding it into small pieces, reheating it at 400 °C for 5 min, then grinding it into a fine powder.
   (b) Prepared by heating sugar in a porcelain crucible with Bunsen burner for 6 h and grinding it into small pieces, reheating it for 6 h, then grinding it into a fine powder.
   (c) Carbon black, as received from industry (specific surface area, 125 m^2/g).

2.2. Sample preparation and heating

The starting materials were mixed in acetone at various mol ratios as shown in Tables 1 and 2 and Fig. 1. The mixtures were pressed into pellets of ~1.8 g, CIPed at 100 MPa, and heated under two different conditions:

- Ar atmosphere: The samples were placed in a refractory block lined with carbon paper and covered with powder having the same composition to prevent surface oxidation [6]. They were heated from room temperature to 1600 °C for 1 h at a heating rate 10 °C/min.
- Vacuum: The samples were prefired in Ar atmosphere as described above at 900 °C for 1 h to prevent Al vapor from attacking the carbon lining of the vacuum chamber. After prefiring, the covered powder was removed. The samples were wrapped in carbon paper and placed in a carbon crucible before heating in vacuum at a heating rate 10 °C/min from room temperature to the maximum temperature for 1 h.

Table 2
Al–ZrC–C with amorphous carbon as source of carbon

Composition	Mol ratio of starting materials (Al:ZrC:C)
H (resin)	3:3:4
I (resin)	4:3:3
J (resin)	5.5:3:1.5
K (resin)	6:3:1
L (resin)	3:2.5:4.5
M (resin)	3.5:2.5:4
N (resin)	3:2:3
O (resin)	5:2.5:2.5
P (resin and carbon black)	35:28:37
Q (resin and sugar)	21:14:15

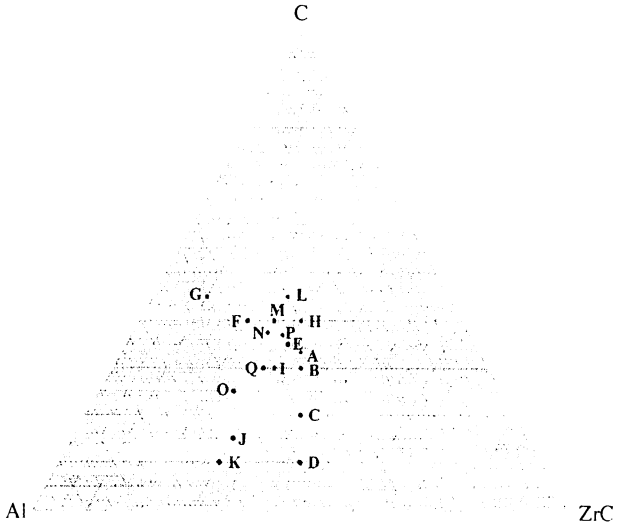

Fig. 1. Composition diagram of Al–ZrC–C mixtures.

2.3. Characterization

Samples were crushed and ground into fine powder. Phase change was characterized by XRD (Shimadzu XD-X1). Thermal analysis was carried out by DTA/TG (Rikaku Thermoplus TG8120) from room temperature to 1200 °C in air to check the exothermic reaction of the residual ZrC around 500–600 °C [7]. After synthesis, fresh crack samples were investigated by SEM (JEOL JSM-6360LV).

3. Results and discussion

3.1. Effect of composition on phase formation

Al–ZrC–graphite mixtures with various mol ratios were heated in Ar atmosphere. Phases formed within the Al–ZrC–graphite pellets after firing at 1600 °C for 1 h are shown in Fig. 2. Phase formation depends on the ratio of the starting materials. Fig. 2a shows the phase formation for an Al:ZrC mol ratio of 1 at varying amounts of graphite. Fig. 2b shows phase formation for an Al:graphite mol ratio of 1 at varying amounts of ZrC. In the middle zone of the composition diagram (Fig. 1), $Zr_2Al_3C_5$ formed after firing. This formation did not depend on the Al:ZrC:graphite ratio, as shown by the XRD patterns of the compositions A, B and E in Fig. 2a and b. The phase formation after firing was completely different away from this middle zone, i.e., closer to the edges of the composition diagram. At a constant mol ratio of Al to ZrC with lower graphite content (compositions C and D in Fig. 2a), no $Zr_2Al_3C_5$ was found. At a constant mol ratio of Al to graphite with lower ZrC content (compositions F and G in Fig. 2b), no $AlZrC_2$ was found

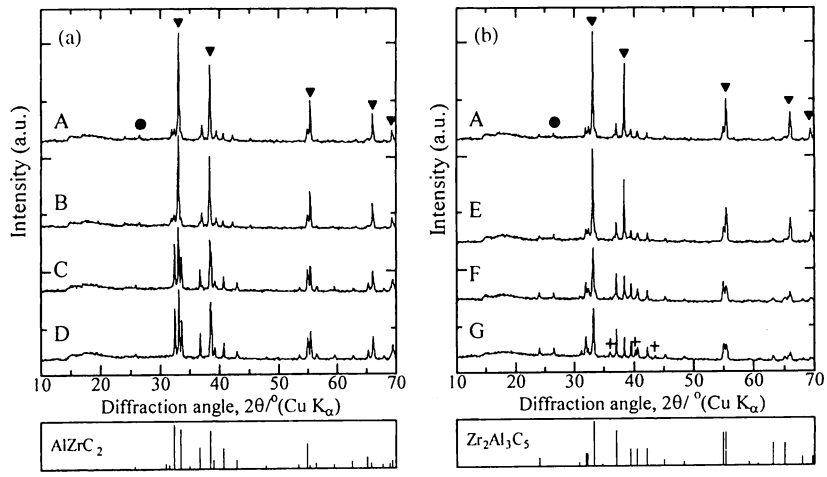

Fig. 2. Phase formation of Al, ZrC and graphite mixtures at various mol ratio after firing at 1600 °C in Ar for 1 h: (a) Al:ZrC = 1; (b) Al:C = 1. (▼) ZrC; (●) graphite; (+) Al_4C_3.

after firing. From Fig. 2, we concluded that the $AlZrC_2$ should be prepared from Al–ZrC–graphite mixture with very low graphite content, however, a very high residual ZrC still remained.

Although the diagram in Fig. 1 is similar to a phase diagram, and the composition axes have to be represented as elements (see Table 1), the carbon from graphite and from ZrC affects Al–Zr–C compound formation differently. Graphite is a carbon compound with hcp structure [8], while carbon in ZrC is in octahedral interstices of Zr close-packed layer [9,10]. Hence, the reaction mechanism of carbon in graphite and the reaction mechanism of carbon in ZrC differ due to differences in the number and type of neighboring atoms or co-ordination number (C.N.). Schuster and Nowotny [5] presented the atomic arrangement of $AlZrC_2$ and $Zr_2Al_3C_5$. The interstitial carbon in both complex carbides shows some relation to the interstitial carbon in ZrC structure. Thus, we describe the mol ratio of the mixtures in terms of the starting compounds, rather than elemental components.

3.2. Effects of carbon phase

We prepared Al–ZrC–C mixtures with compositions A (molar composition equivalent to $AlZrC_2$) and N (molar composition equivalent to $Zr_2Al_3C_5$) with two types of carbon, i.e., graphite and amorphous carbon from phenolic resin, and heated in vacuum at various temperatures for 1 h.

The phase evolutions of the compositions A and N after heating are shown in Fig. 3, where A1, N1 and A2, N2 denote compositions with graphite and amorphous carbon, respectively. The results of thermal analysis of samples, which represent the residual ZrC in samples after firing as exothermic peak [7], are shown in Fig. 4. Based on the discussion in Section 3.1, composition N was expected to yield $Zr_2Al_3C_5$ after heating regardless of the carbon type

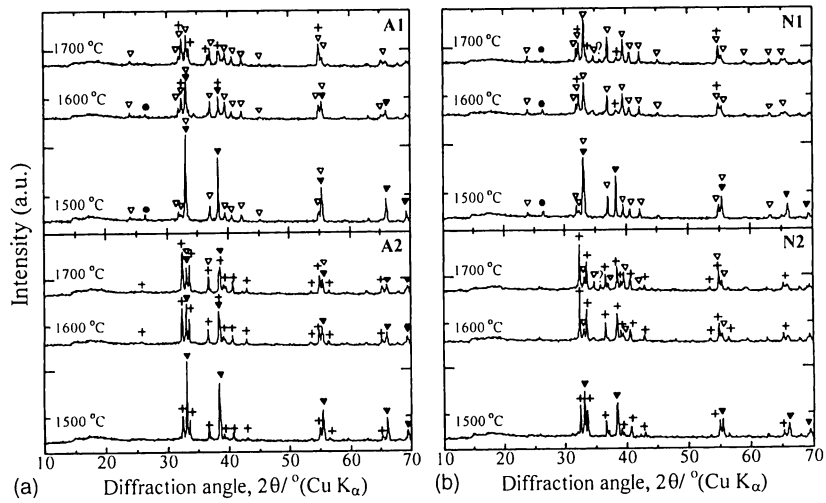

Fig. 3. Phase evolution of Al–ZrC–C mixtures containing different types of carbon upon firing at 1500–1700 °C in vacuum for 1 h; Al, composition A with graphite; A2, composition A with amorphous carbon; N1, composition N with graphite; N2, composition N with amorphous carbon. (▼) ZrC; (●) graphite; (▽) $Zr_2Al_3C_5$; (+) $AlZrC_2$; (?) unknown.

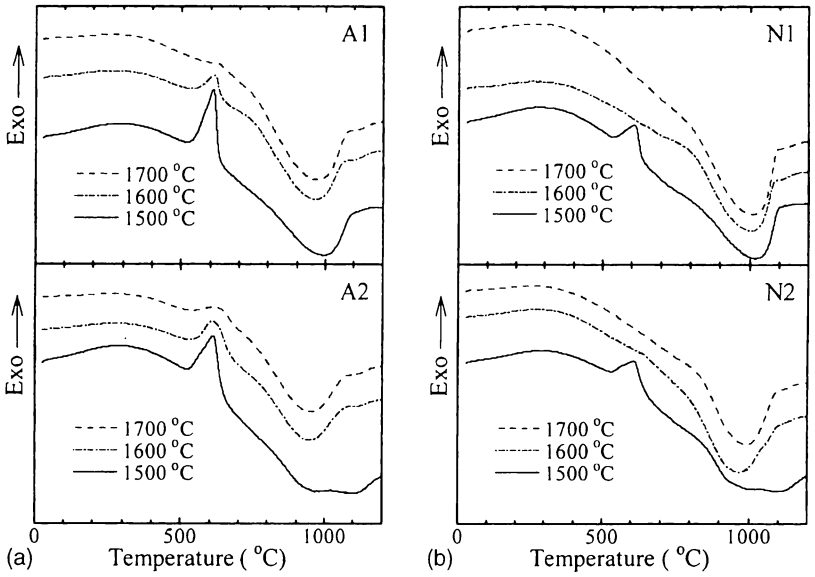

Fig. 4. DTA of Al–ZrC–C mixtures containing different types of carbon after firing at 1500–1700 °C in vacuum for 1 h; Al, composition A with graphite; A2, composition A with amorphous carbon; N1, composition N with graphite; N2, composition N with amorphous carbon.

because this composition lies on the composition line of A–E–F–G (Fig. 1). Fig. 3a and b indicate that $Zr_2Al_3C_5$ formed in the graphite-containing compositions A1 and N1, and $AlZrC_2$ formed in the amorphous carbon-containing compositions A2 and N2. The amounts of $Zr_2Al_3C_5$ and $AlZrC_2$ were higher (Fig. 3) while the amount of ZrC decreased as firing temperature increased (Fig. 4). From Fig. 3, it is obvious that the formation of $Zr_2Al_3C_5$ and $AlZrC_2$ depends on the type of carbon in the composition, not the mol ratio of the starting materials. In other words, the atomic arrangement of carbon in graphite crystal facilitates $Zr_2Al_3C_5$ formation, while the atomic arrangement of amorphous carbon from phenolic resin facilitates $AlZrC_2$ formation.

$AlZrC_2$ in the graphite-containing mixture and $Zr_2Al_3C_5$ in the amorphous carbon-containing mixture heated at 1700 °C presumably came from evaporation during heating because there was weight loss in the samples after heating, and the losses increased as the heating temperature was increased.

Fig. 4b shows that there was no exothermic peak from the ZrC in composition N with both types of carbon after firing at 1600 °C. This means the phase of carbon does not affect the overall reaction between ZrC and other starting materials.

Although the firing atmosphere described in Section 3.1 and here differed, our previous study [7] and the results from studies of other compositions (not shown here) confirm that firing in Ar or in vacuum yields $Zr_2Al_3C_5$ in case of graphite-containing mixtures, and $AlZrC_2$ in case of (phenolic resin-derived) amorphous carbon-containing mixtures. The effects of the firing atmosphere (Ar versus vacuum) were discussed elsewhere [7].

Fig. 3 reveals an interesting fact about Al–Zr–C compound formation. Hashimoto et al. discussed the formation of $AlZrC_2$ in an Al–ZrC–C mixture with a high Al content [6]. After heating, the excess Al–Zr alloy was leached out by HCl. However, as shown in Fig. 3, no Al–Zr alloy was found in samples heated at 1500 °C or above. At 1600 °C, the amount of Al–Zr–C compound still increased. This indicates that there was an Al-containing intermediate phase reacted with ZrC and free carbon to form Al–Zr–C compound, however, this intermediate phase could not be detected. Though we fired the samples at 1600 °C for various short intervals, no Al-containing phase could be detected by XRD. It may be that this Al-containing phase exists only at high temperature. Due to the condition of the vacuum graphite arc furnace, it is impossible to remove the samples from the chamber during the hot stage to characterize this intermediate phase. Our previous study [7] on $Zr_2Al_3C_5$ formation from Al–ZrC–C mixture with a high Al content also confirmed that Al–Zr alloy formed upon firing up to 1400 °C. Thus, the reaction path of Al–Zr–C formation in this present study differs from that in Hashimoto's Al-rich system.

3.3. Amorphism of amorphous carbon

The phenolic resin we used as an amorphous carbon source is widely used as binder in refractory industries [11]. However, carbon obtained from heating phenolic resin is too stiff for grinding. Thus, we used another kind of amorphous carbon, namely carbon black, because it is commercially available as powder. XRD patterns of carbon black, graphite and amorphous carbon from phenolic resin are compared in Fig. 5. Al–ZrC–C mixtures of composition P (see Table 2) with amorphous carbon from phenolic resin and carbon black were fired in vacuum at 1600 °C for 1 h.

The resultant phases are shown in Fig. 6. The mixture with carbon from phenolic resin gave $AlZrC_2$ as a main

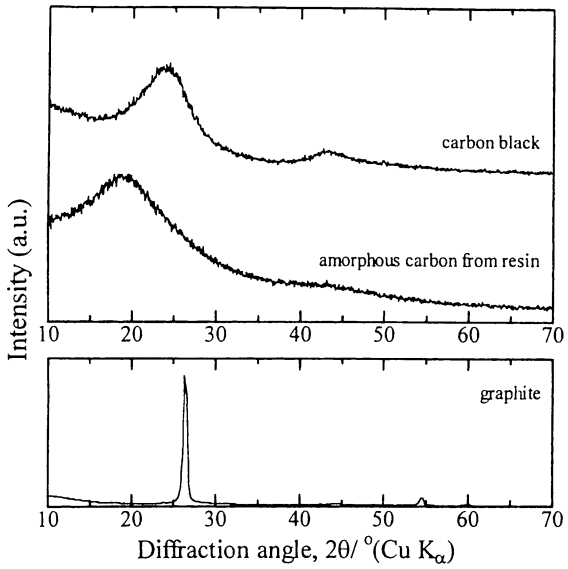

Fig. 5. XRD patterns of carbon black compared with amorphous carbon from resin and graphite.

product with a small amount of $Zr_2Al_3C_5$, while the mixture containing carbon black gave a mixture of $AlZrC_2$ and $Zr_2Al_3C_5$. Although the XRD pattern of carbon black showed the amorphous pattern, the resultant phases in the Al–ZrC–C mixtures after firing differed. This indicated that the amorphisms of the two types differ.

Amorphous carbon obtained by burning phenolic resin is glassy phase [12,13] with a short-range order structure like other inorganic glasses. The glassy material is isotropic and thermodynamically metastable. Therefore, glassy carbon from phenolic resin can be considered as "inherently" amorphous. By contrast, under high TEM resolution [14], carbon black showed very small primary particles surrounded by concentrically deposited carbon layers. The layers were nearly parallel to each other. But the relative position of these layers was random, so that there was no order as in the *c* direction of graphite. Therefore, the carbon atoms arrangement in a carbon black primary particle is non-well crystalline at the surface with an increasing order at the core of the primary particle. For most carbon blacks, these "crystalline" regions are 1.5–2.0 nm in length and 1.2–1.5 nm in height, corresponding to four to five layers. With such small size of "crystalline" regions, carbon black showed "amorphous" XRD pattern since the wavelength of X-ray (Cu Kα, 1.54056 nm) is similar to the "crystalline size" of carbon black.

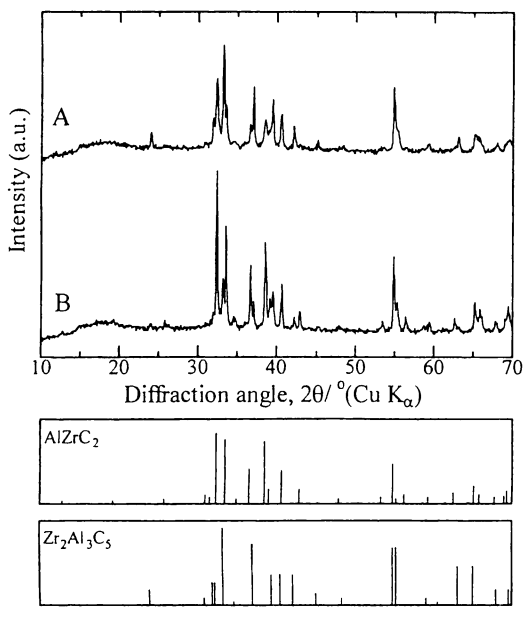

Fig. 6. Effect of type of amorphous carbon as starting material in the same ratio as Al:ZrC:C (mixture P, Al:ZrC:C = 35:28:37) after heating at 1600 °C for 1 h in vacuum. (A) Carbon black and (B) amorphous carbon from phenolic resin.

Based on the results presented in Section 3.2, carbon black in the Al–ZrC–C mixture gave a mixed product of $AlZrC_2$ and $Zr_2Al_3C_5$ because of its mixed characteristic of high reactivity from the non-well crystalline surface and "crystalline" regions within carbon black primary particles.

As mentioned above, the diagram in Fig. 1 is related to phase diagram. However, the results presented in Section 3.2 differ from those presented in Section 3.1. The Al–ZrC–graphite mixture gave the $AlZrC_2$ phase when the main carbon source was ZrC. This means the parent structure of carbon affect the formation of the Al–Zr–C compound. Nowotny et al. compared the crystal structure of Al–Zr–C complex carbides with those of other complex carbides [15]. They found that the degree of filling of the voids by carbon atoms is higher in Al–Zr–C complex carbides than in other complex carbides. Though the mechanism of void filling by carbon atoms in $Zr_2Al_3C_5$ and $AlZrC_2$ was not mentioned, the difference in atomic size between Zr and Al affects this mechanism. Carbon atoms in graphite and glassy carbon are different in many ways, e.g., C.N., bond type between the atom, and thermodynamic state. These factors affect the mechanism of reaction between the Al-containing intermediate phase, ZrC and carbon. The above results suggest that the mechanism of void filling by glassy carbon atoms may be similar to that of the interstitial carbon in ZrC. Thus, at the same Al–ZrC–C composition, the glassy carbon-containing mixture yielded a different Al–Zr–C phase from the graphite-containing composition.

3.4. Composition line

We fired various compositions of Al–ZrC–amorphous carbon in vacuum at 1600 °C for 1 h to find the zone in the composition diagram yielding the lowest amount of $Zr_2Al_3C_5$ and ZrC. Phase analyses of a number of compositions after firing are represented as composition line in Figs. 7 and 8; the two figures show the XRD patterns of composition line H–E–I–J–K and L–M–N–O, respectively. Because the ZrC and $Zr_2Al_3C_5$ peaks in the XRD patterns overlap (at $2\theta \approx 33^\circ$), we conducted thermal analysis of all samples in Figs. 7 and 8 to detect the

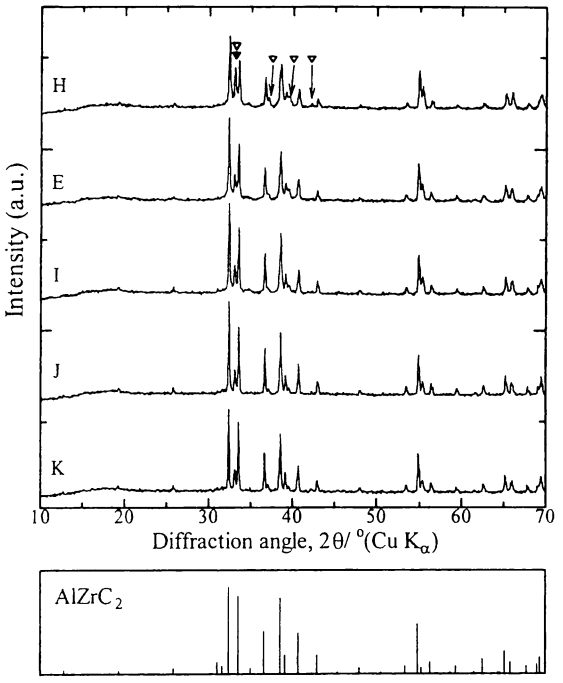

Fig. 7. XRD patterns of Al–ZrC–C composition line "H–E–I–J–K" after firing at 1600 °C in vacuum for 1 h. (▼) ZrC; (▽) $Zr_2Al_3C_5$ (C, amorphous carbon front phenolic resin).

residual ZrC after firing (DTA diagrams of compositions not presented here). The compositions in Fig. 7 gave $AlZrC_2$ as the main product upon firing, with a small amount of $Zr_2Al_3C_5$ and trace amounts of ZrC. The compositions in Fig. 8, slightly richer in Al than those in Fig. 7, gave $AlZrC_2$ as the main product with a small amount of $Zr_2Al_3C_5$. These results indicate that during the $AlZrC_2$ formation, another

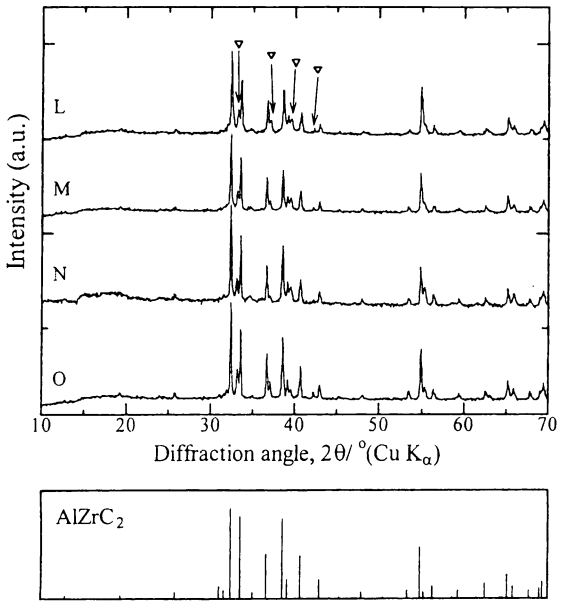

Fig. 8. XRD patterns of Al–ZrC–C composition line "L–M–N–O" after firing at 1600 °C in vacuum for 1 h. (▽) $Zr_2Al_3C_5$ (C, amorphous carbon from phenolic resin).

phase of Al–Zr–C phase ($Zr_2Al_3C_5$) started to form although there was some ZrC left in the system.

3.5. *Effect of excess aluminum*

Schuster and Nowotny [5] studied Al–Zr–C phase diagram at 700 °C and 1000 °C and found that ZrC is very stable and still existed after very long annealing time (longer than 100 h). Gesing and Jeitschko [16] prepared $Zr_3Al_3C_5$ by melting the mixture of ZrC and Al at very high weight ratio of Al (1:5) under Ar for 2 days at 1500 °C to make sure that ZrC was completely reacted with Al and no ZrC was found. The phases of product after melting were $ZrAl_3$ and $Zr_3Al_3C_5$. It is believed that ZrC is very stable and need excessive amount of Al as flux. It is known that ZrC starts to oxidize even at low temperature (300 °C) under low oxygen partial pressure [3]. But no research had studied about the effect of oxygen amount on Al–Zr–C compound formation.

From our previous work, we proved that the significant amount of oxygen in Ar dissolved in ZrC and formed Zr–C–O solid solution which is stable and do not react with other starting materials. The Al–ZrC–graphite mixture of same composition after heating at 1600 °C for 1 h in vacuum and in Ar showed different XRD pattern and no ZrC phase was found in sample heated in vacuum. Therefore, the very excessive amount of Al is needed when the Al–ZrC–C mixture is heated in Ar to form Al melt and cover ZrC grains to protect them from oxidation. However, Al evaporation occurred during heating in vacuum. The excess Al is necessary for Al–Zr–C compound formation, but at much less amount than heating in Ar.

From Section 3.2, the temperature which is suitable for Al–Zr–C compounds formation is 1600 °C. Aluminum has the lowest melting point (660 °C) in the Al–Zr–C system. Excess Al in the mixture may reduce the reaction

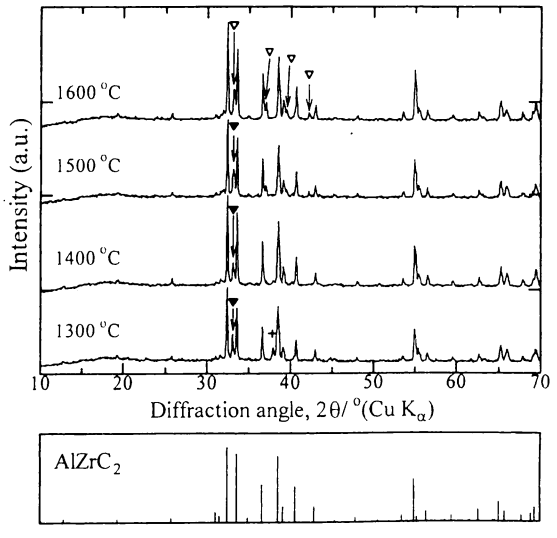

Fig. 9. Phase evolution of Al–ZrC–C at excess-Al-composition (O) after firing in vacuum at various temperatures for 1 h. (▼) ZrC; (▽) $Zr_2Al_3C_5$; (+) Al_3Zr (C, amorphous carbon from phenolic resin).

temperature so that ZrC might be completely consumed in the reaction. The excess-Al composition (composition O) with amorphous carbon from phenolic resin was fired in vacuum at 1300–1600 °C to determine the effect of excess Al on reaction temperature.

As shown in Fig. 9, although the main phase after firing was $AlZrC_2$, Al_3Zr alloy was found after firing at 1300 °C. Residual ZrC was found after firing up to 1500 °C, and $Zr_2Al_3C_5$ was found from 1500 °C. Moreover, fracture surface of samples fired at 1500 °C revealed an inhomogeneous color pattern inside the sample, suggesting that the reaction between the starting materials was incomplete. Thus, excess Al in the Al–ZrC–C mixture facilitates $Zr_2Al_3C_5$ formation at lower temperatures. These results indicate that the optimal temperature for a complete reaction of the mixture (i.e., one in which ZrC is completely reacted) is 1600 °C.

3.6. Graphitization

Composition Q, which lies between composition lines H–E–I–J–K and L–M–N–O, was selected because it gave only trace amounts of residual ZrC and lowest amount of $Zr_2Al_3C_5$ after firing at 1600 °C for 1 h in vacuum. Mixtures of composition Q with amorphous carbon from phenolic resin and from sugar were fired in vacuum at 1600 °C for 1 h. As shown in Fig. 10, the sample with amorphous carbon from sugar gave $AlZrC_2$ with a least amount of $Zr_2Al_3C_5$. The fracture surface of Al–ZrC–amorphous carbon from sugar with composition Q heated in vacuum at 1600 °C for 1 h (Fig. 11), exhibited hexagonal platelets of $AlZrC_2$. The true density of powder obtained from this sample using kerosene as medium is 4.91 g/cm^3.

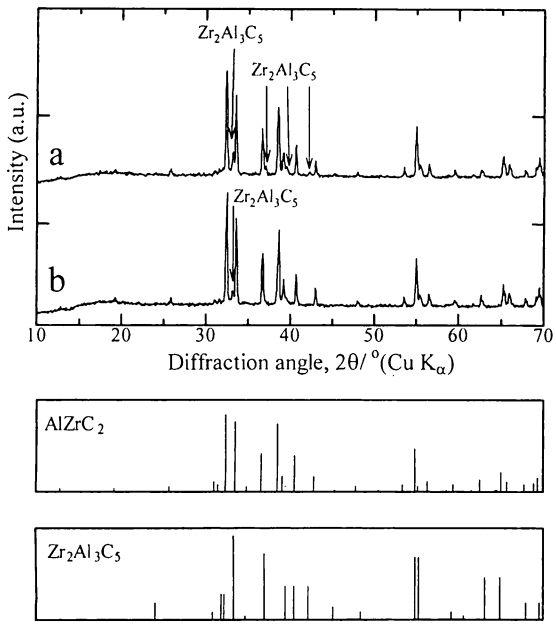

Fig. 10. XRD patterns of composition Q (Al:ZrC:C = 21:14:15) after firing at 1600 °C in vacuum for 1 h compared with ideal XRD pattern of $AlZrC_2$ and $Zr_2Al_3C_5$; with amorphous carbon from (a) phenolic resin and (b) sugar.

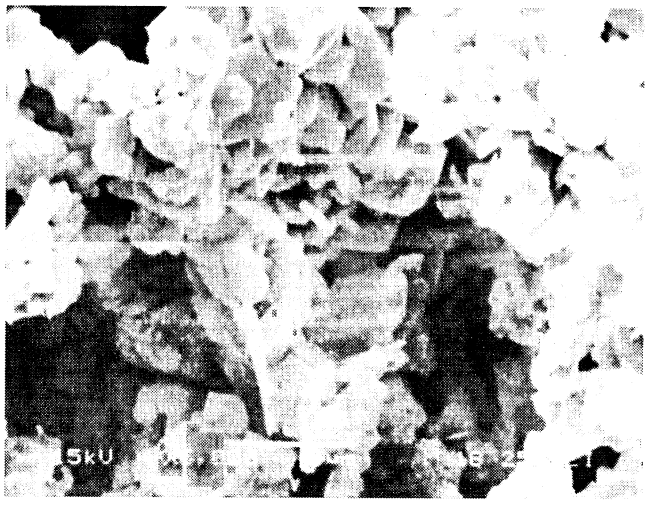

Fig. 11. Fracture surface of pellet of composition Q containing amorphous carbon from sugar after heating in vacuum at 1600 °C for 1 h.

The results presented in Section 3.2 indicate that the phase formation of $AlZrC_2$ and $Zr_2Al_3C_5$ formed in the sample after firing depends on the carbon phase in the starting material. Glassy carbon can transform to a crystalline phase (graphite) at high temperature, so-called graphitization [17]. Graphitization of glassy carbon has been performed at high temperatures and high pressure [18], but the graphitization of glassy carbon in vacuum remains unproven. Thus, we performed a small test to confirm the graphitization of glassy carbons as starting materials. Glassy carbon powder from phenolic resin and glassy carbon powder from sugar were wrapped with clean carbon paper and fired in vacuum at 1600 °C for 1 h, i.e., under the same firing conditions used for our samples.

As evidenced by the high-intense peak in Fig. 12, graphitization occurred in amorphous carbon from phenolic resin while amorphous carbon from sugar showed a lower degree of graphitization. Thus, a small amount of $Zr_2Al_3C_5$ formed spontaneously, and a sample with amorphous carbon from sugar yielded $AlZrC_2$ with less $Zr_2Al_3C_5$ compared with the sample with amorphous carbon from phenolic resin. In general, graphitization is an important step in the manufacture of carbon/carbon composite [17,19]. At this stage, carbon/carbon composites are heated up and disordered carbon transforms into well-ordered graphite structure. Although we prepared amorphous carbon from phenolic resin and sugar by heating in oxidizing atmosphere, a certain amount of organic functional group presumably remained as significant (ppm-level) impurities. Phenolic resin is viscous, high-molecular-weight hydrocarbon. There might be some functional groups left in amorphous carbon after heating phenolic resin at higher amount than heating sugar, which is lower molecular weight. There is a similar phase transformation in the silica glass, i.e., devitrification [20]. The significant amount of impurities in the glassy phase behaves as a mineralizer and initiate crystallization. Thus,

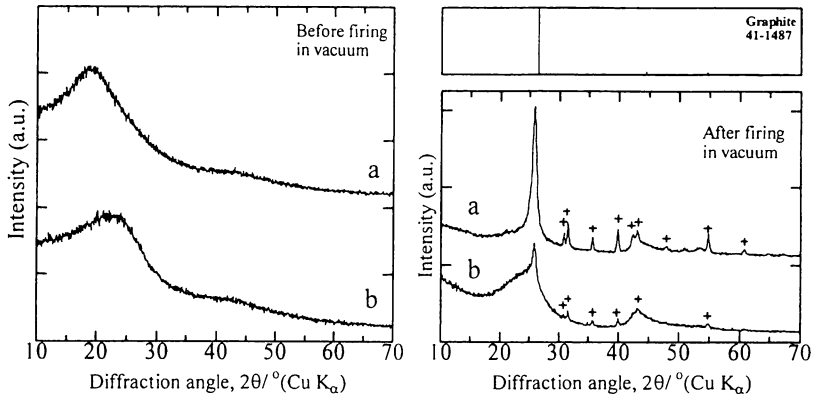

Fig. 12. Phase change of amorphous carbon before and after firing in vacuum at 1600 °C for 1 h; amorphous carbon from (a) phenolic resin and (b) sugar; (+) Al_4C_3.

the graphitization of glassy carbon observed in this study resembles the devitrification in silica glass.

There are some foreign peaks in the XRD patterns of both amorphous carbon powders; they correspond to Al_4C_3. Although the amorphous carbon powders were wrapped with carbon paper, the samples still had to be placed in a small carbon crucible before being loaded into the carbon crucible of the vacuum furnace. Since all of firing tests were done in the same small crucible, Al_4C_3 from the reaction between Al vapor and the crucible may have accumulated on the inner surface of the crucible. Under vacuum, Al_4C_3 evaporated from the crucible surface at high temperature and diffused through the slit in the wrapping. Some of our results (not presented here) indicated that Al_4C_3 has some relation to $AlZrC_2$ and $Zr_2Al_3C_5$ formation. Therefore, Al_4C_3 as impurity during firing the samples does not have negative effect on Al–Zr–C compound formation.

Studies on graphitization of glassy carbon have generally been conducted without presence of other additives. In this work, however, there were other starting materials (Al and ZrC). Therefore, the graphitization of the amorphous carbon in our samples during heating was presumably stronger than graphitization of pure amorphous carbon powder because the other starting materials acted as mineralizer, reducing the graphitization temperature of the amorphous carbon, and hence, accelerating the graphitization process.

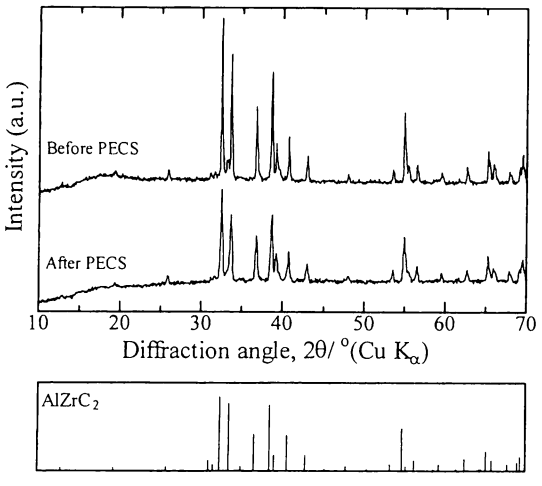

Fig. 13. XRD pattern of compact (composition Q) after sintering by PECS at 1700 °C and 40 MPa in vacuum without soaking.

3.7. *Effect of pressure*

We incidentally found that high purity $AlZrC_2$ from composition Q (with amorphous carbon from sugar as source of carbon) shows only $AlZrC_2$ phase after a 5-min reheat under pressure with electric current by PECS [21]. Therefore, we prepared the mixture of composition Q from Al, ZrC and amorphous carbon from sugar, and heated it at 1600 °C in vacuum for 1 h. Subsequently, we ground it into a fine powder, heated it in PECS under high pressure (40 MPa) in vacuum from room temperature to 1700 °C, and then suddenly stopped. No $Zr_2Al_3C_5$ phase was found, as shown in Fig. 13. The pressure during sintering under PECS may suppress the formation of the $Zr_2Al_3C_5$ phase and rearrange the atomic packing. The effect of pressure on $Zr_2Al_3C_5$ after sintering by PECS [22] also showed the same phenomena.

4. Conclusions

1. The atomic arrangement of carbon in the starting materials affects the Al–Zr–C compound formation.
2. Excess Al does not accelerate the reaction between ZrC and other starting materials.
3. Graphitization of glassy carbon occurs spontaneously as it reacts with the other starting materials at high temperature and affects the Al–Zr–C compound formation.
4. $AlZrC_2$ can be prepared from a mixture of Al, ZrC, and amorphous carbon from sugar at a mol ratio of 21:14:15 by firing the mixture in vacuum at 1600 °C for 1 h and grinding the product into a fine powder, then reheating this powder up to 1700 °C under high pressure and applied electric current.

Acknowledgement

We thank the Royal Thai Government for providing a scholarship to the first author to pursue her Ph.D. studies at the Nagoya Institute of Technology under the OECF–Thailand Japan Technology Transfer Project (TJTTP–OECF) of Chulalongkorn University, Thailand.

References

[1] R.H. Jones, L. Giancarli, A. Hasegawa, Y. Katoh, A. Kohyama, B. Riccardi, L.L. Snead, W.J. Weber, Promise and challenges of SiC_f/SiC composites for fusion energy application, J. Nucl. Mater. 307–311 (2002) 1057–1072.

[2] J.C. Viala, J. Bouix, G. Gonzalez, C. Esnouf, Chemical reactivity of aluminium with boron carbide, J. Mater. Sci. 32 (1997) 4559–4573.

[3] S. Shimada, T. Ishii, Oxidation kinetics of zirconium carbide at relatively low temperatures, J. Am. Ceram. Soc. 73 (10) (1990) 2804–2808.

[4] T. Wang, A. Yamaguchi, Antioxidation behavior and effect of $Al_8B_4C_7$ added to carbon-containing refractories, J. Ceram. Soc. Jpn. 108 (9) (2000) 818–822.

[5] J.C. Schuster, H. Nowotny, Investigations of the ternary systems (Zr, Hf, Nb, Ta)–Al–C and studies on complex carbides, Z. Metallkd. 71 (6) (1989) 341–346.

[6] S. Hashimoto, A. Yamaguchi, M. Yasuda, Fabrication and properties of novel composites in the system Al–Zr–C, J. Mater. Sci. 33 (1998) 4835–4842.

[7] U. Leela-adisorn, A. Yamaguchi, Synthesis of $Zr_2Al_3C_5$ material, Key Eng. Mater. 280–283 (2005) 1379–1384.

[8] C. Hammond, The Basics of Crystallography and Diffraction, second ed., Oxford University Press, New York, 2001, pp. 33–37.

[9] A.F. Wells, Structural Inorganic Chemistry, fifth ed., Oxford University Press, New York, 1993, pp. 950–951, 1320–1321.

[10] P.J. Durrant, B. Durrant, Introduction to Advanced Inorganic Chemistry, second ed., Longman, London, 1970, pp. 630–631.

[11] Uhlmann's Encyclopedia of Industrial Chemistry, vol. A19, fifth ed., VCH, Weinheim, 1986, p. 384.

[12] Materials science and technology, Glasses and Amorphous Materials, vol. 9, VCH, Weinheim, 1991, pp. 554–559.

[13] Uhlmann's Encyclopedia of Industrial Chemistry, vol. A5, fifth ed., VCH, Weinheim, 1986, p. 121.

[14] Uhlmann's Encyclopedia of Industrial Chemistry, vol. A5, fifth ed., VCH, Weinheim, 1986, pp. 140–141.

[15] H. Nowotny, P. Rogl, J.C. Schuster, Structural chemistry of complex carbides and related compounds, J. Solid State Chem. 44 (1982) 126–133.

[16] Th.M. Gesing, W. Jeitschko, The crystal structure of $Zr_3Al_3C_3$, $ScAl_3C_3$, and UAl_3C_3 and their relation to the structures of $U_2Al_3C_4$ and Al_4C_3, J. Solid State Chem. 140 (1998) 396–401.

[17] Uhlmann's Encyclopedia of Industrial Chemistry, vol. A5, second ed., VCH, Weinheim, 1986, p. 110.

[18] X. Wang, G.M. Zhang, Y.L. Zhang, F.Y. Li, R.C. Yu, C.Q. Jin, G.T. Zou, Graphitization of glassy carbon prepared under high temperatures and high pressures, Carbon 41 (2003) 188–191.

[19] E. Fitzer, L.M. Manocha, Carbon Reinforcements and Carbon/Carbon Composites, Springer Verlag, Berlin, 1998, pp. 34, 109.

[20] B.C. Schmidt, F.M. Holtz, J.-M. Bény, Incorporation of H_2 in vitreous silica, qualitative and quantitative determination from Raman and infrared spectroscopy, J. Non-Cryst. Solids 240 (1998) 91–103.

[21] U. Leela-adisorn, S.-M. Choi, N. Tera, T. Takeuchi, S. Hashimoto, S. Honda, H. Awaji, K. Hayakawa, A. Yamaguchi, Sintering and mechanical properties of $AlZrC_2$, J. Ceram. Soc. Jpn. 133 (2005) 188–190.

[22] U. Leela-adisorn, S.-M. Choi, S. Hashimoto, S. Honda, H. Awaji, K. Hayakawa, A. Yamaguchi, Sintering and characterization of $Zr_2Al_3C_5$ monolith, Key Eng. Mater., submitted for publication.

Key Engineering Materials Vols. 317-318 (August 2006) pp. 27-30
online at http://www.scientific.net
© 2006 Trans Tech Publications, Switzerland

Sintering and Characterization of $Zr_2Al_3C_5$ Monolith

U. Leela-adisorn[1,a], S-M. Choi[1,b], S. Hashimoto[1,c], S. Honda[1,d], and H. Awaji[1,e],

K. Hayakawa[2,f], A. Yamaguchi[3,g]

[1]Department of Materials Science and Engineering, Nagoya Institute of Technology, Gokiso-cho, Showa-ku, Nagoya 466-8555 Japan
[2]Japan Fine Ceramic Center, 2-4-1, Matsuno, Atsuta-ku, Nagoya 456-8587, Japan
[3]Okayama Ceramics Research Foundation Research Laboratory, 1406-18 Nishi Katakami, Bizen, Okayama 705-0021 Japan

[a]luraiwan@hotmail.com, [b]choism@zymail.mse.nitech.ac.jp, [c]hashimoto.shinobu@nitech.ac.jp, [d]honda@nitech.ac.jp, [e]awaji@mse.nitech.ac.jp, [f]ka.hayakawa@jfcc.or.jp, [g]yamaguchi@optic.or.jp

Keywords: $Zr_2Al_3C_5$, Pulse Electric Current Sintering (PECS), Complex carbide, Mechanical properties, Oxidation resistance, Hydration resistance

Abstract $Zr_2Al_3C_5$ has been successfully synthesized via solid state reaction between Al, ZrC and carbon powder at 1600℃ in vacuum. This complex carbide has very strong bond between metal atoms and carbon atoms. Thus, this material has a potential to be utilized as structural materials. Some properties of $Zr_2Al_3C_5$ powder from solid-state reaction in vacuum had been tested. It was found that this powder was completely oxidized in air at 900℃ 1 h, and can be hydrated in moist air. These drawbacks might come from the high reactivity of the powder due to synthesis in vacuum. $Zr_2Al_3C_5$ powder from solid state reaction in vacuum was sintered at various temperatures from 1500℃ to 2000℃ under vacuum with pulse electric current sintering (PECS) and pressureless sintering. $Zr_2Al_3C_5$ started to sinter at 1500℃ and got partially dense from 1700℃. Physical properties and mechanical properties of this material were investigated and discussed.

Introduction

Many research works have been studied on properties of carbides and complex carbides. But no research on properties of $Zr_2Al_3C_5$ though this phase was found in 1980 [1]. Schuster and Nowotny found that this phase was always coexist with ZrC. This phase was successfully synthesized as single phase by Leela-adisorn and Yamaguchi [2]. The purpose of this work is to sinter and characterize the properties of this complex carbides.

Experimental procedure

The starting material of Al, ZrC, and graphite powders were mixed throughly at mol ratio 3:1:1. Then the mixture was pressed and CIPed at 100 MPa as pellet before heating at 1600℃ in vacuum for 1 h [2]. After heating, the pellet was ground to fine powder. About 3 g of powder was sintered in vacuum without pressure and with pressure (PECS) under various times and temperatures. After sintering, the samples were characterized by XRD. The density of samples was tested by Archimedes' method in kerosene. The mechanical properties, i.e., fracture strength and Vickers' hardness were tested. The fracture surface of samples were observed by SEM. The oxidation test was done by heating small pieces of samples from room temperature to 1200℃ in air. The hydration resistance was estimated by measuring the weight gain of the samples in a humid chamber at 70°C, 90 R.H.

Results and discussion

The phase change of samples after sintering at various conditions was shown in Figs. 1 and 2. The samples sintered in vacuum without pressure were gradually changed from $Zr_2Al_3C_5$ to ZrC at longer soaking time or higher sintering temperature due to loss of some components during sintering. Though the samples sintered with PECS did not show phase change but their XRD patterns reached to ideal XRD pattern calculated by Schuster and Nowotny (JCPDS No. 41-0814). Since the pressure of synthesis was not specified by Schuster and Nowotny, we assume that these work was done at normal atmosphere. $Zr_2Al_3C_5$ in this work was prepared in vacuum. Therefore, our starting material is a defect structure of $Zr_2Al_3C_5$ occurred at vacuum. The structure of carbide get closed to the ideal structure under high pressure from PECS.

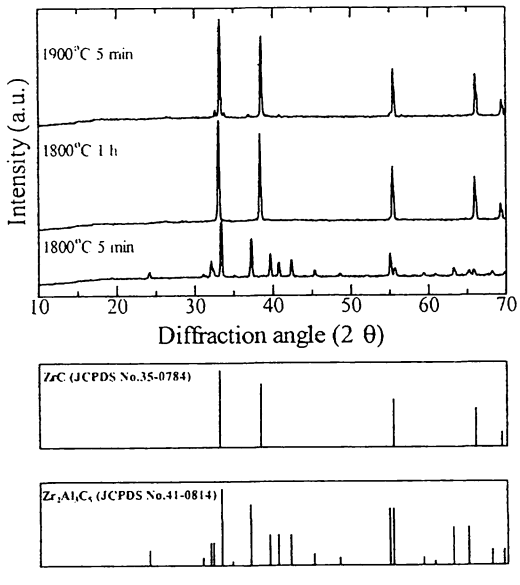

Fig. 1 Phase change of $Zr_2Al_3C_5$ after sinter by pressureless sintering in vacuum at different time and temperature.

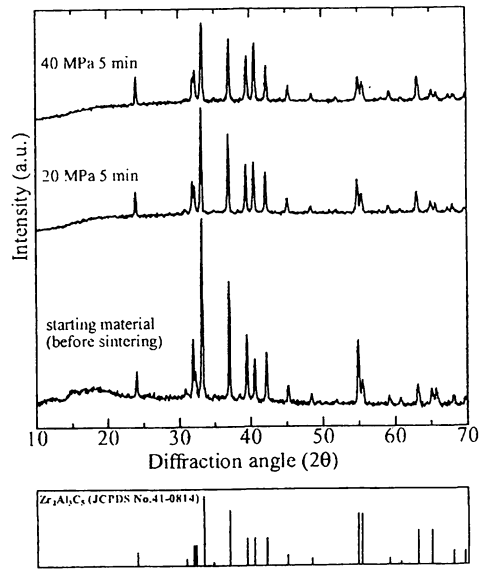

Fig. 2 XRD patterns of $Zr_2Al_3C_5$ after sinter at 1800°C under different pressures compared with starting material

The density of samples after sintering at the same temperature and the same soaking time under different pressures as shown in Table 1 confirmed our assumption, i.e., the density of this carbide increased as the pressure of sintering increased.

Table 1 Density of $Zr_2Al_3C_5$ before and after sinter at 1800℃ for 5 min under various conditions

Condition	Density (g/cm^3)
T. D. (JCPDS No. 41-0814)	4.983
$Zr_2Al_3C_5$ powder (as prepared)	4.49
Pressureless sintering in vacuum	2.42
20 MPa in vacuum (PECS)	3.92
40 MPa in vacuum (PECS)	4.45

The effects of sintering parameters on density of $Zr_2Al_3C_5$ monolith are shown in Fig. 3. This carbide can be sintered as dense monolith from 1800℃ under 20 MPa for 20 min and 40 MPa for 5 min. At 2000℃, the pressure and the soaking time had no effect on the density of monolith.

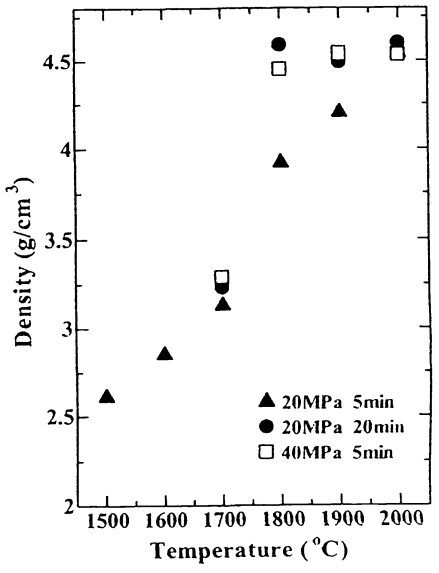

Fig. 3 Relationship between density and sintering conditions.

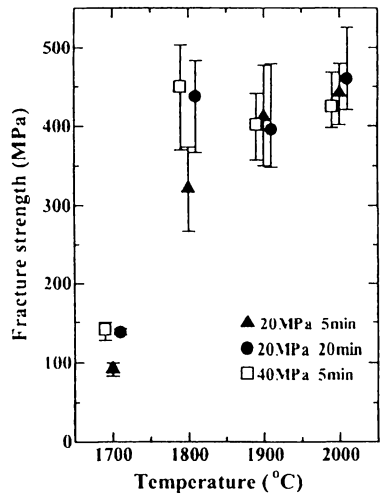

Fig. 4 Fracture strength of samples sintered at various conditions.

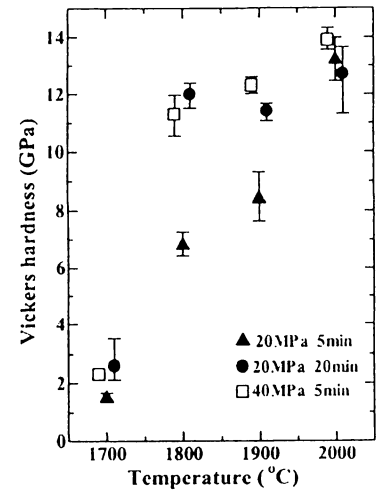

Fig. 5 Vickers hardness of samples sintered at various conditions.

Fracture strength and Vickers hardness of $Zr_2Al_3C_5$ monolith sintered by PECS under various parameters are illustrated in Figs. 4 and 5. At 1700℃ for all parameters, the monolith showed very poor strength and hardness. The fracture strength and hardness were improved by sintering at higher temperature and higher pressure. This can be seen from monolith sintered at 1800℃ at various sintering condition. At 2000℃ the fracture strength and hardness of monolith under different sintering time and pressure are similar. The mechanical properties and density of monolith were compared in Table 2.

Table 2 Several properties of samples after sinter by PECS method.

Sample	Bulk Density	Elastic Modulus	Shear Modulus	Poisson's ratio
	g/cm^3	GPa	GPa	-
1700°C 40M5m	3.969	234.0	98.1	0.191
1800°C 40M5m	4.390	340.4	142.1	0.198
1900°C 40M5m	4.558	361.8	150.9	0.199
2000°C 40M5m	4.580	368.1	157.9	0.165

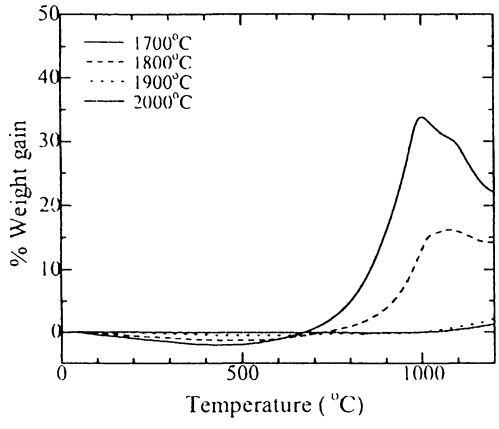

Fig. 6 Weight gain from oxidation of $Zr_2Al_3C_5$ after sintering at various temperatures by PECS under 20 MPa for 5 min

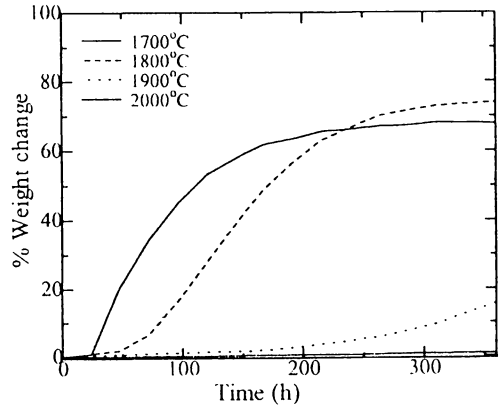

Fig. 7 Weight change from hydration of $Zr_2Al_3C_5$ sintered at various temperatures by PECS under 20 MPa for 5 min

The oxidation resistance of $Zr_2Al_3C_5$ monoliths was tested under DTA/TG (Fig. 6). The weight gain of monoliths after oxidation was compared and illustrated in Fig. 6. $Zr_2Al_3C_5$ after sintering by PECS at 1700℃ and 1800℃ under 20 MPa for 5 min show very poor oxidation resistance. The oxidation resistance of this carbide get improved by sinter at higher temperature. The small weight loss of samples sintered at 1700℃ and 1800℃ at the beginning of oxidation is due to the loss of moisture at the sample surface. The surface of sample is very easy to hydrated with moisture at ambient temperature. The result from hydration test in Fig.7 confirms this effect and shows the relation between oxidation resistance and hydration resistance of $Zr_2Al_3C_5$ monolith.

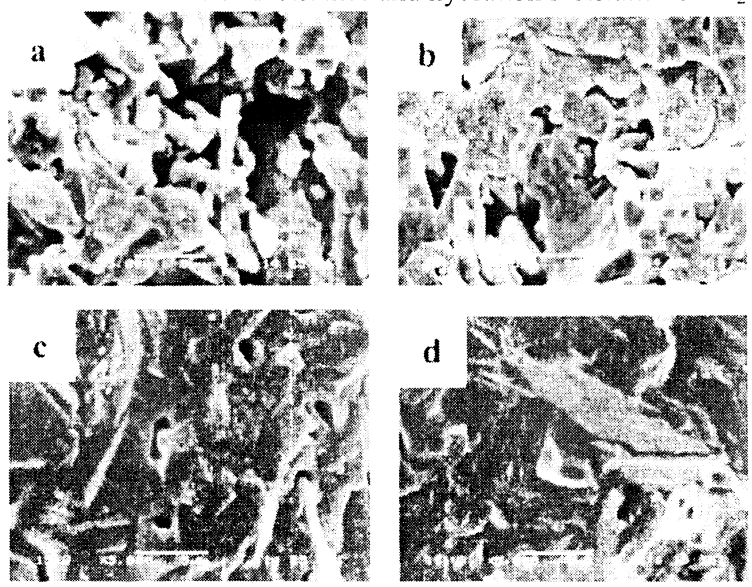

Fig. 8 Microstructure of $Zr_2Al_3C_5$ monolith sintered at various temperatures by PECS under 20 MPa for 5 min; a) 1700℃, b) 1800℃, c) 1900℃, and d) 2000℃

The microstructures of $Zr_2Al_3C_5$ monoliths shown in Fig. 8 indicate the porous structure of samples sinter at 1700℃ and 1800℃ as well as the dense structure of samples sintered at 1900℃ and 2000℃, which confirmed the relation with other properties of monolith and sintering condition.

Summary

The sintering condition had effects on the properties of $Zr_2Al_3C_5$ monolith. The dense $Zr_2Al_3C_5$ monolith with good mechanical properties and better oxidation resistance as well as good hydration resistance were prepared by sintering at 2000℃ under 20 MPa and 40 MPa.

Acknowledgement

The authors thank the Royal Thai Government for providing a scholarship to the first author to pursue her PhD. studies at Nagoya Institute of Technology under the TJTTP-OECF of Chulalongkorn University, Thailand.

References

[1] J.C. Schuster and H. Nowotny, Z. Metallkde., 71[6], 341-346 (1980).

[2] U. Leela-adisorn and A. Yamaguchi, Key Engineering Materials (Proceedings of the Third China International Conference on High-Performance Ceramics (CICC-3) 2004), Vols. 280-283, 1379-1384 (2005).

「材料」(Journal of the Society of Materials Science, Japan), Vol. 55, No. 7, pp. 670-674, July 2006
論　文

リン酸塩結合材を用いたパッチング耐火物の作業性（可塑性）の低下機構†

崎田真一*　山本祐一**　難波徳郎**
三浦嘉也***　林　徹浩****　山口明良*****

Hardening Mechanism of Refractory Patching Materials with Phosphate Binder

by

Shinichi SAKIDA*, Yuichi YAMAMOTO**, Tokuro NANBA**, Yoshinari MIURA***,
Tetsuhiro HAYASHI**** and Akira YAMAGUCHI*****

The hardening mechanism of refractory patching materials with a phosphate binder was investigated by means of ^{31}P static and magic angle spinning (MAS) nuclear magnetic resonance (NMR) spectroscopy. Ten refractory patching materials were made of refractory powders of SiO_2 and fused alumina and five mixed solutions of phosphoric acid and aluminum biphosphate as phosphate binders. ^{31}P static and MAS NMR spectra were measured of five phosphate binders and twenty soft and hard refractory patching materials, respectively, to reveal the local structure around P atoms. The ^{31}P static and MAS NMR spectra revealed that PO_4 tetrahedra in the phosphate binders have no P–O–P linkage between PO_4 tetrahedra and that as the patching materials become hard, the ratio of PO_4 tetrahedra with bridging oxygens increases, respectively. This result suggests that the hardening of the patching materials is caused by the condensation of the phosphate binder. But the ratio of PO_4 tetrahedra with bridging oxygens was not enough to form the network by P–O–P linkage between PO_4 tetrahedra. On the basis of these results, the hardening mechanism of refractory patching materials with a phosphate binder is proposed.

Key words : Refractory patching material, Phosphate binder, SiO_2, Fused alumina, ^{31}P MAS NMR spectroscopy, Local structure, Hardening mechanism

1　緒　　言

大量生産，大量消費，大量廃棄の仕組みの中で，狭い国土での高効率な土地活用および，最終処分場の延命化が求められている日本にとって，一般廃棄物の社会的コンセンサスを得ている処理方式は「焼却し，埋め立てる」方法である．日本の一般廃棄物の量は，年間約5000万トンであり，そのうち80%弱を焼却に頼っている.[1)]

焼却処理に使用される焼却炉の材料としては大きく分けて，耐火レンガなどの定形耐火物と，キャスタブル材，プラスチック材などの不定形耐火物の二種類がある．不定形耐火物は「粒状または練土状の耐火物」とJISで定義されており，耐スポーリング性（耐火物の亀裂や剥離による損傷への耐性）・気密性・低熱伝導性・緊急修理などへの適応性，複雑異型で多種少量の煉瓦使用の場合の置きかえ，損傷の激しい部分への熱間補修による炉の延命など優れた機能を持つ．

パッチング材は，プラスチック材に属する柔らかい練り土状の不定形耐火物であり，耐火性の高い原料とバインダー（結合材）とを水で練り合わせて作製する．現在，ダイオキシン対策用高温溶融炉など高温溶解型産業で使用される炉の補修材として主に使われている．中でも，リン酸塩系のバインダーを用いたパッチング材は，耐火粘土を結合材とした材料に比べて冷間・熱間での強度に優れ，耐摩耗性に優れている．また，冷間・熱間で既存炉壁への吸着性が良いなどの特徴があるので広く利用されている.[2)~4)]

しかし製造後，密封保存しても時間が経過するにつれて作業性（可塑性）の低下により硬化する性質がある．しかも，硬化速度が比較的速いため長期間の保存には耐えられないのが現状である．硬化すると作業性が非常に悪くなるのみならず，製造段階より数倍硬くなり使用困難になる場合すらある．従って，硬化速度を今まで以上に抑制することにより長期間保存を可能にするような硬化速度の制御技術の確立が現在必要とされている．

そこで本研究では硬化速度の制御の前段階として，まずリン酸塩結合材を用いたパッチング材中のリン原子の

†　原稿受理　平成17年10月5日　Received Oct. 5, 2005
*　岡山大学保健環境センター　〒700-8530　岡山市津島中，Health and Environment Center, Okayama Univ., Tsushima-Naka, Okayama, 700-8530
**　岡山大学環境理工学部環境物質工学科　〒700-8530　岡山市津島中，Dept. of Environmental Chemistry and Materials, Faculty of Environmental Sci. and Tech., Okayama Univ., Tsushima-Naka, Okayama, 700-8530
***　正会員　岡山大学環境理工学部環境物質工学科　〒700-8530　岡山市津島中，Dept. of Environmental Chemistry and Materials, Faculty of Environmental Sci. and Tech., Okayama Univ., Tsushima-Naka, Okayama, 700-8530
****　林ロザイ㈱　〒709-0223　備前市吉永町南方，Hayashi Rozai Co., Ltd., Yoshinaga-cho, Bizen, 709-0223
*****　岡山セラミックス技術振興財団　〒705-0021　備前市西片上，Okayama Ceramics Res. Foundation, Nishikatakami, Bizen, 705-0021

局所構造を^{31}Pマジック角回転 (MAS) 核磁気共鳴 (NMR) 分光法を用いてパッチング材の作業性（可塑性）の低下機構の解明を試みた．

2 実験方法

2・1 パッチング材の作製

リン酸塩結合材を用いたパッチング材の耐火性の原料には，電融アルミナ，ムライト，ベントナイト，焼ロー石，バン土頁岩などがあり，いずれも主成分はSiO_2とAl_2O_3（アルミナ）である.[5),6)]そこで今回は代表的な原料の主成分であるSiO_2とAl_2O_3としてSiO_2試薬 (quartz) および電融アルミナ粉末をそれぞれ原料として使用した．

バインダーにはリン酸75%水溶液と重リン酸アルミニウム50%水溶液の混合溶液を選んだ．その混合割合をリン酸100，75，50，25，0vol%とした5種類の溶液をバインダーとして使用した．

パッチング材は，各原料粉末3gに各混合割合のバインダーを加えて混合，混練することにより作製した．バインダーの使用量はSiO_2で1.5ml，電融アルミナで0.5mlであった．パッチング材の作業性（可塑性）の低下の原因として(1) 骨材，骨材中にある石灰，マグネシア，アルカリなどの不純物との反応，(2) 用水の揮散による可塑性の変化，が挙げられる.[3),4)]しかし，本研究で用いたSiO_2試薬は純度99.9%，電融アルミナは白色でいずれも高純度なので,[6)]不純物の影響は無視できると考えた．ビニール袋で密封されたパッチング材は，硬化するときに袋の内側に水滴がつく現象が見られた．この事から，パッチング材の硬化はパッチング材から水分が蒸発する事が原因と考え，110℃の乾燥機で完全に硬化させたパッチング材を作製した．

2・2 ^{31}P静止およびMAS NMR測定

パッチング材中のリン原子周辺の局所構造を明らかにするために，5種類のバインダー溶液，作製後約12h経過した練り土状の柔らかいパッチング材と110℃の乾燥機でパッチング材を完全に硬化させた後粉末状にした試料について，^{31}P静止およびMAS NMR測定を行った．測定装置はVarian UNITY INOVA 300 MAS FT-NMRスペクトロメーター (7.05T) を使用した．測定条件は共鳴周波数121.425MHz，MAS NMR測定時の回転速度は5500～6500Hzとし，標準試料として$NH_4H_2PO_4$を用いた．パルス幅2.0μs，繰り返し時間2.0s，バインダー液は80回，パッチング材は400～1000回の積算回数で測定を行った．

柔らかい練り土状のパッチング材は，MAS NMR測定時，高速回転による遠心力のため，試料中の水分がいくらか失われた状態になっていた．しかし，完全に乾燥したわけではなく，試料の中に水分がいくらか残っている状態であった．また，作製直後ほどではないが，練り土状の柔らかさを保っていた．よって今回得られたスペクトルは，作製直後の水分が豊富な時の状態を反映しているわけではないが，水分を含んだ柔らかい練り土状のパッチング材の状態を反映しているといえる．

3 結果と考察

3・1 リン酸 (H_3PO_4) および重リン酸アルミニウム ($Al(H_2PO_4)_3$) 中のリン原子の基本構造

リン酸および重リン酸アルミニウム中のリン原子は酸素四配位であり，PO_4四面体から成っている．一般的にPO_4四面体の基本構造は架橋酸素の数によって分類し，架橋酸素数nの基本構造をQ_nと表記する．リン酸中のPO_4四面体は，リン原子と結合した4つの酸素のうち1つが二重結合酸素，残り3つが一重結合酸素でさらに水素と結合した$O=P(-O-H)_3$という構造をしており，この四面体は脱水縮合により-P-O-P-連結の形成が可能である．従って，リン酸中のPO_4四面体の基本構造は架橋酸素の数によって，Q_0，Q_1，Q_2，Q_3の4種類に分類できる．Fig. 1 (a) にその基本構造Q_0～Q_3を示す．図中のBOは2個のリン原子と結合し-P-O-P-連結を作る架橋酸素である．他方，NBOは1個のリン原子とのみ結合し-P-O-P-連結は作らない非架橋酸素を示している．DBOは二重結合酸素である．PO_4四面体によるネットワーク形成が可能な構造は，架橋酸素数の多いQ_2，Q_3である．

重リン酸アルミニウム結晶[7)]はPO_4四面体とAlO_6八面体とが交互に頂点共有で連結することで直鎖を形成し，その直鎖間はP-OH基間の水素結合で互いに連結した構造をしている．この結晶は非常に吸湿性が強いため，大気中では普通水を含んだ形で存在する．従って，重リン酸アルミニウム中のPO_4四面体は，PO_4四面体の4つの酸素のうち2つが別々のAlO_6八面体と頂点共有して鎖を作るのに使われる (Fig. 1 (b))．よって，脱水縮合により-P-O-P-連結形成可能な酸素は2つである．また，このPO_4四面体はリン酸の場合とは異なり二重結合がないので，リン酸のPO_4四面体とは異なる結合状態をしていると考えられる．そこで，リン酸のPO_4四面体とは異なることを示すために，重リン酸アルミニウム中のPO_4四面体の基本構造をQ_n'と表記した．従って，重リン酸アルミニウム中のPO_4四面体の基本構造は架橋酸素数によってQ_0'，Q_1'，Q_2'の3種類に分類できる．Fig. 1 (b) にその基本構造Q_0'～Q_2'を示す．重リン酸アルミニウムの場合，元々PO_4四面体とAlO_6八面体とから成る直鎖によるネットワークがすでに形成されているが，架橋酸素数が増大するにつれてより複雑に絡み合ったネットワーク形成が可能となる．

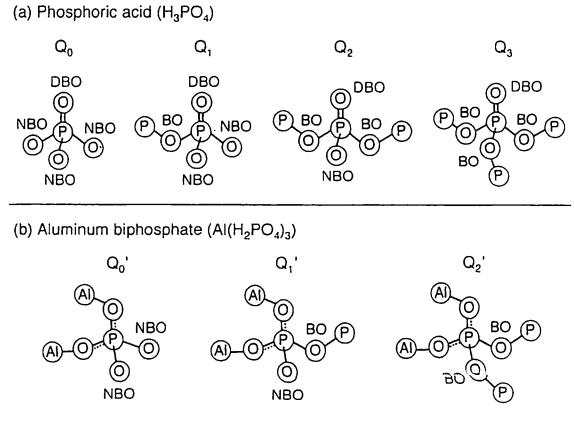

Fig. 1 Basic structures of PO_4 tetrahedra in phosphoric acid (H_3PO_4) (a) and aluminum biphosphate ($Al(H_2PO_4)_3$) (b).

3・2 ^{31}P NMR における PO_4 四面体の基本構造と等方性化学シフトとの関係

Table 1 に PO_4 四面体の基本構造と等方性化学シフト δ (ppm) との関係を示す．Q_n (n = 0 ～ 3)，Q_n' (n = 0 ～ 2) のいずれも架橋酸素数が増加するにつれて，等方性化学シフト値は小さくなっている．Q_n (n = 0 ～ 3) および Q_0' と Q_2'の等方性化学シフト範囲についてはすでに明らかにされているが，[3)～10)] Q_1'の範囲については未だ明らかにされていない．しかし上で述べたように，架橋酸素数の増加とともに等方性化学シフト値が小さくなる傾向があるので，Q_1'の範囲は Q_0'と Q_2'の間にくるものと考えられる．従って，Q_1'の範囲を-15 ～-30ppm と考えて考察を行った．この関係に基づいて，本研究で測定した試料の ^{31}P NMR スペクトルピークの帰属を行った．

3・3 バインダー溶液の ^{31}P 静止 NMR スペクトル

Fig. 2 は，5 種類のバインダー溶液の ^{31}P 静止 NMR スペクトルを示している．図中の数値は等方性化学シフト値を示している．一番上のスペクトルがリン酸 75% 水溶液のみのものであり，下にいくにつれて重リン酸アルミニウム 50% 水溶液の割合が増大し，一番下が重リン酸アルミニウム 50% 水溶液のみのスペクトルである．いずれもシャープなピークが得られており，重リン酸アルミニウム溶液の割合が増大するにつれて，ピークが高磁場側 (右側) にシフトしていることが分かる．リン酸，重リン酸アルミニウム溶液の等方性化学シフト値は 0.1，-7.8ppm であり，これらはそれぞれ O=P(–O–H)$_3$，(Al–O)$_2$–P(–O–H)$_2$ 構造をしているので，それぞれ Q_0，Q_0'構造に帰属できる．

混合溶液のピークはリン酸，重リン酸アルミニウム溶液の間に出現している．このことは，バインダー溶液同士の混合だけではリン酸塩間での脱水縮合は起こらないことを示している．ピークの線幅は十分狭いので，混合溶液のピークはリン酸，重リン酸アルミニウムのそれぞれのピークが合成されてできたピークではなく，リン酸，重リン酸アルミニウムが液中で十分に混ざり合って一本のシャープなピークになっていると考えられる．

Table 1　Isotropic chemical shift ranges of basic structures Q_n and Q_n' of PO_4 tetrahedra in phosphoric acid (H_3PO_4) and aluminum biphosphate ($Al(H_2PO_4)_3$), respectively. Symbol n in Q_n and Q_n' denotes the number of bridging oxygen.

H_3PO_4		$Al(H_2PO_4)_3$	
Q_n	δ (ppm)	Q_n'	δ / ppm
Q_0	+14 ～ -6 [6)]	Q_0'	-15 [7)]
Q_1	4 ～ -22 [6)]	Q_1'	-15 ～ -30 *
Q_2	-16 ～ -27 [6)]	Q_2'	-30 ～ -52 [7), 8)]
Q_3	-32 ～ -46 [6)]		

* Estimated range as the isotropic chemical shift range between Q_0' and Q_2'. The isotropic chemical shift range of Q_1' has not been reported so far.

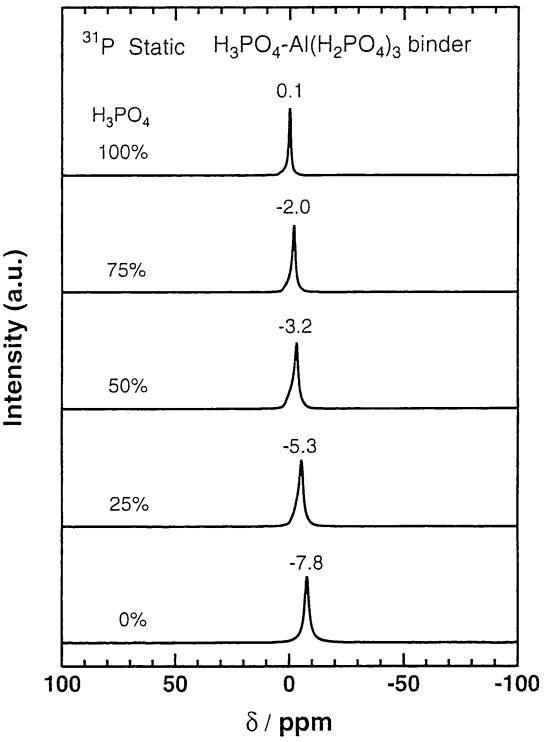

Fig. 2　^{31}P static NMR spectra of five phosphate binders composed of mixed solutions of phosphoric acid and aluminum biphosphate.

3・4 パッチング材の ^{31}P MAS NMR スペクトル

Fig. 3 は SiO_2 原料のパッチング材の ^{31}P MAS NMR スペクトルを示している．左図が柔らかい練り土状のパッチング材，右図が完全に硬化したパッチング材の ^{31}P MAS NMR スペクトルを示している．図中の数値はピーク位置，* 印はスピニングサイドバンドを表している．一番上のスペクトルがリン酸 75% 水溶液のみのものであり，下にいくにつれて重リン酸アルミニウム 50% 水溶液の割合が増大し，一番下が重リン酸アルミニウム 50% 水溶液のみのスペクトルである．Table 1 に基づいて各ピークの帰属を行った．また，リン酸 75，50，25vol% のバインダー溶液の各ピークの帰属に関しては，Table 1 の他に各ピークの強度比，バインダー溶液の体積比，リン酸 100，0vol% でのピーク位置も考慮した．その結果得られた各ピークに帰属できる PO_4 四面体の基本構造を図中に示した．

左図のピークは 0.1 ～-11.7ppm の範囲で現れており，Fig. 2 の等方性化学シフト値に近いことから，水分をいくらか含む柔らかい練り土状のパッチング材中のリンは Q_0，Q_0'構造に帰属でき，リン酸塩間の縮合は起こっていないと考えられる．

右図では，リン酸を 50 ～ 100vol% 含むバインダーで 0ppm 付近の鋭いピークと-13ppm 付近の小さいピークが現れた．リン酸を 25vol% 含むバインダーでは，-0.8ppm の鋭いピークの他に-15.8ppm と-31.1ppm にピークが出現した．また，重リン酸アルミニウム溶液では-15.3ppm のブロードな 1 本のピークが得られた．

いずれのバインダー溶液でも，パッチング材の硬化とともに Q_0，Q_0'構造のみから Q_1，Q_1'構造が現れているの

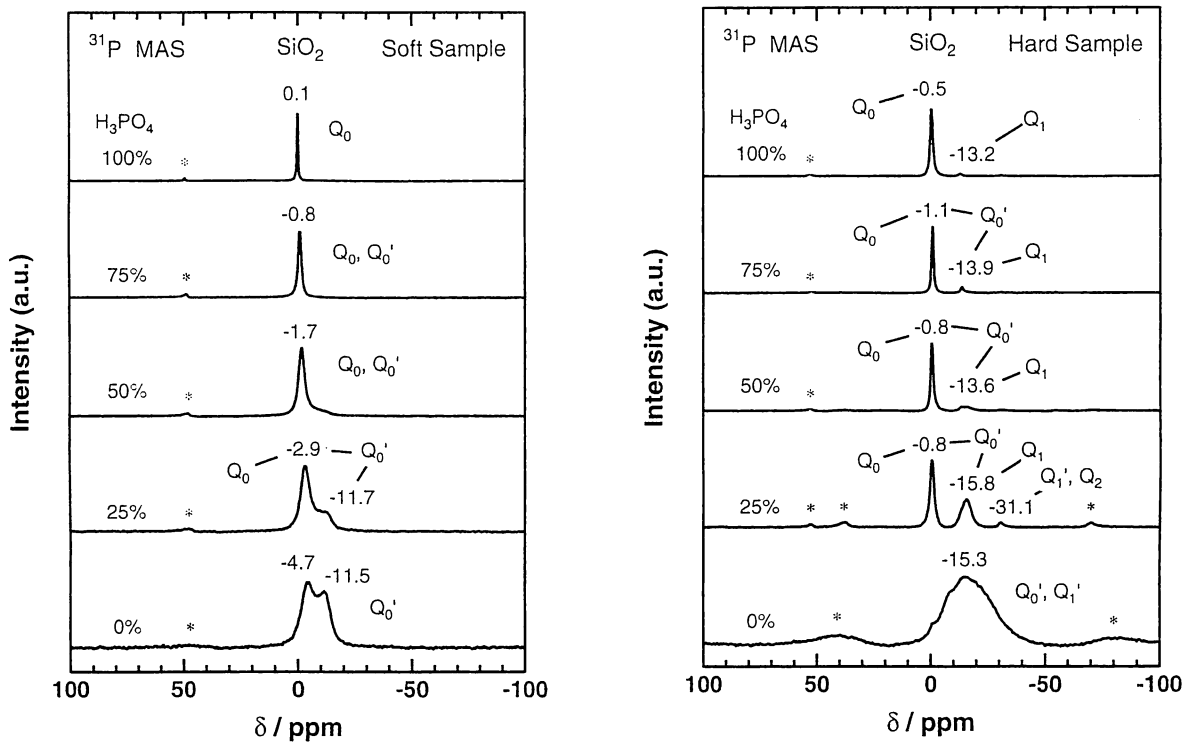

Fig. 3　^{31}P MAS NMR spectra of soft (left) and hard (right) refractory patching materials made by SiO_2. Asterisks denote spinning side bands.

で，パッチング材が硬化するにつれて，架橋酸素をもつリン原子の割合が増加していることが分かる．このことは，パッチング材の硬化により脱水縮合が起こっていることを示している．しかし硬化したパッチング材では，いずれもネットワーク形成能をもたない Q_0，Q_1 構造またはネットワーク形成能に乏しい Q_0'構造が主であり，比較的高いネットワーク形成能をもつ Q_1'，Q_2 構造は少数であった．

Fig. 4 は電融アルミナ原料のパッチング材の ^{31}P MAS NMR スペクトルを示している．左図が柔らかい練り土状のパッチング材，右図が完全に硬化したパッチング材の ^{31}P MAS NMR スペクトルを示している．

左図のピークは 1.6 ～−11.7ppm の範囲で現れているので，水分をいくらか含む柔らかい練り土状のパッチング材中のリンは Q_0，Q_0'構造に帰属でき，SiO_2 の場合と同様にリン酸塩間の縮合は起こっていないと考えられる．

右図では，リン酸を 50 ～ 100vol% 含むバインダーで −16ppm 付近の鋭いピークが現れた．リン酸を 25vol% 含むバインダーでは，−15.9ppm と −21.3ppm にピークが出現した．また，重リン酸アルミニウム溶液では−18.6ppm のブロードな 1 本のピークが得られた．

いずれのバインダー溶液でも，SiO_2 の場合と同様にパッチング材の硬化とともに Q_0，Q_0'構造のみから Q_1，Q_1'構造が現れた．従って，パッチング材の硬化により，架橋酸素をもつリン原子の割合が増加し，脱水縮合が起こったと考えられる．硬化したパッチング材のうち，リン酸を 0 ～ 25vol% 含むバインダーでは，Q_1'構造が増加してきているが，いずれもネットワーク形成能をもたない Q_1 構造とネットワーク形成能に乏しい Q_0'構造が主であった．

Fig. 3 と Fig. 4 の硬化した試料のスペクトル同士を比較すると，リン酸を 25 ～ 100vol% 含むバインダーでは，SiO_2 原料の硬化したパッチング材で見られた 0ppm 付近の鋭いピークが，電融アルミナ原料の硬化したパッチング材では消えていた．また，Q_1，Q_1'，Q_2 構造に帰属できる−13 ～−31ppm のピーク強度は，電融アルミナ原料の方が，SiO_2 原料よりも高かった．Q_0'，Q_1'構造を含む重リン酸アルミニウム溶液のピーク位置は，電融アルミナ原料の方が，SiO_2 原料よりも高磁場側（右側）にあった．以上の結果より，同じバインダー溶液における脱水縮合したリン原子の割合は，電融アルミナ原料の方が SiO_2 原料よりも高いといえる．

3・5　パッチング材の作業性(可塑性)の低下機構

パッチング材の ^{31}P MAS NMR 測定結果から，パッチング材の作業性（可塑性）の低下に伴う硬化によりリン酸塩の一部が脱水縮合していることを明らかにした．しかし，パッチング材中のリン原子はいずれもネットワークを形成しない Q_0，Q_1 構造とネットワーク形成能に乏しい Q_0'構造が主であり，比較的高いネットワーク形成能をもつ Q_1'，Q_2 構造は少数であった．つまり，脱水縮合による−P−O−P−連結によって形成されるネットワークの割合は小さいと考えられるので，リン酸塩の脱水縮合によるネットワーク化のみで硬化するとは考えにくい．しかし実際には硬化している．これは，パッチング材の硬化に影響を及ぼす別の原因が存在することを示唆している．

リン酸結晶[11]は無水和物のとき無色の結晶であり，非常に吸湿性が強い．この結晶は PO_4 四面体の OH 基同士がすべて水素結合で連結した層状構造を作っている．上で述べたように，無水の重リン酸アルミニウム結晶[5]も PO_4 四面体と AlO_6 八面体とから成る直鎖間は P−OH 基間の水素結合で互いに連結した構造をしている．本研究

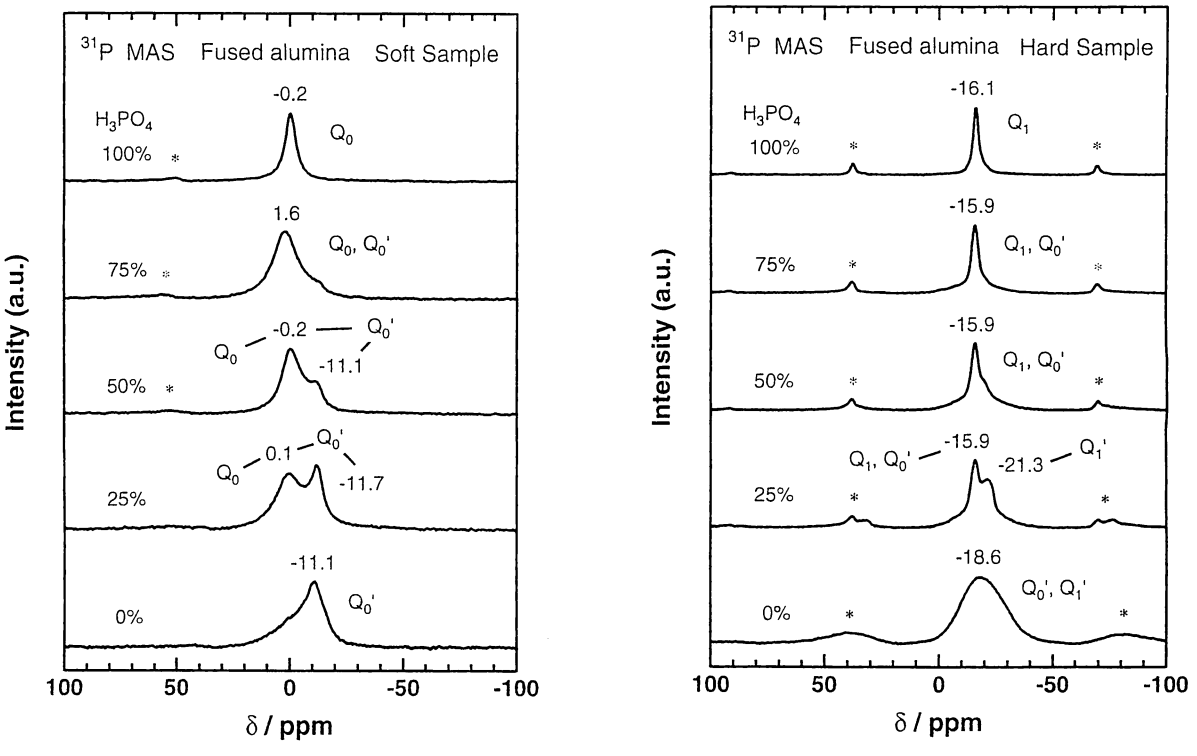

Fig. 4　^{31}P MAS NMR spectra of soft (left) and hard (right) refractory patching materials made by fused alumina. Asterisks denote spinning side bands.

におけるパッチング材は上記のリン酸（塩）を使用しているので，無水状態では上の２つの結晶と類似の連結が存在すると考えられる．即ち，パッチング材中の水分の蒸発に伴うリン酸（塩）同士の水素結合による連結が生じると考えられる．

以上より，水分の減少によって引き起こされる水素結合と脱水縮合が，パッチング材の作業性（可塑性）の低下の原因と考えられる．

4　結　　論

リン酸および重リン酸アルミニウム水溶液の混合溶液から成るバインダー溶液，SiO_2 および電融アルミナ粉末とリン酸塩バインダーから作製したパッチング材の乾燥前，乾燥後の試料について ^{31}P 静止および MAS NMR 測定を行い，パッチング材中のリン原子の局所構造を明らかにすることでパッチング材の作業性（可塑性）の低下機構の解明を試みた結果，次の結論を得た．

(1)　硬化後の試料は硬化前の試料に比べて脱水縮合したリン原子の割合は多くなったが，ネットワークを作らない Q_0，Q_1 構造とネットワーク形成能に乏しい Q_0'構造が主であり，比較的高いネットワーク形成能をもつ Q_1'，Q_2 構造をもつリン原子は少数であった．

(2)　同じバインダーを用いた場合，原料の種類によって脱水縮合したリン原子の割合が変化し，電融アルミナ材質の方が SiO_2 材質よりも脱水縮合したリン原子の割合が多かった．

(3)　パッチング材の作業性（可塑性）の低下の原因は，水分の減少によって引き起こされる水素結合によるリン酸塩間の連結ならびにリン酸（塩）同士の脱水縮合によるネットワークの形成と考えられる．

参　考　文　献

1) Haikibutsugakkai-Hen, "Haikibutsu handbook", pp.157-158 (1997) Ohmsha, Japan.

2) The Ceramic Society of Japan, "Handbook of ceramics" 2nd Edition, Ohyou, pp.844-846 (2002) Gihodoshuppan, Japan.

3) T. Taniguchi, "Aluminium phosphate bonded refractory specialities", Ceramics Japan, Vol.1, No.2, pp.66-71 (1966).

4) S. Nagahama and S. Yamamoto, "Aluminum-phosphate binders for refractories", Taikabutu, Vol.29, No.8, pp.412-425 (1977).

5) The Ceramic Society of Japan, "Handbook of ceramics" 2nd Edition, Ohyou, pp.44-47 (2002) Gihodoshuppan, Japan.

6) The Ceramic Society of Japan, "Handbook of ceramics" 2nd Edition, Ohyou, pp.784-788 (2002) Gihodoshuppan, Japan.

7) R. Kniep and M. Steffen, "Aluminium-tris (dihydrogenphosphat)", Angewandte Chemie, Vol.90, No.4, p.286 (1978).

8) M. W. G. Lockyer, D. Holland, A. P. Howes and R. Dupree, "Magic-angle spinning nuclear magnetic resonance study of the structure of some PbO-Al_2O_3-P_2O_5 glasses", Solid State Nuclear Magnetic Resonance, Vol.5, pp.23-34 (1995).

9) R. K. Brow, R. J. Kirkpatrick and G. L. Turner, "Local structure of $xAl_2O_3 \cdot (1-x)NaPO_3$ glasses : an NMR and XPS study", Journal of the American Ceramic Society, Vol.73, No.8, pp.2293-2300 (1990).

10) I. L. Mudrakovskii, V. P. Shmachkova, N. S. Kotsarenko and V. M. Mastikhin, "^{31}P NMR study of I-IV group polycrystalline phosphates", Journal of the Physics and Chemistry of Solids, Vol.47, No.4, pp.335-339 (1986).

11) M. Nakahara, "Mukikagoubutu · sakutaiziten", pp.1056-1057 (1997) Koudansyasaienthifiku, Japan.

Advances in Science and Technology Vol. 45 (2006) pp 2284-2291
online at http://www.scientific.net
© 2006 Trans Tech Publications, Switzerland

Investigation into Hydration Resistance of CaO-containing Materials

Wei Lin[1, a], Jianli Zhao[1, b], Junji Ommyoji[1, c] and Akira Yamaguchi[1, d]

[1]Okayama Ceramics Research Foundation, Japan
[a]linwei@optic.or.jp, [b]zhaojl@optic.or.jp, [c]ommyoji@optic.or.jp
and [d]yamaguchi@optic.or.jp

Keywords: CaO, Al_2O_3, Fe_2O_3, SiO_2, TiO_2, ZrO_2, NiO, Hydration, Steel, Nozzle.

Abstract: In order to develop an ideal material for the nozzle used in steel continuous casting process, the hydration resistance of some CaO-containing complex oxides and CaO-NiO solid solutions were investigated systematically. The hydration resistance of the complex oxides was CT >CZ>CS>CF>C_3T_2>C_2S>>C_2F>C_3A>CA_2>CaO. CT should be a promising material for the nozzle. A large number of fine secondary-NiOss particles were separated from the CaOss crystal grains in CaO-NiO solid solution and improved the hydration resistance.

I. Introduction

A submerged entry nozzle is used to introduce molten steel into a mold in steel continuous casting process. The refractory material of the nozzle is generally alumina-graphite. In this case, one problem frequently occurs, that is, an adhesion layer which causes nozzle clogging is produced on the inner wall of the nozzle during casting of Al-deoxidized steel. CaO has been considered to be an effective material to prevent the nozzle clogging according to some basic researches, but it is difficult to utilize CaO for the easy-hydration. So CaO-ZrO_2 material containing CaO of approximately 50 mol% is now applied in some nozzles. However, this material is not effective enough for prevention of the nozzle clogging and leads to ZrO_2 inclusions, which tend not to float out of molten steel due to the high density of ZrO_2.

In order to develop an ideal material for the nozzle, we systematically investigated the hydration resistance of CaO-containing materials in the present work. The effect of some added oxides, fluorides and chlorides on the hydration resistance of CaO has been reported in past literatures [1-5]. It can be known that free CaO remains in the sintered compacts if the amount of added components is small from the results. Once the sintered compacts are processed into grains of < 1 mm for the use to the nozzle as the raw material, the grains will be hydrated. Therefore, we paid attention to CaO-containing complex oxides and solid solutions, non-including free CaO.

CaO combines with many oxides to form the complex oxides as shown in Table 1. Taking into

Table 1. Complex oxides in system containing CaO

1	Al_2O_3	$3CaO \cdot Al_2O_3$, $6CaO \cdot 7Al_2O_3$, $CaO \cdot Al_2O_3$, $CaO \cdot 2Al_2O_3$, $CaO \cdot 6Al_2O_3$
2	B_2O_3	$3CaO \cdot B_2O_3$, $2CaO \cdot B_2O_3$, $CaO \cdot B_2O_3$, $CaO \cdot 2B_2O_3$
3	Bi_2O_3	$7CaO \cdot 3Bi_2O_3$, $7CaO \cdot 5Bi_2O_3$, $CaO \cdot Bi_2O_3$
4	Cr_2O_3	$CaO \cdot Cr_2O_3$
5	Fe_2O_3	$2CaO \cdot Fe_2O_3$, $CaO \cdot Fe_2O_3$
6	Ga_2O_3	$3CaO \cdot Ga_2O_3$, $CaO \cdot Ga_2O_3$, $CaO \cdot 2Ga_2O_3$
7	GeO_2	$CaO \cdot GeO_2$
8	HfO_2	$CaO \cdot HfO_2$
9	Mn_2O_3	$CaO \cdot Mn_2O_3$, $CaO \cdot MnO_2$
10	MoO_3	$CaO \cdot MoO_3$
11	Nb_2O_5	$3CaO \cdot Nb_2O_5$, $2CaO \cdot Nb_2O_5$, $CaO \cdot Nb_2O_5$
12	P_2O_5	$4CaO \cdot P_2O_5$, $3CaO \cdot P_2O_5$, $2CaO \cdot P_2O_5$
13	PbO	$PbO \cdot 2CaO$
14	SiO_2	$2CaO \cdot SiO_2$, $3CaO \cdot 2SiO_2$, $CaO \cdot SiO_2$
15	TiO_2	$3CaO \cdot 2TiO_2$, $CaO \cdot TiO_2$
16	UO_2	$2CaO \cdot UO_2$, $CaO \cdot UO_2$
17	V_2O_5	$3CaO \cdot V_2O_5$, $2CaO \cdot V_2O_5$
18	WO_3	$CaO \cdot WO_3$
19	ZrO_2	$CaO \cdot ZrO_2$

account the resource of oxides, we selected Al_2O_3, Fe_2O_3, SiO_2, TiO_2 and ZrO_2 as the second components in the complex oxides. In addition, CaO reacts with CeO_2, FeO, La_2O_3, MgO, MnO, NiO, Pr_2O_3 and Y_2O_3 to produce the solid solutions. We took up CaO-NiO system in our experiment because the solid solubility of NiO in CaO is comparatively high and the hydration resistance of this system has never been studied.

II. Experimental Procedures

For promotion of the sintering, a light $CaCO_3$ obtained by blowing CO_2 gas into a $Ca(OH)_2$ aqueous solution was used as the starting raw material of CaO. The grain sizes were below about 1 μm, markedly smaller than the general $CaCO_3$ reagent, as seen in the microstructure shown in Fig.1. Al_2O_3, Fe_2O_3, SiO_2, TiO_2, ZrO_2 and NiO reagents were used as the second components.

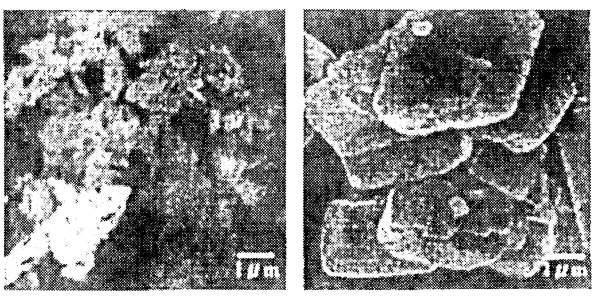

Light　　Reagent

Fig.1. Microstructure of $CaCO_3$ raw materials.

In the case of the complex oxides, the proportion of the raw materials for the preparation of $CaO{\cdot}2Al_2O_3(CA_2)$, $CaO{\cdot}Fe_2O_3(CF)$, $CaO{\cdot}SiO_2(CS)$ and $CaO{\cdot}TiO_2(CT)$ specimens followed each stoichiometric ratio. While for the preparation of $3CaO{\cdot}Al_2O_3(C_3A)$, $2CaO{\cdot}Fe_2O_3(C_2F)$, $2CaO{\cdot}SiO_2(C_2S)$, $3CaO{\cdot}2TiO_2(C_3T_2)$ and $CaO{\cdot}ZrO_2(CZ)$ specimens, the amount of the second components was fixed to be 3 mol % higher than each stoichiometric ratio to completely prevent free CaO to remain in the sintered compacts, because these compounds adjoin free CaO on the phase diagrams. After the raw materials on the proportion were pulverized, mixed with ethanol in an agate mortar, the mixtures were dried in a rotating-vacuum processor. 2 g of each mixture was uniaxially pressed at 50 MPa and then sintered for 5 hr in atmosphere. The sintering temperature was set at 1100°C for CF specimen, 1300°C for C_2F, 1400°C for C_3A, 1500°C for CA_2, C_2S, CS, C_3T_2 and CT, 1600°C for CaO and CZ depending on the fusion point of the complex oxides. The sintered C_2S compact powdered due to the phase transition during cooling. Each of the sintered compacts was pulverized immediately after taken out the electric furnace. A part of the powder was used for the phase identification analysis by X-ray diffraction (XRD), the other (0.5 g) being for the test of hydration resistance.

In the hydration test, the powdery specimen was put in a temperature-humidity chamber (70°C×90%-relative humidity) up to 48 hr. The hydrated specimen was weighed, and the mass-increasing percentage, α or β, was calculated by Eq.(1), (2).

$$\alpha=\Delta M/M_0\times 100\% \qquad (1)$$

$$\beta=\Delta M/M_{CaO}\times 100\% \qquad (2)$$

where, ΔM is the mass increase, M_0 and M_{CaO} are the total mass and the CaO mass of the specimen before the hydration test, respectively. For comparison, an Al_2O_3 regent powder was also tested.

In the case of CaO-NiO solid solutions, the sintered CaO-NiO compacts with NiO of 0, 10, 20, 30, 40, 50 and 60 mol% were prepared by the same method as mentioned above, the sintering temperature being 1600°C. The sintered compacts were directly used in the hydration test. XRD and EPMA analysis were conducted on the sintered compacts prepared under the same condition.

III. Results

(1) Case of complex oxides

The XRD results of the sintered specimens are shown in Fig.2. A small quantity of $Ca(OH)_2$ existed in CaO specimen due to the hydration of CaO upon pulverizing. The phases of $12CaO{\cdot}7Al_2O_3$, $CaO{\cdot}FeO_2$, $3CaO{\cdot}2SiO_2$, $4CaO{\cdot}3TiO_2$ and ZrO_2 were included in C_3A, C_2F, C_2S, C_3T_2 and CZ specimens, respectively, because the added second components were higher than the stoichiometric ratios in them. Each of CA_2, CF, CS and CT specimens was composed of only the single phase.

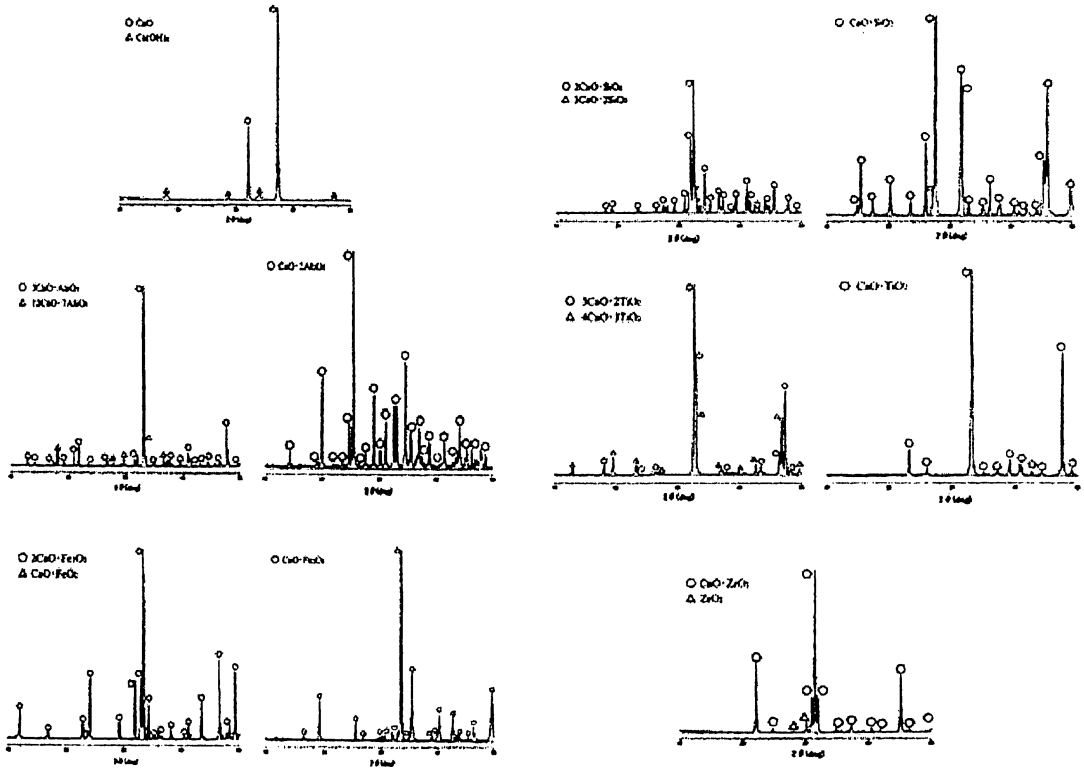

Fig.2. XRD analysis of sintered complex oxide specimens.

The change of the mass-increasing percentage α of the specimens as a function of the hydration time is given in Fig.3. CaO, CF, CS, CZ and CT as well as Al_2O_3 specimens showed a similar change tendency, i.e., the mass increased rapidly in the time to 1 hr and then the increase rate became very slow, whereas the mass of the other specimens increased gradually over the whole period up to 48 hr.

The mass of CaO, CA_2, C_3A and C_2F specimens had a marked increase, reaching 10-45% at 48 hr hydration (Fig.3 (a)). C_2S, C_3T_2 and CF showed a relatively small increase, 1.5-2.5% (Fig.3 (b)). CS, CZ and CT were all below 1%; especially, CT increased only 0.45%, almost same as Al_2O_3 (Fig.3(c)).

Defining a hydration index $I_\alpha=\alpha/\alpha_{CaO}$, I_α of each specimen hydrated for 48 hr is presented in Fig.4. As can be seen in Fig.4, the order of the hydration resistance was

$$CT>CZ>CS>CF>C_3T_2>C_2S>>C_2F>C_3A>CA_2>CaO$$

In addition, the mass-increasing percentage β based on the mass of CaO (M_{CaO}) was calculated

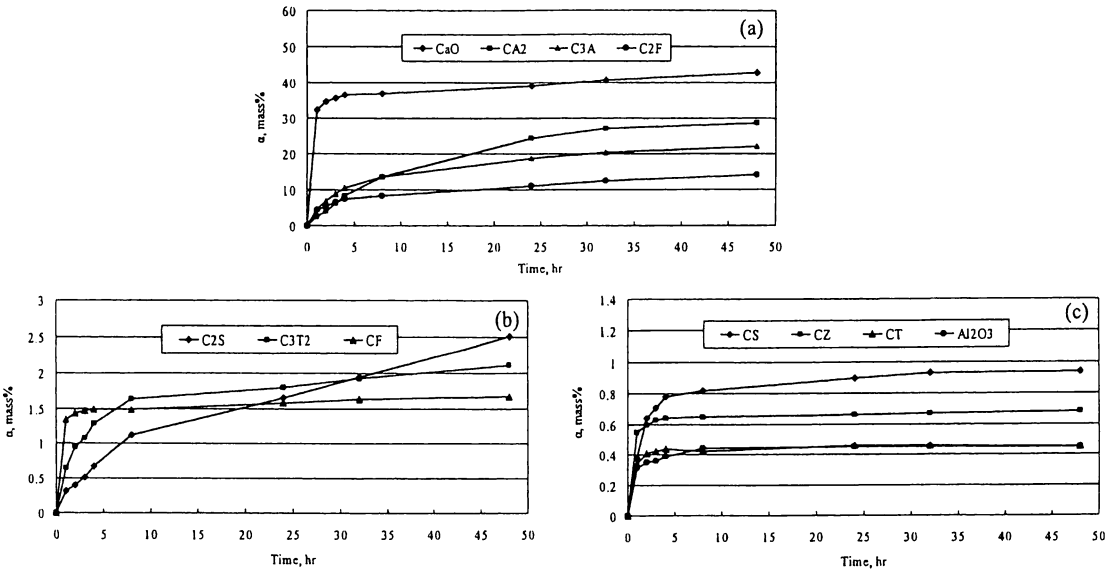

Fig.3. Mass-increasing percentage α of complex oxide specimens.

by Eq.(2) and another hydration index defined as $I_\beta=\beta/\alpha_{CaO}$ was obtained as shown in Fig.5 (values at 48hr hydration). This result indicates that TiO_2, SiO_2 and ZrO_2 have large addition effect and the effect of Al_2O_3 is small for improvement of CaO hydration resistance.

Moreover, all specimens hydrated for 48 hr were heated up to 1000°C in atmosphere. The mass-decreasing percentage of them is shown in Fig.6, which nearly agreed with the mass-increasing percentage α in the hydration test (Fig.3).

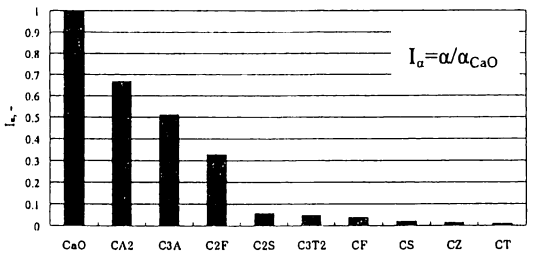

Fig. 4. Hydration index I_α on total mass of specimens (M_0).

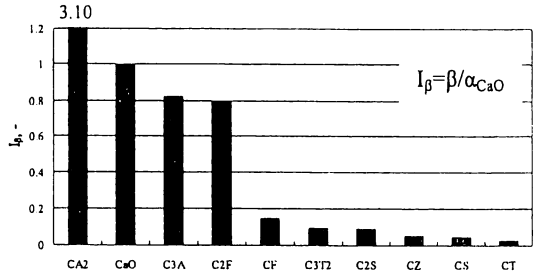

Fig. 5. Hydration index I_β on CaO mass of specimens (M_{CaO}).

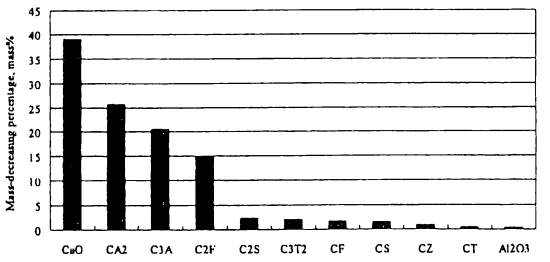

Fig.6. Mass-decreasing percentage of hydrated specimens with heating up to 1000°C.

(2) Case of CaO-NiO solid solutions

The sintered CaO-NiO compacts all had an apparent porosity of 0.8% or less. Fig.7 shows the

mass-increasing percentage β of the compacts during the hydration test, which rose almost linearly with passage of the hydration time, but reduced with increase in NiO content of the compacts.

The average value of the hydration rate, equal to the ratio of the mass-increasing percentage β to the hydration time, of the compacts is pointed in Fig.8. The hydration rate decreased sharply until NiO content of 20 mol% and then decreased slowly on further NiO increasing.

The microstructure of the sintered compacts is shown in Fig.9(a), which consists of white grains and a dark matrix. EPMA analysis indicated that the white grains are a NiO rich solid solution (primary-NiOss) containing around 7 mol% of CaO.

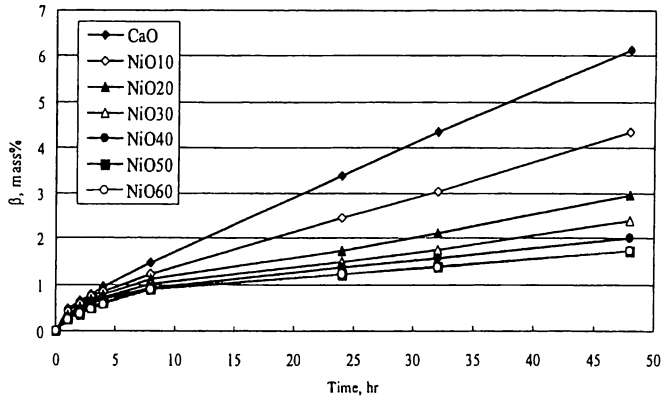

Fig.7 Mass-increasing percentage β of CaO-NiO compacts.

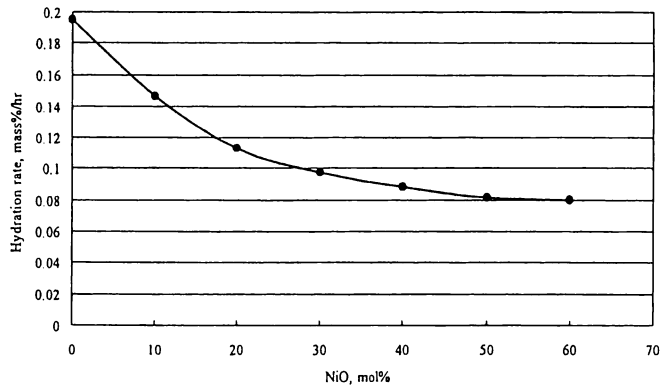

Fig.8 Hydration rate of CaO-NiO compacts.

Fig.9(b) provides the microstructure of the matrix observed at a high magnification. A large number of fine particles (< 0.3 μm) were found to uniformly distribute in the matrix. According to EPMA analysis, the fine particles were also a NiO rich solid solution (secondary-NiOss), while the phase around secondary-NiOss was a CaO rich solid solution containing about 4 mol% NiO. As an example, the analysis result of NiO20 specimen is given in Fig.9(c).

Only a small amount of primary-NiOss existed in NiO10 (Fig.9(a)), so the hydration rate of NiO10 being 30% lower than CaO is considered to be mainly due to the action of secondary-NiOss.

IV. Discussion

(1) Hydration mechanism

Analyzing CaO specimens hydrated for 1 and 48 hr by XRD, $Ca(OH)_2$ was detected in the former and $CaCO_3$ besides $Ca(OH)_2$ in the latter. This signifies that the following reactions occurred in CaO on hydrating.

$$CaO(s)+H_2O(g)=Ca(OH)_2(s) \quad (3)$$

$$Ca(OH)_2(s)+CO_2(g)=CaCO_3(s)+H_2O(g) \quad (4)$$

The CO_2 gas mostly came from the distilled water used in the temperature-humidity chamber.

In C_3A specimen, the reaction expressed by Eq.(5) might has occurred, because $Ca(OH)_2$ and $CaCO_3$ were formed and the ratio of the XRD-peak intensity of C_3A to $C_{12}A_7$ became small after the hydration test.

$$7[3CaO\cdot Al_2O_3](s)+9H_2O(g)=12CaO\cdot 7Al_2O_3(s)+9Ca(OH)_2(s) \quad (5)$$

$Al(OH)_3$ was also identified in the hydrated CA_2 specimen, which suggests occurrence of the

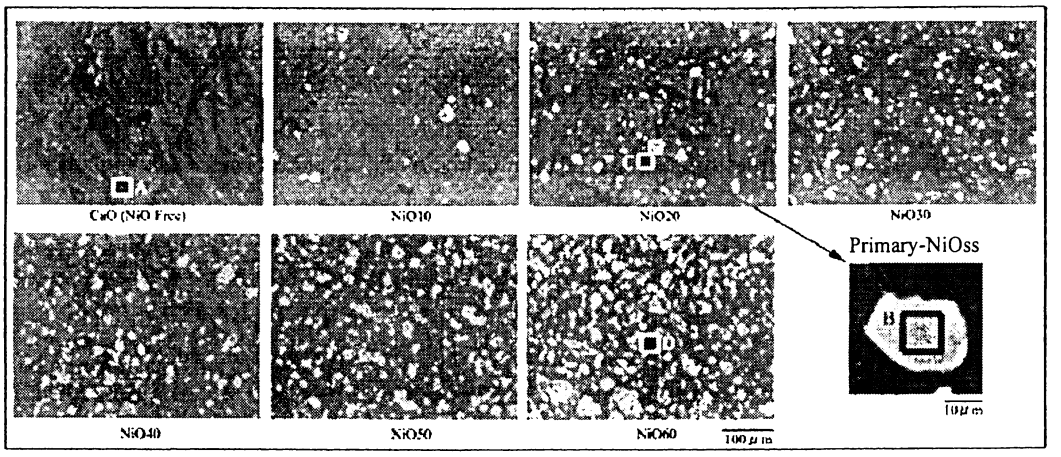

(a)

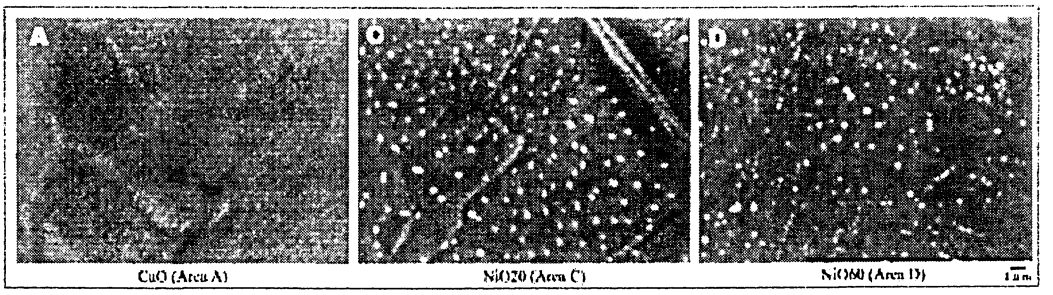

(b)

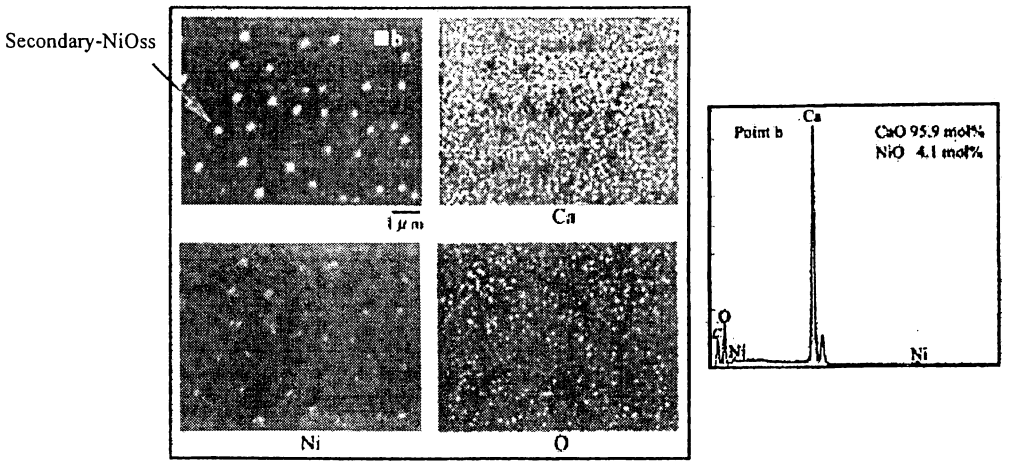

(c)

Fig.9. Microstructure of sintered CaO-NiO compacts.

reaction of Eq.(6).

$$CaO{\cdot}2Al_2O_3(s)+7H_2O(g)=Ca(OH)_2+4Al(OH)_3 \qquad (6)$$

There were some phases that cannot be judged definitely from the XRD charts of both C_2F and C_2S specimens hydrated. Perhaps, the phases were hydrates such as $2CaO{\cdot}Fe_2O_3{\cdot}xH_2O$ and $2CaO{\cdot}SiO_2{\cdot}xH_2O$.

The reaction of Eq.(7) is thought to have happened in C_3T_2 specimen, based on existence of $Ca(OH)_2$ and $CaCO_3$ and decrease in the ratio of the XRD-peak intensity of C_3T_2 to C_4T_3.

$$3[3CaO{\cdot}2TiO_2](s)+H_2O(g)=2[4CaO{\cdot}3TiO_2](s)+Ca(OH)_2(s) \qquad (7)$$

No difference was observed between the XRD chart of CF, CS, CT and CZ specimens before and after the hydration test, same as the case of Al_2O_3 specimen. However, since these specimens, particularly CF and CS showed a mass increase on hydrating (Fig.3), it is possible that the hydrates formed in these specimens were amorphous or of low crystallization degree.

In CaO-NiO system, the reactions of Eq.(3) and (4) occurred, like the case of CaO specimen.

(2) Formation mechanism of secondary-NiOss in CaO-NiO system

CaO-NiO phase diagram[6] shows that the solid solubility of NiO in CaO decreases with temperature falling, for example, being 12.6 mol% at 1600°C and 3.7 mol% at 1200°C. Based on this point as well as the size, shape, number and distribution state of the secondary-NiOss particles (Fig.9), the particles can be judged to have been separated from the CaOss during the cooling stage in the heating process. This suggests that the cooling condition e.g. the cooling rate influences the separation behavior of secondary-NiOss (the cooling rate was 5°C /min from 1600 to 1200°C in our experiment). It is a future research subject to quantitatively clarify the relations among the cooling condition, the separation behavior of secondary-NiOss and the hydration resistance.

The solid solubility of CaO in NiO decreases also with temperature falling, 8.4 mol% at 1600°C and 1.2 mol% at 1200°C. However, no secondary-CaOss particles were observed in the primary-NiOss in the CaO-NiO specimens (Fig.9). This may signify that the diffusion rate of Ca^{2+} in NiO is slow, so that the formation of CaO nucleus is difficult.

(3) Possibility of suitable CaO-containing material for nozzles

The hydration test results mentioned above showed that CT material has the best hydration resistance. In addition, CT contains CaO of 41 mass%, 10 mass% higher than CZ, which is applied now in some nozzles, as listed in Table 2. The fusion point of CT is 1970°C, about 200°C higher than the temperature of molten steel and so the refractoriness is enough, although it is 370°C lower than CZ. Consequently, CT should be a more promising material for the nozzles.

Table 2. Characteristic comparisons between CT and CZ

-	CT	CZ
Hydration index I_α, -	0.01	0.02
CaO content, mass%	41	31
Fusion point, °C	1970	2340
Density, g/cm^3	4.03	4.62

V. Conclusion

1) The hydration resistance of the complex oxides in CaO-Al_2O_3, Fe_2O_3, SiO_2, TiO_2 and ZrO_2 systems was investigated on condition of 70°C and 90%-humidity, and the order of the hydration resistance was

$$CT > CZ > CS > CF > C_3T_2 > C_2S >> C_2F > C_3A > CA_2 > CaO$$

CT should be a more promising material than CZ for the submerged entry nozzle.

2) In the case of CaO-NiO solid solutions, a large number of fine secondary-NiOss particles were separated from the CaOss crystal grains during the cooling stage in the heating process and improved the hydration resistance.

References

1) M. Chen and A. Yamaguchi: J. Ceram. Soc. Japan, 110 [12] 1058 (2002).
2) S. Chen, G. Chen and J. Cheng: J. Am. Ceram. Soc., 83 [7] 1810 (2000).
3) H. Yoshimatus, K. Kawauchi, K. Kawabata, T. Yabuki and Y. Miura: J. Ceram. Soc,. Japan, 106 [11] 1138(1998).
4) A. Harabi and S. Achour: J. Mater. Sci. Lett., 18 [12] 955 (1999).
5) J. T. Song, J. Y. Kim, D. W. Ryu, S. Y. Go and K. S. Han: J. Korean. Ceram. Soc., 35 [2] 185(1998).
6) D. E. Smith, T. Y. Tien and L. H. Van Vlack: J. Am. Ceram. Soc., 52 [8] 459 (1969).

Journal of the Ceramic Society of Japan 115 [1] 42-46 (2007)

Paper

Synthesis of Magnesium Aluminum Oxynitride by Carbothermal Reduction and Nitridation Process

Wenbin DAI,*,** Wei LIN,* Akira YAMAGUCHI,* Jyunji OMMYOJI,* Jingkun YU** and Zongshu ZOU**

*Okayama Ceramics Research Foundation, 1406-18, Nishikatakami, Bizen-shi 705-0021
**School of Materials and Metallurgy, Northeastern University, Shenyang, 110004, China

炭素熱還元窒化法による MgAlON の合成

Wenbin Dai*,** · Wei Lin* · 山口明良* · 隠明寺準治* · Jingkun Yu** · Zongshu Zou**

*岡山セラミックス技術振興財団, 705-0021 備前市西片上 1406-18
**School of Materials and Metallurgy, Northeastern University, Shenyang, 110004, China

Carbothermal reduction and nitridation (CRN) process was utilized to prepare magnesium aluminum oxynitride (MgAlON) and the influence of reaction variables, such as heating temperature, soaking time and the source of carbon, on the formation of MgAlON was investigated. In addition, the density of samples prepared under different route was compared. The results show that volatile gases, Mg (g) in chief, lead to variation in lattice constant and chemical composition at high temperature, and decrease the sintering effect. Since high temperature and low CO partial pressure are favorable to the CRN reaction in view of thermodynamic reason and high temperature also favors the transport of gases, the rate of CRN reaction increases with the increasing temperature. Due to the difference in reactivity between graphite and carbon black, CRN reaction may be the rate controlling step when graphite is used and solid solution of AlN may be the controlling step when carbon black is utilized. CRN reaction can increase surface energy of reaction materials and results in higher final density. However, gases in the system retard the densification effect.

[Received July 10, 2006; Accepted November 16, 2006]

Key-words: Carbothermal reduction and nitridation (CRN), Magnesium aluminum oxynitride (MgAlON), Synthesis

1. Introduction

Magnesium aluminum oxynitride (MgAlON) is a cubic solid solution crystal material with excellent optical and mechanical properties and attracts lots of researchers' interest after the introduction of Jack.[1),2)] Moreover, since MgAlON and its oxidized material, magnesium aluminate spinel ($MgAl_2O_{4ss}$) and Al_2O_3, has high melting point and nitrogen in the material can increase the viscosity of slag to retard the further corrosion,[2)-5)] it can be considered as a promising superior refractory. To prepare this material, the following synthesis methods were utilized: (1) solid phase reaction of AlN, Al_2O_3 and MgO;[2),5)-7)] (2) reaction of Al, Al_2O_3 and MgO;[8)] (3) carbothermal reduction and nitridation (CRN) of Carbon, Al_2O_3 and MgO.[9)]

The MgAlON formation mechanism through solid phase reaction has been well investigated:[2),5)-7)] MgO reacts with Al_2O_3 to form $MgAl_2O_{4ss}$ above 1000°C. At higher temperatures, AlN and Al_2O_3 dissolve into $MgAl_2O_{4ss}$ to form MgAlON. The maximal amount of AlN and Al_2O_3 dissolved into $MgAl_2O_{4ss}$ increases with the increasing heating temperature[7)] and N diffusion is considered to be the rate controlling of MgAlON formation.[2)]

From the viewpoint of the purity of product, preparation of the raw materials and potential for large-scale production, the CRN process is considered to have advantages. However, the synthetic process and other details on preparing MgAlON through CRN were seldom discussed except for few reports proposed that AlON, prepared through CRN process, could be stabilized at low temperature by adding MgO or $MgAl_2O_{4ss}$.[9)]

Since density is probably the most important parameter in the study of sintering and it relates to the sintering kinetics and correlates with many properties of sintering materials,[10)] the sintering characteristics of various routes could be surveyed by the comparison of the density of samples heated at the same condition.

In present investigation, CRN process was utilized to prepare MgAlON and the influence of reaction variables, such as heating temperature, soaking time and the source of carbon, on the formation of MgAlON was investigated. Moreover, density of the samples prepared by different route was compared. Based on the results, evaporation of MgAlON was analyzed, MgAlON formation mechanism through CRN process was discussed, and sintering characteristics of CRN process were surveyed.

2. Experimental procedure

2.1 Starting materials and synthesis procedure

Table 1 gives information about the starting materials used in present investigation. According to **Table 2**, the raw materials were meticulous weighted and then mixed by ball milling with alumina balls in ethyl alcohol. After evaporating the solvent in vacuum rotary, the mixtures were uniaxial pressed under 150 MPa. As described in Table 2, the green compacts were heated in a graphite furnace under various conditions. Gas pressure of the furnace was constant at 0.1 MPa and flowing rate of N_2 gas (purity > 99.999%) was 1 $L \cdot min^{-1}$.

2.2 Characterization

In present work, Bulk density and apparent porosity were measured by SGM-6 automatic gravimeter, true density was analyzed by IONICS multi pycnometer, and specific surface area was tested by IONICS monosorb. The phase composition

Table 1. Some Information of Staring Materials

	MgO*1		Al_2O_3		Carbon		AlN	Al
	M1	M2	AO1	AO2	Graphite	Carbon black*2		
Purity (wt%)	99.9	99.9	99.9	99.99	99.4	99.2	99.2	99.5
Particle size (μm)	<10	0.24	<75	0.1	<45	0.023	0.7	<20
Specific surface area (m^2/g)					12	106		

*1 The materials for chemical analysis were preheated at 1000℃. The ignition loss of M1 and M2 was 3.6% and 8.2%, respectively, and it was considered during the weighting.
*2 Amorphous

Table 2. Composition of the Compacts in Molar ratio and Heating Conditions

Sample No.	MgO		Al_2O_3		Carbon		AlN	Al	Heating conditions
	M1	M2	AO1	AO2	Graphite	Carbon black			
A_1	8		29		9				1100℃, 6h
A_2	8		29		9				1300℃, 6h
A_3	8		29		9				1350℃, 6h
A_4	8		29		9				1400℃, 6h
A_5	8		29		9				1450℃, 6h
A_6	8		29		9				1500℃, 6h
A_7	8		29		9				1600℃, 6h
A_8	8		29		9				1650℃, 6h
A_9	8		29		9				1700℃, 6h
A_{10}	8		29		9				1800℃, 6h
B_1	8		29		9				1500℃, 96h
B_2	8		29		9				1700℃, 3h
B_3	8		29		9				1700℃, 6h
B_4	8		29		9				1700℃, 9h
C_1	8		29			9			1500℃, 6h
C_2	8		29			9			1700℃, 6h
D	4		13				3		1700℃, 6h
E	4		13					3	1700℃, 6h
F		8		29	9				1700℃, 6h
G		8		29		9			1700℃, 6h
H		4		13			3		1700℃, 6h
I		4		13				3	1700℃, 6h

was identified by RINT2200 X-ray diffraction (XRD) and the relative intensity of the random i phase (R_i) was calculated according to the following equation,

$$R_i = \frac{I_i}{I_1 + I_2 + \ldots + I_i + \ldots} \times 100\% \quad (1)$$

where the subscripts represent the detected phases, I_i is the intensity of the strongest peak of i phase.

To analyze formation process in quantity, chemical composition of intermediate product should be concerned. However, it is difficult to determine composition of $MgAl_2O_{4ss}$ and MgAlON only by chemical analysis when Al_2O_3 exists in the sample. In present work, chemical composition of $MgAl_2O_{4ss}$ and MgAlON is calculated by the combination of chemical composition and lattice constant. As lattice constant of $MgAl_2O_{4ss}$ and MgAlON, designated as $\alpha_{MgAl_2O_{4ss}}$ and α_{MgAlON}, can be calculated through the following equations,[7]

$$\alpha_{MgAl_2O_{4ss}} = 0.7900 + 0.0375[MgO]_{MgAl_2O_{4ss}}\% \text{ (nm)} \quad (2)$$

$$\alpha_{MgAlON} = 0.7900 + 0.0375[MgO]_{MgAlON}\% + 0.0150[AlN]_{MgAlON}\% \text{ (nm)} \quad (3)$$

with [MgO] or [AlN] in mol% of each component. Chemical composition of $MgAl_2O_{4ss}$ could be calculated from Eqs. (4)-(6) on the condition that entire Mg exists in $MgAl_2O_{4ss}$ struc-

ture.

$$[Mg]_{MgAl_2O_{4ss}}\% = \frac{(\alpha_{MgAl_2O_{4ss}} - 0.7900) \times 80}{(15 - (\alpha_{MgAl_2O_{4ss}} - 0.7900) \times 240)} \times 100\% \quad (4)$$

$$[Al]_{MgAl_2O_{4ss}}\% = \frac{6 - (\alpha_{MgAl_2O_{4ss}} - 0.7900) \times 160}{(15 - (\alpha_{MgAl_2O_{4ss}} - 0.7900) \times 240)} \times 100\% \quad (5)$$

$$[O]_{MgAl_2O_{4ss}}\% = 1 - [Mg]\% - [Al]\% \quad (6)$$

When entire N and Mg exist in MgAlON structure, chemical composition of MgAlON can be figured out in the following equations:

$$[Mg]_{MgAlON}\% = \{(\alpha_{MgAlON} - 0.7900) \times (Mg)\%\} / \{(2.5575 \times (Mg)\% + 2.445 \times (N)\% - \alpha_{MgAlON} \times ((Mg)\% + (N)\%) \times 3)\} \times 100\% \quad (7)$$

$$[Al]_{MgAlON}\% = \{(1.655 \times (Mg)\% + 0.82 \times (N)\% - ((Mg)\% \times 2 + (N)\%) \times \alpha_{MgAlON})\} / \{(2.5575 \times (Mg)\% + 2.445 \times (N)\% - \alpha_{MgAlON} \times ((Mg)\% + (N)\%) \times 3)\} \times 100\% \quad (8)$$

$$[N]_{MgAlON}\% = \{(\alpha_{MgAlON} - 0.7900) \times (N)\%\} / \{(2.5575 \times (Mg)\% + 2.445 \times (N)\% - \alpha_{MgAlON} \times ((Mg)\% + (N)\%) \times 3)\} \times 100\% \quad (9)$$

$$[O]_{MgAlON}\% = 1 - [Mg]_{MgAlON}\% - [Al]_{MgAlON}\% - [N]_{MgAlON}\% \quad (10)$$

where [Mg, Al and O]$_{MgAl_2O_{4ss}}$% or [Mg, Al, O and N]$_{MgAlON}$% are mol% of elements in these two phases. (Mg and N)% are mol% of Mg and N in the sintered sample. In present investigation, lattice constant of $MgAl_2O_{4ss}$ and MgAlON was determined by XRD by using high purity silicon (purity > 99.999 mass%) as internal standard material, and the content of Mg and Al was measured by Simultix12 X-ray fluorescence spectroscope (XRFS), O, N by EMGA650 oxygen and nitrogen analyzer, and Carbon by EMIA810 carbon analyzer.

3. Results and discussion

3.1 Influence of heating temperature

The content of residual carbon in the samples of A_1-A_{10} is plotted in **Fig. 1**. At temperatures below 1300°C, the content of residual carbon in these samples (3.16 mass%) approximated to that in the raw material (3.19 mass%) and when above it, especially above 1400°C, the rate of graphite consumption increased with the increasing temperature.

Figure 2 reveals the relative intensities of detected phases in the samples of A_1-A_{10}. MgO could not be detected in samples even as low as 1100°C, because entire MgO reacted with Al_2O_3 to form $MgAl_2O_{4ss}$. In view of lattice constant of $MgAl_2O_{4ss}$ decreased from 0.8079 nm at 1100°C to 0.8050 nm at 1300°C, as shown in **Fig. 3**, chemical composition of $MgAl_2O_{4ss}$ calculated by equations (4)-(6) could be represented as $Mg_4Al_{8.76}O_{17.14}$ (1100°C) and $Mg_4Al_{12}O_{22}$ (1300°C), respectively. Since the amount of Al_2O_3 dissolved into $MgAl_2O_{4ss}$ increased with the increasing temperature and the molar weight of graphite and $MgAl_2O_{4ss}$ had not obvious change below 1300°C, the relative intensity of Al_2O_3 decreased, while that of graphite and $MgAl_2O_{4ss}$ increased from 1100°C to 1300°C. By making use of chemical analysis and XRD detection, it was confirmed that MgAlON was formed in the samples heated above 1350°C. Based on the result of lattice constant, as shown in Fig. 3 chemical composition of the synthesized MgAlON could be calculated by Eqs. (7)-(9) and some of them were $Mg_4Al_{13.40}O_{23.94}N_{0.11}$ (1350°C), $Mg_4Al_{17.48}O_{29.08}N_{0.76}$ (1450°C) and $Mg_4Al_{27.86}O_{41.40}O_{2.93}$ (1600°C). When over 1650°C, mono-

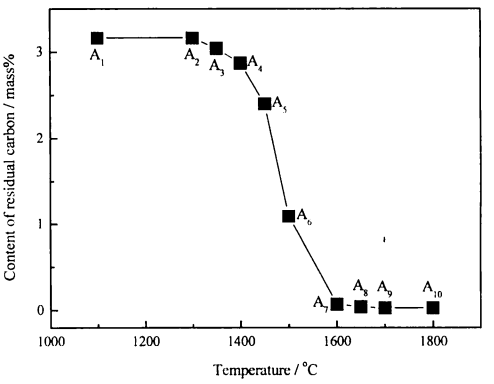

Fig. 1. Content of residual carbon in the samples of A_1-A_{10}.

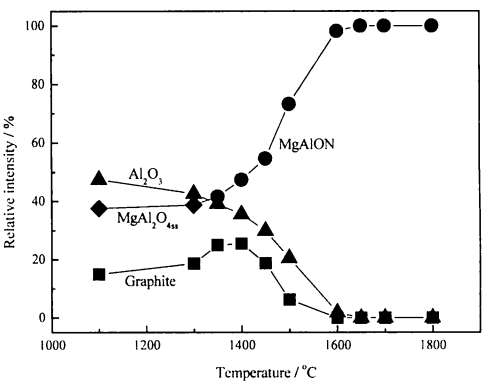

Fig. 2. Change of relative intensities of detected phases in the samples of A_1-A_{10}.

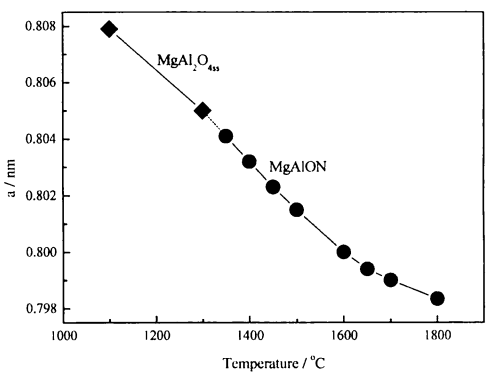

Fig. 3. Lattice constant of $MgAl_2O_{4ss}$ and MgAlON in the samples of A_1-A_{10}.

phase MgAlON was obtained and chemical composition of these samples was calculated by making use of chemical analysis and they were $Mg_4Al_{31.62}O_{46.75}N_{3.12}$ (1650°C), $Mg_4Al_{32.20}O_{47.60}N_{3.13}$ (1700°C) and $Mg_4Al_{32.79}O_{48.44}N_{3.16}$ (1800°C), respectively. It is indicated that Mg content decreased with the increasing temperature and as a consequence, lattice constant of MgAlON decreased according to equation (3). Through the further discussion in Section 3.5, it is known that volatile gases of MgAlON caused the variation.

3.2 Effect of the soaking time

In the sample of B_1, which was heated at 1500°C for 96 h, AlN, Al_2O_3 and MgAlON were detected and the residual car-

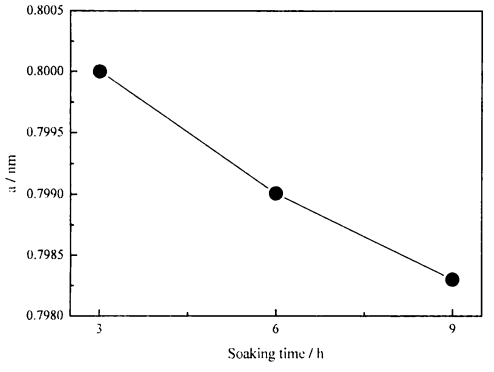

Fig. 4. Lattice constant of MgAlON in the samples of B_2–B_4.

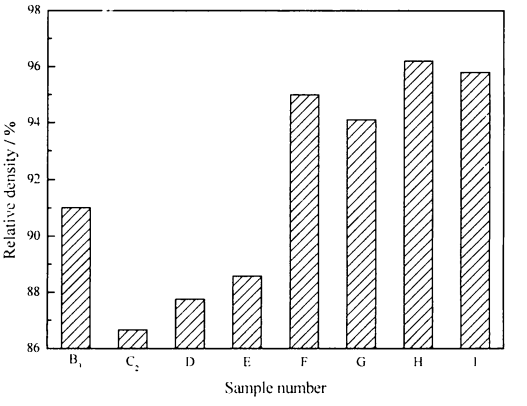

Fig. 5. Relative density of samples heated at 1700°C for 6 h.

bon was 0.09 mass%. The AlN provided by CRN reaction did not dissolve into $MgAl_2O_{4ss}$ entirely and it was different from the sample of A_6, which was heated at 1500°C for 6 h, for that AlN could not be detect. As the amount of AlN dissolved into $MgAl_2O_{4ss}$ has a maximal value at a temperature,[7] the AlN provided by CRN reaction in the sample of B_1 is excessive for $MgAl_2O_{4ss}$ at this temperature. Considering the phase composition of samples of A_3–A_{10} heated at different temperature for 6 h, as mentioned in Section 3.1, it can be concluded that the generating rate of AlN by CRN of graphite is slower than the potential maximal solid solution rate of AlN before a critical point. In the samples of B_2–B_4, which were heated at 1700°C for different soaking time, the content of residual carbon was less than 0.03 mass% and only MgAlON detected. According to the result of chemical analysis, their chemical composition could be expressed as $Mg_4Al_{29.87}O_{44.33}N_{2.98}$ (3 h), $Mg_4Al_{32.20}O_{47.60}N_{3.13}$ (6 h), and $Mg_4Al_{33.58}O_{49.53}N_{3.23}$ (9 h), respectively. It implies that Mg content decreased with the soaking time and the decrease caused variation in lattice constant (**Fig. 4.**). Evaporation of MgAlON at high temperature leads to it and the reason was further discussed in Section 3.5.

3.3 Effect of the source of carbon

In the sample of C_1, which was made from carbon black and heated at 1500°C for 6 h, AlN, Al_2O_3 and MgAlON were detected and the content of residual carbon was 0.11 mass%. Its composition was close to the sample of B_1, which was made from graphite and heated at 1500°C for 96 h, and its residual carbon was much lower than that the sample of A_6, which was made from graphite and heated at 1500°C for 6 h. Hence, the carbon consumption rate in the sample made from carbon black was much higher than that made from graphite. Since the amorphous carbon black used in this work has smaller size (about 0.023 μm) and higher surface area (106 $m^2 \cdot g^{-1}$), the reactivity of it is much higher than that of graphite.

3.4 Density of samples prepared by different route

In present investigation, all the samples heated at 1700°C for 6 h were monophase MgAlON and the chemical composition was close to each other. However, as shown in **Fig. 5**, the relative density was different with the synthesis route. Among the samples B_3, C_2, D, and E, which were made from coarser MgO and Al_2O_3, the sample of B_3, which was made from graphite by CRN process, had the highest density and that of C_2, which was made from carbon black, was the most porous one. As to the samples made from finer MgO and Al_2O_3 (F, G, H, and I), the density was much higher than that of samples made from coarser materials. The density of samples F and G, which was prepared by CRN process, was lower than that of others and the sample of H, which was made from

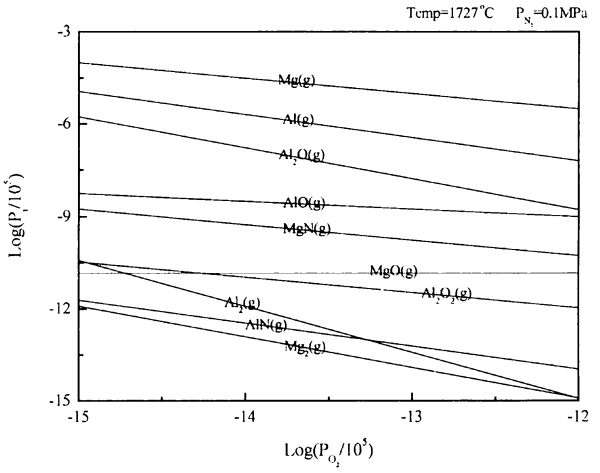

Fig. 6. Equilibrium gas partial pressures of $Mg_4Al_{29}O_{43}N_3$ at 1727°C.

MgO, Al_2O_3, and AlN, had the highest density. However, due to volatile gases of MgAlON at high temperature, which was discussed in Section 3.5, closed pores were formed in the matrix and full dense samples could not be obtained in present condition even the apparent porosity approximated to 0.

3.5 Evaporation of MgAlON

Based on the thermodynamics data,[6),11)] equilibrium partial pressure of gases of $Mg_4Al_{29}O_{43}N_3$ at 1727°C in nitrogen atmosphere are calculated and plotted in **Fig. 6**. These gases, Mg (g) in chief, may be entrained by the flowing nitrogen gas and then evaporation occurs at high temperature. In this way, as mention in Sections 3.1 and 3.2, Mg content in the sample decreased and lattice constant was also decreased according to Eq. (3). Moreover, the volatile gases lead to closed pores formed in the matrix and it is difficult to obtain full dense MgAlON sample in present condition without any auxiliary means, such as spark plasma.[4)]

3.6 MgAlON formation mechanism by CRN process

As mentioned in Section 3.1, entire MgO react with Al_2O_3 to form $MgAl_2O_{4ss}$ below 1100°C. The reaction is considered as the first step and similar to solid phase reaction system. In the CRN process, it is certain that nitride, AlN, must be provided before its solid solution reaction. Hence, in the second step, AlN supplies by the following overall reaction.[12)]

$$Al_2O_3 + 3C + N_2 = 2AlN + 3CO \qquad (11)$$

Figure 7 shows the equilibrium partial pressure of CO of

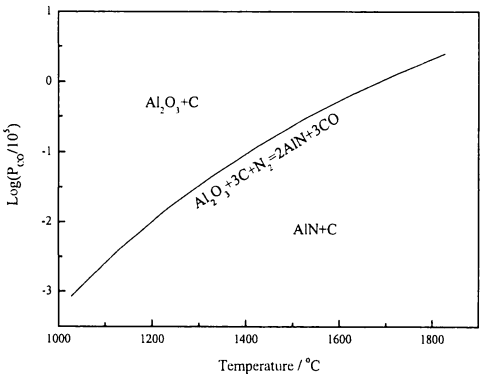

Fig. 7. Equilibrium partial pressure of CO of CRN reaction.

CRN reaction when the partial pressure of nitrogen is given as 0.1 MPa. Obviously, high temperature and low CO partial pressure are favorable to the CRN reaction. In the inner of the sample, the partial pressure of CO would be increased and that of N_2 would be decreased when CRN reaction proceeds with, because of the consumption of N_2 and formation of CO. If the diffusivity of gases is too slow, CRN reaction would be retarded or even ceased. On the other hand, since the diffusivity of gases increases with the increasing temperature, high heating temperature is also favorable to the transport of gases and favors the CRN reaction. Hence, the rate of CRN reaction increases with the increasing temperature. In the third process, Al_2O_3 and AlN, which was provided by CRN reaction, dissolve into $MgAl_2O_{4ss}$ to form MgAlON. In the sample made from graphite, the reaction rate of the second step should be slower than the maximum potential rate of the third step considering that AlN could not be detected in the samples of A_3-A_{10}. While in the sample made from carbon black, the reaction rate of the second step is much faster for the higher reactivity of carbon black and the third step is assumed as the rate limiting steps.

3.7 Characteristics of CRN process

When CRN reaction occurs, the reaction of carbon and Al_2O_3 can increase the surface energy of Al_2O_3 and the product of CRN reaction, AlN, has high surface energy. Since raw materials with higher surface energy always lead to higher final density,[10] the CRN process is favorable to the densification of samples and the sample of B_3, which was made from graphite, has the highest density. On the other hand, being the reactivity of carbon black is higher than graphite, lots of gases might be generated from the sintering body at one time and the sinterability of C_2 would be decreased. So, the density of C_2 is lower than that of B_3. The densities of Al and AlN are 2.702 $g \cdot cm^{-3}$ and 3.26 $g \cdot cm^{-3}$, respectively,[13] and the volume expansion caused by the nitridation of Al, which occurs at 600-800°C, is about 26%. Hence, the density of E is increased before the solid phase reaction of MgO-Al_2O_3-AlN system and the final density of E is higher than that of D, which was made from AlN.

When fine MgO and Al_2O_3 are used as raw materials, the materials themselves have high surface energy and the influence of the rise in the surface energy caused by CRN process could be neglected. Moreover, since CRN reaction is a kind of gas solid reaction and gases in the system are not favorable to the densification. Hence, the density of samples made from CRN process is lower than that of samples made from the other processes.

4. Conclusions

The process of carbothermal reduction and nitridation (CRN) on the synthesis of magnesium aluminum oxynitride (MgAlON) was investigated in present investigation. Being the volatile gases of MgAlON, Mg (g) in chief, there was variation in lattice constant and chemical composition at high temperature. In addition, these gases resulted in closed pores formed in the matrix and decreased the density of sample. Considering that high temperature and low CO partial pressure are favorable to the CRN reaction in view of thermodynamics reason and high temperature also favors the transport of gases, increasing the heating temperature is an efficient means to increase CRN reaction rate. Because of the difference in reactivity between graphite and carbon black, CRN reaction was the rate controlling step when graphite was used and solid solution of AlN was the controlling step when carbon black was utilized. CRN reaction could increase surface energy and lead to higher final density. However, gases in the system tended to decrease the final density.

Acknowledgments We are grateful to T. Mimura and to S. Takeuchi for their help.

References

1) Jack, K. H., *J. Mater. Sci.*, Vol. 11, pp. 1135-1158 (1976).
2) Bandyopadhyay, S., Rixecker, G., Aldinger, F. and Maiti, H. S., *J. Am. Ceram. Soc.*, Vol. 87, pp. 480-482 (2004).
3) Lofaj, F., Doráková, F. and Hoffmann, M. J., *J. Mater. Sci.*, Vol. 40, pp. 47-51 (2005).
4) Dai, W., Yamaguchi, A., Lin, W., Ommyoji, J., Yu, J. and Zou, Z., Submitted to *J. Ceram. Soc.Japan.*
5) Weiss, J,. Greil, P. and Gauckler, L. J., *J. Am. Ceram. Soc.*, Vol. 65, pp. C68-C69 (1982).
6) Wang, X. D., Li, W. C. and Seethararnan, S., *Z. Metallkd.*, Vol. 93, pp. 540-544 (2002).
7) Granon, A., Goeuriot, P., Thevenot, F., Guyader, J., L'Haridon, P. and Laurent, Y., *J. Eur. Ceram. Soc.*, Vol. 13, pp. 365-370 (1994).
8) Wang, X. T., Wang, H. Z., Zhang, W. J., Sun, J. L. and Hong, Y. R., *Key Engineering Materials*, Vol. 226, pp. 373-378 (2002).
9) Li, Y. W., Li, N. and Yuan, R. Z., *J. Mater. Sci.*, Vol. 32, pp. 979-982 (1997).
10) German, R. M., "Sintering Theory and Practice," John Wiley & Sons, New York (1996) pp. 9 and 181-191.
11) Chase, M. W., Jr., NIST-JANAF Thermochemical Tables, 4th ed. the American Ceramic Society and the American Institute of Physics for the National Institute of Standards and Technology, Maryland, 1998.
12) Lefort, P. and Billy, M., *J. Am. Ceram. Soc.*, Vol. 76, pp. 2295-2299 (1993).
13) Lide, D. R., "CRC Handbook of Chemistry and Physics-72nd Edition 1991-1992"; Chemical Rubber Publishing Company, Boston (1991) pp. 4-50.

Journal of the Ceramic Society of Japan 115 [3] 195-200 (2007)

Paper

Oxidation Behavior of Magnesium Aluminum Oxynitride

Wenbin DAI,*,** Akira YAMAGUCHI,* Wei LIN,* Junji OMMYOJI,* Jingkun YU** and Zongshu ZOU**

*Okayama Ceramics Research Foundation, 1406-18, Nishikatakami, Bizen-shi, Okayama 705-0021

**School of Materials and Metallurgy, Northeastern University, Liao Ning, 110004, China

Oxidation behavior of spark plasma sintered (SPS) magnesium aluminum oxynitride (MgAlON) was investigated in this study. Monophase MgAlON without pores was easily obtained and evaporation was sufficiently limited by the utilization of the SPS process. The MgAlON powder was oxidized above 750°C, and a detectable mass gain of the MgAlON plate could not be obtained below 1200°C, because the oxidation reaction was of a very low level and occurred only on the surface. High temperature were favorable to oxidation reaction. According to the isothermal mass gain and evolution of oxidized morphology of the plates oxidized at different temperature, it could be deduced that the oxidation of MgAlON was limited by interface reaction. To analyze more profoundly, an oxidation model was proposed. [Received November 1, 2006; Accepted December 18, 2006]

Key-words : *Magnesium aluminum oxynitride (MgAlON), Oxidation behavior, Spark plasma sintering (SPS), Interface reaction, Controlling step*

1. Introduction

Magnesium aluminum oxynitride (MgAlON), a solid solution material with high melting point, was proposed by Jack in 1976.[1] And some relative studies, such as oxidation behavior,[2),3)] reactivity,[4)] and synthesis processes,[5)-7)] have been carried out recently. As an oxynitride, oxidation behavior is one of the most important high-temperature properties and the overall oxidation reaction follows

$$MgAlON + O_2 \longrightarrow MgAl_2O_{4SS} + Al_2O_3 + N_2 \qquad (1)$$

Wang et al.[2),3)] have investigated some properties of hot pressed MgAlON and proposed that the oxidation of MgAlON would be limited by gas diffusion because of the protective of oxidized layer. However, as shown in **Fig. 1**, the oxidized layer of MgAlON is porous though the tested sample is in full density. Obviously, gas diffusion in the oxidized layer may not be the controlling steps during the oxidation of MgAlON. So the oxidation behavior of MgAlON needs further research.

On the other hand, according to the thermodynamic analysis,[7)] it is known that evaporation occurs at high temperature and rapid heating process might be favor to decrease the effect. Though some efforts have been taken to decrease the evaporation of MgAlON, they are not so efficient because of their long soaking time at high temperature.[5)] Moreover, to decrease the effect of impurity and pores on the investigation of oxidation behavior, dense samples in high purity are required. Fortunately, a newly developed sintering technical, spark plasma sintering (SPS), with application of mechanical pressure and an on-off DC current, is an efficient means to prepare dense samples in short time.[8)] That's why SPS is used to prepare MgAlON in our present experiment.

Raw materials with the composition same as Wang et al.[2)] are utilized and our objective here is to further study the oxidation behavior of MgAlON and find a more reasonable oxidation model.

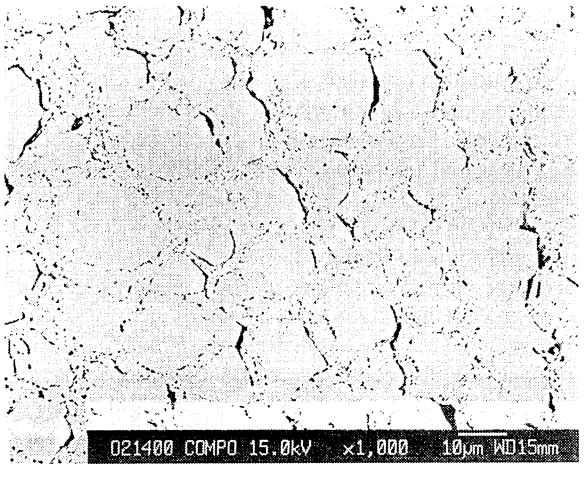

Fig. 1. Morphology of MgAlON oxidized at 1400°C for 14.5 h, black areas are pores or cracks.

2. Experimental procedure

2.1 Sample preparation

High purity starting materials in small size, MgO (0.24 μm, >99.9%), Al_2O_3 (0.1 μm, >99.99%), and AlN (0.7 μm, >99.2%), with molar proportions of 4 : 13 : 3 were meticulous weighed before milled in pet with alumina balls by using ethanol as dispersion. Subsequently, the slurry was vacuum dried in rotary evaporator (Model BUCHI R-134 rotavapor, SIBATA, Tokyo, Japan) and then the dried powders were placed in a graphite die and then set in SPS system (Model DR. SINTER 820S, Sumitomo Heavy Industries, Ehime, Japan). After the chamber was evacuated to less than 5 Pa and flushed with nitrogen (purity >99.999%), repeatedly, the green samples were heated to 1700°C in 20 min and then held at 1700°C for 10 min under the pressure of 30 MPa.

The plates for oxidation test were cut from SPSed samples by using a conventional mechanical cutting procedure. After ground with a diamond wheel to 10×10×3.6 mm, the plates were rough polished and the edges were chamfered at 45°. On the other hand, some SPSed samples were pulverized into less than 10 μm in an agate mortar to prepare powders for oxidation test.

2.2 Oxidation test

Oxidation tests of the powders and plates prepared by SPS were conducted under dry air flowing on thermo-gravimeter (TG, Model TG/DTA 6300, Seiko Instruments, Tiba, Japan) (Pt crucible, 0.2 l min^{-1}) and $MoSi_2$ furnace (ventilating Pt net, 2 l min^{-1}), respectively. Moreover, the mixed raw powders after drying were also tested by TG. The non-isothermal tests of powders and plates were conducted with the warming

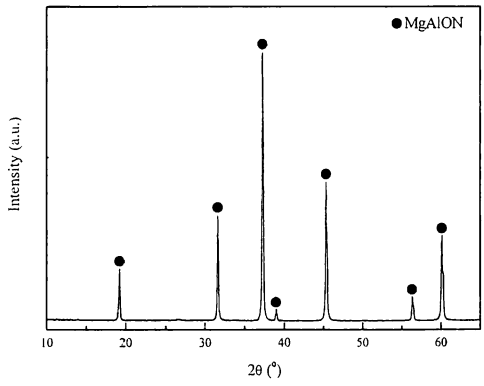

Fig. 2. XRD pattern of synthesized material.

up rate at 5°C min^{-1}. As to the isothermal oxidation of plates, they were placed into the furnace later after that had arrived the setting temperature for 30 min. The oxidized plates were cut parallel and about 5 mm to the edge and the cross sections were polished up to 0.5 μm. All the polished plates were ultrasonically cleaned in ethanol and then kept in desiccators before characterization.

2.3 Characterization

Microstructure and element distribution were characterized by field emission scanning electron microscope (FE-SEM, Model JSM6340F, JEOL, Tokyo, Japan) equipped with energy-dispersive X-ray spectroscope (EDAX). Phase composition was determined by X-ray diffraction (XRD, Model RINT2200, Rigaku, Tokyo, Japan). The content of Mg and Al was measured by X-ray fluorescence spectroscope (XRFS, Model Simultix12, Rigaku, Tokyo, Japan), and O, N by oxygen and nitrogen analyzer (Model EMGA650, HORIBA, Kyoto, Japan). Bulk density was measured by automatic gravimeter (Model SGM-6, Mettler-Toledo International, Ohio, USA) and true density was analyzed by multi pycnometer (Model MVP-1, YUASA IONICS, Massachusetts, USA).

3. Results and discussion

3.1 Phase composition and structure of prepared sample

As shown in **Fig. 2**, monophase MgAlON was obtained by SPS in a rapid heating process. Excitingly, as listed in **Table 1**, the difference of chemical composition between raw materials and prepared MgAlON was so small that the evaporation was sufficiently limited in present work. Moreover, as shown in **Fig. 3**, the synthesized sample was so dense that pores could not be seen in the matrix, and by the further testing, the density of sample was higher than 99.9% and it was denser than the ever reported.[9] So, SPS process should be a better choice to prepare MgAlON than other processes.

3.2 Oxidation behavior of powders

Figure 4 shows the weight change of mixed raw powders and SPSed MgAlON powders. As the grain size of the raw powders was so small, it was inevitable that some water was attached, which may be reasonable to explain why the weight loss below 700°C. Oxidation of MgAlON powders and raw powders almost started at about 750°C and maximum weight change of raw powders caused by oxidation reaction was about 1.8% while that of prepared MgAlON powders was about 4.0%. As the chemical composition of raw powders had not obvious difference to the MgAlON powders (Table 1), there was an abnormal weight change during the oxidation MgAlON according to Eq. (1). The possible reason for the abnormal weight change was still unknown and it need further study.

Table 1. Chemical Composition of Mixed Raw Powders and SPS Prepared Sample (mass%)

	Raw materials	Prepared sample	Difference
Mg	5.98	5.98	0
Al	48.59	48.51	0.08
O	42.97	42.89	0.08
N	2.35	2.19	0.16

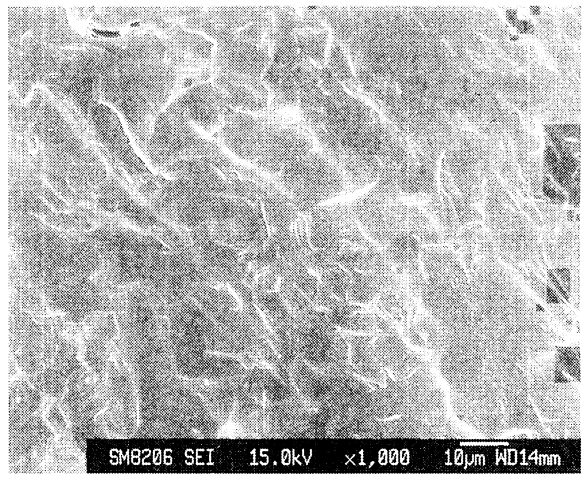

Fig. 3. Cross section micrograph of prepared sample.

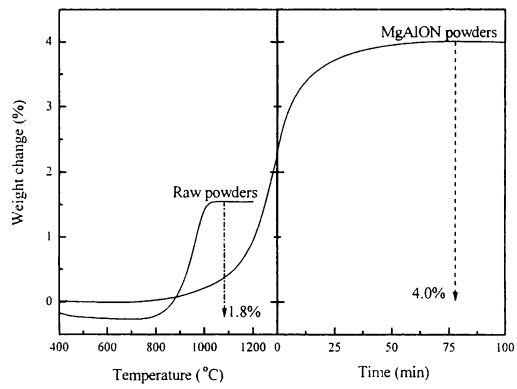

Fig. 4. Weight change ($W=\Delta m/m$) of mixed raw powders and prepared MgAlON powders.

3.3 Oxidation behavior of plates

Isothermal mass gain of plates oxidized at different temperature is shown in **Fig. 5**. Mass gain of plates oxidized at 1200°C followed a parabolic law and that of plates oxidized at higher temperature close obeyed linear laws. As mass gain would obey a parabolic rate law when the reaction was limited by gas diffusion and follow a linear law when controlled by interface reaction,[10] interface reaction might be the controlling step during the oxidation of MgAlON. However, Wang et al.[2] considered that the gas diffusion would be the controlling step from 1200°C-1500°C except for the short initial surface oxidation reaction. On the other hand, since lots of pores and cracks existed in the oxidized region (Fig. 1), the resistance of gas diffusion was in low level. So, there were some flaws in the proposition of Wang et al. To clarify the oxidation behavior, the evolution of morphology of oxidized plates was dis-

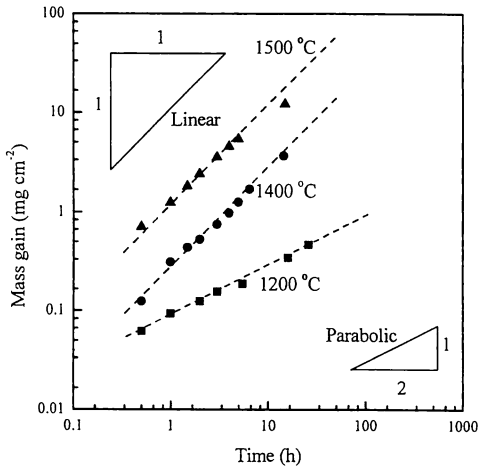

Fig. 5. Isothermal mass gain ($\alpha = W/S$, S is geometrical surface exposed to oxidation) of MgAlON plates oxidized at different temperature.

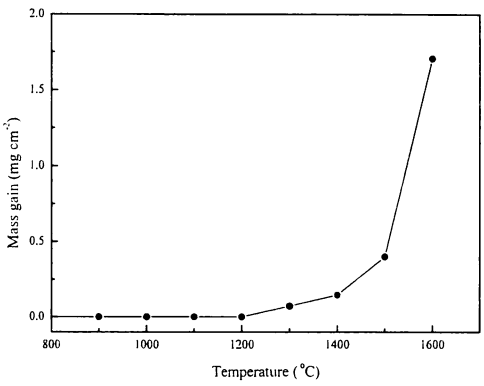

Fig. 6. Mass gain of MgAlON plates with respect to temperature.

cussed in Section 3.4. **Figure 6** illustrates the oxidation behavior of plates with respect to temperature. Detectable mass gain could not be obtained lower than 1200°C even the powder could be oxidized as low as 750°C (Fig. 5). Over 1200°C, the oxidation rate increased with the increasing of temperature and it got to a high speed at 1600°C.

3.4 Morphology of oxidized plates

Figure 7 shows the morphology of plate oxidized at 1200°C for 26 h. Since grain-boundary/surface intersections in single-phase ceramics were the most active centers for oxidation, stress concentrations might occur at these areas and pores or cracks would be formed.[12] In Fig. 7(a), cracks were recognized and micron-sized grains were discontinuously distributed on the surface of the oxidized plate, which implied that oxidation reaction had occurred and stress was generated during the oxidation process. According to the change of elemental distribution plotted in Fig. 7(c), an interface about 40 μm below the surface could be identified and the region with some change of element distributions was considered as oxidized layer and the region without obvious changes was un-oxidized layer. In the oxidized layer, cracks propagated along the grain boundaries, which implied that the stress caused by oxidation reaction was not so strong to crack the big grains. As cracks were formed on the surface and in the oxidized layer, the gas diffusivity would be in high level[10] and the gas partial pressures near the surface and the interface should not have big

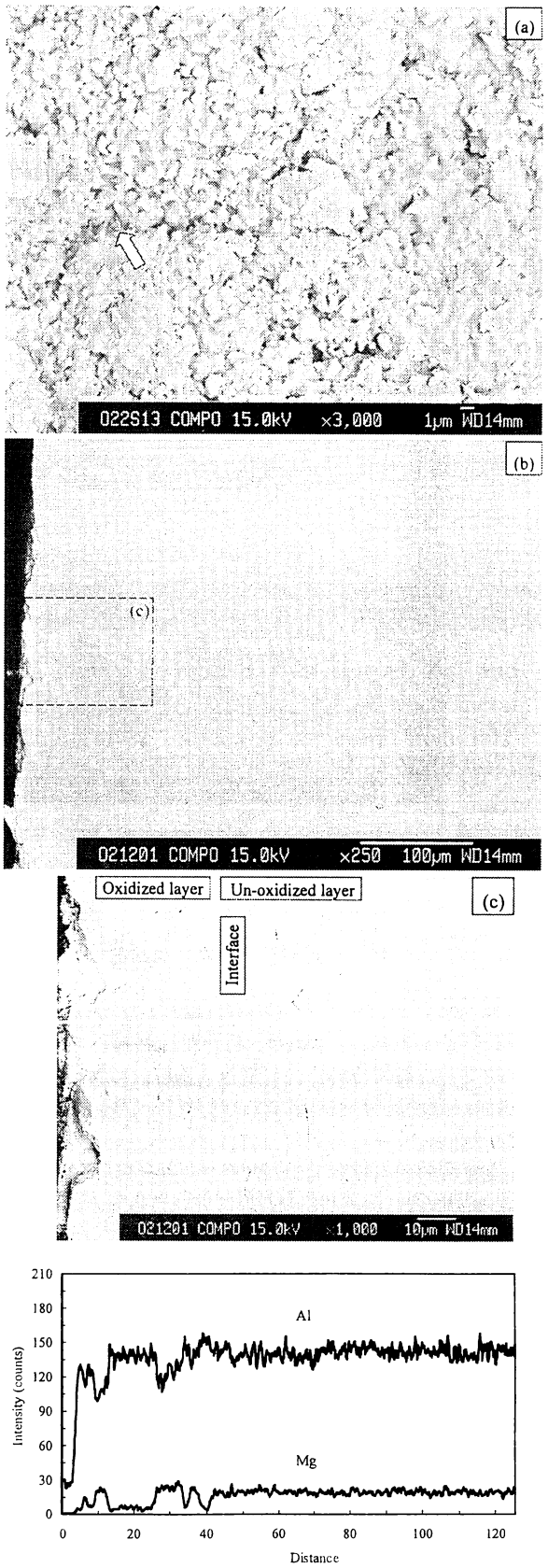

Fig. 7. Morphology of MgAlON plates oxidized at 1200°C (a) Surface, the arrow shows one of cracks on the surface, (b) polished cross section, and (c) magnified microstructure showing in (b) with the pattern of elemental distribution.

difference. Hence, oxidation reaction could not be prevented by the oxidized layer and gas diffusion should not be the con-

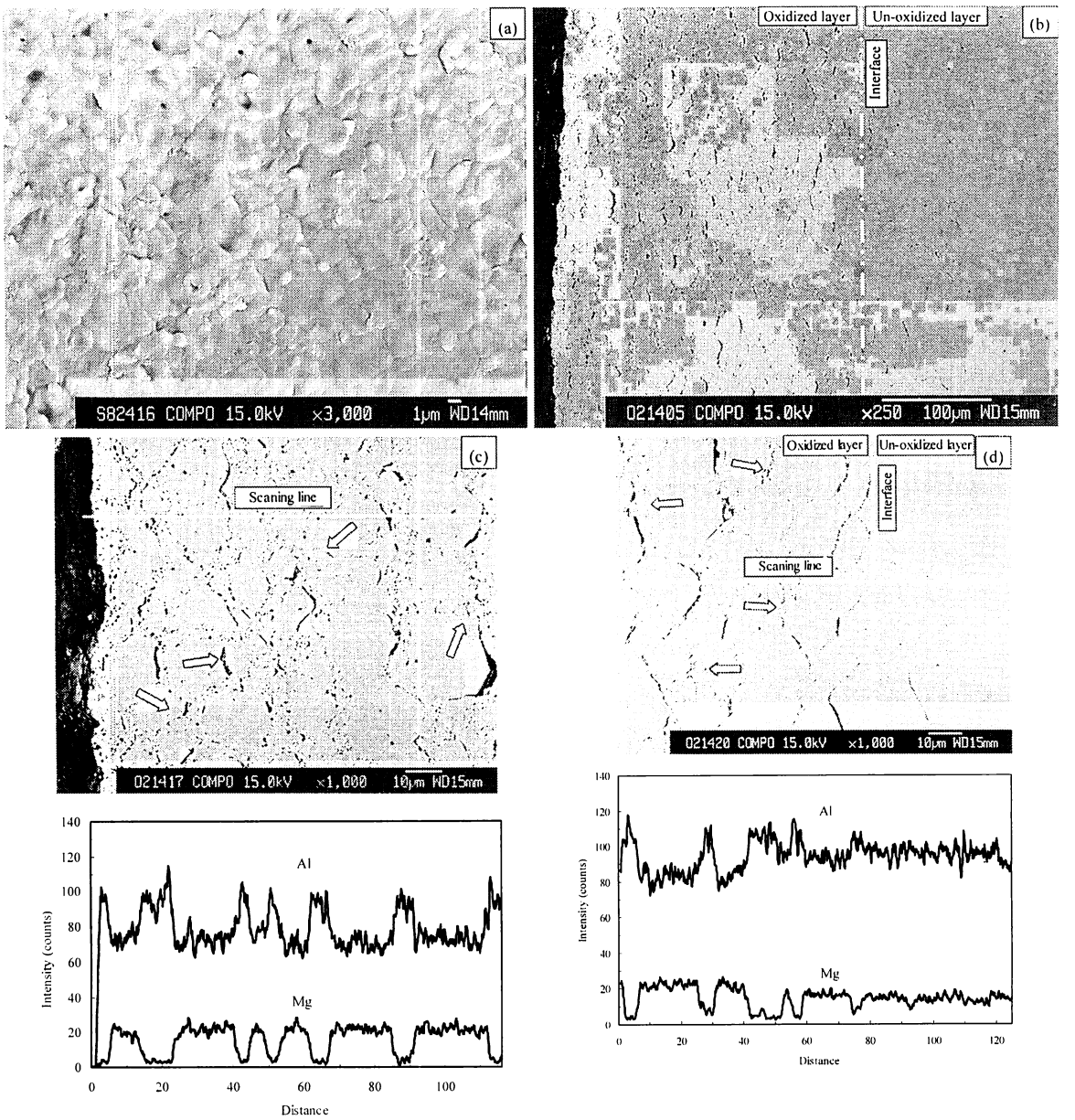

Fig. 8. Morphology of MgAlON plates oxidized at 1400°C (a) surface, (b) low magnified cross section, (c, d) high magnified cross sections near the surface and the interface with the pattern of elemental distribution, arrows show cracks of grains.

trolling step, though the mass gain followed a parabolic law (Fig. 5). Even oxidized at 1200°C for 26 h, the oxidation of MgAlON was kept in low level. Consequently, detectable mass gain could not be obtained below 1200°C during non-isothermal testing (Fig. 6). As stress was generated during oxidation process, the stability of grain boundary was decreased and some stresses would transfer to un-oxidized layer. Consequently, areas with residual stress, which was formed during sintering process, were very active and cracks were favor to be formed in these areas. Hence, as shown in Fig. 7(c), cracks along the grain boundary could be observed even about 70 μm below the interface. **Figures 8**(a) and (b) show the surface and inner morphology of plate oxidized at 1400°C. An interface between oxidized layer and un-oxidized layer could be distinguished easily. The morphology was very different to that of plate oxidized at 1200°C and lots of pores and cracks existed in the oxidized layer. Elemental distributions of Mg and Al near the surface and the interface are plotted in Figs. 8 (c) and (d). The dense thin surface layer (about 1 μm) and reticular materials around big grains were made of Al_2O_3. As the big grains were surrounded by Al_2O_3 and the content of Mg of the big grains in oxidized layer was higher than that in the un-oxidized layer, it could be deduced that Al_2O_3 were precipitated from big grains during oxidation reaction. If the oxidation of MgAlON was controlled by the gas diffusion, gradient of gas partial pressure should exist,[10),11)] and the morphology near the surface would be different to that near the interface. However, the morphology near the surface (Fig. 8 (c)) was very similar to that near the interface (Fig. 8(d)). Moreover, as lots of pores and cracks were formed in the oxidized layer, the resistance of gas diffusion by oxidized layer should in low level. In addition, as described in Fig. 5, the mass gain behavior of plates oxidized at 1400°C followed a linear law. Hence, gas diffusion would not be the controlling step during oxidation of MgAlON and interface reaction should be the case. In samples oxidized at 1400°C, the stress yielded by oxidation reaction was so stronger that that big grain could not withstand and cracks of big grain were

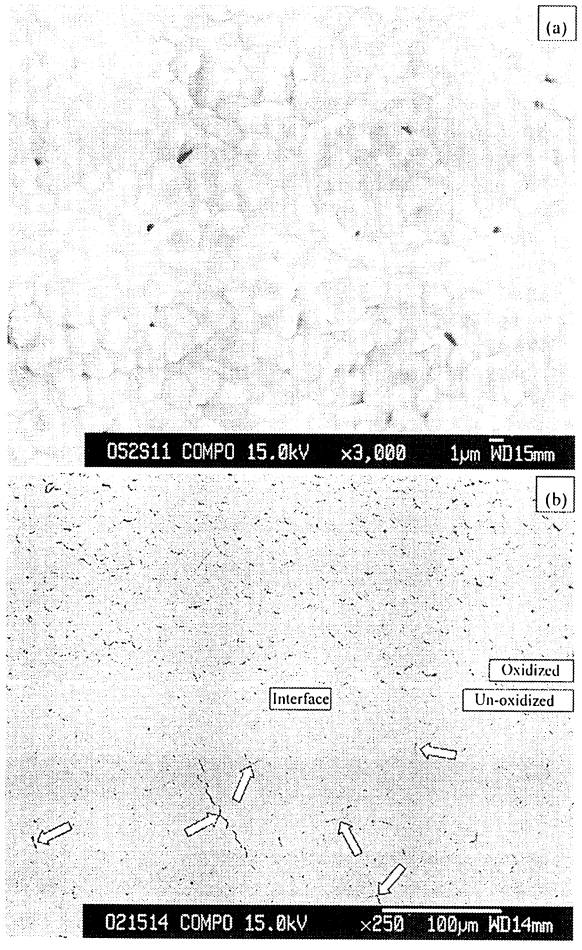

Fig. 9. Morphology of MgAlON plates oxidized at 1500°C (a) surface, (b) polished cross section, arrows show cracks along grain boundary below the interface.

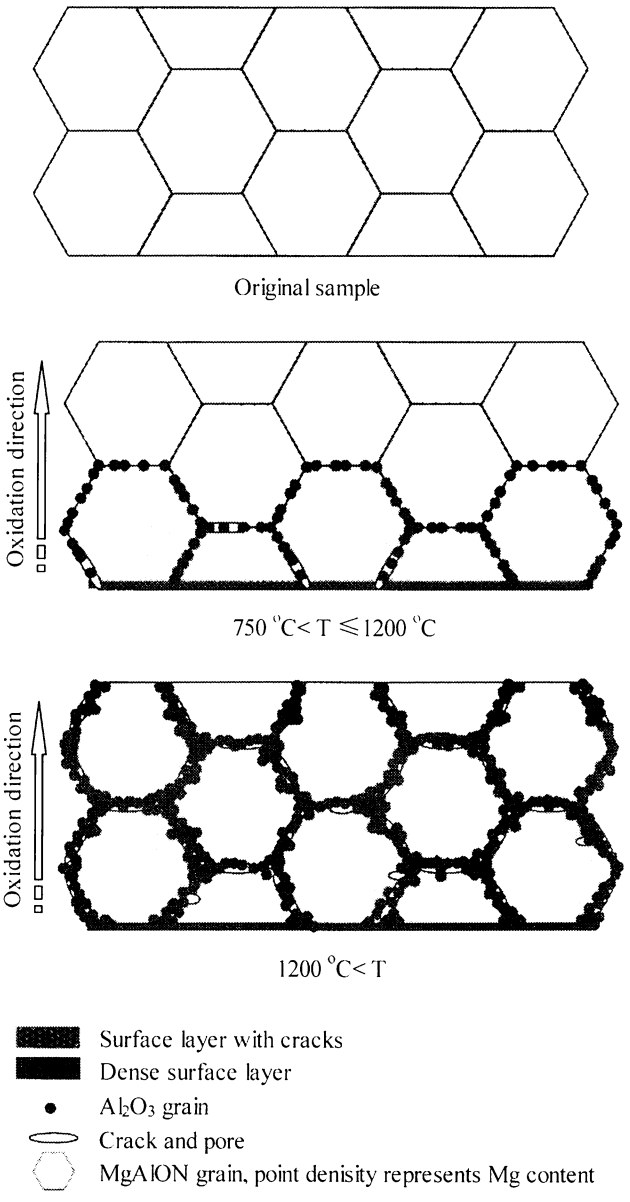

Fig. 10. Schematic of oxidation model of MgAlON at different temperature.

observed. Consequently, the amount of stress transferred from oxidized layer to un-oxidized layer was increased and the cracks in the inner of the interface were more obvious. Hence, the resistance of interface was decreased and the oxidation reaction was in high rate. As to the MgAlON plate oxidized at 1200°C, the stress caused by oxidation was in low level and the interface could not be damaged easily. Hence, the oxidation rate was low and mass gain followed a parabolic law. But, the oxidation of MgAlON at 1200°C would also be controlled by interface reaction. The morphology of plate oxidized at 1500°C is shown in **Fig. 9**. Because of the increasing of oxidation temperature, the precipitated Al_2O_3 grains on the dense thin surface were more homogenous. Considering that the width of precipitated Al_2O_3 between big grains was thicker and the original big grains became smaller and smoother with the increasing of oxidation degree, it could be deduced that the big grains in oxidized region should be MgAlON. The oxidation interface became more illegible than that of plate oxidized at 1400°C and the amount of cracks in the inner of the interface was increased, which implied that the stress was increased with temperature. Hence, it was reasonable to assume that at 1600°C, the stress was much higher than 1500°C and as a result, the oxidation rate was very high (Fig. 6).

3.5 Oxidation model

According to the above discussion, an oxidation model could be schematically drawn in **Fig. 10**. When lower than 1200°C, the stress caused by oxidation was in low level, the interface could not be damaged easily and the further oxidation reaction was retarded. At higher temperature, stress caused by oxidation reaction was increased and even over the critical values that MgAlON grain could resist, the interface could not withstand the stress then oxidation proceeded on from surface to inside step by step in relative high rate.

4. Conclusions

Monophase magnesium aluminum oxynitride (MgAlON) without pores was obtained by spark plasma sintering (SPS) process and utilized to further investigate the oxidation behavior. Oxidation reaction of MgAlON powder started at about 750°C, and detectable mass gain of MgAlON plate could not observed below 1200°C because oxidation reaction was in very low level and occurred only on the surface. Higher temperature was favor to oxidation reaction and the reaction continued on from surface to inside step by step because the interface could not withstand the stress caused by oxidation reaction. From this work, it was clear that the oxidation of

MgAlON was limited by interface reaction and not by gas diffusion, which was proposed before. According to the evolution of morphology, a model for oxidation of MgAlON was proposed.

References

1) Jack, K. H., *J. Mater. Sci.*, Vol. 11, pp. 1135-1158 (1976).
2) Wang, X., Wang, F. and Li, W., *J. Inorganic Mater.*, Vol. 18, pp. 83-90 (2003) [In Chinese].
3) Wang, X., Li, W. and Seetharaman, S., *Z. Metallkd.*, Vol. 93, pp. 545-553 (2002).
4) Weiss, J., Greil, P. and Gauckler, L. J., *J. Am. Ceram. Soc.*, Vol. 65, pp. C68-C69 (1982).
5) Granon, A., Goeuriot, P., Thevenot, F., Guyader, J., L'Haridon, P. and Laurent, Y., *J. Eur. Ceram. Soc.*, Vol. 13, pp. 365-370 (1994).
6) Wang, X., Wang, H., Zhang, W., Sun, J. and Hong, Y., *Key Eng. Mater.*, Vol. 226, pp. 373-378 (2002).
7) Dai, W., Lin, W., Yamaguchi, A., Ommyoji, J., Yu, J. and Zhou, Z., *J. Ceram. Soc. Japan*, Vol. 115, pp. 42-46 (2007)
8) Shen, Z., Johnsson, M., Zhao, Z. and Nygren, M., *J. Am. Ceram. Soc.*, Vol. 85, pp. 1921-1927 (2002).
9) Granon, A., Goeuriot, P. and Thevenot, F., *J. Eur. Ceram. Soc.*, Vol. 15, pp. 249-254 (1995).
10) Luthra, K. L., *J. Am. Ceram. Soc.*, Vol. 74, pp. 1095-1103 (1991).
11) Narushima, T., Goto, T., Yokoyama, Y., Hagiwara, J., Iguchi, Y. and Hirai, T., *J. Am. Ceram. Soc.*, Vol. 77, pp. 2369-2375 (1994).
12) Cubicciotti, D., Lau, K. H. and Jones, R. L., *J. Electrochem. Soc.*, Vol. 12, pp. 1955-1956 (1977).

Journal of the Ceramic Society of Japan 115 [7] 409-413 (2007)

Paper

Oxidation Behavior of Magnesium Aluminum Oxynitride with Different Composition

Wenbin DAI,*,** Akira YAMAGUCHI,* Wei LIN,* Junji OMMYOJI,* Jingkun YU** and Zongshu ZOU**

*Okayama Ceramics Research Foundation, 1406-18, Nishikatakami, Bizen-shi 705-0021

**School of Materials and Metallurgy, Northeastern University, Liao Ning, 110004, China

Oxidation behavior of spark plasma sintered (SPS) magnesium aluminum oxynitride (MgAlON) with different composition was investigated in present work. Results showed that the variation in composition had not obvious effect on the density of MgAlON, but had some effect on excess weight change. Also found that the oxidation behavior of MgAlON was different with oxidation temperature, which was attributed to the transformation from γ-Al_2O_3 to α-Al_2O_3. Moreover, the excess weight change was ascribed to the existence of lots of vacancies in γ-Al_2O_3 and magnesium aluminate spinel ($MgAl_2O_4$ss).

[Received December 13, 2006; Accepted June 14, 2007]

Key-words: Magnesium aluminum oxynitride (MgAlON), Oxidation, Composition, Weight change

1. Introduction

As known, MgAlON can be inevitably oxidized under oxidation atmosphere at high temperature and the oxidation behavior is one of its most important properties. When MgAlON is oxidized under certain condition, α-Al_2O_3 and magnesium aluminate spinel ($MgAl_2O_4$ss) are detected in the oxidized product. The oxidation reaction of MgAlON proposed by Wang *et al.* is as fellows[1]

$$MgAlON + O_2 \longrightarrow MgAl_2O_{4ss} + Al_2O_3 + N_2 \qquad (1)$$

In their report, no intermediate oxidized products have been obtained. On the other hand, it has been reported that the solid solution of Al_2O_3 and AlN into $MgAl_2O_{4ss}$ forms MgAlON and the amount of dissolved materials has relatively wide ranges at high temperature.[2] So, oxidation behavior and density of MgAlON might change with the composition. In addition, we have obtained an excess weight change during the oxidation of MgAlON powder in the previous study.[3] But, the effect of chemical composition on density and oxidation behavior has not been mentioned in the earlier reports.

Our objective here is to investigate the influence of chemical composition of MgAlON on its density and excess weight change, and to further discuss the oxidation mechanism of MgAlON at elevated temperature.

2. Experimental procedure

2.1 Preparation of MgAlON

The raw materials of MgO (particle size, ~0.24 μm; purity, >99.9%), Al_2O_3 (~0.1 μm; >99.99%), and AlN (~0.7 μm; >99.2%) were meticulously weighed according to **Table 1**, and milled with alumina balls by using ethanol as dispersion. Subsequently, the slurry was dried in a vacuum rotary evaporator (Model BUCHI R-134 rotavapor, SIBATA, Tokyo, Japan) and then the dried powders were placed in a graphite die and set in a SPS machine (Model DR. SINTER 820S, Sumitomo Heavy Industries, Ehime, Japan). After the chamber was repeatedly evacuated to less than 5 Pa and flushed with nitrogen (purity>99.999%), the samples were heated to 1700°C in 20 min and then held at 1700°C for 10 min under the pressure of 30 MPa.

2.2 Oxidation test

In present work, the oxidation behavior of MgAlON powders and plates was integrally surveyed. The powders less than 10 μm were pulverized from the SPSed samples in an agate mortar. The plates were cut from the SPSed samples by using a conventional mechanical cutting procedure. After ground with a diamond wheel to 10×10×3.6 mm, the plates were roughly polished with the edges chamfered at 45°. The oxidation tests of the powders and plates were conducted under flowing dry air by a thermo-gravimetry (TG, Model TG/DTA 6300, Seiko Instruments, Tiba, Japan) (Pt crucible, 0.2 l min^{-1}) and a $MoSi_2$ furnace (ventilating Pt net, 2 l min^{-1}), respectively. The oxidation tests of powders were carried out with the heating rate at 5°C min^{-1} and then soaked at different temperature for presetting time. The plates were placed into the furnace later after the furnace had arrived the setting temperature for 30 min. Then, the oxidized plates were cut along the middle lines and the cross sections were well polished. All the polished plates were ultrasonically cleaned in an ethanol and then kept in a desiccate before characterization.

Table 1. Composition of Raw Materials in Molar Ratio and Mass Percent

	S1		S2		S3*		S4*		S5*		S6*	
	Molar ratio	Mass%	Molar ratio	Mass%	Molar ratio	Mass%	Molar ratio	Mass%	Moral ratio	Mass%	Molar ratio	Mass%
MgO	1	3.38	4	17.49	4	9.94	5.21	12.57	6.41	15.04	7.62	17.38
Al_2O_3	10	86.22	7	78.03	13	82.41	13	80.01	13	77.75	13	75.61
AlN	3	10.40	1	4.48	3	7.64	3	7.42	3	7.21	3	7.01

* S4-S6 is 3 mass%, 6 mass%, and 9 mass% of additional MgO added into S3, respectively.

2.3 Characterization

Microstructures and elemental distributions were observed by field emission scanning electron microscope (FE-SEM, Model JSM-6340F, JEOL, Tokyo, Japan) equipped with energy-dispersive X-ray spectroscopy (EDAX) and SEM (Model JXA-8621MX, JEOL, Tokyo, Japan) equipped with wavelength dispersion spectrometer (WDS). Phases were identified by X-ray diffraction (XRD, Model RINT2200, Rigaku, Tokyo, Japan) by using Si (purity > 99.999 mass%) powders as internal standard material. The contents of Mg and Al were measured by X-ray fluorescence spectroscopy (XRFS, Model Simultix12, Rigaku, Tokyo, Japan), and those of O and N were tested by oxygen and nitrogen analyzer (Model EMGA650, HORIBA, Kyoto, Japan). The bulk density was measured by an automatic gravimetry (Model SGM-6, Mettler-Toledo International, Ohio, USA) and the true density was analyzed by a multi pycnometer (Model MVP-1, YUASA IONICS, Massachusetts, USA).

3. Results and discussion

3.1 Properties of prepared samples

All the SPSed samples were identified by XRD as monophase MgAlON. The relative densities were higher than 99.9%, and as shown in **Fig. 1**, pores were seldom in these samples.

As listed in **Table 2**, though the samples had some difference in chemical composition, the deviation of the true densities was very small. So, the influence of the amount of dissolved Al_2O_3 and AlN could be neglected. The conclusion expanded the viewpoint on the solid solution of cubic spinel, for Nakagawa has proposed that the amount of dissolved Al_2O_3 has a minor influence on the density of $MgAl_2O_{4ss}$.[4)]

3.2 Effect of oxidation conditions on weight change and product

Figures 2 and **3** show XRD patterns of S3 oxidized at variation conditions and their maximum weight changes (W_M) during oxidation process, respectively. The oxidation rate was very slow below 1000°C. When above it, the oxidation rate dramatically increased. Worth to note that though the weight changes were obtained in the samples oxidized as low as 900°C, the XRD patterns of their products were still similar to that of MgAlON until to 1100°C. When oxidized at 1200°C, α-Al_2O_3 was detected in the oxidized products besides the cubic spinel crystalline.

3.3 Effect of oxidation conditions on the microstructure of plates

Figures 4(a)-(d) show the BSE image and X-ray dot maps for Mg, Al, and O obtained from an area beside the interface of oxidized layer and un-oxidized layer of S1 oxidized at 1400°C for 14.5 h. Figure 4(e) shows the distribution of N of a big grain in the oxidized layer approaching to the interface.

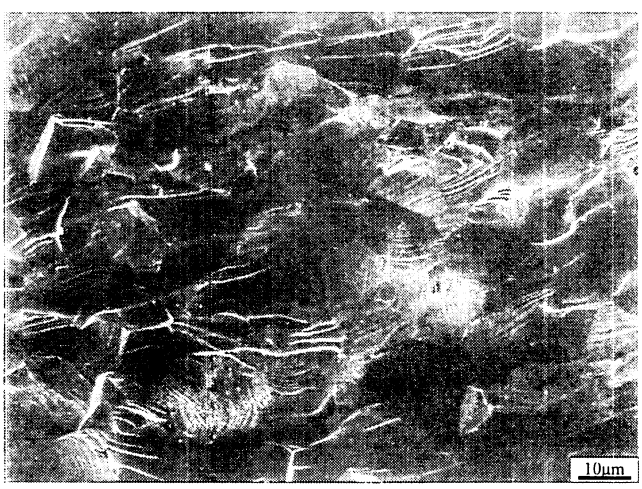

Fig. 1. SE image of cross section of S1.

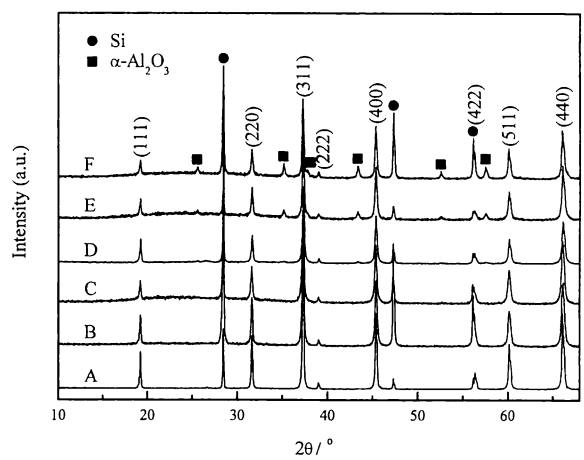

Fig. 2. XRD patterns of the oxidized products of S3 oxidized at different condition. (A) synthesized SPSed sample, (B) oxidized at 900°C for 12 h, (C) oxidized at 1000°C for 12 h, (D) oxidized at 1100°C for 6 h, (E) oxidized at 1200°C for 3 h, and (F) oxidized at 1300°C for 3 h.

Table 2. Chemical Composition (mol%) and True Densities of the SPSed Samples as well as Some Results about Weight Change

	S1	S2	S3	S4	S5	S6
Mg	1.67	8.68	5.10	6.28	7.54	8.68
Al	39.82	33.74	36.80	35.82	34.91	34.01
O	53.85	56.09	54.90	54.83	54.65	54.55
N	4.66	1.49	3.20	3.08	2.90	2.75
True density (g cm^{-3})	3.67	3.62	3.65	3.64	3.64	3.63
Theoretical weight change (W_T)	2.28	0.73	1.56	1.51	1.42	1.35
maximum weight change(W_M)	4.77	2.13	4.01	3.59	3.33	2.76
Excess weight change (W_E)	2.49	1.40	2.45	2.08	1.91	1.41

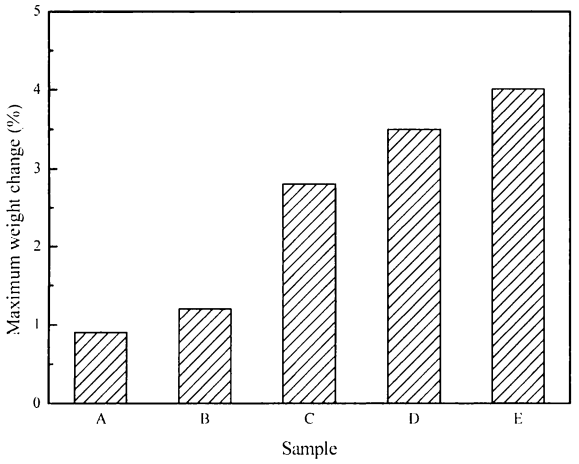

Fig. 3. Maximum weight change of S3 oxidized at different condition. (A) oxidized at 900°C for 12 h, (B) oxidized at 1000°C for 12 h, (C) oxidized at 1100°C for 6 h, (D) oxidized at 1200°C for 3 h, and (E) oxidized at 1300°C for 3 h.

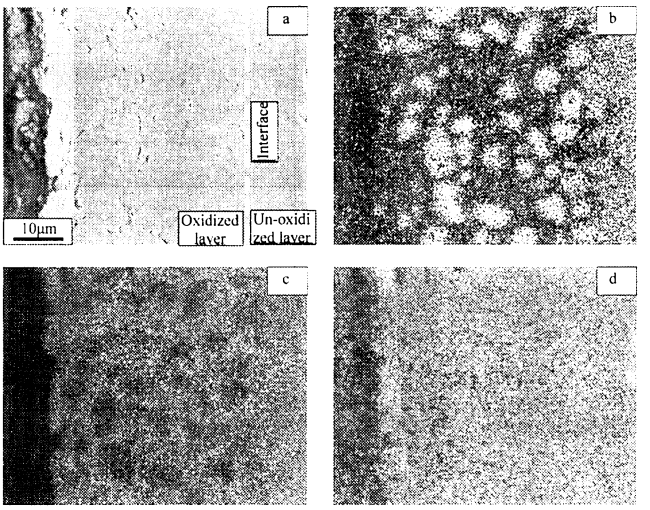

Fig. 5. (a) BSE image and X-ray dot maps for (b) Mg, (c) Al, and (d) O obtained from a polished cross section of S1 oxidized at 1200°C.

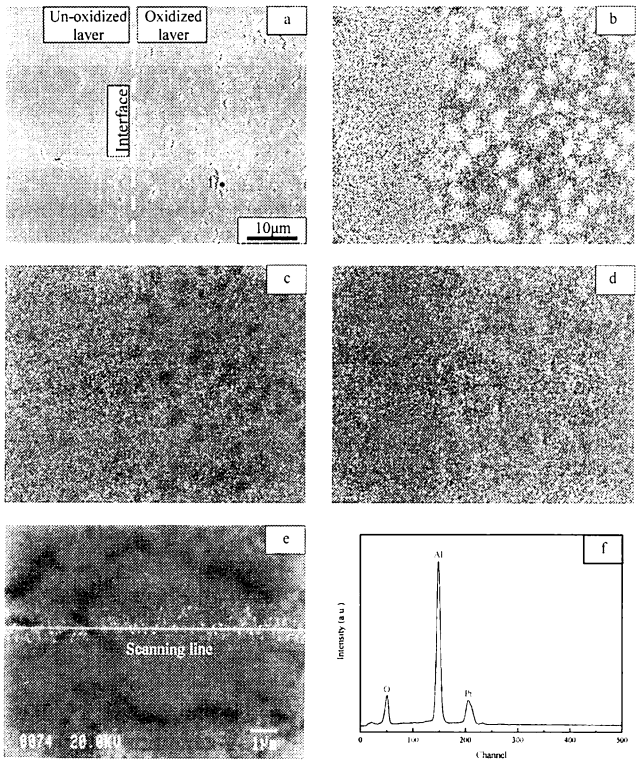

Fig. 4. (a) BSE image and X-ray dot maps for (b) Mg, (c) Al, and (d) O, (e) the distribution of N determined by WDS, (f) EDS result of the point in (a).

Moreover, an EDS result of the material surrounding a big grain in the oxidized layer is illustrated in Fig. 4(f). As shown in Fig. 4(a), even the oxidized layer was very porous, only small amount of cracks and pores was in the un-oxidized layer. From Figs. 4(b)-(e), it was very interesting to found that N remained in the big grain and the content of Mg of the big grains was higher than that in the un-oxidized layer. So, the big grains were MgAlON with high content of Mg. Moreover, as shown in Fig. 4(f), only Al and O existed in the materials surrounding the big grains. Hence, during the oxidation of MgAlON, the precipitation of Al_2O_3 caused the enrichment of Mg of MgAlON grains in the oxidized layer.

Figures 5(a)-(d) illustrate BSE image and X-ray dot maps for Mg, Al, and O obtained from S1 oxidized at 1200°C for 26 h. Worth to note that though lots of Al_2O_3 were precipitated in the oxidized layer, the amount of pores and cracks was small. In addition, the size of MgAlON grains in the oxidized layer was much bigger than that in the S1 oxidized at 1400°C.

3.4 Oxidation mechanism of MgAlON

During the oxidation of single phase ceramics, stress always concentrated at grain-boundary/surface intersections. When the stress exceeded a critical value, pores and cracks were formed in the structure. In respect that the densities of MgAlON (Table 2) approximated to those of γ-Al_2O_3 ($\sim$3.5 g cm^{-3})[5] and $MgAl_2O_{4ss}$ ($\sim$3.6 g cm^{-3})[4] and much lower than that of α-Al_2O_3 ($\sim$3.97 g cm^{-3}),[5] stress aroused from the oxidation of MgAlON was much lower when γ-Al_2O_3 was the oxidation product rather than α-Al_2O_3. Thus, the amount of formed pores and cracks was small when γ-Al_2O_3 was the main phase in the precipitated Al_2O_3; When α-Al_2O_3 was the main phase, lots of pores and cracks were formed. On the other hand, even γ-Al_2O_3 could transfer to α-Al_2O_3 as low as 1000°C, the rate of conversion was very low until to 1200°C. At higher temperatures, the rate of the phase transformation increased with temperature.[6] Figure 5 revealed that the microstructure of the plate oxidized at 1200°C kept dense with lots of Al_2O_3 precipitation. So, γ-Al_2O_3 must form during the oxidation of MgAlON and it was the main product of the precipitated Al_2O_3 at this condition. Because of phase transformation, stress was intense when oxidized at 1400°C. As shown in Fig. 4, lots of pores and cracks were formed in the oxidized layer. In addition, in view of the similarity of XRD patterns among γ-Al_2O_3, $MgAl_2O_{4ss}$, and MgAlON, the formation of γ-Al_2O_3 was not observable by XRD pattern of necessity (Fig. 2). So, Wang et al. did not found the intermediate oxidation product.

According to the above discussion, the oxidation reaction of MgAlON could be divided into two regimes:

(I) $750°C < T \leq 1200°C$

$$\text{Step1: } (\text{MgAlON})_{(\text{low Mg})} + O_2 \longrightarrow \text{MgAlON}_{(\text{high Mg})} + \gamma\text{-}Al_2O_3 + N_2 \quad (2)$$

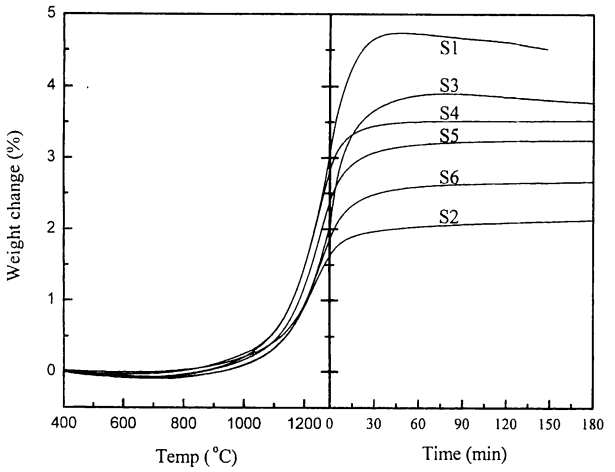

Fig. 6. Weight changes ($W=\Delta m/m$, m is the weightiness before testing, Δm is the change of weightiness) of prepared samples with different composition with respect to the oxidation temperature and soaking time.

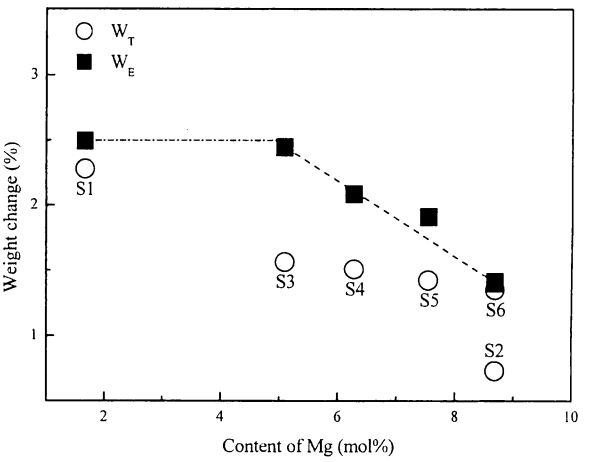

Fig. 7. Theoretical weight change (W_T) and excess weight change (W_E) of prepared samples with respect to content of Mg.

Step2: $(MgAlON)_{(high\ Mg)} + O_2 \longrightarrow MgAl_2O_{4ss} + \gamma\text{-}Al_2O_3 + N_2$ (3)

(II) $1200°C < T$

Step1: $(MgAlON)_{(low\ Mg)} + O_2 \longrightarrow MgAlON_{(high\ Mg)} + \gamma\text{-}Al_2O_3 + N_2$ (4)

Step2: $\gamma\text{-}Al_2O_3 \longrightarrow \alpha\text{-}Al_2O_3$ (5)

Step3: $(MgAlON)_{(high\ Mg)} + O_2 \longrightarrow MgAl_2O_{4ss} + \alpha\text{-}Al_2O_3 + N_2$ (6)

3.5 Effect of composition on excess weight change

Weight changes of the MgAlON powders with different composition versus oxidation temperature and soaking time are shown in **Fig. 6**. All the samples were oxidized above 750°C, and the weight changes of S1 and S3 had a decrease with the prolonging soaking time. According to Eq. (1), the theoretical weight changes (W_T) were calculated and shown in **Fig. 7** and Table 2. But, all of them were lower than W_M obtained from TG analysis. In present work, the excess weight changes (W_E) were defined as

$$W_E = W_M - W_T \quad (7)$$

and shown in Fig. 7.and Table 2. From Fig. 7, it was very interesting to observe that W_E decreased almost in linear according to the equation,

$$W_E = -29.07 \times [Mg]\% + 3.9285 \quad (5 < [Mg] < 9) \quad (8)$$

with [Mg]% in mol% in the MgAlON phase. But, when the content of Mg was less than 5 mol%, W_E had not obvious change.

It was reported that the oxidation of oxynitride was the substitution of N by O, and the discharged N was in atomic state.[6] In addition, if oxidized product had vacancies, the N and other elements had chance to occupy the vacancies when the elements diffused through the material. Thus, excess *weights change was obtained.*[7] In Eqs. (2)-(6), $\gamma\text{-}Al_2O_3$ and $MgAl_2O_{4ss}$ were the materials with lots of vacancies.[8)-10)] So, excess weight changes occurred during the oxidation of MgAlON.

Referring to relative diagram,[11] the MgAlON with higher content of N and lower content of Mg led to more $\gamma\text{-}Al_2O_3$ formation, and vice versa. In view of the law of phase transformation,[6] it was known that the amount of remained $\gamma\text{-}Al_2O_3$ could be neglected when the samples with high content of Mg and low content of N oxidized at 1300°C. Hence, the excess weight changes of these samples were solely ascribed to the dissolution of elements into $MgAl_2O_{4ss}$. As $MgAl_2O_{4ss}$ was stable at this condition, the weight changes were constant with the prolonging soaking time (Fig. 6). On the contrary, some $\gamma\text{-}Al_2O_3$ might remain initially when the samples with high content of N and low content of Mg oxidized at 1300°C. So, the excess weight changes were caused by the dissolution of elements into $\gamma\text{-}Al_2O_3$ and $MgAl_2O_{4ss}$. Since $\alpha\text{-}Al_2O_3$ was the crystal with fewer vacancies, the dissolved elements in $\gamma\text{-}Al_2O_3$ in the initial stage were discharged with the prolonging soaking time. Thus, as shown in Fig. 6, the weight change of S1 and S3 had a decrease.

In addition, due to the decrease of the Mg site to accept the excess Al ion, the solubility of elements increased with the decreasing of the content of Mg.[12] Thus, the excess weight change decreased with the content of Mg (Fig. 7). However, it was unknown until now why the excess weight change had not obvious change when the content of Mg was less than 5 mol%.

4. Conclusions

The present work mainly investigated the oxidation behavior of spark plasma sintered (SPS) magnesium aluminum oxynitride (MgAlON) with different composition. The variation of composition almost no affect on density but had some effects on excess weight change. Because of the transformation from $\gamma\text{-}Al_2O_3$ to $\alpha\text{-}Al_2O_3$ at high temperature, the oxidation behavior of MgAlON was different with oxidation temperature. Moreover, the excess weight change was ascribed to the vacancies of $\gamma\text{-}Al_2O_3$ and magnesium aluminate spinel ($MgAl_2O_{4ss}$).

References

1) Wang, X., Li, W. and Seetharaman, S., *Z Metallkd.*, Vol. 93, pp. 545-553 (2002).
2) Weiss, J., Greil, P. and Gauckler, L. J., *J. Am. Ceram. Soc.*, Vol. 65, pp. C68-C69 (1982).
3) Dai, W., Lin, W., Yamaguchi, A., Ommyoji, J., Yu, J. and Zhou, Z., *J. Ceram. Soc. Japan*, Vol. 115, pp. 195-200 (2007).
4) Nakagawa, Z., *Ceram. Trans.*, Vol. 71, pp. 283-94 (1996).
5) Lide, D. R., "CRC Handbook of Chemistry and Physics-72nd

ed., 1991-1992", Chemical Rubber Publishing Company, Boston (1991) pp. 4-50.
6) Goursat, P., Billy, M., Goeuriot, P., Labbe, J. C., Villechenoux, J. M., Roult, G. and Bardolle, J., *Materials chemistry*, Vol. 6, pp. 81-94 (1981) [in France].
7) Goursat, P., Goeuriot P., and Billy M. *Materials chemistry*, Vol. 1, pp. 131-149 (1976) [in France].
8) Wang, Y., Bronsveld P., and DeHosson, J., *J. Am. Ceram. Soc.*, Vol. 81, pp. 1655-1600 (1998).
9) Sickafus, K, and Wills, J., *J. Am. Ceram. Soc.*, Vol. 82, pp. 3279-3292 (1999).
10) Kryukova, G., Klenov, D., Ivanova, A. and Tsybulya, S., *J. Euro. Ceram. Soc.*, Vol. 20, pp. 1187-1189 (2000).
11) Howald, R. and Roy, B., *Calphad: Comput. Coupling Phase Diagrams Thermochem.*, Vol. 15, pp. 159-172 (1991).
12) Okuyama, Y., Kurita, N. and Fukatsu, N., *Solid State Ionics*, Vol. 177, pp. 59-64 (2006).

Available online at www.sciencedirect.com
ScienceDirect
materials letters
Materials Letters 61 (2007) 45–49
www.elsevier.com/locate/matlet

Preparation of slaking resistant CaO aggregate from lightweight $CaCO_3$ with oxide addition

Min Chen [a,*], Nan Wang [a], Jingkun Yu [a], Akira Yamaguchi [b]

[a] School of Materials and Metallurgy, Northeastern University, 3-11 Wen-Hua Road, Shenyang, 110004, China
[b] Okayama Ceramics Research Foundation, 1406-18 Nishi Katakami, Bizen, Okayama, 705-0021, Japan

Received 8 January 2006; accepted 2 April 2006
Available online 5 May 2006

Abstract

CaO aggregate was sintered from reagent-grade lightweight $CaCO_3$ powder by the addition of 0–20% (molar ratio) MgO and ZrO_2, respectively. The results showed that the CaO derived from lightweight $CaCO_3$ was highly sinterable and compact CaO aggregate with relative density above 96% was obtained after sintering at 1400 °C for 2 h, but further increase of compactness was restrained due to the occurrence of abnormal grain growth. The densification of the aggregate was promoted due to the behavior of oxide addition on restraining the grain growth of CaO. With increasing the amount of oxide addition, the microstructure of CaO aggregate underwent a restructuration process. Homogeneous microstructure, with well growing MgO grains occupying most of the boundary triple points of CaO grain, formed by the addition of 20% MgO. Especially when 20% ZrO_2 was added, $CaZrO_3$ layer formed around CaO grains. The slaking resistance of the aggregate was appreciably improved due to the promotion of densification, the formation of CaO solid solution (while MgO added) and the modification of microstructure.
© 2006 Elsevier B.V. All rights reserved.

Keywords: Lime refractories; Lightweight $CaCO_3$; MgO; ZrO_2; Sintering; Slaking resistance

1. Introduction

Lime has the properties of high melting temperature, low vapor pressure, and thermodynamic stability in the presence of carbon as well as high alkalinity, thus it has long been considered to be used as the raw materials for high temperature ceramics (such as crucible and ceramic filter), refractories and metallurgical accessories (such as refining slag and tundish covering powder) [1–5]. With the development of high temperature technology, lime containing materials are acting more and more important roles [6–11]. It is considered that application of CaO containing refractories is one of the essential directions for the development of metallurgical industries and other high temperature fields [12]. However, the application of CaO containing materials has been inhibited due to their drawback of poor slaking resistance, and many studies have been carried out on this subject [13–15].

Oftentimes, the slaking resistance of lime aggregate is improved by increasing its compactness, and the traditional manufacture technology to produce lime aggregate is by two steps: firstly lightburnt lime is derived from limestone, and then the deadburnt lime aggregate is obtained by heating lightburnt lime at temperature above 1700 °C which leads to high energy consumption. Therefore, it is essential to develop a new technology to produce compact slaking resistant lime aggregate.

It is reported that CaO derived directly from the decomposition of lightweight $CaCO_3$ is very reactive and highly sinterable [16,17]. In the present work, the sintering property and effect of oxide addition on densification and slaking resistance were studied using synthetic lightweight $CaCO_3$ as raw materials. The purpose of this work is to find a new economic way for producing dense slaking resistant lime aggregate.

2. Experimental procedure

The starting materials were lightweight $CaCO_3$ powder and oxide additives. The lightweight $CaCO_3$ powder was reagent

* Corresponding author. 312#, Northeastern University, 3-11 Wen-Hua Road, Shenyang, 110004, China. Tel.: +86 24 6368 2241; fax: +86 24 8368 1576.
E-mail address: slakejpa@163.com (M. Chen).

0167-577X/$ - see front matter © 2006 Elsevier B.V. All rights reserved.
doi:10.1016/j.matlet.2006.04.002

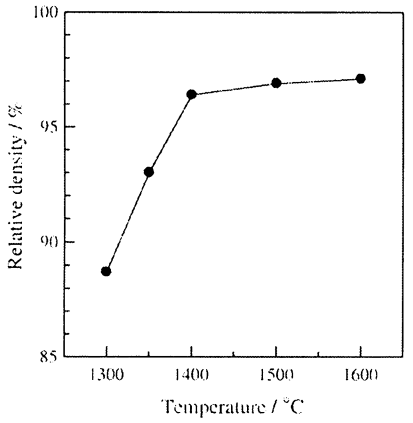

Fig. 1. The dependence of temperature on relative density of CaO aggregate sintered from lightweight $CaCO_3$.

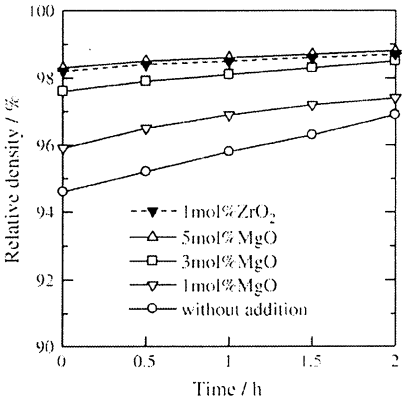

Fig. 3. Change of relative density of CaO aggregate with oxide additions sintered at 1500 °C for various times.

grade with average diameter of 0.9 μm that was prepared from reagent grade $CaCO_3$ by precipitation reaction (details as described in a previous work [16]). Oxide additives were MgO and ZrO_2 powders. The former, MgO powder, was derived from heating reagent-grade $Mg(OH)_2$ powder at 600 °C, while the later, ZrO_2 powder, was from Sumidomo Ltd, with average diameter of 0.046 μm and purity of 99.7%.

The two kinds of oxide powders were added to lightweight $CaCO_3$ respectively and wet-mixed with acetone using a ball mill in the molar proportion of CaO/oxide additive=$(100-x)/x$ (x=0–20). After being dried completely, the mixed powder was shaped into a 20 mm by 20 mm by ~7 mm sized compact by using a cold isostatic press (CIP) under a pressure of 100 MPa. The compacts were then heated to 1300–1600 °C at a rate of 10 °C/min in an electric furnace. After soaking at different temperatures, the sample was cooled at the same rate as that of heating.

The sintered samples were characterized by carrying out bulk density, phase composition, and microstructural analyses as well as a slaking test. Bulk density was measured by liquid displacement using Archimedes' principle in kerosene. Phase compositions were analyzed by X-ray powder diffraction (Cu target, 30 kV and 30 mA). Lattice parameter of the sintered CaO was calculated by program according to the d values of the 4 strongest diffraction lines of (111), (200), (220) and (311) detected by X-ray diffraction. The microstructure was observed by SEM (scanning electron microscopy) attached with EPMA (electric probe micro analysis) on the polished surface after etching. The slaking resistance of CaO aggregates was evaluated by measuring the mass gain after soaking the sintered bodies under the conditions of 70 °C and 90% humidity.

3. Results and discussion

3.1. Densification

Fig. 1 shows the relative density of the CaO aggregate without oxide addition. It is observed that the relative density abruptly increased with temperature increasing from 1300 to 1400 °C when the relative density was 96.9%. This result shows that the lightweight $CaCO_3$ had considerable highly sintering activity, and the sintering temperature was much lower than that of the traditional one. But when further increasing temperature from 1400 to 1600 °C, there was only a slight increase in compactness.

Fig. 2 shows the relative density of aggregate with different amounts of oxide addition sintered at 1500 °C for 2 h. The relative density was appreciably increased by addition of MgO and ZrO_2. The relative density was 96.9% for the sample without addition, which

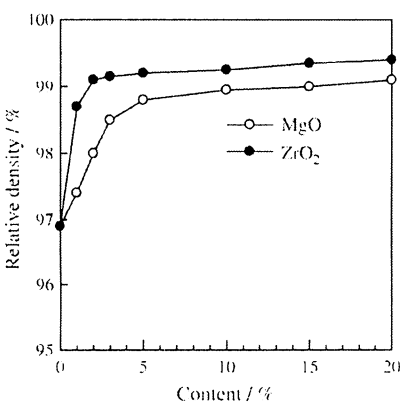

Fig. 2. Effect of oxide addition on densification of CaO aggregate.

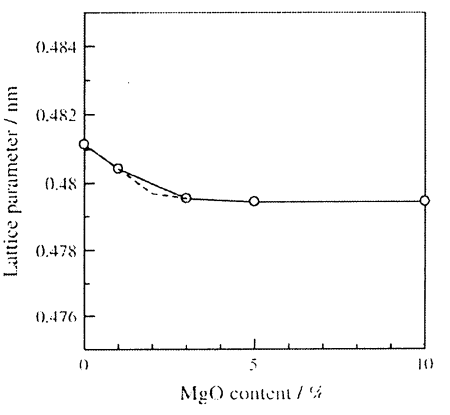

Fig. 4. Lattice parameter of cubic CaO solid solution sintered at 1500 °C for 2 h by the addition of MgO.

increased to 98.5% and 99.0% when 3% MgO and 3% ZrO_2 were added respectively. It is also observed that the densification was very sensitive to a small amount of additions (below 3%), and ZrO_2 addition was more effective than MgO on promotion of densification.

The changes of relative density with soaking time at 1500 °C are shown in Fig. 3. It is observed that for the sample without addition, the densification process was still in progress after soaking at 1500 °C for 2 h. By addition of oxides, the time necessary for completion of sintering was effectively shortened. Thus, it is considered that the shrinkage of the compact, or the full densification of compacts, was promoted by addition of oxides. In addition, it is also observed that the values of the line with 1% ZrO_2 is almost equal to that of 5% MgO added, indicating that the effect of 1% ZrO_2 addition was equivalent to 5% MgO addition on promotion of densification.

3.2. Phase composition and microstructure

XRD patterns showed that the added ZrO_2 reacted with CaO to form $CaZrO_3$, but there was not any new phase formed when MgO was added. The lattice parameter of CaO is shown in Fig. 4. It was 0.4811 nm (theoretic value is 0.4813 nm) for the sample sintered without MgO, which decreased to 0.4795 nm with increasing the addition of MgO to 3%, and no change was found with further increasing the content of MgO. From this result it is considered that the added MgO had formed solid solution with CaO and the solubility limit of MgO in CaO was around 2% under the present sintering conditions. But when ZrO_2 was added, there is no change in the value of lattice parameter, indicating that the added ZrO_2 did not form solid solution with CaO.

Microstructure observation shows that coarse CaO grains (53 μm), with irregular grain boundaries and most of pores within the individual grains, were observed for the aggregate without oxide addition, indicating the occurrence of discontinuous or abnormal grain growth (Fig. 5). While MgO was added, the grain size of CaO was sharply decreased (Fig. 6), with the elimination of most pores, and the fine MgO particles were found within CaO grains (Fig. 7a). This result shows that the densification of CaO compact was promoted by inhibiting grain growth when MgO was added. With increasing MgO content, the grain size of CaO decreased further, and the added MgO grew up and preferred to gather between CaO grains, often at grain-boundary triple points (Fig. 7b). Homogeneous microstructure, with well growing MgO grains occupying most of the grain-boundary triple points, formed when 20% MgO was added (Fig. 7c). When ZrO_2 was added, it was more effective on inhibiting grain growth of CaO (Fig. 7d–f), and a homogeneous microstructure with $CaZrO_3$ layers around CaO grains formed when 20% ZrO_2 was added.

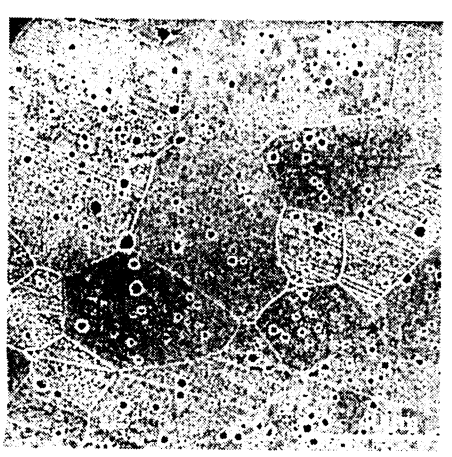

Fig. 5. Microstructure of CaO aggregate sintered at 1500 °C for 2 h.

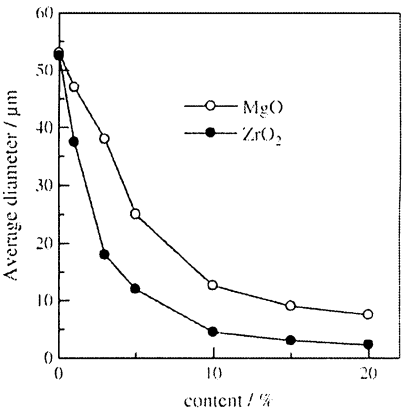

Fig. 6. Grain size of CaO as a function of oxide content.

3.3. Slaking resistance

Fig. 8 illustrates the dependence of oxide content on mass gains after the CaO aggregates were slaked under the conditions of 70 °C and 90% humidity for 96 h. The mass change was expressed by mass gain percent to the original mass of the samples. It is observed that the slaking resistance was effectively improved by oxide addition, and the addition of less than 5% was more effective. The mass gain after 96 h was 10% for the sample without MgO, and it decreased to 3.5% and 2.1% by addition of 5% MgO and 20% MgO, respectively. It is also observed that the addition of ZrO_2 was more effective on improving the slaking resistance of CaO aggregate. The mass gain was 1.9% when 5% ZrO_2 was added, and it decreased to merely 0.6% by addition of 20% ZrO_2.

4. Discussion

4.1. Effect of oxide addition on densification and microstructure

Discontinuous grain growth or secondary recrystallization is a common phenomenon that occurs on the sintering of oxide ceramics, giving rise to non-uniform microstructures. Due to the high sintering activity of the CaO derived from lightweight $CaCO_3$, discontinuous grain growth preferred to happen in the present work, with formation of coarse CaO grains containing many pores. With increasing the sintering temperature, the grain growth was promoted and the escaping of pores was inhibited, thus it is observed that there was only a slight increase in relative density when the temperature was increased from 1400 to 1600 °C (Fig. 1).

When oxides were added, these fine particles dispersed in the structure and inhibit the discontinuous growth by increasing the energy necessary for the movement of grain boundaries [18]. Thus, the movement of CaO grain boundaries was slowed down and the escaping of pores was promoted. When a small amount of oxides was added, these oxide particles were so small that the

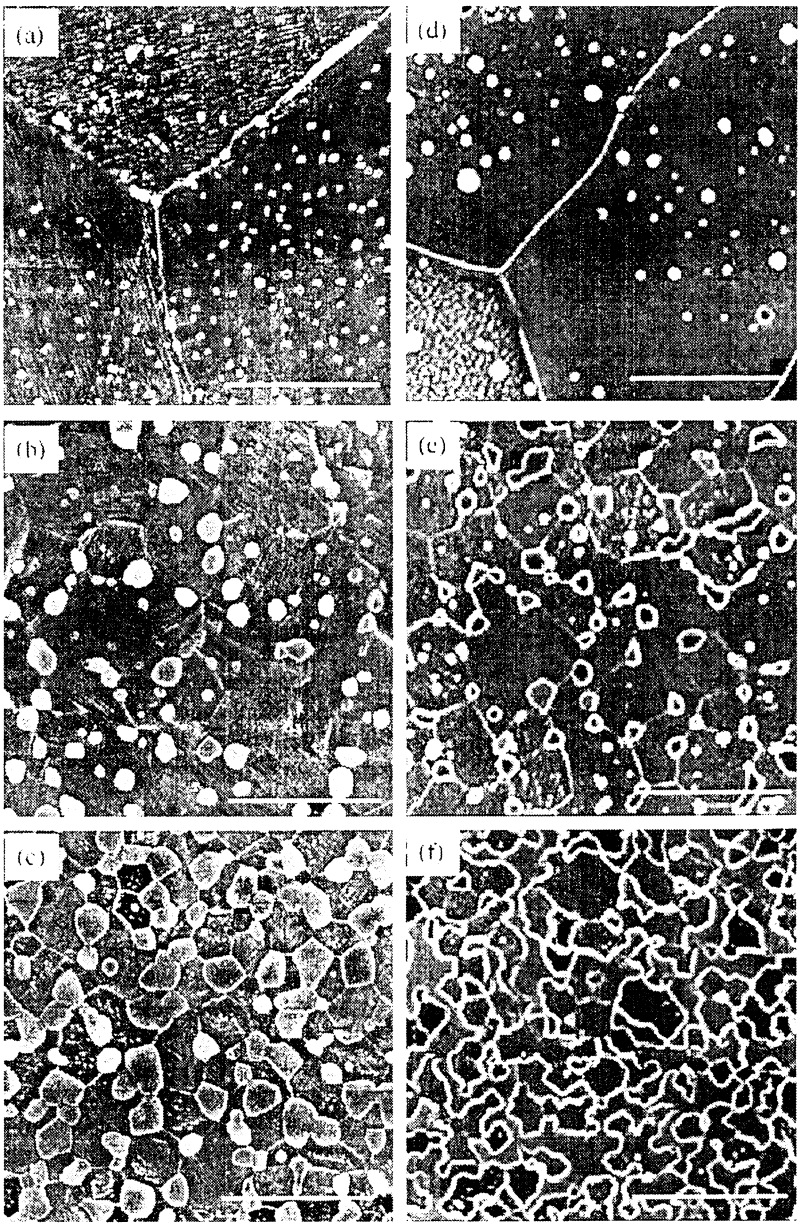

Fig. 7. Microstructure of CaO aggregate with oxide addition sintered at 1500 °C for 2 h. The scale bar is 10 μm.

grain boundaries of CaO were easily passed over, with the fine oxide particles inside CaO grains (Fig. 7a and d). When these oxide particles were so big with their content increasing that the grain boundaries would not pass over, thus these additives were observed at the grain boundaries, often at boundary triple points.

Since a part of the added MgO formed solid solution with CaO, only a part of it acted as inhibitor of grain growth. But when ZrO_2 was added, it did not form solid solution with CaO, and all of the added ZrO_2 reacted with CaO by solid phase reaction and acted as inhibitor of grain growth. Thus it was observed that the addition of a small amount ZrO_2 was more effective on restraining grain growth of CaO. Owing to the solid phase reaction happening, the microstructure was modified, with protective $CaZrO_3$ layer formed around CaO grains.

4.2. Improvement of slaking resistance

It is known that the slaking resistance of CaO aggregate is dependent to the reaction specific surface area that is related to the microstructure, including the relative density, pore distribution as well as grain size, etc. The CaO aggregate with high compactness and large CaO grains is considered to be more slaking resistant. In the present work, when MgO and ZrO_2 were added, the slaking resistance of CaO aggregate was improved due to the following reasons:

First, CaO solid solution was formed when MgO was added. Since the radius of Mg^{2+} cation (0.86×10^{-10} m) is smaller than that of Ca^{2+} cation (1.14×10^{-10} m) [19], the substitution of Ca^{2+} cation by Mg^{2+} cation contributed to the shrinkage of the lattice of CaO crystal, resulting in enhancement of the electrostatic

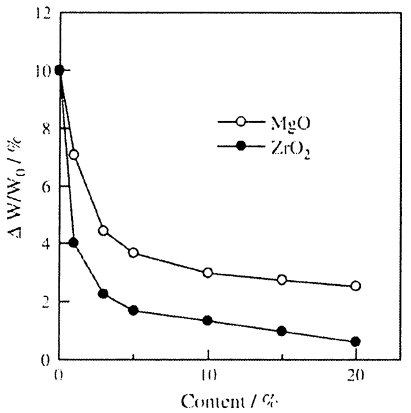

Fig. 8. Mass gains of CaO aggregate with oxide addition after slaking at 70 °C in 90% humidity for 96 h.

force among the ions in CaO lattice [20]. Thus the slaking resistance of CaO was improved by the formation of solid solution when MgO was added.

Second, the CaO grain was stabilized due to the promotion of densification by addition of MgO and ZrO_2, which effectively decreased the reaction specific surface area of the CaO aggregate.

Lastly, the slaking resistance was improved due to the modification of microstructure when the addition of MgO and ZrO_2 increased. It is well known that the slaking reaction always begins from the sites with crystal defects. Thus, the grain boundaries, especially the boundary triple points, are the poor slaking resistant sites. While enough MgO was added, and the well growing MgO grains occupying these sites, the slaking resistance of CaO aggregate could be effectively improved. Especially when $CaZrO_3$ layer formed by addition of enough ZrO_2, CaO grains were effectively isolated to circumstance, thus the slaking reaction was retarded and the slaking resistance was improved.

5. Conclusions

Based on the above results, the following conclusions were drawn when CaO aggregate was sintered from lightweight $CaCO_3$ by addition of MgO and ZrO_2.

1) The lightweight $CaCO_3$ was highly sinterable, and compact CaO aggregate with relative density above 96% was obtained after soaking at 1400 °C that was much lower than the present commercial sintering temperature. However, further increase of compactness was restrained due to the occurrence of abnormal grain growth.
2) The densification of CaO aggregate was promoted by addition of MgO and ZrO_2 due to their effect on restraining grain growth. In addition, the microstructure was modified by addition of MgO and ZrO_2. Homogeneous microstructure, with well growing MgO grains occupying most of the boundary triple points of CaO grain, formed by the addition of 20% MgO. Especially when 20% ZrO_2 was added, homogeneous $CaZrO_3$ layer formed around CaO grains.
3) The slaking resistance of CaO aggregate was improved due to the promotion of densification, the formation of CaO solid solution (while MgO was added) and the modification of microstructure. Especially when 20% ZrO_2 was added and $CaZrO_3$ layer formed around CaO grains, the slaking resistance of CaO aggregate was appreciably improved.

References

[1] F. Nadachowski, Interceram 24 (1975) 42–45.
[2] R.E. Moore, Interceram 35 (1986) 19–21.
[3] F. Nadachowski, Ceramurgia International 2 (1976) 55–61.
[4] T. Degawa, Ceramics (Japan) 23 (1988) 1052–1055.
[5] W.M. Yuan, B.L. Shang, Technology of Casting (China) 179 (1) (1994) 6–8.
[6] J. Kijac, P. Kovac, E. Steranka, V. Masek, P. Marek, Metalurgija 43 (2004) 59–62.
[7] Z.Y. Chen, S.X. Tian, Refractories/Naihuo Cailiao (China) 38 (2004) 219–225.
[8] Y.W. Wei, N. Li, J.C. Kuang, F.Y. Chen, InterCeram: International Ceramic Review 51 (2002) 200–205.
[9] W.X. Feng, J.G. Niu, H.M. He, S.H. Su, Y. Liu, L.Y. Chen, H.K. Liu, Kang T'ieh/Iron and Steel (China) 37 (2002) 25–27.
[10] Y.W. Wei, N. Li, American Ceramic Society Bulletin 81 (2002) 32–35.
[11] H.J. Wu, Z.Q. Cheng, S.T. Jin, W.Z. Wang, Naihuo Cailiao/Refractories (China) 36 (2002) 145–147.
[12] X.C. Zhong, Refractories/Naihuo Cailiao (China) 37 (2003) 1–10.
[13] S. Motoi, Gypsum & Lime (Japan) 154 (1978) 123–127.
[14] K. Hamano, Gypsum & Lime (Japan) 157 (1978) 20–29.
[15] Y. Oda, Taikabutsu (Japan) 41 (1989) 690–700.
[16] M. Chen, S. Ito, A. Yamaguchi, Journal of the Ceramic Society of Japan 110 (2002) 512–517.
[17] Y. Shi, G.L. Messing, R.C. Bradt, Journal of the American Ceramic Society 63 (1984) 109–111.
[18] W.D. Kingery, Introduction to Ceramics, John Wiley & Sons Inc., New York, 1960, pp. 353–370.
[19] Nippon Kagakukai (Ed.), Kaguku-Benran, vol. 2, Maruzen, Tokyo, 1975, p. 1407, [in Japanese].
[20] L. Zhang, Z. Wang, F. Li, in: N. Li, X. Zhong (Eds.), Proceeding of the International Symposium on Refractories, Haikou, 1996, p. 405.

論文

耐火物　59〔6〕288～295（2007）

アルミナと黒鉛を出発原料としたAl4O4Cの合成

趙　建立*,**，林　煒*，山口明良*，隠明寺準治*，孫　加林**

*岡山セラミックス技術振興財団 研究所　〒705-0021 岡山県備前市西片上1406-18

**北京科技大学（中国）材料科学工学科　〒100083 北京市学院路30

Synthesis of Al_4O_4C from Starting Raw Materials of Alumina and Graphite

Jianli Zhao*,**, Wei Lin*, Akira Yamaguchi*, Junji Ommyoji* and Jialin Sun**

*Research Laboratory, Okayama Ceramics Research Foundation　1406-18 Nishikatakami Bizen, Okayama, 705-0021 Japan

**School of Material Science and Engineering, University of Science and Technology Beijing,　100083 China

Abstract：Al_4O_4C has been reported to be a good additive for carbon-containing refractories. The present study investigated various factors influencing the synthesis of Al_4O_4C by heating mixtures of Al_2O_3 and graphite in argon atmosphere. The reactions in the powder mixtures were faster than those in the pressed compacts. The formation of Al_4O_4C began from a temperature between 1500 and 1550℃. The optimum molar ratio of graphite to Al_2O_3 was 1.5 for the synthesis of Al_4O_4C. The quantity of Al_4O_4C was decreased and Al_2O_3 remained more when the ratio was below 1.5, contrastively, Al_4C_3 was formed with a decrease of Al_4O_4C when above 1.5. As the heating time was extended, Al_4O_4C was increased gradually in cases of $C/Al_2O_3 \leq 1.5$, but Al_4O_4C was decreased after an increase and at the same time Al_4C_3 was increased in cases of $C/Al_2O_3 > 1.5$. The formation mechanism of Al_4O_4C was also discussed.

Key words：Al_4O_4C, Synthesis, Al_2O_3, Graphite, Carbon-containing refractories.

要　旨：　Al_4O_4Cは，炭素含有耐火物に対して良い添加剤であると報告されている。本研究では，Al_2O_3と黒鉛の混合物をAr雰囲気で加熱することによるAl_4O_4Cの合成に及ぼす影響因子について検討した。空隙率の大きい粉体での反応は，空隙率の小さい成形体に比べて速かった。Al_4O_4Cの生成は1500～1550℃の間から始まった。Al_4O_4Cの合成に適した黒鉛とAl_2O_3のモル比は1.5であった。1.5より小さくなると，Al_4O_4Cの量が少なくなり，残留Al_2O_3の量が多くなったが，1.5を超えると，Al_4O_4Cの量が減少すると同時に，Al_4C_3が生成した。加熱時間が長くなるにつれて，$C/Al_2O_3 \leq 1.5$ではAl_4O_4Cの量が徐々に増加したが，$C/Al_2O_3 > 1.5$ではAl_4O_4Cの量が始めのうち増加し，その後Al_4C_3の生成に伴って減少した。Al_2O_3と黒鉛の反応メカニズムについても考察を行った。

キーワード：　Al_4O_4C，合成，Al_2O_3，黒鉛，炭素含有耐火物

1　緒言

Al_2O_3-C系やMgO-C系などの炭素含有耐火物において，炭素の酸化を防止し，耐火物の熱間特性を改善するなどの目的で，添加剤として金属アルミニウム（Al）が広く適用されているが，いくつかの問題がある。それは，金属Alは高温で耐火物中の炭素と反応して炭化アルミニウム（Al_4C_3）を生成し[1-3]，このAl_4C_3が冷却時に大気中の水分と水和反応を起こすため，再昇温の際に耐火物の崩壊をもたらすこと[4]，また，これが水と反応しやすいため，水系結合剤を用いる不定形耐火物に使用することはできないこと[5]，さらに，微細な金属Al粉末が燃焼し易いので，その取り扱いに危険が伴うことなどである。

図1にAl_2O_3-Al_4C_3系相平衡の状態図[6]を示す。この系には，常温から1890℃まで安定である化合物のAl_4O_4Cが存在する。この化合物は，P_{CO}=0.101325MPa（=1 atm）のCO雰囲気において約800℃からCOガスと反応してAl_4C_3の生成を経由せずにAl_2O_3と炭素へ変化

平成18年11月10日受付，平成19年2月14日受理

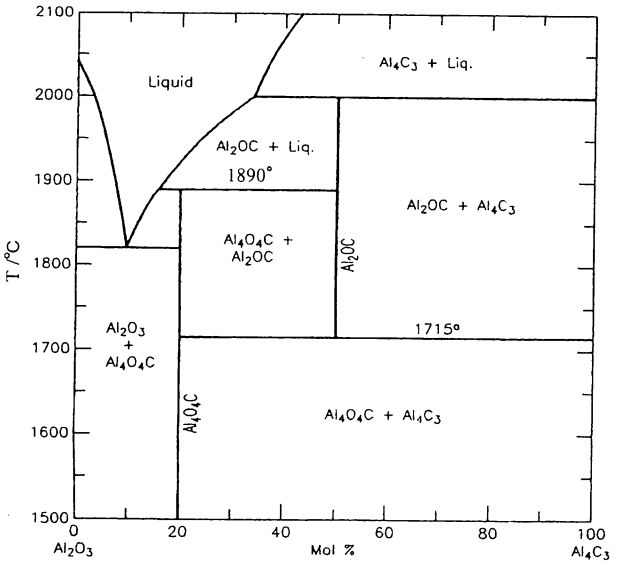

Fig. 1　Phase diagram of Al_2O_3-Al_4C_3 system.

し，また水和しない特徴を有するため，金属Al粉末よりも良い耐火物の添加剤であると報告されている[7]。そのため，Al_4O_4C原料を多量に合成する方法についての研究が必要となっている。

Al_2O_3-C耐火物での金属Alの挙動に関して，ZhangとYamaguchi[7]は，Al_2O_3，金属Alおよび黒鉛からなる混合物をAr雰囲気中で加熱して結晶相の変化を調べている。その結果，900℃でAl_4C_3，1300℃でAl_4O_4Cが生成し，1700℃まで昇温するとAl_4C_3の消失に伴ってAl_4O_4Cが主要相となることを示し，その反応機構として，金属Alと黒鉛の反応で先に生じたAl_4C_3は，さらにAl_2O_3と反応しAl_4O_4Cを生成することを説明した。

一方，金属Alの製錬分野において，Al_2O_3の炭素熱還元による溶融金属Alの製錬方法についての研究が報告されている。それらによると，金属Alの生成には高い加熱温度が必要であり，またAl_4O_4C, Al_2OCおよびAl_4C_3の中間相の生成が伴う。例えば，Waiら[8]は2300-2550KでのプラズマによるAl_2O_3の炭素還元について検討し，Katkobら[9]は2600K以上の還元温度が必要であることを述べた。また，Kibbyら[10]はAl_4O_4CおよびAl_4C_3を経て金属Alを生成する反応モデルを構築し，Qiuら[11]およびLihrmannら[12]はAl_4O_4Cの標準生成自由エネルギーを求めた。

本研究では，Al_4O_4C合成プロセスの開発に基礎的な知見を提供するため，金属Alを使用せず，Al_2O_3と黒鉛のみを出発原料としたAl_4O_4Cの合成方法について検討した。Ar雰囲気においてAl_2O_3と黒鉛との混合物を加熱し，生成物の結晶相に及ぼす炭素とAl_2O_3の混合比，混合物の状態（粉体および成形体），加熱温度および加熱時間などの因子の影響を実験的に調査し，反応の機構を考察した。

2　実験方法

純度99.99mass%以上のアルミナ（大明化学工業㈱）および純度99mass%以上の黒鉛試薬（和光純薬工業㈱）を出発原料とした。前者の平均粒度は0.1μmであり，後者の粒度は45μm以下と称されているが，顕微鏡の観察によると，大部分は20～30μmであった。

所定比例の黒鉛とアルミナ（C/Al_2O_3モル比は0.5，1，1.5，2および3）にエタノールを加え，メノウ乳鉢で混合した後，真空回転式の乾燥装置で混合物を乾燥した。次に，混合物の粉体（2g）を高純度の黒鉛るつぼに入れ，電気炉(発熱体は黒鉛)の中に設置し，炉内を真空にした後，Arガスを送入した（Arガスは純度が99.9999%以上の超高純度のもので，1700℃での酸素分圧をZrO_2酸素センサーで測定した結果，その分圧は10^{-20}MPaである)。Arガスの流量を1L/minと一定にし，10℃/minの速度で1500～1700℃まで昇温してから，3～9時間保持した。その後，電源を切って試料を炉内で冷却した(1700℃から1000℃までの平均冷却速度は64℃/min)。室温まで冷却した試料からサンプルを採取し，X線回折(XRD）により結晶相を同定した。また，微構造の観察およびEPMA分析を行った。

混合物の状態（粉体または成形体）の加熱後試料の結晶相に及ぼす影響を明確にするため，予備実験として，混合物の粉体を予め100MPaで加圧成形して得られた成形体を用いた実験も行った。

3　結果

3・1　混合物の状態の影響

C/Al_2O_3=1.5の混合物の粉体および成形体の1700℃，9時間加熱後各試料のXRDパターンを図2(a)，(b)に示す。加熱前の粉体試料中の空隙率は75%，成形体は39%であった。各結晶相のXRD最大強度を図3(a)にまとめた。いずれの場合もAl_4O_4Cが生成していたが，粉体でのAl_4O_4Cの生成量は成形体の場合より多かった。

また，C/Al_2O_3=3の混合物の粉体（空隙率：80%）および成形体（空隙率：37%）を1600℃で3時間加熱した場合の各結晶相の最大強度を図3(b)に示す。成形体の場合は，新しい相は生成せず，加熱前の結晶相と同じ

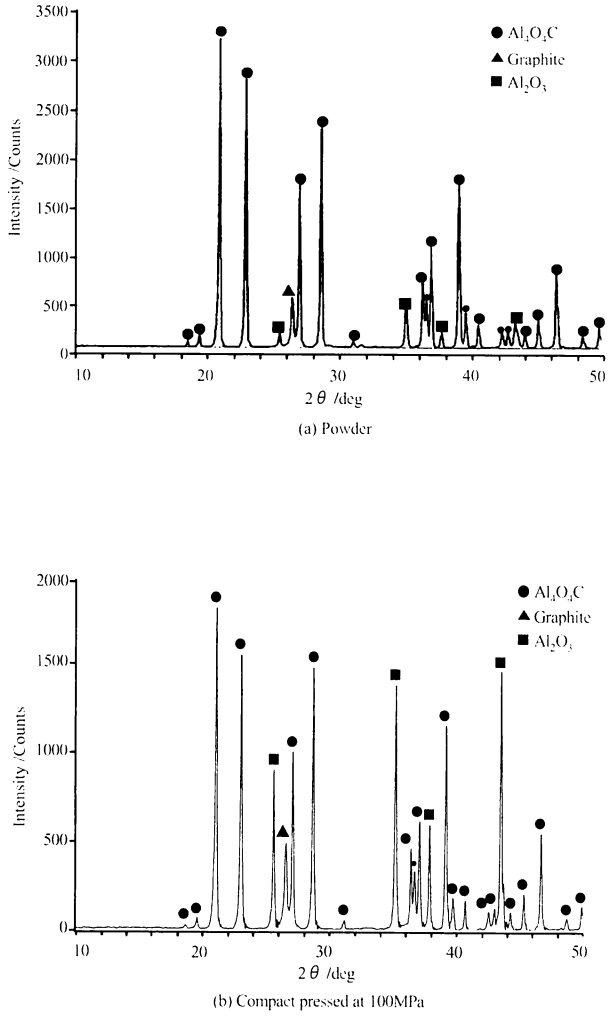

Fig. 2　XRD patterns of C/Al_2O_3=1.5 samples heated at 1700℃ for 9h.

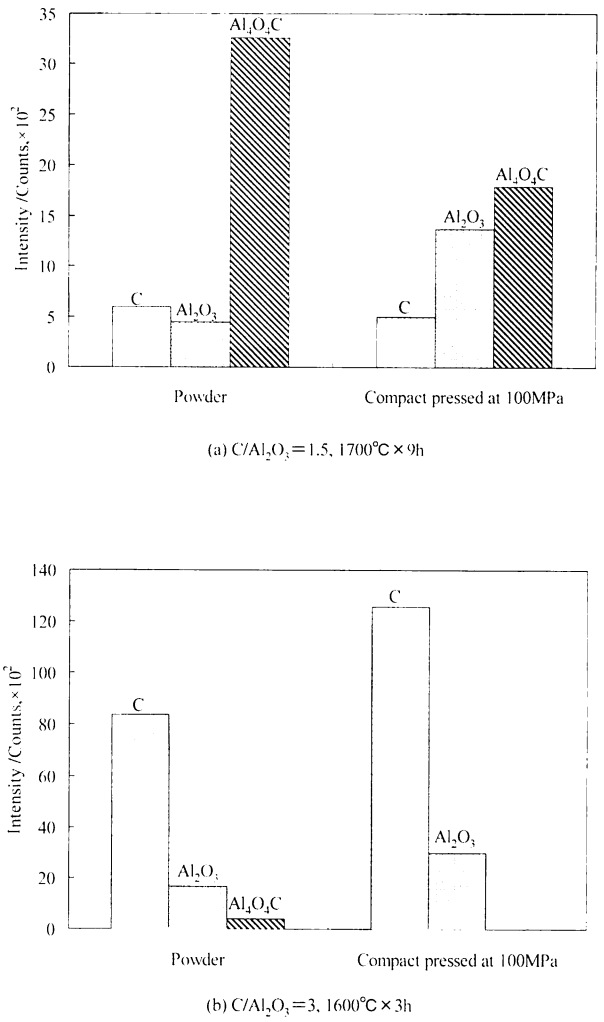

Fig. 3　Phases of powder samples and pressed compact samples heated.

であるのに対して，粉体の場合は，Al_2O_3および黒鉛の量が低減し，Al_4O_4Cが生成していた。

以上の結果は，成形体よりも粉体の反応速度の方が速いことを意味している。したがって，以下の実験では，すべて混合物の粉体を用いた。

3・2　加熱温度の影響

C/Al_2O_3=1.5および3の混合物をそれぞれ1500, 1550, 1600, 1650および1700℃で3時間加熱した。加熱後試料の結晶相の最大強度変化を図4(a),(b)に示す。

いずれの場合も，1550℃以上で加熱した試料からAl_4O_4Cにが検出され，加熱温度が高くなるにつれてAl_4O_4Cの生成量が増加し，同時にAl_2O_3および黒鉛の量が減少していた。1500℃で加熱した試料からはAl_4O_4Cは検出されなかった。このことは，Al_4O_4Cの生成開始温度が1500～1550℃の間にあることを示している。ただし，C/Al_2O_3=1.5のときは，1600℃まではAl_4O_4Cの生成量が少なく，1600℃を超えるとその量は多くなった。C/Al_2O_3=3のときは，Al_4O_4Cの生成量は加熱温度の増加にしたがって徐々に増加し，また1600～1650℃の間からAl_2OCおよびAl_4C_3も少量ながら生成しはじめた。

3・3　C/Al_2O_3の影響

1700℃でC/Al_2O_3=0.5, 1, 1.5, 2および3の混合物をそれぞれ3と9時間加熱した。加熱後各試料中の各結晶相の最大強度変化を図5(a),(b)に示す。

いずれの場合も，Al_4O_4Cの生成量は当初C/Al_2O_3の増加にしたがって増加し，C/Al_2O_3=1.5で最大値となった。C/Al_2O_3がさらに増すと，Al_4O_4Cの量が減少すると同時に，Al_2OCおよびAl_4C_3が生成した。9時間加熱の時はAl_2OCは生成せず，Al_4C_3が生成し，その量はC/Al_2O_3の増加につれて大幅に増加した。

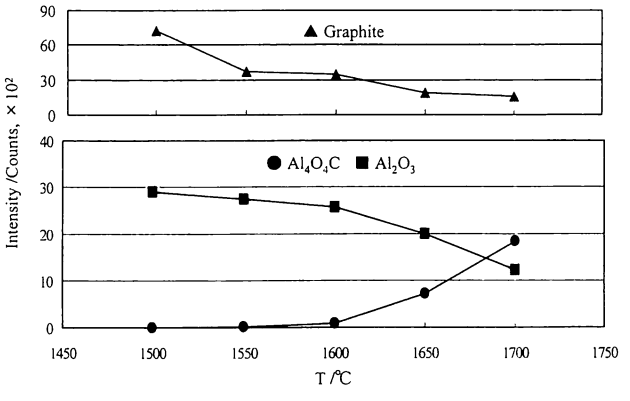

(a) $C/Al_2O_3=1.5$

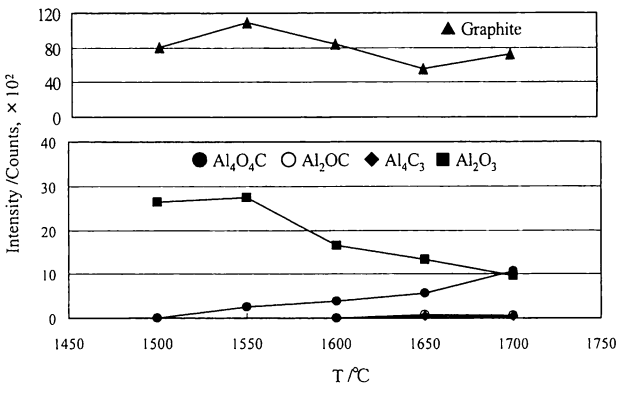

(b) $C/Al_2O_3=3$

Fig. 4 Phases of samples heated at different temperatures for 3h.

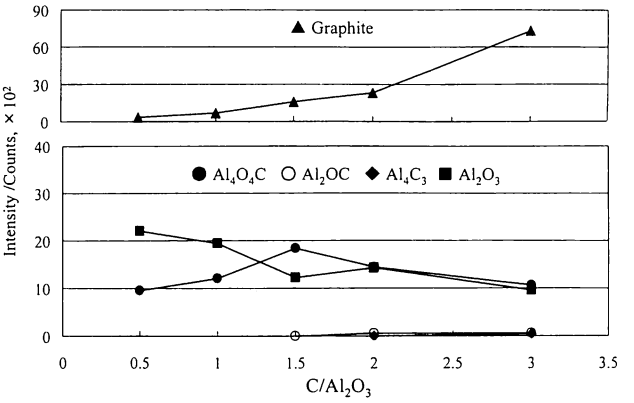

(a) 1700℃ × 3h

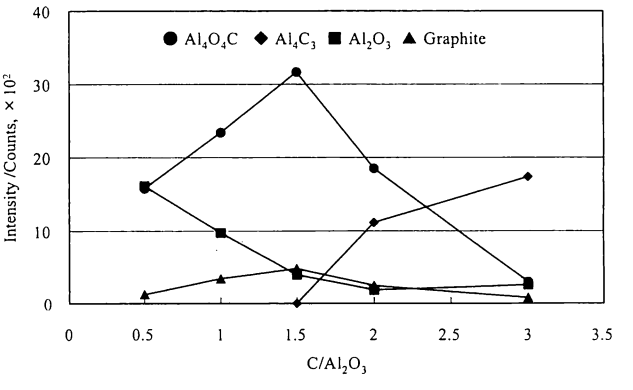

(b) 1700℃ × 9h

Fig. 5 Phases of heated samples with different C/Al_2O_3 ratios.

この結果から，$C/Al_2O_3=1.5$のときはAl_4O_4Cの生成量が最も多く，またAl_2OCおよびAl_4C_3が生じないため，Al_4O_4Cの合成には最も良い混合比であると判断される。ただし，本実験において，Al_2O_3および黒鉛を含まない純粋なAl_4O_4Cは得られなかった。

3・4　加熱時間の影響

1700℃で$C/Al_2O_3=1.5$および3の混合物をそれぞれ3，5，7および9時間加熱し，加熱後試料の時間による結晶相の最大強度変化を図6(a)，(b)に示す。

$C/Al_2O_3=1.5$のときは，Al_4O_4Cのみが生成し，加熱時間が長くなるにつれて，Al_4O_4Cの量が徐々に増加し，Al_2O_3および黒鉛の量が減少していた。

$C/Al_2O_3=3$のときは，Al_4O_4CのほかAl_2OCおよびAl_4C_3も生成した。Al_4O_4Cの量は5時間までは増加の傾向，その以後は減少の傾向を示した。Al_2OCは5時間までは少量生成したが，7時間になると消失した。Al_4C_3は，加熱時間が長くなるにしたがって増加した。この結果から，この混合比ではAl_4O_4Cを最大限に生成すると同時に，Al_2OCおよびAl_4C_3量を抑制するには適した加熱時間があり，この場合は5時間であった。

3・5　合成物の微構造

$C/Al_2O_3=1.5$の混合物の1700℃，9時間加熱試料を樹脂に埋め込み研磨し微構造観察を行った。研磨面のSEM写真を図7(a)，EPMA分析結果の一例を図7(b)に示す。粒径は10～100μm程度で，30～50μmのものが多かった。また，粒の内部には気孔がなく，緻密になっていた。EPMA面分析によると粒の構成元素はAl, Oおよびcであり，図2(a)に示したXRD分析結果と合わせると，その結晶相はAl_4O_4Cであると判断される。ただし，少数の粒の内部には，小さな鱗状の黒鉛が存在していることが観察された。それは，未反応で残留していた黒鉛と考えられる。

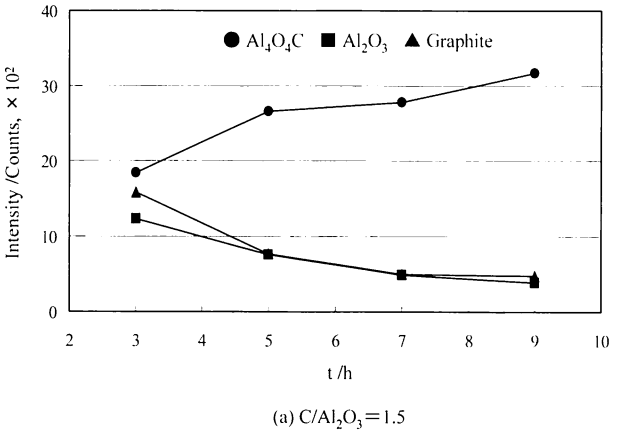

(a) $C/Al_2O_3=1.5$

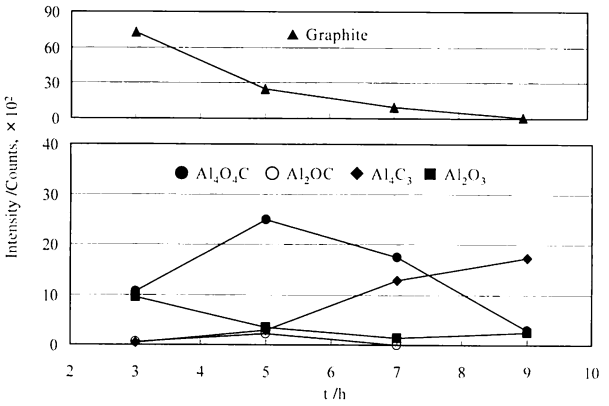

(b) $C/Al_2O_3=3$

Fig. 6　Phases of samples heated at 1700℃ for different times.

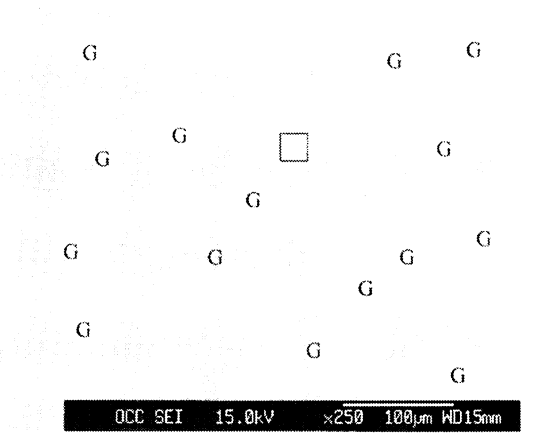

(a) SEM photograph (G: Grain)

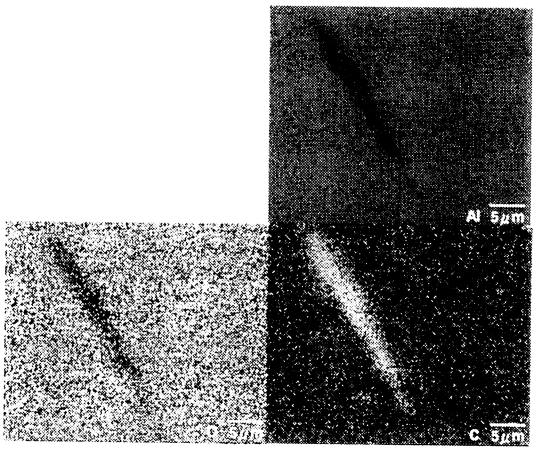

(b) EPMA analysis

Fig. 7　SEM photograph and EPMA analysis of C/Al_2O_3=1.5 sample heated at 1700℃ for 9h.

XRD分析結果によれば，この試料には少量のAl_2O_3も含まれていたが，その量は少なく，またサイズが小さすぎるためか，EPMA分析では検出されなかった。

4　考察

4・1　Al_4O_4Cの生成およびAl_4C_3への変化の反応

C/Al_2O_3が1.5以下で結晶相としての生成物がAl_4O_4Cのみであった結果（図5）から，この場合は次のような反応が生じたと考えられる。すなわち，Al_2O_3と黒鉛の粒が接触している最初の段階では，固相－固相間の反応

$$2Al_2O_3(s)+3C(s)=Al_4O_4C(s)+2CO(g) \quad (1)$$

が起こった。粒の間が接触しなくなると，固相－COガス間の反応

$$2Al_2O_3(s)+4CO(g)=Al_4O_4C(s)+3CO_2(g) \quad (2)$$

$$CO_2(g)+C(s)=2CO(g) \quad (3)$$

が生じた。反応(2)と(3)の全反応は反応(1)と同じ形になるが，Al_4O_4C(s)生成の主反応になったと推定される。

C/Al_2O_3が1.5を超えると，Al_4C_3も生成し，また加熱時間の延長につれてAl_4O_4Cの生成量は増加の後Al_4C_3の生成に伴って減少した結果（図5，6(b)）から，反応(1)に対してCが過剰なので，反応(1)～(3)で生成したAl_4O_4CはさらにCOと反応してAl_4C_3へ変化したと考えられる。すなわち，

$$Al_4O_4C(s)+8CO(g)=Al_4C_3(s)+6CO_2(g) \quad (4)$$

反応(3)と(4)の全反応は，

$$Al_4O_4C(s)+6C(s)=Al_4C_3(s)+4CO(g) \quad (5)$$

になる。

Al_2OCは，Al_4O_4CがAl_4C_3へ変化している過程で不安定な中間相として生成した後，Al_4C_3へ変わったと考えられる。すなわち，

$$Al_4O_4C(s)+4CO(g)=2Al_2OC(s)+3CO_2(g) \quad (6)$$

$$2Al_2OC(s)+4CO(g)=Al_4C_3(s)+3CO_2(g) \quad (7)$$

全反応を表す反応(1), (5)にしたがい，各化合物の標準生成自由エネルギー($\triangle_fG^0$)から，本実験の加熱温度における炭素共存下でのAl_2O_3, Al_4O_4CおよびAl_4C_3の安定領域とCOガス分圧（P_{CO}）の関係を求めた。本実験の最高加熱温度の1700℃（1973K）での結果を図8に示す（状態図[6]により，1715℃以下ではAl_2OCが不安定なので，本計算にAl_2OC-C系を入れなかった)。計算に用いたAl_4O_4Cの$\triangle_fG^0$はLihrmannら[12]の示した式から算出し，Al_2O_3, Al_4C_3およびCOのそれは“JANAF熱力学表”[13]のデータを基に回帰処理で得られたものである。基準圧力（P^0）は，いずれも0.101325MPa（≒1 atm）とした。

図8により，炭素共存下の1700℃において，Al_2O_3がAl_4O_4Cへ変化する臨界CO分圧$P_{CO}(Al_2O_3 \rightarrow Al_4O_4C)$は$5.685\times10^{-3}$MPa($\log(P_{CO}/P^0)=-1.251$)，$Al_4O_4C$の$Al_4C_3$へ変化するそれ$P_{CO}(Al_4O_4C \rightarrow Al_4C_3)$は$4.099\times10^{-3}$MPa($\log(P_{CO}/P^0)=-1.393$)であり，すなわち，$Al_4O_4C$の安定領域は，$P_{CO}=(4.099\sim5.685)\times10^{-3}$MPaである。言い換えれば，実際のCO分圧が$4.099\times10^{-3}$MPa以下で，また炭素が共存している条件では，結晶相の生成物はAl_4O_4Cとならず，Al_4C_3となる。

前述したように，本実験においては，酸素分圧P_{O2}が10^{-20}MPaの超高純度のArガスを1 L/minの流量で流していた。Arガス中の酸素は発熱体のカーボンと反応し($1/2O_2+C(s)=CO(g)$) COガスを発生するとすれば，そのCOガス分圧は，1500～1700℃で約0.5×10^{-20}MPaとなる。これによると，本実験の加熱中において，試料の上部にあるCO分圧は4.099×10^{-3}MPaの臨界値より顕著に小さかったと推定される。$C/Al_2O_3\leqq1.5$の場合にAl_4C_3が生成せずAl_4O_4Cのみが生成した理由としては，Al_4O_4Cが生じた後黒鉛はほぼなくなり，Al_4O_4Cと共存する状態ではなくなったことが推測される。

また，求められた各温度での臨界CO分圧$P_{CO}(Al_2O_3 \rightarrow Al_4O_4C)$, $P_{CO}(Al_4O_4C \rightarrow Al_4C_3)$を図9に示す。これによると，熱力学上では，$Al_4O_4C$および$Al_4C_3$生成の開始温度は，いずれも雰囲気中COガス分圧の増大につれて高くなるが，P_{CO}が0.5×10^{-20}MPaより顕著に高い10^{-6}MPaであってもそれぞれ1180℃と1200℃になる。これらに比べて，図4に示したように，実際のAl_4O_4C生成の開始温度は1500～1550℃，Al_4C_3のそれは1600～1650℃と300～500℃高かった。これは，Al_4O_4Cおよび

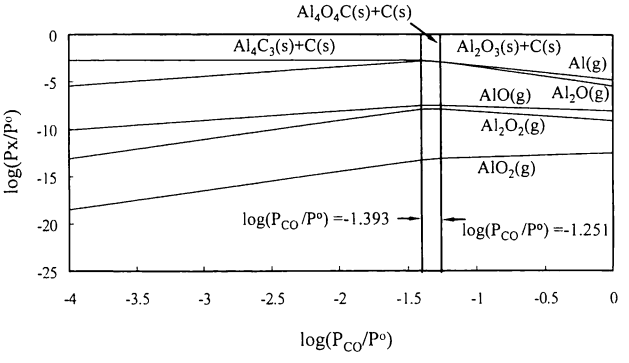

Fig. 8 Stable zone of Al_2O_3, Al_4O_4C and Al_4C_3 coexisting with carbon at 1973K (1700℃).

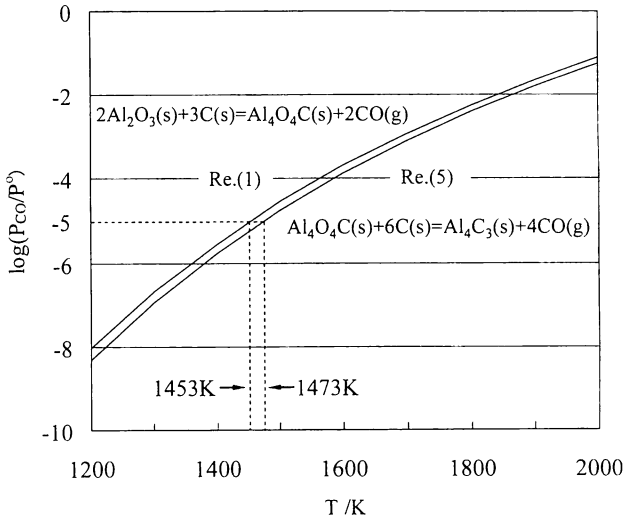

Fig. 9 Equilibrium CO partial pressures as a function of temperature for Reaction(1) and (5).

Al_4C_3の生成にはその温度差に応じる活性化エネルギーが必要であることを示唆していると考えられる。

なお，上述したことから，炭素共存下でAl_4O_4Cが安定となるCO分圧および温度の範囲はいずれも狭いことがわかる。この例によれば，1700℃での$P_{CO}(Al_4O_4C \rightarrow Al_4C_3)/P_{CO}(Al_2O_3 \rightarrow Al_4O_4C)$の比は0.72であり，$P_{CO}=10^{-6}$MPaでの温度範囲は20℃である。したがって，将来Al_4O_4C原料を多量に合成する場合には，雰囲気および温度を精密に制御することが必要であることが示された。

4・2 Al-O系気相の生成反応

加熱実験後，炉の内壁およびガス出口の付近には付着物が付いていることが観察された。この付着物は，SEM観察によるとナノサイズの粒子の凝集物であり，XRD分析によると，C, Al_2O_3, Al_4C_3およびAl_4O_4Cからなっていることが判明した。これらの生成は，加熱中に試料から

発生した気相の揮発に起因したものと推定される。気相種としては，(1)～(7)式に示したCO，CO_2ガス以外に，Al(g)，Al_2O(g)，AlO(g)，Al_2O_2(g)およびAlO_2(g)などの気相も考えられる。

図8には，一例として1700℃でのAl_2O_3-C，Al_4O_4C-CおよびAl_4C_3-C系におけるAl(g)，Al-O系気相種の平衡分圧も示されている。これによると，いずれの系でも，ほかの気相よりAl(g)およびAl_2O(g)の分圧が高い。例えば，Al_2O_3-Al_4O_4C-Cの平衡位置において，P_{CO}(=5.685×10^{-3}MPa) を1とすれば，P_{Al}，P_{Al_2O}，P_{AlO}，$P_{Al_2O_2}$およびP_{AlO_2}はそれぞれ2.237×10^{-2}，1.943×10^{-2}，5.529×10^{-7}，2.018×10^{-7}，1.323×10^{-12}となる。本実験の最低加熱温度の1500℃においても，同じ傾向がある。それゆえ，Alを含む気相は，主にAl(g)およびAl_2O(g)と推定される。これらの生成の反応として，(8)～(11)の反応が考えられるが，全反応は(8)，(10)の反応となる。

$$Al_2O_3(s)+3C(s)=2Al(g)+3CO(g) \quad (8)$$

$$Al_2O_3(s)+3CO(g)=2Al(g)+3CO_2(g) \quad (9)$$

$$Al_2O_3(s)+2C(s)=Al_2O(g)+2CO\ (g) \quad (10)$$

$$Al_2O_3(s)+2CO(g)=Al_2O(g)+2CO_2(g) \quad (11)$$

生じた気相は，さらにAl_2O_3(s)と反応するとAl_4O_4C，Al_4C_3を生成する。例えば，

$$Al_2O_3(s)+2Al(g)+CO(g)=Al_4O_4C(s) \quad (12)$$

$$Al_2O_3(s)+3Al_2O(g)+2CO(g)=2Al_4O_4C(s) \quad (13)$$

となるが，式(8)+(12)=(1)，1.5×(10)+0.5×(13)=(1)となるので，気相を介しての反応も(1)式と同じ式で示される。

一部の気相は，温度の低い炉の上部へ揮発し，観察された付着物を生成したと考えられる。例えば，

$$2CO(g)=C(s)+CO_2(g) \quad (14)$$

$$4Al(g)+3CO_2(g)=2Al_2O_3(s)+3C(s) \quad (15)$$

$$4Al(g)+3C(s)=Al_4C_3(s) \quad (16)$$

$$2Al_2O(g)+CO_2(g)=Al_4O_4C(s) \quad (17)$$

である。将来Al_4O_4Cを多量に合成する場合は，原料のロスを減らすため，付着物回収の必要性が生じると考えられる。

4・3　微構造の形成機構

本実験に用いたAl_2O_3原料は平均粒度が0.1μmと微細なものであり，黒鉛原料は平均粒度が20～30μmと比較的大きなものである。加熱前での2種類の原料の分布状態を表すモデルを図10(a)に示す。すなわち，Al_2O_3の粒は，黒鉛粒子を被覆している状態である。以下C/Al_2O_3=1.5の場合について微構造形成機構の推定を行う。

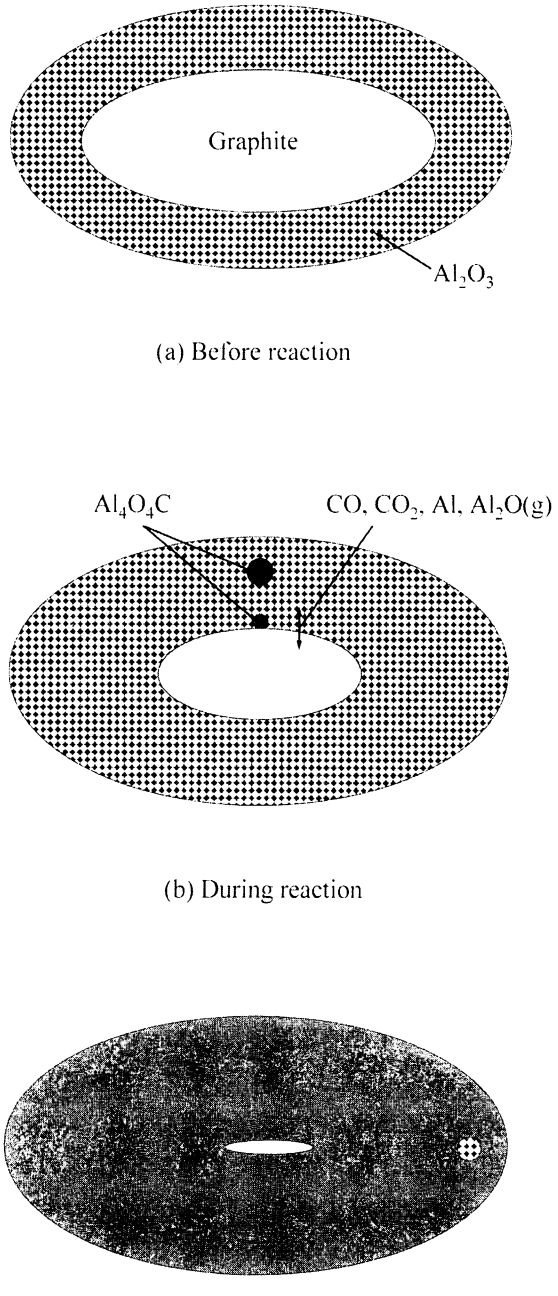

Fig. 10　Model for reaction between Al_2O_3 and graphite.

最初は，黒鉛とAl_2O_3の界面で反応(1)，および反応(8)，(10)のような反応が起こり，結晶相のAl_4O_4Cが生成すると同時に，CO，AlやAl_2Oなどの気相が生じる。生じた気相は，空隙を通して界面から離れているAl_2O_3粒の間へ逸散し，Al_2O_3と反応(2)，および反応(9)，(11)～(13)のような反応を起こし，続いてAl_4O_4Cを生成す

ると同時に，再びCO，AlやAl$_2$Oなどの気相を発生し，CO$_2$ガスも生じる。CO$_2$ガスは，周囲へ逸散し黒鉛と接すると，反応(3)を起こすことにより黒鉛を消耗し，COガスへ変わる（図10(b)）。

上述のような反応過程が続くと，Al$_4$O$_4$Cの生成量が増え，Al$_4$O$_4$C粒の間の焼結も起こる。焼結で緻密なAl$_4$O$_4$Cの粗粒が生じると，粒の中で気相の逸散ができなくなり，反応が停止する。未反応の黒鉛が存在すれば，Al$_4$O$_4$C粗粒の内部に残留し，すなわち，図7(b)に示したような微構造が形成する（図10(c)）。同様な理由で，未反応のAl$_2$O$_3$もその内部に残留していると考えられる。

また，以上のことによって，加熱前の混合物において空隙が少なく，または空隙の大きさが小さくなると，前述した気相の逸散が難しくなるため，Al$_4$O$_4$Cの生成速度が遅くなる。これは，混合物の成形体に比べて，粉体の場合はAl$_4$O$_4$Cの生成量が多かった（図2，3）原因であると考えられる。

5　結言

Al$_2$O$_3$と黒鉛との混合物をアルゴン雰囲気において加熱し，Al$_4$O$_4$Cの生成に及ぼすいくつかの因子の影響を調べた結果，次のことが判明した。

1）空隙率の小さい混合物の成形体より空隙率の大きい粉体を用いたほうが反応速度は速い。これは，粉体の場合は気相の逸散が起こりやすいためである。

2）Al$_4$O$_4$Cの生成開始温度は1500～1550℃の間であり，熱力学的計算温度より高い。また，加熱温度の増加にしたがって，Al$_4$O$_4$Cの生成量が増加する。

3）Al$_4$O$_4$Cの合成に最も適した黒鉛とAl$_2$O$_3$のモル比は1.5である。1.5より小さくなると，Al$_4$O$_4$Cの生成量が少なくなり，残留Al$_2$O$_3$の量が多くなる。1.5を超えると，Al$_4$O$_4$Cの量が減少すると同時に，Al$_4$C$_3$が生成する。また，Al$_4$C$_3$の生成量がC/Al$_2$O$_3$の増加につれて増加する。

4）加熱時間が長くなるにつれて，C/Al$_2$O$_3$≦1.5ではAl$_4$O$_4$Cの量が増加するが，C/Al$_2$O$_3$＞1.5ではAl$_4$O$_4$Cの量が増加の後Al$_4$C$_3$の生成に伴って減少する。

Al$_2$O$_3$と黒鉛から純粋なAl$_4$O$_4$C化合物を合成することは困難であるが，そのAl$_2$O$_3$，黒鉛を少量に含んでいるAl$_4$O$_4$C合成原料でも，炭素含有耐火物の添加剤として用いることができると考えられる。

文献

1）京田　洋，西尾英昭，伊東克則，堀田修三：耐火物，38［4］242-250（1986).

2）山口明良：耐火物，38［8］506-512（198).

3）渡辺　明，高橋宏邦，高長茂幸：耐火物，38［11］740-746（1986).

4）S. Zhang and A.Yamaguchi：J. Ceram. Soc. Japan, 103［3］235-239（1995).

5）S. Zhang and A.Yamaguchi：Proceedings of Unified International Technical Conference on Refractories, 1997, New Orleans, USA, 861-869.

6）Y. Larrere, B. Willer, J. M. Lihrmann and M. Daire：Rev. Int. Hautes Temp. Refract., 21［1］3-18（1984).

7）S. Zhang and A.Yamaguchi：J. Ceram. Soc. Japan, 104［3］393-398（1996).

8）M. Wai and S.G. Hutchison：Metall. Trans. B, 121［2］406-408（1990).

9）O. M. Katkob：Izv. Vyssh. Uchebn. Zaved. Tsven. Metall., No.5, 38-42（1985).

10）R. M. Kibby and A. F. Saavedra：Light Met., 263-268（1987).

11）C. Qiu and R. Metselaar：Z. Metalkkd., 86［3］198-205（1995).

12）J.M. Lihrmann, J. Tirlocq, P. Descamps and F. Cambier：J. Eur. Ceram. Soc., 19, 2781-87（1999).

13）D.R.Stull and H.Prophet：JANAF Thermochemical Tables, United States Government Doc. No. NSRDS-NBS, 37, 2nd ed., 1971；supplements in J. phys. Chem. Ref. Data, 3［2］(1974)；4［1］(1975)；7［3］(1978)；11［3］(1982).

「材料」(Journal of the Society of Materials Science, Japan), Vol. 56, No. 6, pp. 526-530, June 2007
Original Papers

Sintering of Al_2O_3-Cr_2O_3 Powder Prepared by Sol-Gel Process †

by

Motonari FUJITA*, Keisuke INUKAI**, Shinichi SAKIDA***, Tokuro NANBA***, Junji OMMYOJI****, Akira YAMAGUCHI**** and Yoshinari MIURA*****

The sol-gel method was applied to create Al_2O_3-Cr_2O_3 ceramics using aluminum ethylacetoacetate diisopropylate and chromium (III) chloride hexahydrate as starting materials. In the calcination at 600-1200°C it was found that the grains of Cr_2O_3-rich solid solution grew when they were exposed to the surrounding Al_2O_3-rich amorphous particles. The composition of the powders obtained by the sol-gel process changed with calcining temperature. Cr_2O_3-rich solid solutions firstly crystallize at low temperature and the composition of the crystallites changes as the crystals grow and react with the surrounding Al_2O_3-rich phases. The final sintered bodies fired under an Ar atmosphere showed higher relative densities as compared with those fired in air. A dense sintered body was not obtained when abnormal grains grew when calcining occurred.

Key words : Al_2O_3, Cr_2O_3, *Solid solution, Sol-gel process, Sintering*

1 Introduction

The amount of municipal wastes in Japan is about 50 million tons/year. About 80% of waste disposal relies on incineration. In this case, however, endocrine disrupters such as dioxin are present in the gas and fly ash exhausted from the incineration facilities. This problem has become serious social issues. Melting type incinerators such as gasification melting furnaces have been developed as a solution to this problem. In high temperature melting type incinerators the wastes are burnt and melted above 1300°C. Generally Al_2O_3-Cr_2O_3 refractories are used in such conditions.[1),2)]

The alkali and alkali-earth elements such as Na, K and Ca are present in the municipal wastes and corrode furnace lining refractories. Porous microstructure refractories are attacked so a dense body is used to avoid damage. Hirata et al. investigated densification and corrosion of Al_2O_3-Cr_2O_3 by addition of TiO_2.[3),4)]

Aluminium organometallic compound[5)~7)] starting materials were used to obtain dense ceramics. The powders obtained from the starting material contained uniformly dispersed fine particles. The sintered Al_2O_3-Cr_2O_3 body seemed to have corrosion resistance when the material was used in the same way.

Al_2O_3-Cr_2O_3 ceramic is a solid solution of Al_2O_3 and Cr_2O_3 has high chemical stability even at high temperatures and hence it is used as a refractory brick in gasification melting furnaces. Both Al_2O_3 and Cr_2O_3 are chemically stable at high temperature and take a corundum crystal structure forming a solid solution $(Al_{1-x}Cr_x)_2O_3$ in the entire composition region at high temperature (Fig. 1). At relatively low temperatures a miscibility gap is present in which two crystalline phases of Al_2O_3-rich and Cr_2O_3-rich solid solutions are present. As shown in Fig. 1, the critical temperature Tc depends on the surrounding pressure.[8)~10)] A thermodynamically stable solid solution is necessary to obtain, and some conditions of the metastability are being researched now. Murakami et al.[11)] confirmed a metastable two-phase region at around 1300°C. Bondioli[12)] investi-

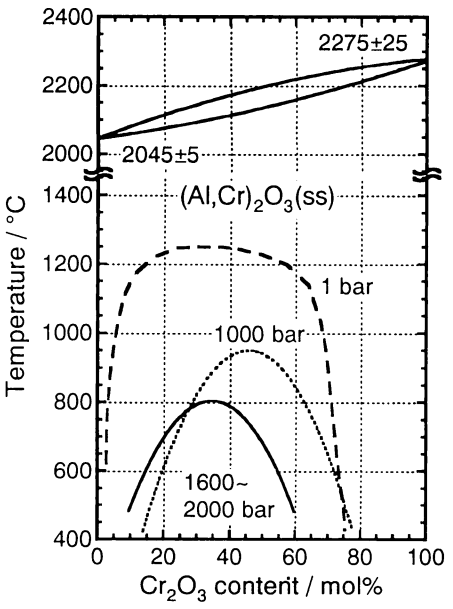

Fig. 1 Phase diagram of alumina-chromia (Al_2O_3-Cr_2O_3) system.[8)~10)]

† Received Oct 13, 2005 ©2007 The Society of Materials Science, Japan
* Okayama Ceram. Res. Fndn., Nishikatakami, Bizen, 705-0021 Japan, Present address : Kyushu Refractories Co., Ltd., Urainbe, Bizen, 705-0002 Japan.
** Grad. School Nat. Sci. Tech., Okayama Univ., Tsushima-Naka, Okayama, 700-8530 Japan, Present address : Shinagawa Refractories Co., Ltd., Chiyoda-ku, Tokyo, 102-0073 Japan
*** Health Environ. Center, Okayama Univ., Tsushima-Naka, Okayama, 700-8530 Japan
**** Okayama Ceram. Res. Fndn., Nishikatakami, Bizen, 705-0021 Japan
***** Member : Grad. School Environ. Sci., Okayama Univ., Tsushima-Naka, Okayama, 700-8530 Japan

gated two metastable phase by solid phases reaction and coprecipitation. When the different phases were observed in the heat-treated powder, reactivity was thought to influence sintering behavior.

Moreover, the vapor pressure of CrO_3 and CrO_2 is high so that the sintered body of Cr_2O_3 becomes porous due to the evaporation of Cr-compounds when fired in air.

We prepared uniform precursor powder mixed at a molecular level, and then got Al_2O_3-Cr_2O_3 dense ceramics. In this paper we investigated the mechanism for the formation of solid solution. The effects of powder size and sintering atmosphere on sintering were investigated.

2 Experimental Procedures

The raw materials used were aluminum ethylacetoacetate diisopropylate (ALCH, Kawaken Fine Chemicals Co., Ltd.) and $CrCl_3 \cdot 6H_2O$ (Wako Pure Chemical Industries Ltd.). ALCH and $CrCl_3 \cdot 6H_2O$ were dissolved in a 10 times the amount of raw material mole ratio of ethanol and were stirred and mixed with a homogenizer for 30 minutes and a supersonic homogenizer for 5 minutes. 30 times mole ratio of ion exchange water was slowly dropped with stirring and was mixed for 30minutes with a magnetic stirrer to obtain gels at room temperature. The gels were dried in a rotary evaporator and calcined at 600–1200°C for 1h in air. After the calcinations the powders were mixed with a ball mill for 10h using an ethanol solvent and pressed into pellets of about 25mm in diameter. The green bodies were sintered at 1600°C for 1h in an atmosphere of air or Ar. Fig. 2 shows the sample preparation procedures.

For comparison Al_2O_3-Cr_2O_3 ceramics were also prepared by a conventional solid phase reaction. The starting powders of Cr_2O_3 (Kanto Chemical Co., Inc.) and α–Al_2O_3 (AES-12 Sumitomo Chemical Co., Ltd.) were mixed with a ball mill for 10h using an ethanol solvent.

The bulk densities of the sintered bodies were measured and the relative densities were also estimated from the experimental values and the theoretical densities calculated from the compositions. The crystalline phases were identified by X-ray diffraction (XRD ; Rigaku RINT2200VHF + /PC) with CuKα radiation. The microstructures of the specimens were observed by optical microscope and scanning electron microscope (SEM ; JEOL JSM-6340F).

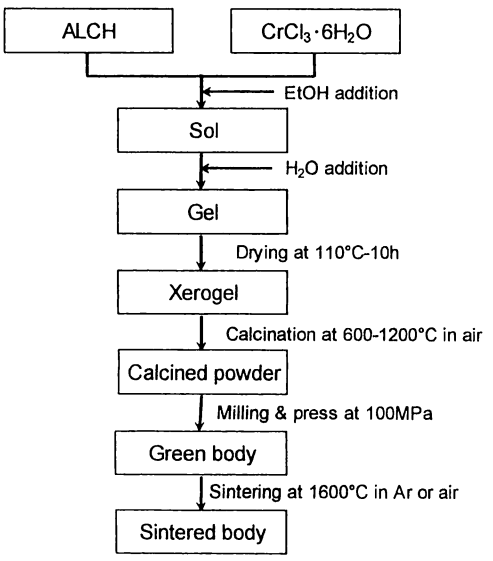

Fig. 2 Sample preparation procedures.

3 Results and Discussion

3.1 Formation of solid solution

Fig. 3 shows the XRD patterns of the sol-gel derived powders of 10, 30 and 50 mol% Cr_2O_3 calcined at 600–1200°C. A/C = 50/50 implies an equimolar ratio of Al_2O_3 and Cr_2O_3. Two phases in the A/C = 50/50 sample calcined at 600°C with a Cr_2O_3 content richer than the nominal composition, were observed. The double peak turned into a single peak above 700°C. In the A/C = 70/30 sample, no peak appeared when calcined at 600°C, and a phase was found when calcined above 800°C. In A/C = 90/10 sample no peak appeared when calcined at 800°C, and a crystalline phase was found as calcined above 900°C. In all the compositions as the calcination temperature increased the peak shifted to the higher diffraction angle side (Al_2O_3-rich side). These results indicate that Cr_2O_3-rich solid solutions firstly crystallize at low temperature and the composition of the crystallites changes

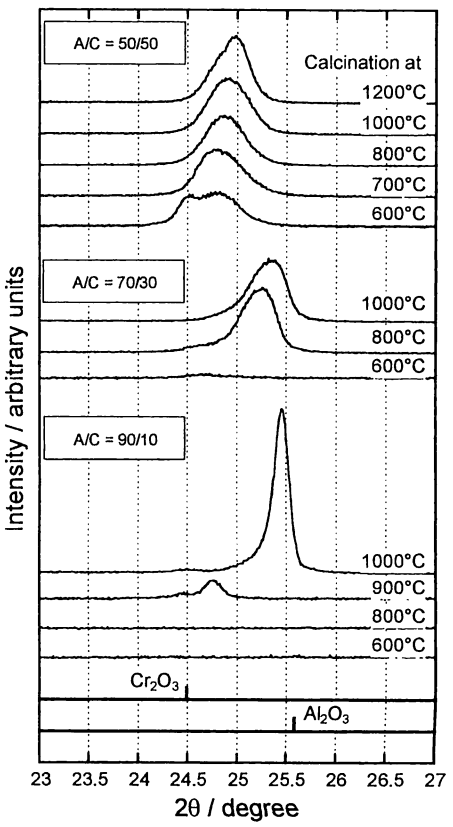

Fig. 3 XRD patterns of the sol-gel derived powders of A/C = 90/10, A/C = 70/30 and A/C = 50/50 calcined at 600°–1200°C. Solid lines indicate the position of respective (012) plane in pure Cr_2O_3 and Al_2O_3.

as they grow and react with the surrounding Al_2O_3-rich phases. When Cr_2O_3-rich phase was formed, the remained composition must be more excessive about Al_2O_3 content than the mixed composition. However, no Al_2O_3 excessive XRD peaks were seen. Hence Al_2O_3-rich phases are considered to be amorphous.

Fig. 4 shows the SEM micrographs of the A/C = 50/50 sol-gel derived powders calcined at 1000° and 1200°C. There was one peak in the sample of A/C = 50/50 whose critical temperature is reported to be 1250°C[10] even when calcined at 700° and 800°C. These powders, which were calcined at 1000° and 1200°C, are thought to be metastable. At 1000°C fine particles adhere to the larger particles however at 1200°C the fine particles disappear and hexagonal plates with smooth surfaces are observed. This suggests that the fine particles which vanish at 1200°C are the Al_2O_3-rich amorphous phases.

Fig. 5 shows the lattice constants of the sol-gel derived Al_2O_3-Cr_2O_3 powders calcined at 1000°C for 1h. The straight line of Fig. 5 is the theoretical line of the solid solution, which is a line drawn between the lattice constants[14), 15)] of corundum (a = 0.476nm, c = 1.295nm) and eskolite (a = 0.496nm, c = 1.360nm). As the results in Fig. 3 show, the XRD peak of A/C = 70/30 and A/C = 50/50 were broader than A/C = 90/10. It is thought that, with a high Cr_2O_3 content, the particles are divided into Cr_2O_3-rich crystalline and Al_2O_3-rich amorphous phases which resist unification into theoretical composition.

3.2 Sintering behavior of Al_2O_3-Cr_2O_3 system

Fig. 6 shows the relative density of Al_2O_3-Cr_2O_3 ceramics sintered at 1600°C in Ar and air atmospheres. As for the sample in Ar with A/C = 70/30 and with A/C = 50/50 prepared by the sol-gel method, the relative density increases up to 95% at all calcining temperatures. When the calcining temperature was high, relative density was low at A/C = 90/10. In the sintered bodies that were made from the powder prepared by a solid state reaction, the relative density was about 92% at all the content levels. As for the sintering atmospheres the samples sintered in air show lower density and the samples with higher Cr_2O_3 content have loosely packed structures. When the powder prepared by sol-gel method was used and calcined at 1000°C, the relative density of the sintered bodies was about 60% at all the Cr_2O_3 content levels.

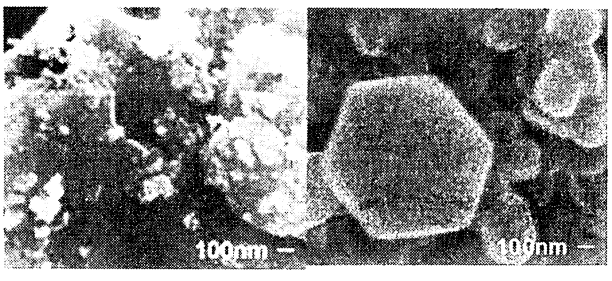

Fig. 4　SEM micrographs of the sol-gel derived powders of A/C = 50/50 calcined at 1000° (left) and 1200°C (right).

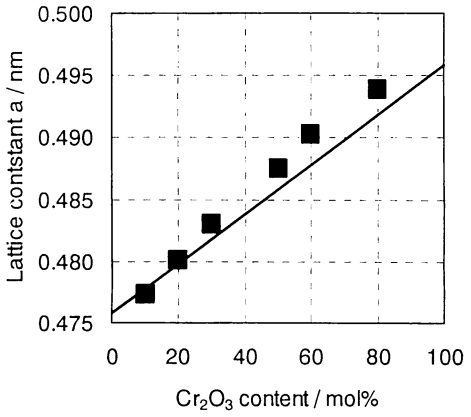

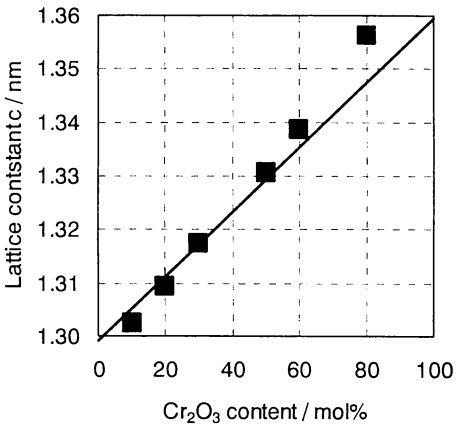

Fig. 5　Lattice parameters of the sol-gel derived powders of (Al, Cr)$_2O_3$ calcined at 1000°C for 1h.

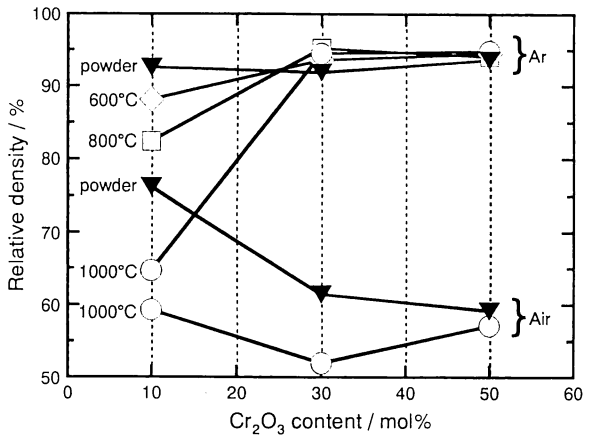

Fig. 6　Relative densities of Al_2O_3-Cr_2O_3 ceramics sintered at 1600°C in Ar and air atmospheres. Temperatures in the figure indicate the calcination temperature of the sol-gel derived samples. The samples prepared by the solid phase reaction are shown as "powder".

Fig. 7 shows the vapor pressure diagrams of the compounds of Al-O and Cr-O at 1900K. Pressure is shown

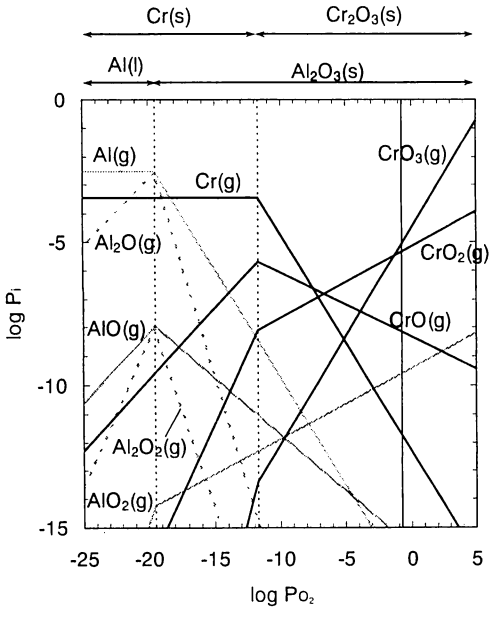

Fig. 7　Vapor pressure diagrams of Al-O and Cr-O compounds at 1900K.[13)]

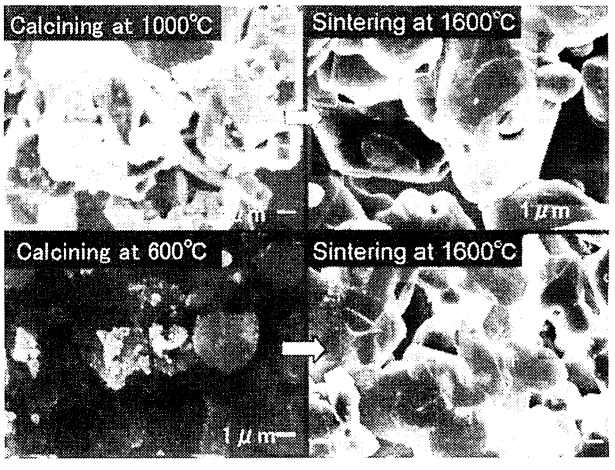

Fig. 8　SEM micrographs of the A/C = 90/10 samples after the calcination at 1000°C and 600°C in air and after sintering at 1600°C for 1h in Ar.

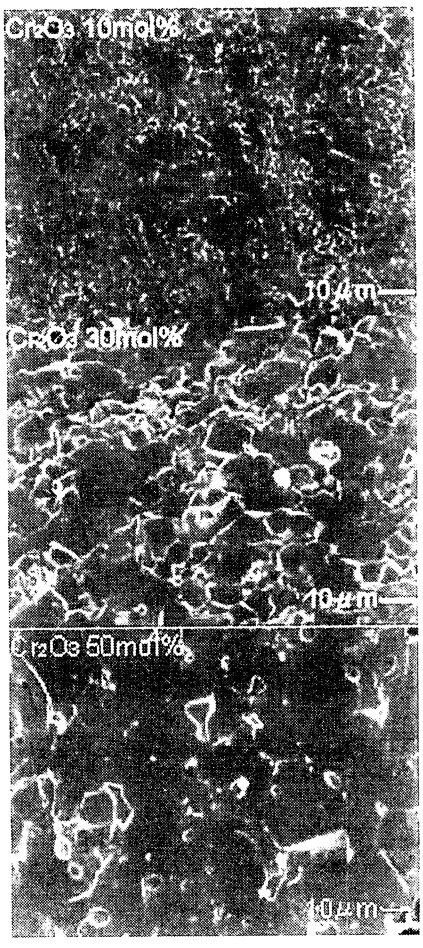

Fig. 9　SEM micrographs of the sol-gel derived Al_2O_3-Cr_2O_3 ceramics sintered at 1600°C in Ar after the calcination at 600°C.

without the dimension standardized under the standard-state pressure (10^5Pa). None of the sample heated in air were dense. This results can be explained as follows, based on the Fig. 7. CrO_3 (g) and CrO_2 (g), which partial pressure is the highest in Cr-O system, undergo high pressure increase under O_2 partial pressure. In air atmosphere, CrO_3 (g) partial pressure has $\log P_{CrO_3} = -5$. Therefore, the powder was sintered without shrinkage because of the vaporization and condensation mechanism.

Although Cr_2O_3 may discharge Cr (g) under low P_{O_2} conditions, the sintered bodies did not loses weight in an Ar atmosphere nor did the metal Cr (s) separate. This suggests that the evaporation speed was very slow. Therefore dense sintered bodies were obtained in an Ar atmosphere.

Fig. 8 shows the SEM micrographs of the A/C = 90/10 samples after calcination at 1000°C and 600°C in air and after sintering at 1600°C for 1h in Ar. The particle diameter of powder calcined at 600°C was 0.1μm, and grain growth to 5μm was confirmed when sintered at 1600°C. The powder calcined at 1000°C had a 5μm particle diameter which grew to 10μm when sintered. When calcining temperature was changed to 1000°C from 600°C, grain diameter also changed from 5μm from 0.1μm. This is the result of unusual grain growth during calcination. In the A/C = 90/10 samples the relative density of the final products decreased with an increase in calcination temperature.

Fig. 9 shows the microstructure of the sol-gel derived Al_2O_3-Cr_2O_3 ceramics sintered at 1600°C in Ar after the calcination at 600°C. The particle size increases with increasing Cr_2O_3 content. This tendency was also seen in the sintered bodies made from the powder prepared by the solid state reaction.

Fig. 10 shows a relation between the grain size of the calcined powder and the relative density of the sintered body at 1600°C in Ar by the sol-gel method. For the A/C = 50/50 samples, the relative density was 95% and the

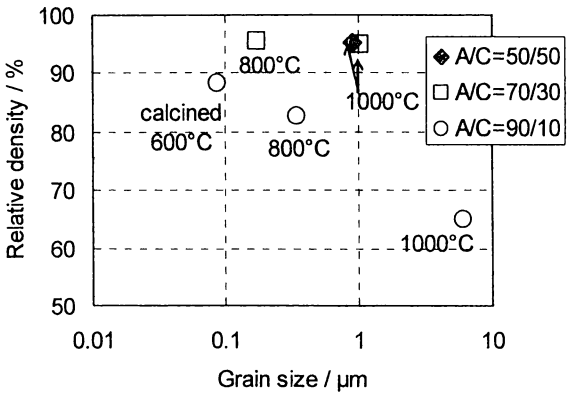

Fig. 10 Relation between grain size of calcined powder and relative density of body sintered at 1600°C in Ar by sol-gel method.

grain size of the powder calcined at 1000°C was 1μm. For the A/C = 70/30 samples, the relative density was 95% and the grain size of the powder calcined at 1000°C was 1μm and at 800°C was 0.2μm. In the A/C = 90/10 sample, the relative density increased in inverse proportion to the logarithmic grain size. This tendency was very different from that for A/C = 30/70 and 50/50. The separated phase state of the calcined powder was divided into Cr_2O_3-rich crystalline and Al_2O_3-rich amorphous phases. This is considered to be the cause for dense sintering to proceed.

4 Conclusions

Al_2O_3-Cr_2O_3 ceramics were prepared by the sol-gel method and the formation mechanism of solid solution and the sintering process were examined.

(1) The composition of the crystallized phases changes with the calcined temperature.

(2) Cr_2O_3-rich solid solution firstly crystallize at low temperature and the composition of the crystallites changes as they grow and react with the surrounding Al_2O_3-rich phase.

(3) Al_2O_3-Cr_2O_3 precursor becomes much denser when sintered at 1600°C in Ar.

(4) A dense sintered body was obtained when abnormal grains did not grow when calcining occurred.

REFERENCE

1) A. Yamaguchi, "Present Situation and Problems of Refractories for Waste Melting Furnace", The Japan Society of Waste Management Experts, Vol.13, No.1, pp.47-53 (2002).

2) A. Yamaguchi, "Usefulness and Problem of the Chrome-containing Refractory" Taikabutsu, Japan, Vol.57, No.6, pp.316-320 (2005).

3) T. Hirata, K. Akiyama and H. Yamamoto, "Sintering behavior of Cr_2O_3-Al_2O_3 ceramics", Journal of European Ceramic Society, Vol.20, No.2, pp.195-199 (2000).

4) T. Hirata, T. Morimoto, A. Deguchi and N. Uchida, "Corrosion Resistance of Alumina-Chromia Ceramic Materials Against Molten Slag", Materials Transactions, Vol.43, No.10, pp.2561-2567 (2002).

5) H. Yoshimatsu, K. Kawabata, A. Osaka, Y. Miura and H. Kawasaki, "Preparation of ZrO_2-Al_2O_3 powder by thermal decamposition of gels produced from an aluminium chelate compound and zirconium butoxide", Journal of Materials Science, Vol.31, No.8, pp.4975-4980 (1996).

6) K. Kawabata, H. Yoshimatsu, T. Yabuki, A. Osaka and Y. Miura, "Selective Reduction of Nitrogen Oxide with Propylene on Alumina-Zirconia Prepared from Al Chelate Compound and Zr Alkoxide", Journal of the Ceramic Society of Japan, Vol.104, No.5, pp.458-461 (1996).

7) K. Kawabata, H. Yoshimatsu, T. Yabuki, A. Kubotsu, S. Hayakawa, A. Osaka and Y. Miura, "Properties of Alumina-Zirconia Powder Prepared from Aluminium Chelate Compound and Zirconium Alkoxide", Journal of the Ceramic Society of Japan, Vol.106, No.2, pp.155-159 (1998).

8) A. Neuhaus, "Physics and Chemistry of High Pressure. Edited by the Society of Chemical Industry", p.237 (1963) Gordon and Breach Science Publishers, New York.

9) D. M. Roy and R. E. Barks, "Subsolidus Phase Equilibria in Al_2O_3-Cr_2O_3", Nature Physical Science, Vol.235, No.2, pp.118-119 (1972).

10) W. Sitte, "Investigation of the Miscibility Gap of the System Chromia-Alumina below 1300°C", Materials Science Monographs, Vol.28A, pp.451-456 (1985).

11) Y. Murakami, T. Hirata and Y. Tsuru, "Metastable phase relationship in the Al_2O_3-Cr_2O_3 system and phase equilibria of 1 : 1 composition at 1200°C", Journal of the Ceramic Society of Japan, Vol.110, No.6, pp.541-543 (2002).

12) F. Bondioli, A. M. Ferrari, C. Leonelli, T. Manfredini, L. Linati and P. Mustarelli, "Reaction Mechanism in Alumina/Chromia (Al_2O_3-Cr_2O_3) Solid Solutions Obtained by Coprecipitation", Journal of the American Ceramic Society, Vol.83, No.8, pp.2036-2040 (2000).

13) M. W. Chase, Jr., "NIST-JANAF Thermo chemical Tables Forth Edition Part I Al-Co and Part II Cr-Zr", Journal of Physical and Chemical Reference Data, Monograph No.9 (1998).

14) JCPDS, "powder Diffraction File-Inorganic," Card No.10-173 (1986).

15) JCPDS, "powder Diffraction File-Inorganic," Card No.38-1479 (1986) .

Journal of the Ceramic Society of Japan 115 [4] 272-277 (2007)

Paper

Al-Si-C-N 系組成物の焼結に及ぼす炭素の影響

藤田基成・隠明寺準治・山口明良

岡山セラミックス技術振興財団，705-0021 岡山県備前市西片上 1406-18

Influence of Carbon on Sintering of the Al-Si-C-N System Composite

Motonari FUJITA, Junji OMMYOJI and Akira YAMAGUCHI

Okayama Ceramics Research Foundation, 1406-18, Nishikatakami, Bizen-shi, Okayama 705-0021

The composite in Al_4SiC_4-AlN and Al_4SiC_4-AlN-C system were sintered by a spark plasma sintering method. The powders of metal Al, Si and carbon black and AlN as starting materials were mixed. The mixture was calcined at 1300°C and sintered at 1600° to 1800°C by spark plasma sintering. Shrinkage during sintering, density, microstructure and phase of sintered bodies were measured. X-ray diffraction analysis gave Al_5SiC_4N (15R) and AlN (2H) phases in the bodies sintered at 1750°C. Densification did not occur in some composition in 50 to 80% AlN of the system Al_4SiC_4-AlN, but their densification was accelerated by addition of carbon. By the analysis of shrinkage during sintering and SEM observation of microstructure, the grain of Al_5SiC_4N (15R) and AlN (2H) grew, and pore exclusion was obstructed in the system Al_4SiC_4-AlN, though the grain did not grow, and pore exclusion was accelerated in the system Al_4SiC_4-AlN-C.

[Received July 19, 2006; Accepted February 15, 2007]

Key-words : *Al_4SiC_4, AlN, Spark plasma sintering, Pore exclusion, Reaction sintering*

1. 緒　言

Al と Si の複合炭化物である Al_4SiC_4 は SiC よりも高温での耐酸化性に優れる性質が見出されている[1),2)]．Al_4SiC_4 の緻密焼結体が放電プラズマ焼結で助剤無添加で1700°C程度の比較的低温から得られており[1)~5)]，電気伝導率[3)]，熱膨張率[4)]及び熱伝導率[5)]が計られており，新たな高温材料としての可能性が見出されてきている．

Al-Si 系の炭化物，窒化物の複合は，AlN-C 系[6)~8)]，SiC-AlN 系[9)~11)]，Al_4C_3-SiC 系[12),13)]，Al_4C_3-SiC-AlN 系[14)~16)]などいくつかの系で検討され，新たな特徴の探索や構造解析の研究が行われている．しかし，Al_4SiC_4 に添加物を混合した場合の報告例は少ない．このため，本研究では Al_4SiC_4 に AlN を複合した場合を考え，焼結挙動について検討した．複合の形態を Al_4SiC_4-AlN 系及び Al_4SiC_4-AlN-C 系とし，焼結体を放電プラズマ焼結で作製し，焼結性の評価を行った．Al_4SiC_4 に AlN を添加することにより，焼結性が低下する範囲が確認され，この緻密化阻害を防ぐ方法として炭素を若干過剰とする方法で緻密化が可能となったことについて報告する．

2. 実　験

Al_4SiC_4 のみ及びこれに少量の遊離 C を含む組成に対して AlN を加えた Al_4SiC_4-AlN 系と Al_4SiC_4-AlN-C 系について検討した．出発原料には Al 粉末(試薬，99.99%-200 mesh，三ツ和化学)，Si 粉末 (試薬，99.99%-200 mesh，三ツ和化学)，C 粉末 (カーボンブラック粉末，東海カーボン TOKABLACK#7350) 及び AlN 粉末 (試薬，99% 8.85 μm，三ツ和化学) を使用し，Al_4SiC_4-AlN 系組成物を作製した．また，Al_4SiC_4 に対して C を過剰に外掛けで2.71 mass%添加した組成に AlN を加えることにより Al_4SiC_4-AlN-C 系組成物を作製した．図 1 に作製試料の組成を Al-Si-C-N 系図上に示す．

全量100 g になるように所定量を混合した粉末をアルミナ質ボールミルによってよく混合した後，200 cm^3 の黒鉛るつぼに充填し，黒鉛発熱体炉で Ar 雰囲気下で1300°C, 3 h の仮焼を行った．得られた粉末をアルミナ質ボールミルで粉砕し，約28 g の粉体をφ50 mm の黒鉛ダイに装填し，0.03 MPa の N_2 雰囲気で昇温速度60～80°C min^{-1} で1600°Cから1800°Cまで昇温し20 min 保持の条件で，放電プラズマ焼結装置 (SPS シンテックス製，SPS-820S) を用い，焼結させた．得られた焼結体の上下面を切削して，アルキメデス法で密度測定を行い，破断面を SEM (電解放射型走査電子顕微鏡；日本電子 JSM-6340F) で観察した．残った試片を粉砕し，乾式型ピクノメータ (湯浅アイオニクス；マルチピクノメータ) で試料の真密度を測定した．焼結体の相対密度は真密度に対するかさ密度の値である．また，

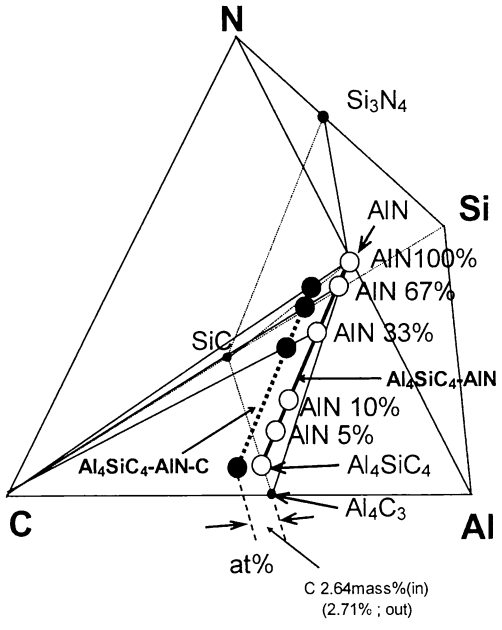

Fig. 1. Prepared sample and Al-Si-C-N system.

Table 1. Phase Present and Densities in Calcined Powder at 1300°C for 3 h and Sintered Bodies by SPS at 1750°C for 20 min

	Al_4SiC_4 / mass%	AlN / mass%	C / mass%	Calcined at 1300°C for 3 h: Phase present Main (Sub)	Packing density (Relative density) of green-body / gcm^{-3}(%)	True density of calcined powder / gcm^{-3}	Sintered by SPS at 1750°C for 20 min: Phase present Main (Sub)	Bulk density (Relative density) of sintered-body / gcm^{-3}(%)	True density of sintered-body / gcm^{-3}
Al_4SiC_4-AlN	100	0	0	Al_4SiC_4(8H)	1.28 (42.6)	3.01	Al_4SiC_4(8H)	3.01 (99.96)	3.01
	95	5	0	Al_4SiC_4(8H)	1.40 (46.3)	3.02	Al_4SiC_4(8H) (Al_5SiC_4N(15R))	2.97 (99.2)	2.99
	90	10	0	Al_4SiC_4(8H) (Al_5SiC_4N(15R))	1.28 (42.2)	3.03	Al_5SiC_4N(15R) (Al_4SiC_4(8H))	2.74 (91.6)	2.99
	80	20	0	Al_5SiC_4N(15R) (Al_4SiC_4(8H))	1.31 (42.7)	3.06	Al_5SiC_4N(15R) (AlN(2H))	2.94 (97.0)	3.03
	67	33	0	AlN(2H) (Al_5SiC_4N(15R)) (Al_4SiC_4(8H))	1.25 (40.5)	3.09	Al_5SiC_4N(15R) (AlN(2H))	2.76 (92.3)	2.99
	50	50	0	AlN(2H) (Al_4SiC_4(8H))	1.27 (40.6)	3.13	AlN(2H) (Al_5SiC_4N(15R))	2.72 (89.6)	3.03
	33	67	0	AlN(2H) (Al_4SiC_4(8H))	1.44 (45.4)	3.17	AlN(2H) (Al_5SiC_4N(15R))	2.40 (75.3)	3.18
	20	80	0	AlN(2H) (Al_4SiC_4(8H))	1.52 (47.4)	3.20	AlN(2H) (Al_5SiC_4N(15R))	2.33 (73.1)	3.19
	0	100	0	AlN(2H)	1.85 (57.2)	3.24	AlN(2H)	2.88 (88.7)	3.24
Al_4SiC_4-AlN-C	100	0	2.71	Al_4SiC_4(8H)	1.31 (43.8)	2.99	Al_4SiC_4(8H)	2.95 (99.4)	2.97
	67	33	2.71	Al_4SiC_4(8H) (Al_5SiC_4N(15R)) (AlN(2H))	1.46 (47.6)	3.06	Al_5SiC_4N(15R) (AlN(2H)*)	3.00 (99.4)	3.02
	33	67	2.71	AlN(2H) (Al_4SiC_4(8H))	1.42 (45.3)	3.14	AlN(2H)* (Al_5SiC_4N(15R))	2.87 (91.5)	3.14
	0	100	2.71	AlN(2H)	1.66 (51.6)	3.22	AlN(2H)	2.95 (96.2)	3.07

* 2 peaks

XRD（理学電機；RINT 2200 VHF +/PC）で結晶相を同定した．

3. 結　果

3.1 仮焼粉末の相と成形体密度

表1に1300°Cで仮焼した粉末と1750°Cで焼結した焼結体のXRD結果及び粉末成形体の充填密度，焼結体の焼結密度を示す．1300°Cで仮焼した粉末ではAl_4SiC_4組成（AlN 0%）でAl_4SiC_4（8H）単相，AlN 100%ではウルツ鉱AlN（2H）の単相になった．Al_4SiC_4-AlN系のAlN 5%ではAl_4SiC_4（8H）のみが観察され，AlN 10%ではAl_4SiC_4（8H）とAl_5SiC_4N（15R）の混相でAl_4SiC_4（8H）が主相であった．AlN 20%ではAl_5SiC_4N（15R）とAl_4SiC_4（8H）の混相でAl_5SiC_4N（15R）が主相であった．AlN 33%ではAlN（2H），Al_4SiC_4（8H）とAl_5SiC_4N（15R）の三つの混相でAlN（2H）が主相であった．AlN 50%以上ではAlN（2H）とAl_4SiC_4（8H）の混相でAlN（2H）が主相となった．Al_4SiC_4-AlN-C系ではAlN 0%ではAl_4SiC_4（8H），AlN 33%ではAlN（2H），Al_4SiC_4（8H）とAl_5SiC_4N（15R）の三つの混相，AlN 67%ではAlN（2H）とAl_4SiC_4（8H）の混相，AlN 100%にCと混合した場合ではAlN（2H）となった．いずれも各Al_4SiC_4/AlN比に対する生成相はAl_4SiC_4-AlN系の場合とAl_4SiC_4-AlN-C系の場合とで変わりのない結果であった．

放電プラズマ焼結前の粉末成形体の充填密度は，Al_4SiC_4-AlN系では1.28～1.85 g cm^{-3}の範囲で，すなわち相対密度としては約41～57%の範囲で変化し，AlNの割合が増加すると高くなった．また，Al_4SiC_4-AlN-C系の粉末成形体の充填密度はAlNの混合比の増大に従って上昇し，1.27～1.66 g cm^{-3}の範囲，すなわち相対密度としては約41～52%の範囲となっており，Al_4SiC_4-AlN系とほぼ同様であった．

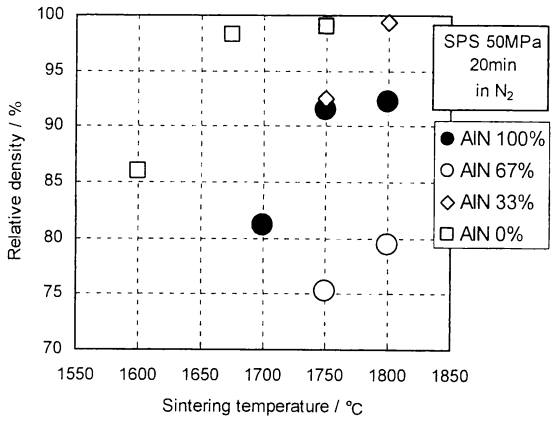

Fig. 2. Relation between sintering temperature and relative density of Al_4SiC_4-AlN bodies sintered by spark plasma sintering.

3.2 Al_4SiC_4-AlN系及びAl_4SiC_4-AlN-C系の緻密化焼結

図2にAl_4SiC_4-AlN系焼結体の焼結温度と相対密度の関係を示す．AlN 0%，33%，67%及び100%いずれの組成も焼結温度が上昇すると相対密度は高くなった．AlN 0%では1675°C及び1750°C，AlN 33%では1800°Cでの焼結温度で，相対密度は98%以上に達しているが，AlNが67%及び100%では1800°Cの焼結温度でも相対密度は80%と92%にとどまった．

図3にAl_4SiC_4-AlN系及びAl_4SiC_4-AlN-C系の*1750°C*での加熱によって得られた焼結体について，AlN含有量に対する見掛気孔率及び全気孔率の関係を示す．Al_4SiC_4-AlN系ではAlN 50%以下では見掛気孔率がほぼ0%程度となり，気孔の形態は

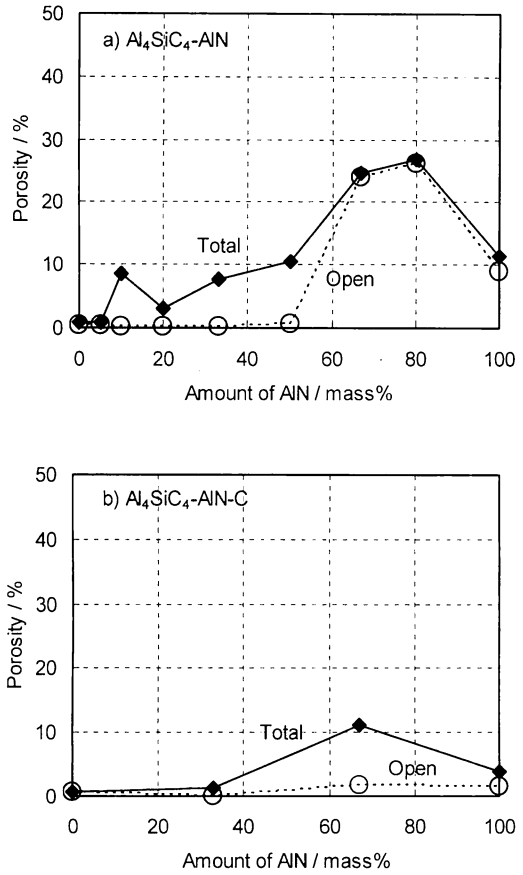

Fig. 3. Relation between amount of AlN and porosities of a) Al_4SiC_4-AlN and b) Al_4SiC_4-AlN-C bodies sintered at 1750°C for 20 min.

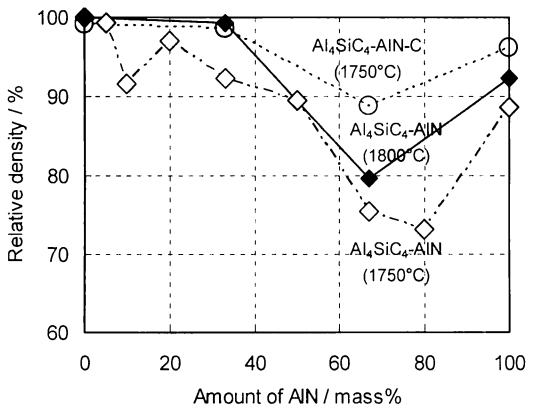

Fig. 4. Relation between amount of AlN and relative densities of bodies sintered at 1750°C and 1800°C for 20 min in Al_4SiC_4-AlN and Al_4SiC_4-AlN-C system.

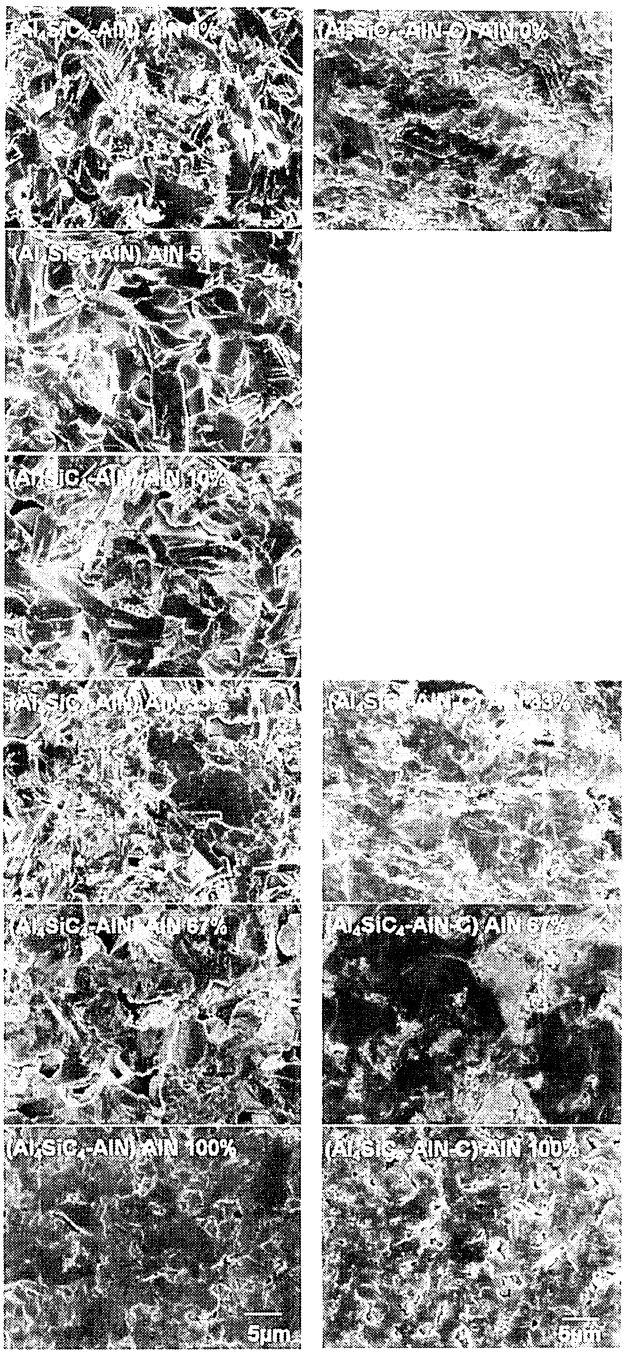

Fig. 5. SEM micrographs of fracture surface for bodies sintered at 1750°C for 20 min.

ほとんど密閉気孔であった．AlN 67～80%では25%程度の開放気孔であった．AlN 100%では10%弱の開放気孔があった．Al_4SiC_4-AlN-C 組成では開放気孔はほとんどなく，AlN 67%で見掛気孔率はもっとも高く，約2%であった．なお，いずれの試料も重量減少はなかった．

図4に1750°C及び1800°Cで焼結させた焼結体の相対密度を出発原料中の AlN 含有量に対して示す．Al_4SiC_4 の理論組成通りの原料組み合わせ（AlN 無添加）では100%近くまで緻密化した．他方 AlN のみでも若干の気孔があるが相対密度90%にまで緻密化した．Al_4SiC_4-AlN 系では1750°Cの場合，AlN 5%以下では98%以上の相対密度であるが，AlN の増加とともに低下し，AlN 67%及び80%では約75%であった．しかし，AlN 100%では90%と上昇した．焼結温度を1800°Cに上げると AlN 33%では98%，AlN 67%では約80%，AlN 100%で92%まで相対密度が上昇した．

これに対し，1750°Cでの Al_4SiC_4-AlN-C 系では AlN 33%で98%，AlN 67%では90%，AlN 100%では95%の相対密度であった．Al_4SiC_4-AlN 系の AlN 67%～100%の領域で焼結温度を上昇させた場合より炭素を添加した方に緻密化の促進が見られた．

図5に1750°Cで作製した焼結体の破断面の SEM 像を示す．

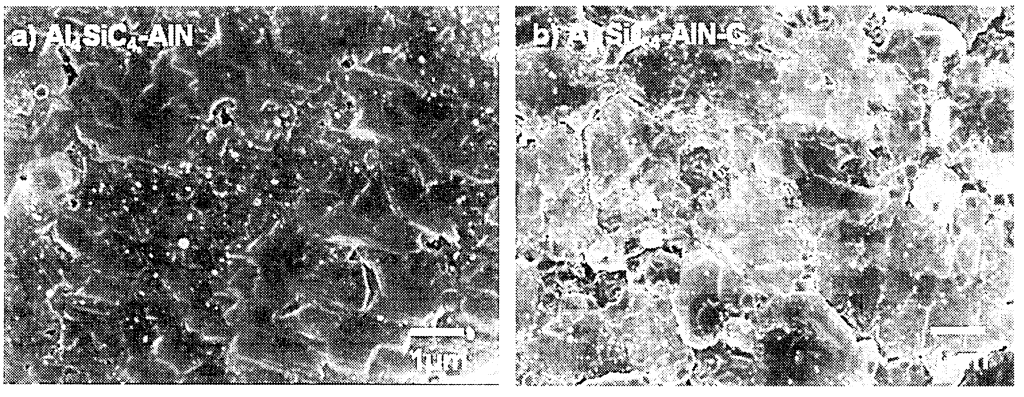

Fig. 6. SEM micrographs of polished and etched surface component for the bodies sintered at 1750°C for 20 min by spark plasma sintering with composition AlN 67% a) Al_4SiC_4-AlN and b) Al_4SiC_4-AlN-C.

Al_4SiC_4-AlN 組成では AlN0%，5%では気孔はほとんど見られず，緻密になっていた．AlN 100%では，1 μm 程度の気孔が少量点在していた．AlN 10%及び33%では若干の密閉気孔が見られた．また，AlN 67%では多くの気孔が観察された．Al_4SiC_4-AlN-C 組成では，AlN 0%では気孔はなく，破断面の組織は Al_4SiC_4-AlN 組成よりも粒が小さく観察された．AlN 33%でも気孔はなく，緻密になった．AlN 67%では気孔は存在するが Al_4SiC_4-AlN 組成のものよりも気孔径は小さく，しかも量的に少なかった．

緻密化に差異のあった Al_4SiC_4-AlN 系と Al_4SiC_4-AlN-C 系の AlN67%の焼結体について，より拡大した組織を観察した．図 6 に研磨面を熱エッチングした表面の SEM 像を示す．Al_4SiC_4-AlN 系では粒の境界が明瞭に見られなかった．これに対して，Al_4SiC_4-AlN-C 系では粒の境界が明瞭である．

3.3 Al_4SiC_4-AlN 系及び Al_4SiC_4-AlN-C 系の焼結体の相と収縮挙動

表 1 に1750°Cで処理した焼結体の XRD 結果を示す．Al_4SiC_4-AlN 系では Al_4SiC_4 組成（AlN 0%）で Al_4SiC_4（8H）単相，AlN 100%ではウルツ鉱 AlN（2H）の単相になった．AlN 10%以下では Al_4SiC_4（8H）と Al_5SiC_4N（15R）の 2 相である．AlN 10%で Al_4SiC_4 とわずかの Al_5SiC_4N の 2 相になった．これに対して Al_4SiC_4-AlN-C 系では AlN 33%，AlN 67%でいずれも AlN（2H）と Al_5SiC_4N（15R）の混相であったが，AlN（2H）の回折図形上では同一反射面に対して二つのピークが観察された．また，過剰に添加した C については，黒鉛として検出されなかった．

図 7 に Al_4SiC_4-AlN 系及び Al_4SiC_4-AlN-C 系試料での AlN 67%の仮焼粉末と焼結体の XRD ピークを示す．仮焼粉末ではどちらの系でも生成相は AlN（2H）と Al_4SiC_4（8H）で大きな差はなかった．焼結体では，仮焼粉末では生成していない Al_5SiC_4N（15R）相が，いずれも生成していた．Al_4SiC_4-AlN 系では仮焼粉末と焼結体で AlN（2H）のピーク位置が異なっており，焼結体では仮焼粉末の AlN（2H）よりも低角側にシフトしていた．これに対して C を2.71 mass%外掛け添加した Al_4SiC_4-AlN-C 系の焼結体では AlN のピークは二つに分かれた．一つは仮焼粉末の AlN（2H）と同様の位置のピークで，他の一つは仮焼粉末よりも低角側にシフトしていた．C の有無により AlN（2H）相の構造の変化がみられる結果となった．

図 8 に1750°C，20 min の放電プラズマ焼結での処理中の加圧方向の試料の変位を温度に対して及び一定温度に保持した後は時間に対して示す．Al_4SiC_4-AlN 系の AlN 0%では1300°C付近

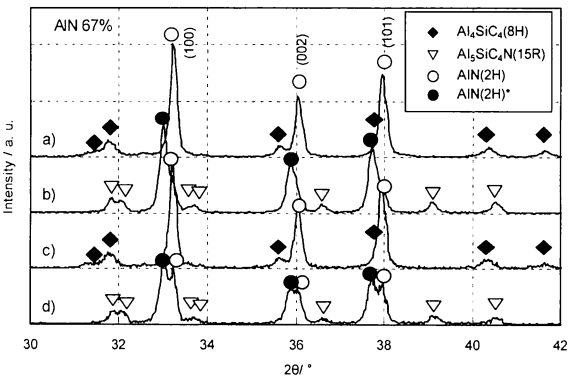

Fig. 7. X-ray diffraction patterns of AlN 67% component for the powder of a) Al_4SiC_4-AlN and c) Al_4SiC_4-AlN-C calcined at 1300°C for 3 h and for the bodies of b) Al_4SiC_4-AlN and d) Al_4SiC_4-AlN-C sintered at 1750°C for 20 min.

で収縮が開始し，その後直線的に収縮量が増加した．この後，1750°Cでの保持後に数分で，収縮は止まった．AlN 5～33%では収縮の開始温度は約1300°CからでAlN 0%とあまり変わらなかったが，1600°C以上の温度域で収縮曲線の傾きは AlN 0%と比べると若干低下した．このうち AlN 10%以上では1750°Cで保持中に収縮が継続された．AlN 量が多いものほど収縮が継続される傾向が強い．AlN 50%以上では収縮開始の温度が低くなり，その後の収縮量が小さくなった．AlN 50%，67%及び AlN 80%の順に収縮量が小さかった．AlN 100%では，収縮開始温度は高かった．

Al_4SiC_4-AlN-C 系では，各試料とも約1300°Cで収縮が開始し，AlN の含有量が異なるごとに収縮曲線の傾きが変化した．AlN 67%が収縮曲線の傾きが小さいが，Al_4SiC_4-AlN-C 系ではいずれのものでも収縮量は Al_4SiC_4-AlN 系より大きかった．Al_4SiC_4-AlN 系と Al_4SiC_4-AlN-C 系の緻密化の度合いの差は大きく，AlN 67%の組成で比較をすると，収縮開始した後の収縮量が Al_4SiC_4-AlN-C 系の方が大きくなっていた．

4. 考　察

4.1 生成相と緻密化について

図 4 で示したように Al_4SiC_4-AlN 系と Al_4SiC_4-AlN-C 系の焼結性に差異が認められ，C が存在する系で緻密化が促進された．この理由は次のように考えられ，表 1 の結果から Al_4SiC_4-AlN

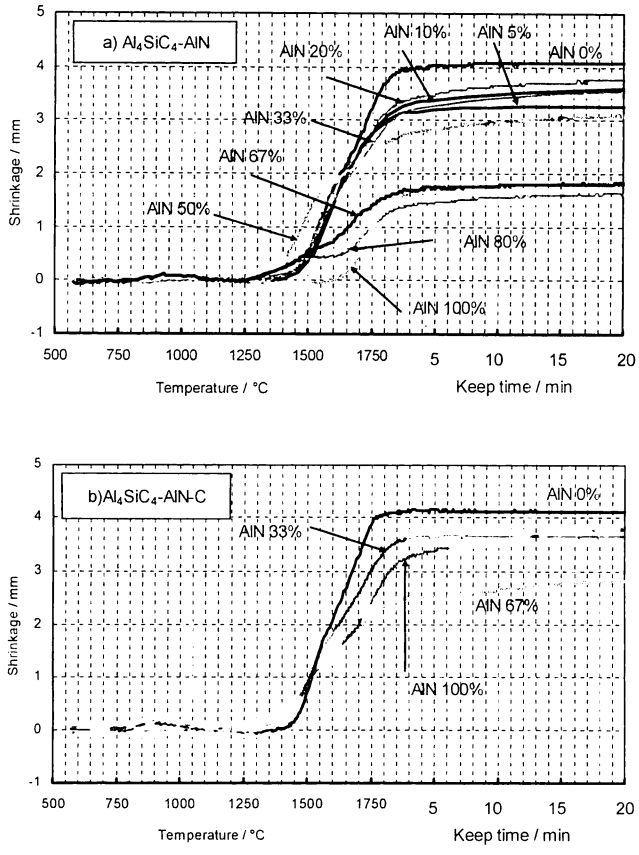

Fig. 8. Shrinkage curves of the samples during spark plasma sintering with composition a) Al_4SiC_4-AlN and b) Al_4SiC_4-AlN-C.

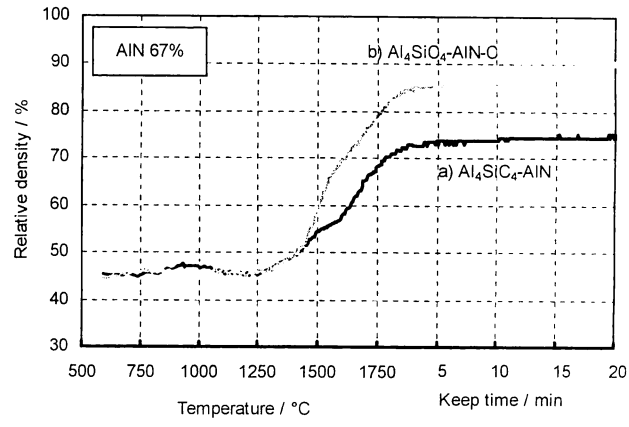

Fig. 9. Change of relative density of the samples during spark plasma sintering with composition AlN 67% a) Al_4SiC_4-AlN and b) Al_4SiC_4-AlN-C.

系では AlN 50～80％のとき1300°Cでの仮焼粉末の結晶相は AlN (2H) と Al_4SiC_4 (8H) である．焼結体は両者が反応して新たに Al_5SiC_4N (15R) を生成して，AlN (2H) との２相となっている．また，図７に示される焼結体の AlN (2H) は，仮焼粉末で現れた AlN (2H) のピークより低角側にずれていた．この AlN (2H) は，Si や C が固溶して生成したものであると考えられる．これによって，ピークのずれが生じたと考えられる．また，焼結中は Al_5SiC_4N や AlN が粒成長し，気孔を囲むことになると考えられる．それぞれの粒は成長し，気孔を排除できず，緻密化が進行しなかったと考えられる．AlN 10～33％では Al_5SiC_4N が主相であるが，同様に粒が成長し，気孔内のガスは排除されなくなり，密閉気孔となったと考えられる．

一方，Al_4SiC_4-AlN-C 系では，1750°Cで加熱された焼結体は Al_5SiC_4N (15R) と AlN (2H) が検出され，その AlN (2H) は図 7d)の(100)面，(002)面及び(101)面のピークが二つに分かれていた．一つは上述の1750°C加熱によって現れた AlN のピークと一致している．他方は仮焼粉末に現れる AlN のピークと一致した．このように C の含有により，生成相に変化が認められたのは次のように考えられる．共存する C は Al_4SiC_4 や AlN と化合物をつくらないので，Al_5SiC_4N や AlN 粒の間隙に点在し Al_4SiC_4 と AlN 粒の接触を妨げたと考えられる．その結果として Al_4SiC_4-C-AlN の粒界面を通じての気孔内のガス排出を容易にした結果であると考えられる．

4.2　焼結時の密度と組織について

Al_4SiC_4-AlN-C 系で緻密化が進行した理由について図６の結果からみると次のように考えられる．Al_4SiC_4-AlN 系においては強固な結合で，気孔を取り囲んでおり，気孔の排除が進行しなかったようにみられるが，これに対し，Al_4SiC_4-AlN-C 系では形成する粒の境界がはっきりしている．この境界は過剰な C の分散により形成された粒界であったと考えられる．粒界が多く存在することにより，粒は成長せず，強固に結合を形成せずに気孔排除が可能となり，緻密化が進行したと考えられる．C の介在によって，粒界が多く存在することによる自己潤滑特性[17]が付与され，気孔排除が容易になり，緻密化が進行したと考えられる．

AlN 67％の Al_4SiC_4-AlN 系と Al_4SiC_4-AlN-C 系の焼結体について，緻密化の進行度合いを相対密度の変化として考えてみた．図９は放電プラズマ焼結での加熱及び加圧時における相対密度変化である．この図は，図８の試料厚みの変化とダイの断面積（焼結体試料の径は焼結中一定である）と装填された粉末重量からかさ密度を算出し，それより求めた相対密度である．仮焼粉末と焼結体の粉砕粉末の真密度はほぼ同じであるので，後者の値を用いて算出した．Al_4SiC_4-AlN系 と Al_4SiC_4-AlN-C 系とも，成形体の相対密度は45％程度で，ほぼ同じである．1750°Cで20 min 保持した後の試料の相対密度は，Al_4SiC_4-AlN 系では75％，Al_4SiC_4-AlN-C 系では90％であり，大きな差が生じていた．両者とも約1300°Cから収縮をし始めているが，約1450°C から Al_4SiC_4-AlN-C 系の相対密度増加が著しくなり，差異が生じ始めている．この差異が生じたのは，C の介在によって Al_4SiC_4-AlN 粒の間隙に炭素が存在する構造となり，気孔排除が容易になったと考えられる．

5.　結　　論

Al_4SiC_4 と AlN の組成に注目し，Al_4SiC_4-AlN 系及び Al_4SiC_4-AlN-C 系の焼結特性を金属 Al 粉末，Si 粉末，カーボンブラック粉末及び AlN 粉末を混合して放電プラズマ焼結により焼結体を作製し，緻密化に及ぼす炭素の影響を調べ，以下の結論を得た．

(1)　Al_4SiC_4-AlN 系の焼結において AlN の量比が50～80％の組成範囲で，C の添加によって緻密化が促進される．

(2)　C 添加により，粒界はより多く形成し，気孔排除は容易になるため，緻密化は促進される．

References

1)　Inoue, K., Yamaguchi, A. and Hashimoto, S., *J. Ceram. Soc. Japan*, Vol. 110, pp. 1010-1015 (2002) [in Japanese].

2) Inoue, K., Mori, S. and Yamaguchi, A., *J. Ceram. Soc. Japan*, Vol. 111, pp. 126-132 (2003) [in Japanese].
3) Inoue, K. and Yamaguchi, A., *J. Ceram. Soc. Japan*, Vol. 111, pp. 267-270 (2003) [in Japanese].
4) Inoue, K., Mori, S. and Yamaguchi, A., *J. Ceram. Soc. Japan*, Vol. 111, pp. 348-351 (2003) [in Japanese].
5) Inoue, K., Mori, S. and Yamaguchi, A., *J. Ceram. Soc. Japan*, Vol. 111, pp. 466-470 (2003) [in Japanese].
6) Bandoh, Y., *Ceramics Japan*, Vol. 26, pp. 754-758 (1991) [in Japanese].
7) Jeffrey, G. A. and Wu, V. Y., *Acta Cryst.*, Vol. 16, pp. 559-566 (1963).
8) Jeffrey, G. A. and Wu, V. Y., *Acta Cryst.*, Vol. 20, pp. 538-547 (1966).
9) Ruh, R. and Zangvil, A., *J. Am. Ceram. Soc.*, Vol. 65, pp. 260-265 (1982).
10) Carrillo-Heian, E. M., Xue, H., Ohyanagi, M. and Munir, Z. A., *J. Am. Ceram. Soc.*, Vol. 83, pp. 1103-1107 (2000).
11) Miura, M., Yogo, T. and Hirano, S., *J. Mater. Sci.*, Vol. 28, pp. 3859-3865 (1993).
12) Barczak, V. J., *J. Am. Ceram. Soc.*, Vol. 44, pp. 299-299 (1961).
13) Inoue, Z., Inomata, Y. and Tanaka, H., *J. Mater. Sci*,, Vol. 15, pp. 575-580 (1980).
14) Oden, L. L. and McCune, R. A., *J. Am. Ceram. Soc.*, Vol. 73, pp. 1529-1533 (1990).
15) Oscroft, R. J. and Thompson, D. P., *J. Am. Ceram. Soc.*, Vol. 74, pp. 2327-2329 (1991).
16) Oscroft, R. J. and Thompson, D. P., *J. Am. Ceram. Soc.*, Vol. 75, pp. 224-226 (1992).
17) Zhien, L., Jianjun, Y. and Zhiyun, X., *J. Mater. Sci.*, Vol. 30, pp. 399-404 (1995).

Available online at www.sciencedirect.com

ScienceDirect

Ceramics International 33 (2007) 1585–1589

CERAMICS INTERNATIONAL

www.elsevier.com/locate/ceramint

Oxidation protection of $CaO–ZrO_2–C$ refractories by addition of SiC

Min Chen [a,*], Nan Wang [a], Jingkun Yu [a], Akira Yamaguchi [b]

[a] *School of Materials and Metallurgy, 312#, Northeastern University, 3-11 Wen-Hua Road, Shenyang 110004, China*

[b] *Okayama Ceramics Research Foundation, 1406-18 Nishi Katakami, Bizen, Okayama 705-0021, Japan*

Received 10 October 2005; received in revised form 24 April 2006; accepted 3 July 2006

Available online 18 September 2006

Abstract

The effect of SiC used as antioxidant in carbon-containing $CaO–ZrO_2$ refractories and the behaviour of SiC in CO gas were studied. SiC was found to react initially with CO to form SiO_2(s) and C(s) at ~1200 °C, and then the formed SiO_2 reacted with CaO in the refractories to form belite ($2CaO·SiO_2$). The refractory microstructure was modified by addition of SiC. Due to the deposition of SiO_2 in the large (2–10 μm) pores of the refractory through the reaction of SiO(g) with CO, the percentage of large pores decreased and a dense layer, mainly consisting of belite, was formed near the surface of the refractory after it was heated at high temperature (1500 °C). The oxidation resistance of $CaO–ZrO_2–C$ refractories was improved by reaction of SiC with CO to deposit C(s) and decrease the size of the large pores. The oxidation resistance of such refractories can be improved significantly when such a dense layer is formed near their surfaces.

© 2006 Elsevier Ltd and Techna Group S.r.l. All rights reserved.

Keywords: $CaO–ZrO_2–C$ refractories; Oxidation resistance; Oxidation; Antioxidant

1. Introduction

Carbon possesses excellent thermal shock and slag resistance properties, and it has become an important component of commercial refractories, however, carbon suffers the drawback of poor oxidation resistance [1]. To improve the oxidation resistance of carbon-containing refractories, antioxidants, such as metals (Mg, Al, Si), alloys (Mg–Al) and carbides (B_4C, SiC) are often added to them. The antioxidant selected varies according to the matrix type of the carbon-containing refractories. For example, Mg and Al are often added to MgO–C refractories, whereas SiC is often added to $Al_2O_3–C$ refractories [2,3].

Lime has the advantages of being abundant, having a high melting temperature, a low vapour pressure and thermodynamic stability in the presence of carbon. Accordingly, CaO–C refractories have long been regarded as potentially attractive for applications in the metallurgical industries [4,5]. In recent years, lime-containing refractories have shown great advantages in dephosphorization and desulphurization of molten steel [6]. Nevertheless, the application of CaO refractories has been inhibited owing to its poor hydration resistance, and the main attention of lime refractories research has been in this area [7,8]. The present authors have also studied this topic and prepared hydration resistant $CaO–ZrO_2$ composites through the formation of a protective $CaZrO_3$ layer around CaO grains [9]. Little attention has been paid to improve the oxidation resistance of CaO–C refractories [10,11].

In the present work, the behaviour of SiC antioxidant in CO gas and the mechanism of improved oxidation resistance of $CaO–ZrO_2–C$ refractories were studied.

2. Experimental procedures

2.1. Starting materials

The starting materials in the present work were $CaO–ZrO_2$ grain prepared by grinding $CaO–ZrO_2$ clinker (sintered from a mixture of reagent grade $CaCO_3$ and ZrO_2 in the molar proportion $CaO:ZrO_2 = 80:20$, with relative density of over 99%) [9] to pass 90 μm, carbon (graphite flake, with purity of over 99.7% and average size of less than 0.5 μm) and SiC (with purity of over 99% and average grain diameter of 2–3 μm).

* Corresponding author. Tel.: +86 24 6368 2241; fax: +86 24 8368 1576.
E-mail address: slakejp@163.com (M. Chen).

0272-8842/$32.00 © 2006 Elsevier Ltd and Techna Group S.r.l. All rights reserved.
doi:10.1016/j.ceramint.2006.07.004

Table 1
Composition of the $CaO–ZrO_2–C$ refractories, mass%

Batch	$CaO–ZrO_2$ grain	Graphite	SiC
1	80	20	0
2	75	20	5

2.2. Sample preparation

Two batches of powder were prepared by wet-mixing (in acetone) $CaO–ZrO_2$ grain, carbon and SiC in the proportions shown in Table 1. Then the mixed powders were shaped to cylindrical compacts of $D15$ mm × ~15 mm and plate compacts of 20 mm × 20 mm × ~12 mm by using CIP (cold isostatic pressing) under 100 MPa with 4 mass% phenolic resin as a binder. Cylindrical compacts were pretreated at 800 °C for 5 h in a carbon powder bed for the carbonization of resin before the oxidation test.

2.3. High temperature behaviour of SiC added to $CaO–ZrO_2–C$ refractories

Approximately 1.5 g of the mixture with SiC addition (with composition of sample 2) was heated in a tube furnace at a heating rate of 10 °C/min. After soaking at different temperatures for 2 h and at 1500 °C for 2–6 h, the heated sample was cooled in the furnace to room temperature at a rate of 10 °C/min. CO gas was bled into the furnace at a flow rate of 0.2 L/min for the duration of the heat treatment. The phase composition of the heat treated mixture was analyzed by using powder XRD (X-ray diffraction, Cu target, 20 kV, 20 mA) and the mass change was measured using an electric balance.

2.4. High temperatures oxidation testing

The oxidation test was carried out by heating the cylindrical bricks in a TG (thermogravimetric) furnace in air (Fig. 1a), with the same heating and cooling rate of 10 °C/min. The pore size distribution of the bricks was examined using mercury porosimetry, and the phase composition of the samples after heating was analyzed using XRD. Cross sections of the heated samples were observed under optical microscopy and SEM (scanning electron microscopy).

Because of the low pressure used, the relative density of the brick was so poor that the cylindrical compact was completely oxidized before it reached the higher temperature (1500 °C). To investigate the oxidation behaviour of the refractory with SiC addition at a higher temperature, the oxidation test was also carried out in another electric furnace by embedding most of a plate compact in carbon powder while keeping its top surface exposed to air, as shown in Fig. 1b. The sample was heated to 1500 °C at a rate of 10 °C/min and kept at this temperature for 4 h. After heating, the microstructure was observed under optical microscopy and the composition near the surface was obtained by spot analyses with interval of 200 μm using EPMA (Electron Probe Micro Analysis).

3. Results and discussion

3.1. Behaviour of SiC added to $CaO–ZrO_2–C$ refractories

It is known that the main gaseous species in the refractories is CO when the oxides coexist with condensed carbon. Therefore, the present work investigated the behaviour of SiC added to the refractories in CO gas. Fig. 2 shows the phase change of the $CaO–ZrO_2–C$ refractories with SiC addition after heating at different temperatures for 2 h and at 1500 °C for 2–6 h in CO gas. The intensity of SiC began to decrease significantly above 1200 °C, and, simultaneously, the intensity of CaO decreased and belite (Ca_2SiO_4) began to be detected. This indicates that the SiC reacted with CO to form SiO_2(s) and C(s) according to reaction (1) from ~1200 °C. The identification of belite indicates that the formed SiO_2 reacted further with CaO. For $CaZrO_3$, no change of its intensity after heating at different temperatures confirmed that it was stable in these

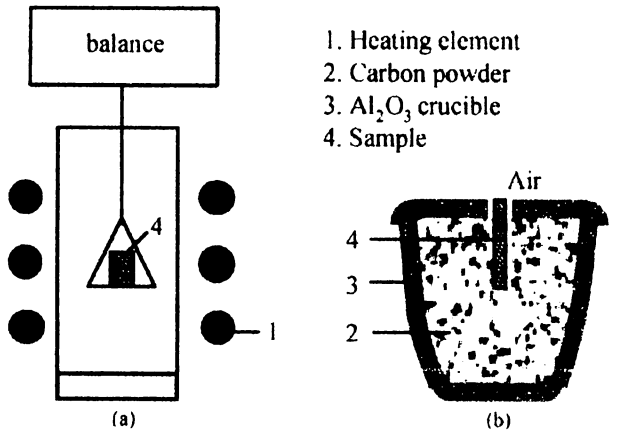

Fig. 1. Schematic diagram of reaction vessel for oxidation test of the $CaO–ZrO_2–C$ refractories.

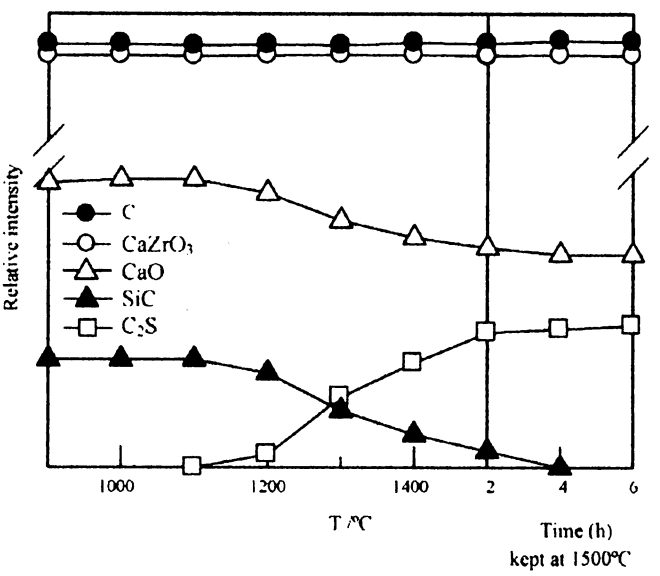

Fig. 2. Phase change of the $CaO–ZrO_2–C$ refractories with SiC addition heated at various temperatures for 2 h and at 1500 °C for different time.

atmospheres and temperature conditions. The intensities of CaO and belite reached a constant value when the sample was heated at 1500 °C for 6 h, indicating the completion of the reaction in the refractories.

$$SiC(s) + 2CO(g) = SiO_2(s) + 3C(s) \quad (1)$$

Fig. 3 shows the mass change of the mixture with SiC addition (with composition of sample 2) after heating at different temperatures for 2 h and at 1500 °C for 2–6 h in CO gas. The abrupt increase of mass gain from 1200 °C also confirmed the occurrence of reaction (1) from this temperature. As previously reported, it is considered that the occurrence of reaction (1) proceeded in the following two steps [2]:

$$SiC(s) + CO(g) = SiO(g) + 2C(s) \quad (2)$$

$$SiO(g) + CO(g) = SiO_2(s) + C(s) \quad (3)$$

Because a part of the SiO(g) volatilized to the atmosphere, it did not completely condense as SiO_2 within the refractories. As a result, after the refractory was heated in CO gas for 6 h, the mass gain of the refractory was only 5.8 mass%, which was less than the theoretical value of 7.0 mass%.

3.2. Improved oxidation resistance of the CaO–ZrO_2–C refractories

Fig. 4 shows the mass changes of the CaO–ZrO_2–C refractories heated to 1300 °C and kept at this temperature for 2 h in air at a heating rate of 10 °C/min. Mass decreased in a similar manner for both samples at lower temperatures, but from 1200 °C, the mass decrease was obviously suppressed and a plateau was found for samples with SiC addition. For samples without SiC, the mass reached a constant value after 11 min at 1300 °C, whereas it was 32 min for samples with SiC. These results indicate that the oxidation of carbon was effectively suppressed by the deposition of C(s) when SiC was added.

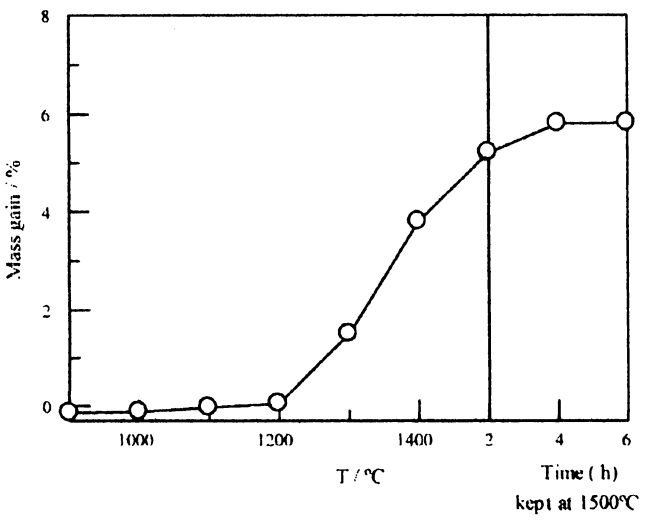

Fig. 3. Mass change of the CaO–ZrO_2–C refractories with SiC addition heated at various temperatures for 2 h and at 1500 °C for different time.

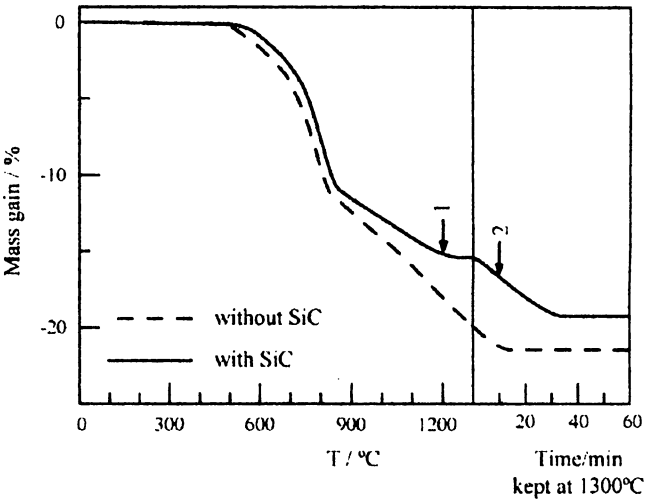

Fig. 4. Mass change of the CaO–ZrO_2–C bricks heated in air at a rate of 10 °C/min.

Fig. 5 shows XRD of the air quenched samples with SiC addition after heating to 1200 °C and holding at 1300 °C for 10 min in air (corresponding to positions 1 and 2 in Fig. 4). It is observed that SiC was still found and no alite or belite [12] formed when samples were heated to 1200 °C, but SiC disappeared and there was an obvious increase in the intensity of alite peaks after the sample was held at 1300 °C for 10 min. Similar to the results shown in Fig. 3, this shows that SiC began to react with CO at ~1200 °C. Because of the occurrence of this reaction, mass loss by carbon oxidation was counterbalanced by deposition of carbon. Thus the oxidation rate was decreased, and a plateau formed (in Fig. 4). Due to the mass increasing while SiC was oxidized to SiO_2, the mass loss of the SiC added refractory was always less than that of the sample without SiC after they were completely oxidized (Fig. 4).

Fig. 6 shows the optical photographs of the CaO–ZrO_2–C refractories after heating at 1300 °C for 10 min. For the sample

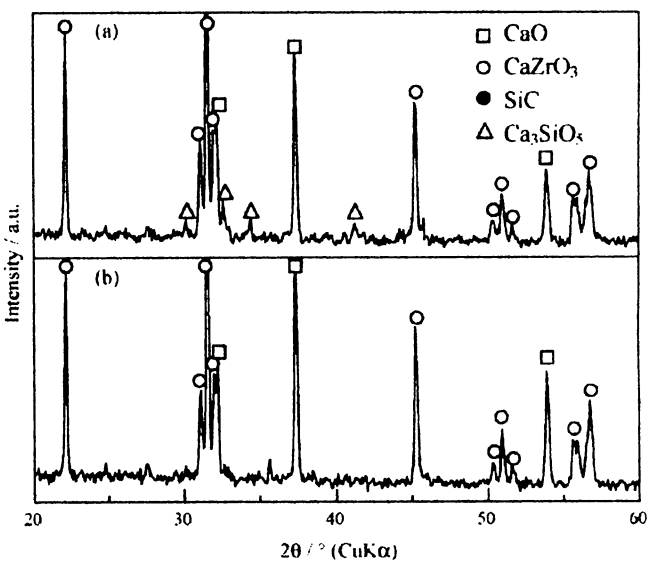

Fig. 5. XRD of the SiC added CaO–ZrO_2–C refractories heated to (a) 1200 °C and (b) kept at 1300 °C for 10 min.

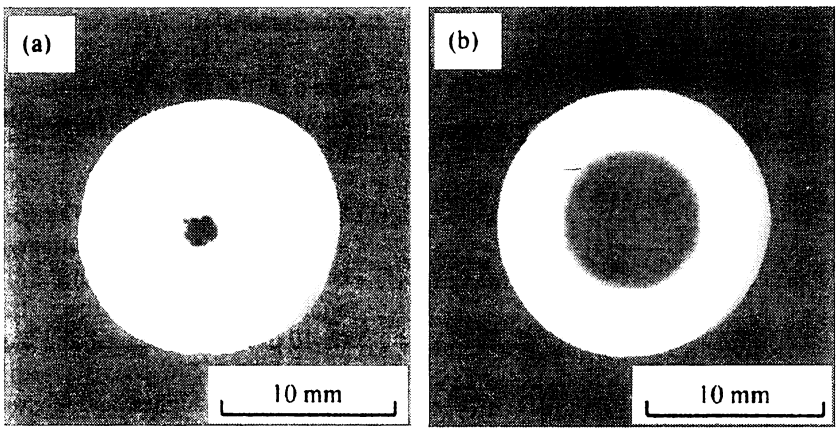

Fig. 6. Section of (a) SiC free and (b) SiC added CaO–ZrO_2–C refractories heated at 1300 °C for 10 min in air.

without SiC, the refractories were almost completely oxidized (the central black zone is the unoxidized core). But for the sample with SiC, a large unoxidized zone was still observed. This result also confirmed that the addition of SiC effectively improved the oxidation resistance of the refractories.

3.3. Modification of microstructure

Fig. 7 shows the pore size distribution of the refractories with and without SiC heated at 1300 °C for 2 h. It is observed that although there was no obvious change in apparent porosity (it was 50% and 49% for the sample without and with SiC addition, respectively), the percentage of large pores (2–10 μm) was decreased when SiC was added. The microstructure observation also identified that the amount of large pores decreased when SiC was added, as shown in Fig. 8.

The modification of microstructure was considered to occur by the reaction of SiC turning to SiO_2. Because of diffusion of SiO(g) at high temperature, SiO(g) was considered likely to condense as SiO_2(s) in the pores. As a result, the pores were filled with SiO_2 (which further reacted with CaO to form belite) and the pore size decreased.

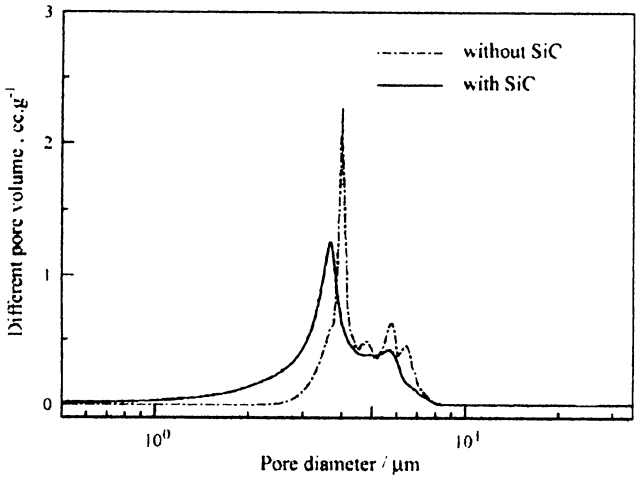

Fig. 7. Pore size distribution of the CaO–ZrO_2–C bricks after 2 h at 1300 °C.

It is known that the partial pressure of $P_{SiO(g)}$ is strongly dependent on temperature. For example, it is calculated that $P_{SiO(g)}$ is 270 Pa at 1300 °C, increasing to 535 Pa when the temperature is elevated to 1500 °C. Because of the low $P_{SiO(g)}$ and limited time of SiC coexisting with carbon due to the complete oxidation of carbon at 1300 °C, SiO(g) would be expected to diffuse only a short distance. As a result, SiO(g) reacted with CO gas to condense as SiO_2 (reaction (3)) just at the original SiC site or the pores nearby.

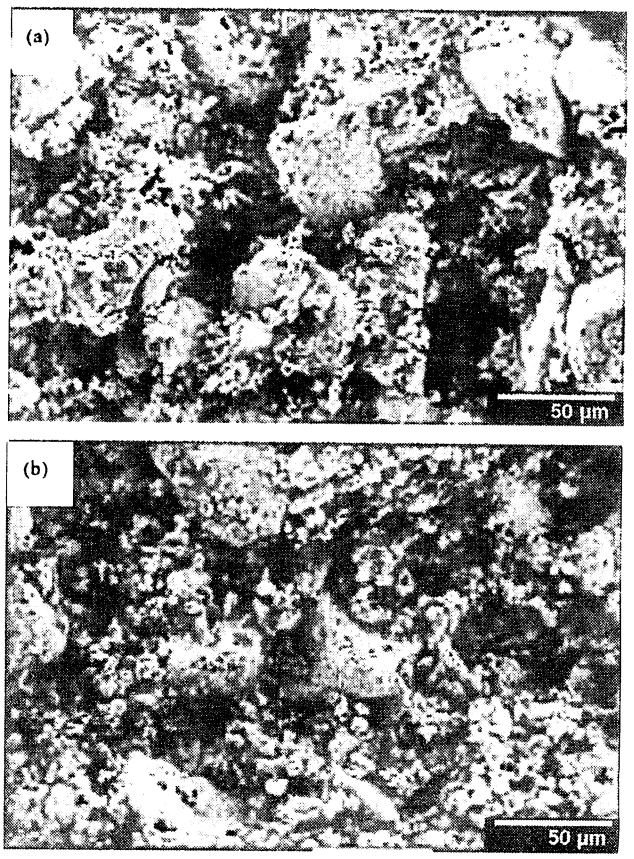

Fig. 8. SEM photographs of the fractured surface of CaO–ZrO_2–C bricks (a) without and (b) with SiC addition after heating at 1300 °C for 2 h.

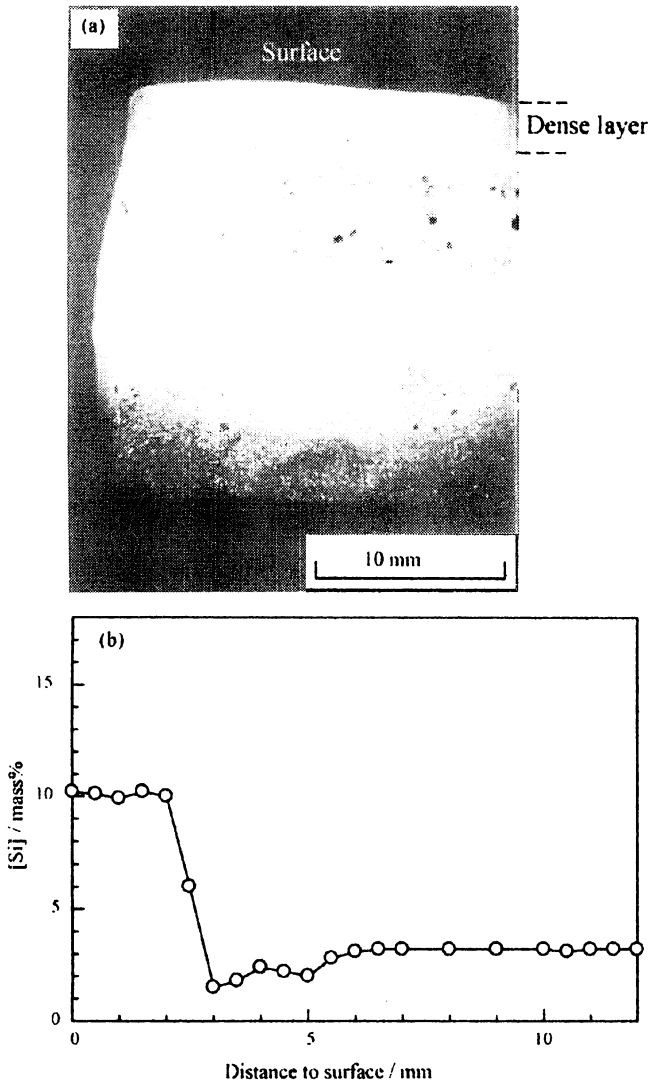

Fig. 9. Reflected light photograph (a) and result of EPMA analysis (b) of the SiC added CaO–ZrO_2–C refractories after heating at 1500 °C for 5 h in carbon bed.

However, when the sample was heated at a higher temperature and SiC coexisted with carbon for a sufficiently long time, the formed SiO(g) diffused continuously to the surface of the refractory and condensed to form SiO_2. Thus, a dense protective layer near the surface of the refractory was formed, as shown in Fig. 9a. EMPA analyses showed that the silicon content in the dense layer was much higher than that in the bulk (Fig. 9b). This confirms that the dense layer formation near the surface arises by the condensation of SiO(g). It is considered that the formation of a dense protective layer can effectively suppress the diffusion of oxygen into the refractories and improve its oxidation resistance.

4. Conclusions

Based on the above results, the following conclusions were drawn when SiC was added as an antioxidant to the CaO–ZrO_2–C refractories:

(1) SiC begins to react with CO gas at ~1200 °C, forming C(s) and SiO_2(s). The latter further reacts with CaO to form belite. Due to the diffusion and condensation of SiO(g), the microstructure was modified. The percentage of large pores (2–10 μm) is decreased and a dense protective layer is formed when SiC coexists with condensed carbon in the refractory at higher temperature (1500 °C) for enough time.

(2) The addition of SiC improves the oxidation resistance of CaO–ZrO_2–C refractories by reaction of SiC with CO gas to deposit carbon and modification of the microstructure. In particular, a dense protective layer formed near the refractories surface is effective in improving the oxidation resistance.

References

[1] Ewais, M. Emad Monhamed, Carbon based refractories, J. Ceram. Soc. Jpn. 112 (10) (2004) 517–532.
[2] A. Yamaguchi, Behaviors of SiC and Al added to carbon containing refractories, Taikabutsu Overseas 4 (3) (1984) 14–18.
[3] A. Yamaguchi, Thermalchemical analysis for reaction process of aluminium and aluminium-compounds in carbon-containing refractories, Taikabutsu Oversea 7 (2) (1987) 11–16.
[4] F. Nadachowski, Refractories based on lime: development and perspectives, Ceram. Int. 2 (2) (1976) 55–61.
[5] T. Degawa, Some properties and application of calcia ceramics, Seramikkusu 23 (11) (1988) 1052–1055.
[6] Y. Wei, N. Li, J.C. Kuang, F. Chen, Desulfurization and dephosphorization of molten iron in basic refractories, InterCeram 51 (3) (2002) 200–205.
[7] Y. Oda, Preventive methods for hydration of calcia and dolomite clinkers, Taikabutsu 41 (12) (1989) 690–700.
[8] H. Nakayama, Study on preventing agent against slaking of calcia clinker, Yogyo-Kyokai-shi 87 (1) (1979) 28–37.
[9] M. Chen, A. Yamaguchi, Sintering of CaO–ZrO_2 composite and its property of slaking resistance, J. Ceram. Soc. Jpn. 110 (12) (2002) 1055–1058.
[10] S. Hashimoto, A. Yamaguchi, Mechanism of oxidation suppression of CaO–C refractories by antioxidant, in: H. Henein, T. Oki (Eds.), Proceedings of the First International Conference Processing Mater, 1993, pp. 255–299.
[11] A. Yamaguchi, Carbon containing complex refractories, Kizoku 64 (11) (1994) 52–152.
[12] Powder Diffraction File, Card No. 35-0790, 31-1232, 31-0301, JCPDS International Center for Diffraction Data, Newtown Square, PA, USA (1997).

Journal of the Ceramic Society of Japan 115 [9] 525-529 (2007)

Paper

Preparation and Properties of Spark Plasma Sintered Magnesium Aluminum Oxynitride

Wenbin DAI,*,** Akira YAMAGUCHI,* Wei LIN,* Junji OMMYOJI,* Jingkun YU** and Zongshu ZOU**

*Okayama Ceramics Research Foundation, Okayama 705-0021

**School of Materials and Metallurgy, Northeastern University, Liao Ning, 110004, China

In this paper, the effects of heating temperature and soaking time on the synthesis of magnesium aluminum oxynitride (MgAlON) by spark plasma sintering (SPS) were investigated. Results showed that the content of N decreased while that of O increased with the increasing of temperature, because of the reaction between Mg_3N_2 and H_2O when the sample heated below 1500°C. Owing to the rapid warming up rate and the reaction between graphite and H_2O, the variation of chemical composition was lowered in the sample heated at higher temperature. During the heating process, shrinkage started above 1000°C and expansion was observed above 1600°C. Moreover, open pores were not detected in the sample heated at 1500°C for 1 min and single phase MgAlON without pores could be obtained when heated at 1700°C for 10 min. With the increasing of the content of Mg and the decreasing of N, all the thermal characteristics were increased and the cold bending strength was decreased, which may provide a standard data about the cold bending strength and the thermal characteristics of MgAlON with different composition. [Received January 12, 2007; Accepted July 19, 2007]

Key-words : *Magnesium aluminum oxynitride (MgAlON), Spark plasma sintering (SPS), Preparation, Property*

1. Introduction

Magnesium aluminum oxynitride (MgAlON) is a solid solution material with high melting point and considered as a promising superior refractory.[1] Investigations on its oxidation behavior[2)-4)] and synthesis processes[1),5)-7)] have been carried out and lots of meaningful results have been achieved. Up to now, three methods about the preparation of MgAlON have been proposed: (1) solid phase reaction of AlN, Al_2O_3 and MgO;[5),6)] (2) reaction of Al, Al_2O_3 and MgO;[7)] and (3) carbothermal reduction and nitridation of carbon, Al_2O_3 and MgO.[1)] Among these methods, the first one has more advantages to prepare high density MgAlON with small sized starting materials,[1)] and its reaction sequences can be described as following: MgO reacts with Al_2O_3 above 1000°C and magnesium aluminate spinel ($MgAl_2O_{4ss}$) is formed at first. Then, with the solid solution of AlN and Al_2O_3 into $MgAl_2O_{4ss}$ above 1350°C, MgAlON is formed, and the potential of the solution of AlN and Al_2O_3 increases with the increasing of temperature.[6)]

As a material to utilize at high temperature, it is necessary to investigate the thermal characteristics, such as thermal expansion, thermal diffusivity, thermal capacitance, and thermal conductivity. To obtain standard data of MgAlON with respect to thermal characteristics and strength, single phase samples without pores need be prepared. In addition, since MgAlON is a solid solution material and its chemical composition has a relatively wide range,[6)] the properties of MgAlON with different composition should be explored.

Considering the advantages of spark plasma sintering (SPS) (schematically shown in **Fig. 1**),[8),9)] it is used to prepare high density MgAlON in this work, and we have successfully prepared single phase MgAlON without pores in very short process by SPS process through solid phase reaction of MgO, Al_2O_3 and AlN.[3),4)] However, the process has not been systemically investigated.

In this paper, our objective is to investigate the effect of synthetical parameters, such as heating temperature and soaking time, on the preparation of MgAlON by SPS process and to obtain the standard data about the cold bending strength and thermal characteristics of single phase MgAlON without pores in different composition.

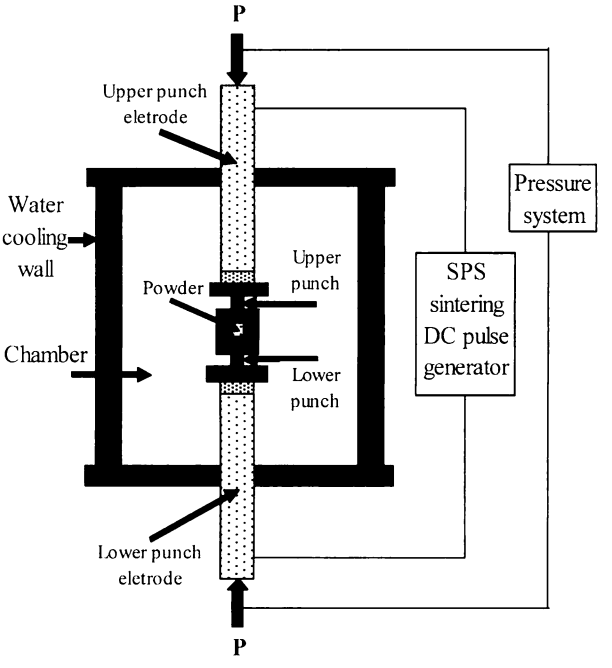

Fig. 1. Schematic of SPS system.

2. Experimental procedure

2.1 Preparation of MgAlON

High purity and small sized starting powders, MgO (0.24 μm, >99.9%), Al_2O_3 (0.1 μm, >99.99%), and AlN (0.7 μm, >99.2%), were meticulously weighed according to the proportion listed in **Table 1**, and milled with alumina balls by using ethanol as dispersion. Subsequently, the slurry was vacuum dried in rotary evaporator (Model BUCHI R-134 rotavapor, SIBATA, Tokyo, Japan) and then the dried powders were placed in a graphite die and set in SPS system (Model DR. SINTER 820S, Sumitomo Heavy Industries, Ehime, Japan). After the chamber was evacuated to less than 5 Pa and flushed with nitrogen (purity>99.999%), repeatedly, the samples were heated following the patterns listed in

Table 1. Chemical Composition of Raw Materials and Heating Conditions

	Chemical composition						Heating conditions	
	Molar ratio			Mass %				
	MgO	Al_2O_3	AlN	MgO	Al_2O_3	AlN	Warming up conditions	Soaking conditions
T0	4	13	3	9.94	82.41	7.64	Just mixed	
T1							R.T.-1100 °C in 12 min	1100 °C for 1 min
T2							R.T.-1500 °C in 16 min	1500 °C for 1 min
T3							R.T.-1700 °C in 20 min	1700 °C for 1 min
H1	4	13	3	9.94	82.41	7.64	R.T.-1700 °C in 20 min	1700 °C for 10 min
C1	1	10	3	3.38	86.22	10.4	R.T.-1700 °C in 20 min	1700 °C for 10 min
C2	4	13	3	9.94	82.41	7.64		
C3	5.21	13	3	12.57	80.01	7.42		
C4	6.41	13	3	15.04	77.75	7.21		
C5	7.62	13	3	17.38	75.61	7.01		
C6	4	7	1	17.49	78.03	4.48		

Table 1 under the pressure of 30 MPa.

2.2 Characterization

The plates for mechanical testing were cut from SPSed samples by using a conventional mechanical cutting procedure. After ground with a diamond wheel to 45×4×3 mm, the plates were rough polished and the edges were chamfered at 45°. The bending strength was measured by a mechanical strength testing machine (Model AG-100kNE autograph, SHIMADZU, Kyoto, Japan).

Similar as the above procedure, plates in 18×4×3 mm for the measurement of thermal expansion and 10×10×4 mm for the test of pore distribution were prepared. The thermal expansion was tested on a thermoflex (Model TMA-8140, Rigaku, Tokyo, Japan) with the warming up rate at 5°C min^{-1} and pore distribution was measured by a mircomeritics (Model MIC-9510 auto pore IV, SHIMADZU, Kyoto, Japan) with mercury as medium.

To measure the thermal conductivity, thermal capacitance, and thermal diffusivity, the specimens were drilled from SPSed samples and ground to Φ12.7×0.2 mm in ahead of looking-glass finish. The measurement was carried out at room temperature and 500°C on a laser flash analyzer (LFA, Model LFA457, NETZSCH, Selb/Bavaria, Germany).

Some SPSed samples were pulverized into less than 10 μm in an agate mortar and the powders were oxidized under flowing dry air on thermo-gravimeter (TG, Model TG/DTA 6300, Seiko Instruments, Tiba, Japan) with warming up rate at 5°C min^{-1}.

The bulk density was measured by automatic gravimeter (Model SGM-6, Mettler-Toledo International, Ohio, USA) and the true density was analyzed by multi pycnometer (Model MVP-1, YUASA IONICS, Massachusetts, USA). Microstructure was characterized by field emission scanning electron microscope (FE-SEM, Model JSM-6340F, JEOL, Tokyo, Japan). Phase composition was determined by X-ray diffraction (XRD, Model RINT2200, Rigaku, Tokyo, Japan) and by using high purity silicon (purity > 99.999%) as internal standard material, lattice constant of $MgAl_2O_{4ss}$ was determined. Content of Mg and Al was measured by X-ray fluorescence spectroscope (XRFS, Model Simultix12, Rigaku, Tokyo, Japan), and O, N by oxygen and nitrogen analyzer (Model EMGA650, HORIBA, Kyoto, Japan).

3. Results and discussion

3.1 Effect of heating conditions on composition

Chemical composition of SPSed samples and that of green compact (T0) are listed in **Table 2**. In these samples, the content of Mg and Al had not obvious variation. When lower than 1500°C, the content of O had a minor increase and that of N had a tiny decrease with the increasing of temperature. However, the difference of the content of O and N between the heated samples and green compact had not obvious change higher than 1500°C.

Phase composition of T0-T3 and H1 is shown in **Fig. 2**. In T1, the reaction of MgO and Al_2O_3 generated $MgAl_2O_{4ss}$, but due to the short heating process, the MgO was not completely consumed. The accurate chemical composition of $MgAl_2O_{4ss}$ could be calculated from the following equations,[1)]

$$[Mg]_{MgAl_2O_{4ss}}\% = \frac{(\alpha_{MgAl_2O_{4ss}} - 0.7900) \times 80}{(15 - (\alpha_{MgAl_2O_{4ss}} - 0.7900) \times 240)} \times 100\% \quad (1)$$

$$[Al]_{MgAl_2O_{4ss}}\% = \frac{6 - (\alpha_{MgAl_2O_{4ss}} - 0.7900) \times 160}{(15 - (\alpha_{MgAl_2O_{4ss}} - 0.7900) \times 240)} \times 100\% \quad (2)$$

$$[O]_{MgAl_2O_{4ss}}\% = 1 - [Mg]\% - [Al]\% \quad (3)$$

when the lattice constant of the determined $MgAl_2O_{4ss}$ in T1 was 0.80826 nm, its chemical composition was $MgAl_{2.11}O_{4.16}$.

From the XRD result of T2, the MgO was entirely consumed and MgAlON was obtained. Combined with the result of **Fig. 3**, where the excess weight change (W_E) of T2 was 1.45%, the content of Mg of MgAlON in T2 calculated from Eq. (4) was 8.52 mol%.

$$W_E = -29.07 \times [Mg]\%3.9285 \quad (4)^{4)}$$

However, the content of Mg in T2 was 5.11 mol% (Table 2). So, it could be deduced that only about three quarters of Al_2O_3 dissolved into the MgAlON in T2. In T3 and H1, single phase MgAlON was obtained. According to Table 2, the chemical composition of MgAlON of T3 and H1 could be represented as $Mg_4Al_{28.84}O_{43.04}N_{2.51}$ and $Mg_4Al_{28.84}O_{43.03}N_{2.51}$, respectively.

Figure 3 shows the weight change of SPSed samples and that of mixed raw materials. The sizes of starting powders

Table 2. Chemical Composition of Samples T0-T3 and Sample H1 (mol%)

	Soaking conditions	Chemical composition			
		Mg	Al	O	N
T0	Mixed raw materials	5.08	36.71	54.78	3.42
T1	1100 °C for 1 min	5.10	36.76	54.88	3.26
T2	1500 °C for 1 min	5.10	36.79	55.01	3.10
T3	1700 °C for 1 min	5.10	36.79	54.90	3.20
H1	1700 °C for 10 min	5.10	36.80	54.90	3.20

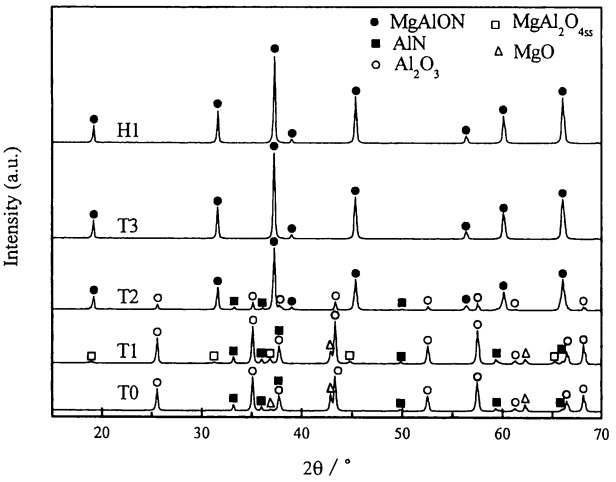

Fig. 2. XRD patterns of T0-T3 and sample H1.

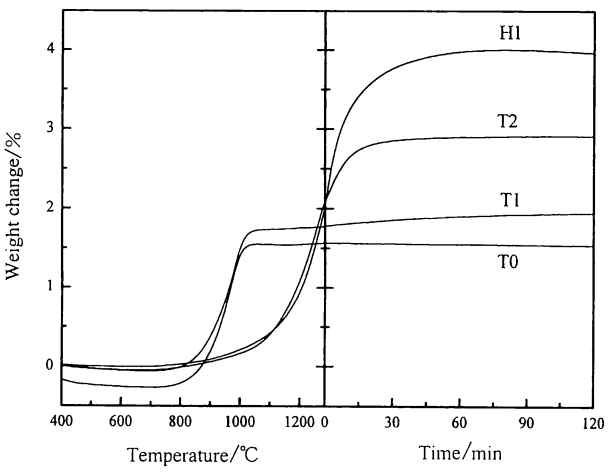

Fig. 3. Weight change of T0-T2, and H1.

were very small, and inevitably, some attached water existed in the mixed raw materials. Hence, the weight decrease of T0 below 700°C was ascribed to the evaporation of attached water.[3] Above 750°C, all the samples were oxidized, however, their oxidation behavior had some difference: T0 and T1 had an obvious oxidation, while T2 and H1 had not obvious oxidation until to 1000°C, though AlN was detected in T1 and T2. Considering that the Al_2O_3 used in present work was very sinterable, un-reacted AlN in T2 might be surrounded by MgAlON and Al_2O_3 grains. Moreover, the oxidation of MgAlON was slow below 1000°C. As a result, the oxidation of AlN was retarded and T2 had not obvious oxidation until 1000°C.

From Fig. 3, it can be also found that the total weight change of T0 had minor difference to that of T1 but obviously lower than that of T2 and H1, even though the chemical composition of these samples had not big difference (Table 2). Considering the overall oxidation reaction of MgAlON and AlN:

$$MgAlON + O_2 \longrightarrow MgAl_2O_{4ss} + Al_2O_3 + N_2 \quad (5)$$
$$AlN + O_2 \longrightarrow Al_2O_3 + N_2 \quad (6)$$

The oxidation reaction of the above two nitrides can be represented as,

$$4N^{3-} + 3O_2 = 2N_2 + 6O^{2-} \quad (7)$$

By using Eq. (7), the theoretical weight change (W_T) could be calculated. Compared with Table 2, the chemical composition of all samples was similar, and the difference of W_T among these samples could be neglected. However, it should be noted that there existed some obvious differences in weight changes achieved by TG analysis. W_E was determined by the equation,[4]

$$W_E = W_M - W_T \quad (8)$$

where, W_M is the maximum weight changes shown in Fig. 3. In present work, W_E of T2 was 1.45% and that of H1 was 2.45%. In ref 4), Dai et al. had proposed that during the oxidation of MgAlON, there was an excess weight change and it related to the content of the content of Mg of the MgAlON phase (Eq. (4)). So, the oxidation behavior of samples agreed well with the proposition.[4]

In the following, a possible reason for the change of the chemical composition at different heating condition (Table 2) was discussed. During the preparation of MgAlON by solid phase reaction, Mg_3N_2 as a volatile material with the vaporizing temperature at 700°C formed through the reaction between MgO and AlN:[10]

$$MgO + AlN \rightarrow Al_2O_3 + Mg_3N_2 \quad (9)$$

In addition, as attached water remained in the green compact, the Mg_3N_2 was favorable to react with H_2O as follows,[10]

$$Mg_3N_2 + H_2O \longrightarrow MgO + H_2 + N_2 \quad (10)$$
$$Mg_3N_2 + Al_2O_3 + H_2O \longrightarrow MgAl_2O_{4ss} + H_2 + N_2 \quad (11)$$
$$Mg_3N_2 + MgAl_2O_{4ss} + H_2O \longrightarrow MgAlON + H_2 + N_2 \quad (12)$$

Taking into account the graphite die as heater, the reaction between H_2O and graphite could also occur according to,

$$C + H_2O \longrightarrow CO + H_2 \quad (13)$$

With the proceeding of the reaction between Mg_3N_2 and H_2O as reactions (10)-(12), the content of N would decrease and

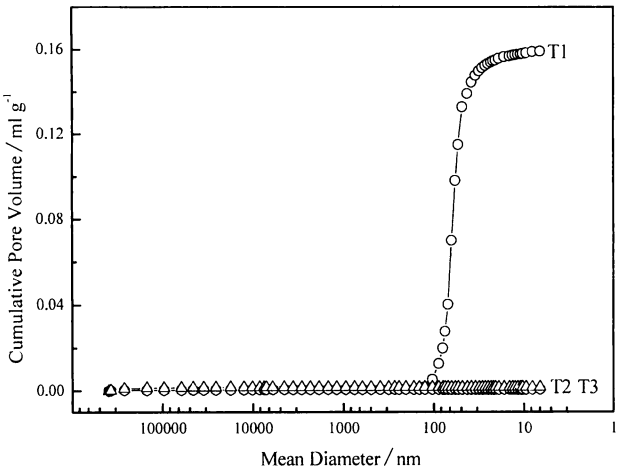

Fig. 4. Pore distribution of T1-T3.

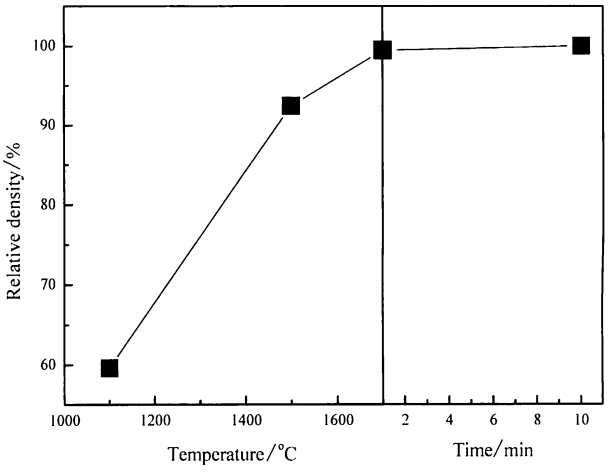

Fig. 5. Relative density of heated T1-T3 and H1.

that of O would increase, and the occurrence of reaction (13) had not effect on the chemical composition of heated sample. As Mg_3N_2 reacts with H_2O at low temperatures and graphite reacts with H_2O only at high temperature, obviously, the change of chemical composition in the samples heated lower than 1500°C mainly caused by the reactions (10)-(12). With the temperature increasing, the solid phase reaction rate among MgO, AlN and Al_2O_3 was increased and the formation of Mg_3N_2 was lowered. Oppositely, with the increasing of temperature, the reactivity between graphite and H_2O increased, thus, lots of H_2O were consumed by the graphite. Hence, the difference of the content O and N between T3 and T0 was lower than that between T2 and T0.

3.2 Effect of heating conditions on microstructure

Pore distributions of samples heated at different temperature are plotted in **Fig. 4**. The volume of pore was about 0.16 ml g^{-1} and mean diameter was less than 100 nm in T1. In T2 and T3, the amount of mercury accessed in the samples could be neglected. Furthermore, the measurement of the bulk density and porosity of T2 and T3 by Archimedes method implied that their apparent porosity almost to zero. Moreover, as shown in **Fig. 5**, the relative densities of T1, T2, and T3 were 59.6%, 92.4%, and 99.5%, respectively. So, some closed pores were remained in T2 and T3.

Figure 6 illustrates the microstructures of samples heated at different condition. With the increasing of temperature, the pores became smaller and the grains got coarser. T1 was very porous and its grains were very small; For T2, the grains and pores were about 1 μm, and pores were distributed around dense grains; For T3, the grains were about 5 μm and few pores were involved in the grain. Especially, the grain size of H1 was about 10 μm and as twice as that of T3, and no pores existed in the inner of grains. Since the sample was heated under vacuum condition, pores involved in the grains were in negative pressure and they could migrate to the grain boundaries and out of the sintering body easily at higher temperature. In this case, the pores were efficiently removed through SPS process. Therefore, SPS process was an effective means to *prepare full density* sample.

3.3 Shrinkage behavior during heating process

Figure 7 shows the shrinkage behavior of H1 during the heating process. The shrinkage behavior had not obvious change until 1000°C because the raw materials kept stable at low temperature. It could be found that the shrinkage rate was rapidly increased from about 1100°C to 1400°C and became

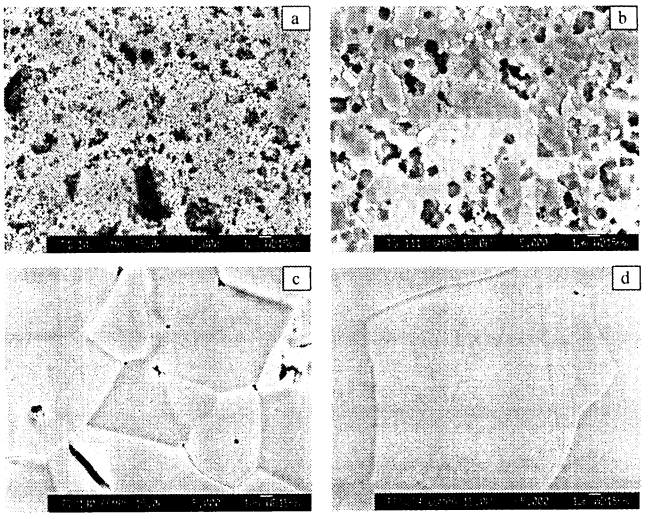

Fig. 6. Polished cross section morphology of T1-T3 and H1 after the treatment of phosphoric acid (a) T1, (b) T2, (c) T3, and (d) H1.

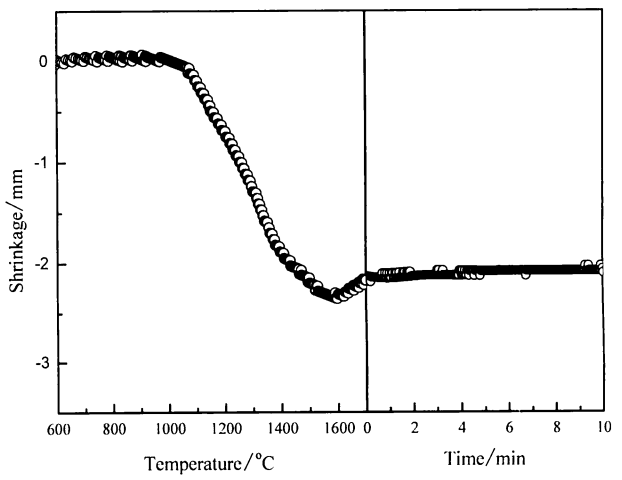

Fig. 7. Shrinkage behavior of H1 during heating process.

slower from 1400°C to 1600°C. As the densities of raw materials were 3.97 g cm^{-3} (Al_2O_3), 3.26 g cm^{-3} (AlN), 3.58 g cm^{-3} (MgO),[11] and the formed $MgAl_2O_{4ss}$ and MgAlON

Table 3. Properties of SPSed MgAlON with Different Composition

	Thermal diffusivity ($mm^2 s^{-1}$)		Thermal capacitance ($J g^{-1} K^{-1}$)		Thermal conductivity ($W m^{-1} K^{-1}$)		Expansivity ($\times E^{-6} °C^{-1}$)	Cold bending strength (MPa)
	R.T.	500 °C	R.T.	500 °C	R.T.	500 °C		
C1	4.156	1.519	0.768	1.142	11.656	6.356	8.01	292
C2	4.258	1.552	0.782	1.145	12.139	6.462	8.22	256
C3	4.348	1.570	0.791	1.146	12.438	6.529	8.21	260
C4	4.426	1.606	0.802	1.149	12.866	6.688	8.26	252
C5	4.532	1.635	0.809	1.151	13.216	6.808	8.29	249
C6	4.586	1.651	0.813	1.152	13.496	6.866	8.41	247

were about 3.6 g cm^{-3} and 3.65 g cm^{-3},[4),12)] respectively, expansion would occur during the solid solution of Al_2O_3 into $MgAl_2O_{4ss}$ and MgAlON. At the beginning of shrinkage (1100°C-1400°C), as the sample was very porous, the expansion caused by the solid phase reaction had minor effect on the dimensional change of sample comparing to the shrinkage induced by the elimination of pores. In the succeeded stage (1400°C-1600°C), as the density of the sample was increased, the effect of the shrinkage caused by elimination of pores was lowered. On the other hand, since the rate of the solid solution of Al_2O_3 was increased at higher temperature, the influence of the expansion aroused from the solid solution reaction increased. When higher than 1600°C, an expansion was obtained. As some residual Al_2O_3 were existed and the density was about 92.4% in T2, it could be deduced that in the sample heated at 1600°C without holding process, some un-reacted Al_2O_3 should remain and the density was relatively high. Since about 8% of volume expansion was generated during the solid solution of Al_2O_3 into MgAlON and $MgAl_2O_{4ss}$, the solution of Al_2O_3 should be the reason for the expansion higher than 1600°C. As the densities of T3 and H1 were about 99.5% and 100%, respectively, the variation of the dimension of sample could be neglected and the sample soaked at 1700°C had not obvious change.

3.4 Effect of composition on the properties of SPSed MgAlON

All the SPSed samples for the measurement of the properties were confirmed to be single phase MgAlON without pores (density >99.9%) by the determination of phase composition and density. According to the properties of SPSed MgAlON listed in **Table 3**, the difference of thermal diffusivity, thermal capacitance, and thermal conductivity at room temperature was greater than that at 500°C and the thermal capacitance had not obvious change with the variation of chemical composition. With the increasing of the content of Mg and the decreasing of N, all the thermal characteristics, thermal expansion, thermal diffusivity, thermal capacitance, and thermal conductivity, were increased and the cold bending strength was decreased. The reason of the relationship between the properties and the composition of MgAlON was still unknown and it need further study.

4. Conclusions

During the synthesis of magnesium aluminum oxynitride (MgAlON) by spark plasma sintering (SPS) process, a minor variation of the content of N and O at temperatures lower than 1500°C was caused by the reaction between Mg_3N_2 and H_2O. At higher temperature, the change of the chemical composition was decreased, because of the high efficiency of the SPS process and the reaction between graphite heater and H_2O. In the course of the heating process, the shrinkage rate was very fast from about 1100°C to 1400°C, and slowed down from 1400°C to 1600°C. When above 1600°C, an expansion was obtained. In addition, Open pores were not existed in the sample heated at 1500°C for 1 min and single phase MgAlON without pores were obtained when heated at 1700°C for 10 min. With the increasing of the content of Mg and the decreasing of N, the cold bending strength was decreased and all the thermal characteristics were increased.

Acknowledgments We are grateful to T. Mimura, S. Takeuchi for their help. Moreover, we should show our appreciation to reviewer and editor for discreet consideration and lots of constructive suggestion.

References

1) W. Dai, W. Lin, A. Yamaguchi, J. Ommyoji, J. Yu and Z. Zhou, *J. Ceram. Soc. Japan*, 115, 42-46 (2007).
2) X. Wang, W. Li and S. Seetharaman, *Z. Metallkd.*, 93, 545-553 (2002).
3) W. Dai, A. Yamaguchi, W. Lin, J. Ommyoji, J. Yu and Z. Zhou, *J. Ceram. Soc. Japan*, 115, 195-200 (2007).
4) W. Dai, A. Yamaguchi, W. Lin, J. Ommyoji, J. Yu and Z. Zhou, *J. Ceram. Soc. Japan*, 115, 409-413 (2007).
5) X. Wang, W. Li and S. Seetharaman, *Z. Metallkd.*, 93, 540-544 (2002).
6) A. Granon, P. Goeuriot, F. Thevenot, J. Guyader, P. L'Haridon and Y. Laurent, *J. Eur. Ceram. Soc.*, 13, 365-370 (1994).
7) X. Wang, H. Wang, W. Zhang, J. Sun and Y. Hong, *Key Engineering Materials*, 226, 373-378 (2002).
8) M. Radwan, T. Kashiwagi and Y. Miyamoto, *J. Eur. Ceram. Soc.*, 23, 2337-2341 (2003).
9) Z. Shen, M. Johnsson, Z. Zhao and M. Nygren, *J. Am. Ceram. Soc.*, 85, 1921-1927 (2002).
10) M. W. Chase, Jr., "NIST-JANAF Thermochemical Tables," 4th ed., the American Ceramic Society and the American Institute of Physics for the National Institute of Standards and Technology, Maryland (1998).
11) D. R. Lide, "CRC Handbook of Chemistry and Physics-72nd ed., 1991-1992", Chemical Rubber Pub. Co., Boston (1991) pp. 4-50.
12) Z. Nakagawa, *Ceram. Trans.*, 71, *283-294 (1996).*

Journal of the Ceramic Society of Japan 115 [10] 654-660 (2007)

Paper

Influence of Heating Temperature, Keeping Time and Raw Materials Grain Size on Al_4O_4C Synthesis in Carbothermal Reduction Process and Oxidation of Al_4O_4C

Jianli ZHAO,*,** Wei LIN,*,† Akira YAMAGUCHI,* Junji OMMYOJI* and Jialin SUN**

*Okayama Ceramics Research Foundation, Nishikatakami, 1406-18, Bizen, Okayama 705-0021

**School of Material Science and Engineering, University of Science and Technology Beijing, 100083 China

Several factors, influencing synthesis of Al_4O_4C in carbothermal reduction process from Al_2O_3 and C starting raw materials in argon atmosphere, and oxidation characteristics of Al_4O_4C were investigated. The formed Al_4O_4C in heated specimens was increased and Al_2O_3 and C were decreased with increase of heating temperature and extension of keeping time. Grain size of Al_2O_3 had obvious influence on synthesis of Al_4O_4C and fine Al_2O_3 was more advantageous. The activation energy of the reduction reaction from Al_2O_3 and graphite to form Al_4O_4C was calculated as 358.0 kJ/mol basing on experimental data. Al_4O_4C was observed to be oxidized from about 820°C in air. Al_4O_4C, buried in graphite powder and heated in air, was converted into Al_2O_3 and C.

[Received May 30, 2007; Accepted August 24, 2007]

Key-words: Al_4O_4C, Synthesis, Al_2O_3, Graphite, Carbothermal reduction, Oxidation, Carbon-containing refractories

1. Introduction

Metal Al is frequently used in carbon-containing refractories as an additive to improve oxidation resistance and thermal properties, but it also causes some problems. For example, Al reacts with C in refractories to form Al_4C_3,[1)-3)] which may lead the refractories to collapse for the poor hydration resistance of Al_4C_3.[4)]

Al_4O_4C that is stable until 1890°C exists in Al_2O_3-Al_4C_3 system.[5)] This compound has been confirmed to have good hydration resistance and be transformed into Al_2O_3 and C at $P_{CO}=0.1$ MPa (1 atm). So Al_4O_4C may be a better additive than metal Al for carbon-containing refractories.[6)]

The authors have proceeded some research works about synthesis of Al_4O_4C from Al_2O_3 and graphite starting raw materials in argon atmosphere and it was known that the formation of Al_4O_4C started at a temperature of 1500-1550°C.[7)]

However, more factors influencing synthesis of Al_4O_4C are necessary to be investigated for comprehending synthesis of Al_4O_4C in detail, and characteristics of formed Al_4O_4C are also necessary to be investigated for probable utilization in the future.

In the present work, several factors, influencing synthesis of Al_4O_4C, such as heating temperature, keeping time and grain size of Al_2O_3, and oxidation characteristics of formed Al_4O_4C were investigated.

2. Experimental procedure

2.1 Investigation on factors influencing synthesis of Al_4O_4C

Al_2O_3 (average grain size: 0.1 μm, 30 μm, 60 μm and 1 mm. purity: +99.0 mass%) and graphite (average grain size: 30 μm. purity: +99.0 mass%) were used as starting raw materials. They were weighted in proportions of $C/Al_2O_3=1.5$ (molar ratio), mixed with alcohol and dried in a vacuum-rotary evaporator. Two grams of the powder mixture put in a high purity graphite crucible was set into an electric furnace with a graphite heater (**Fig. 1**). Ar gas (purity: +99.9999 mass%), in which the partial pressure of O_2 was determined 10^{-20} MPa by a ZrO_2 sensor, was poured into the furnace after producing vacuum. The powder mixtures were heated to 1600-1700°C at a rate of 10°C/min and maintained for 3-9 h under flowing Ar of 1 L/min. Finally, the specimens were cooled to room temperature within the furnace through shutting off power supply, where the average cooling rate was 64°C/min from 1700°C to 1000°C. Phases of the heated specimens were identified by using X-ray diffraction (XRD, RINT 2200, Rigaku, Japan). Microstructure was observed using field emission scanning electron microscope (FE-SEM, JSM-6340F, JEOL, Japan). The compositions of a part of heated specimens were determined by using chemical analysis method.

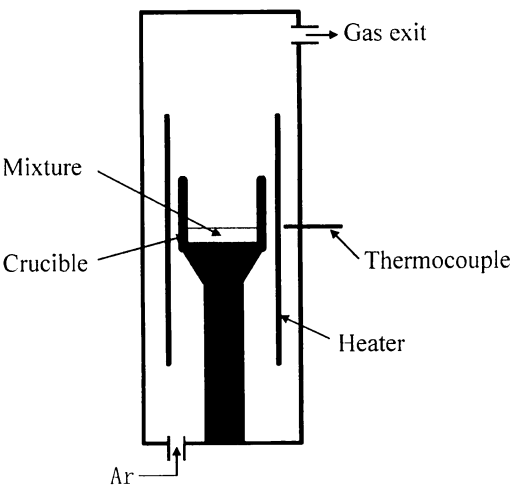

Fig. 1. Schematic diagram of experimental equipment.

2.2 Investigation on oxidation characteristics of Al_4O_4C

1) Oxidation of Al_4O_4C in air

The specimen from mixture with $C/Al_2O_3=1.5$ heated at 1700°C for 9 h, with the highest Al_4O_4C content and a little of Al_2O_3 and graphite, was grounded into grain size of approximate 10 μm and was named Al_4O_4C product, then was used to measure oxidation characteristic in air by using TG-DTA method, where the flow rate of air was 200 ml/min and the temperature rising rate was 5°C/min. In addition, the ground-

† Present address; Shinagawa Refractories Co., Ltd, Imbe 707, Bizen, Okayama, 705-0001 Japan

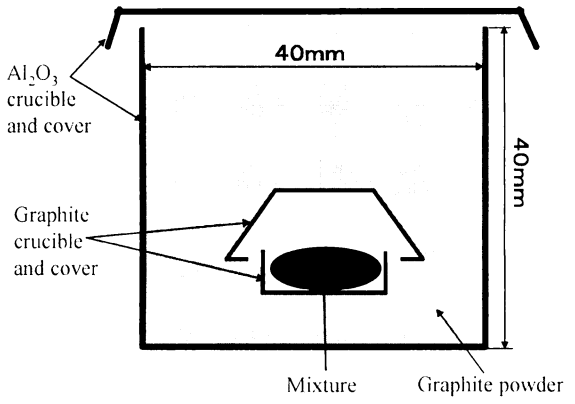

Fig. 2. Structure of set including mixture and crucibles.

ed powder with 10 μm grain size was reheated at 800°C for 2 h in air to remove the residual graphite and was named reheated powder, then was used to measure oxidation characteristic in air by using TG-DTA method. The graphite used in this research was also analyzed by using the same TG-DTA method.

2) Oxidation of Al_4O_4C buried in graphite powder and heated in air

Since Al_4O_4C is probable to be used as an additive into carbon-containing refractories, oxidation characteristic of Al_4O_4C coexisting with C is necessary to be determined. So oxidation characteristic of formed Al_4O_4C, buried in graphite powder and heated in air, was also investigated.

The Al_4O_4C product stated above was mixed with graphite powder in molar ratio of Al_4O_4C : graphite = 1 : 6 (Al_4O_4C product was calculated as 100% Al_4O_4C). This (Al_4O_4C product)-graphite mixture in a graphite crucible with a cover was buried into graphite powder in an alumina crucible as shown in **Fig. 2**. This set was heated at 400-1500°C for 1-3 h in air. The heated specimens were analyzed by using XRD to identify phases.

3. Results

3.1 Influence of various factors on synthesis of Al_4O_4C

1) Influence of heating temperature and keeping time

The powder mixtures with $C/Al_2O_3 = 1.5$ (Al_2O_3: 0.1 μm) were heated at 1600, 1650 and 1700°C for 3-9 h. The heated specimens were analyzed by using XRD and it was known that the phases in the heated specimens were Al_2O_3, Al_4O_4C and graphite, no other substances existing. Mass contents of the elements of Al, O and C in the heated specimens were determined and are shown in **Table 1**.

Figure 3(a), (b) and (c) present mass contents of the phases of Al_2O_3, Al_4O_4C and graphite in heated specimens, which were calculated from Table 1 and according to equations as

$$[Al] = [Al_2O_3] \times 54/102 + [Al_4O_4C] \times 108/184$$
$$[O] = [Al_2O_3] \times 48/102 + [Al_4O_4C] \times 64/184$$
$$[C] = [\text{graphite}] + [Al_4O_4C] \times 12/184$$

Where [Al], [O], [C], [Al_2O_3], [Al_4O_4C] and [graphite] are the mass contents of Al element, O element, C element, Al_2O_3 phase, Al_4O_4C phase and graphite phase in the heated specimens.

As temperature was raised, increase of Al_4O_4C and decrease of Al_2O_3 and graphite were turned into more quick. At the same time, proportion of Al_4O_4C in the heated specimens was

Table 1. Mass Contents of the Elements of Al, O and C in Specimens from Mixtures with $C/Al_2O_3 = 1.5$ Heated at Various Temperatures for Different Times

Mass /%

Temperature /°C	Element	Time /h				
		0	3	5	7	9
1600	Al	45.00	47.18	48.94	49.96	51.28
	O	40.00	39.49	38.64	37.51	36.49
	C	15.00	13.33	12.42	12.53	12.23
1650	Al	45.00	48.12	50.64	52.88	54.87
	O	40.00	38.67	37.27	35.83	34.32
	C	15.00	13.21	12.09	11.29	10.81
1700	Al	45.00	52.53	55.02	55.93	56.89
	O	40.00	37.11	35.56	34.9	34.69
	C	15.00	10.36	9.42	9.17	8.42

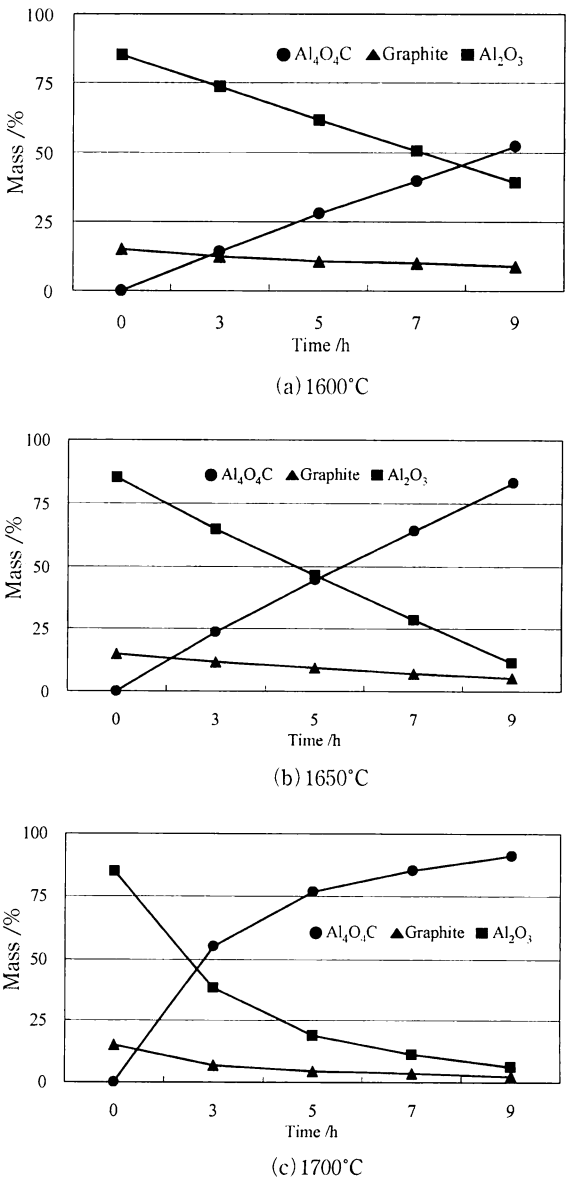

Fig. 3. Mass contents of the phases of Al_2O_3, Al_4O_4C and graphite in specimens from mixtures with $C/Al_2O_3 = 1.5$ heated at various temperatures for different times.

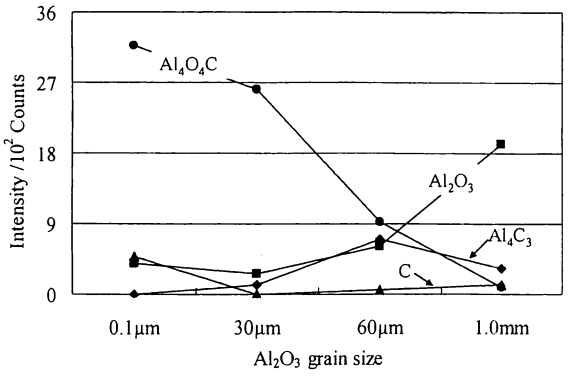

Fig. 4. Phases in specimens from mixtures with various Al_2O_3 grain sizes and $C/Al_2O_3 = 1.5$ heated at 1700°C for 9 h. ($(h\,k\,l)$ of the highest peak of each phase: C = (003); Al_2O_3 = (104); Al_4O_4C) = (111); Al_4C_3 = (012)).

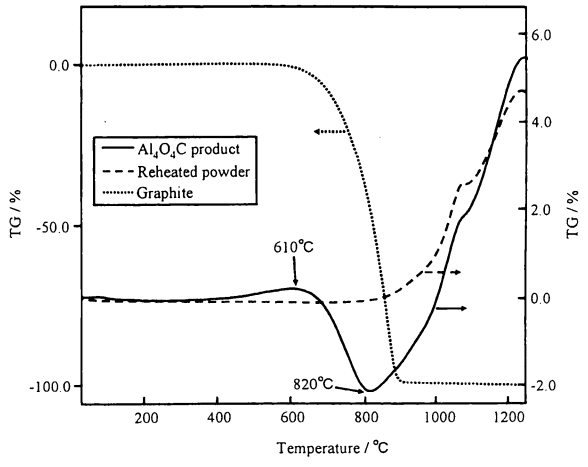

Fig. 5. TG patterns of Al_4O_4C product, reheated powder and graphite (air: 200 ml/min; temperature rising: 5°C/min).

increased and those of Al_2O_3 and graphite were decreased for same keeping time. It was assumed that increase of heating temperature would increase reaction speed of Al_2O_3 and graphite to form Al_4O_4C.

As keeping time was extended, proportion of Al_4O_4C in the heated specimens was gradually increased and those of Al_2O_3 and graphite were gradually decreased at each temperature. The conclusion was gained that extension of keeping time would increase reaction extend of Al_2O_3 and graphite to form Al_4O_4C.

The highest Al_4O_4C proportion was obtained at 1700°C for 9 h. In this specimen, mass content of Al_4O_4C was 91.3% and those of Al_2O_3 and graphite were 6.2% and 2.5%, respectively. According to SEM observations on this specimen,[7] the formed Al_4O_4C grains had size in range of 10–100 μm, mainly 30–50 μm, and they hardly included pores, very dense. The residual graphite existed in the center of some Al_4O_4C grains. The residual Al_2O_3 could not be observed due to the too small size and low content.

2) Influence of grain size of Al_2O_3

The powder mixtures with $C/Al_2O_3 = 1.5$ (Al_2O_3: 0.1 μm, 30 μm, 60 μm and 1 mm) were heated at 1700°C for 9 h. The intensity of the highest XRD peak of each phase in the heated specimens is shown in **Fig. 4**.

The decrease of grain size of Al_2O_3 was advantageous for synthesis of Al_4O_4C. Increasing grain size of Al_2O_3, the reduction rate of Al_2O_3 was decreased and at the same time, Al_4C_3 was increased with Al_4O_4C decreased. It was assumed that enough fine Al_2O_3 as starting raw material is necessary for synthesis of Al_4O_4C and in this research the best grain size of Al_2O_3 was 0.1 μm.

3.2 Oxidation characteristics of Al_4O_4C

1) Oxidation of Al_4O_4C in air

The reheated powder was analyzed by using XRD and it was known that all residual graphite was oxidized; only Al_4O_4C and Al_2O_3 existed (Fig. 10(a)).

TG patterns of the Al_4O_4C product, the reheated powder and the graphite used in this research are shown in **Fig. 5**.

From Fig. 5, the mass of the Al_4O_4C product decreased obviously from about 610°C and again increased obviously from about 820°C. Comparing to the pattern of the graphite, it is known that the temperature of about 610°C is the starting temperature that the residual graphite was oxidized. And comparing to the pattern of the reheated powder, it is known that the temperature of about 820°C is the starting temperature

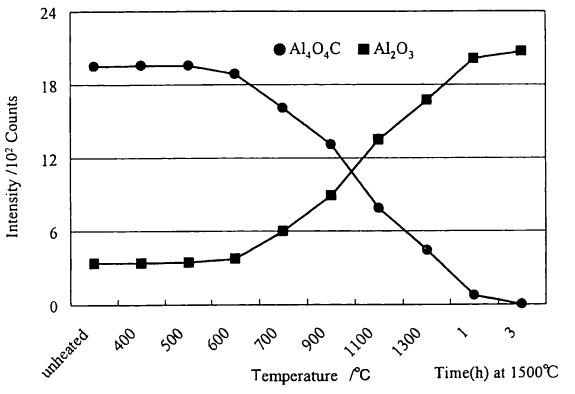

Fig. 6. Phases in specimens from mixture of Al_4O_4C: graphite = 1 : 6 heated at various temperatures for 1 h and 1500°C for 1 h and 3 h. ($(h\,k\,l)$ of the highest peak of each phase: Al_2O_3 = (104); Al_4O_4C) = (111)).

that Al_4O_4C was oxidized.

2) Oxidation of Al_4O_4C buried in graphite powder and heated in air

Phases of specimens from (Al_4O_4C product)-graphite mixture heated at various temperatures and different times are shown in **Fig. 6**, where the intensity of graphite phase was omitted.

With increase of heating temperature and extension of keeping time, Al_4O_4C was decreased, simultaneously that of Al_2O_3 was increased. Al_4O_4C was converted into Al_2O_3 from about 600°C × 1 h and the conversion was finished at 1500°C × 3 h.

4. Discussion

1) Al_4O_4C's formation and conversion into Al_4C_3

Figure 7 presents change of condensed phases for various partial pressures of $CO(g)$ in the Al-O-C system, which was calculated thermodynamically (Since Al_2OC is unstable below 1715°C, Al_2OC is not included.). The formation free energy of Al_4O_4C reported by Lihrmann et al.[8] was used in the calculation. Those of Al_2O_3, C, Al_4C_3 and CO were from NIST-JANAF Thermo-chemical Tables.[9] The standard pressure (P^0) was 0.1 MPa (1 atm).

The critical P_{CO}/P^0 of Al_4O_4C and Al_4C_3 formation increases with rise of temperature from Fig. 7. Since the con-

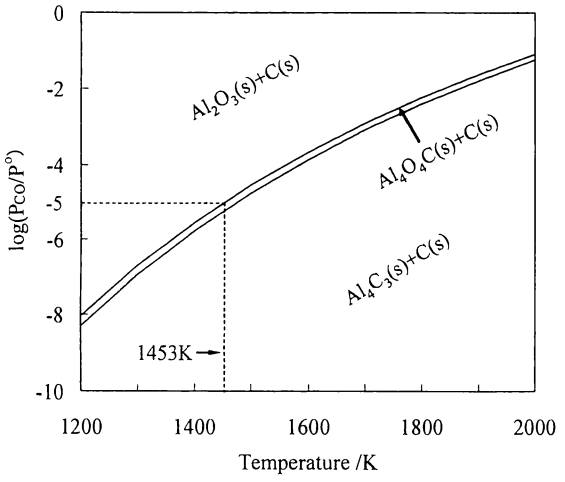

Fig. 7. Stable relation among condensed phases in Al-O-C system for temperature and partial pressure of $CO(g)$.

version critical temperature of $Al_2O_3 \rightarrow Al_4O_4C$ is less than that of $Al_4O_4C \rightarrow Al_4C_3$ at same partial pressure of $CO(g)$, Al_4O_4C would be formed firstly according to Re. (1) and then be conversed into Al_4C_3 according to Re. (2) as temperature was raised.

$$2Al_2O_3(s) + 3C(s) \longrightarrow Al_4O_4C(s) + 2CO(g) \quad (1)$$
$$Al_4O_4C(s) + 6C(s) \longrightarrow Al_4C_3(s) + 4CO(g) \quad (2)$$

The change sequence of condensed phases in the Al-O-C system with increase of temperature is as the following.

$$Al_2O_3 + C \longrightarrow Al_4O_4C + C \longrightarrow Al_4C_3 + C$$

In addition, since the stable area of Al_4O_4C is very narrow, the formed Al_4O_4C would quickly be reducted by C to form Al_4C_3 as temperature was raised.

Re. (1) should only occur in the reaction-starting period of Al_2O_3 and C, after Al_2O_3 was separated from C by formed Al_4O_4C, Al_4O_4C would be formed mainly according to Res. (3) and (4). Similarly, Re. (2) should also only happen in the reaction-starting period of Al_4O_4C and C, as long as Al_4O_4C was separated from C by formed Al_4C_3, Al_4C_3 would be formed mainly according to Res. (5) and (4). Overall reaction of Re. (3) and Re. (4) is same with Re. (1) ((3) + 3 × (4) = (1)). Overall reaction of Re. (5) and Re. (4) is same with Re. (2) ((5) + 6 × (4) = (2)).

$$2Al_2O_3(s) + 4CO(g) \longrightarrow Al_4O_4C(s) + 3CO_2(g) \quad (3)$$
$$CO_2(g) + C(s) \longrightarrow 2CO(g) \quad (4)$$
$$Al_4O_4C(s) + 8CO(g) \longrightarrow Al_4C_3(s) + 6CO_2(g) \quad (5)$$

Since this research was proceeded in argon atmosphere with partial pressure of O_2 as 10^{-20} MPa as statement, O_2 should have reacted with the graphite heater, the graphite crucible and the graphite in mixtures into CO ($1/2O_2(g) + C(s) \rightarrow CO(g)$) with a partial pressure as approximately 2×10^{-20} MPa. But, even if P_{CO} is 10^{-6} MPa, very higher than 2×10^{-20} MPa, the starting temperature of Al_4O_4C formation is 1180°C (1453 k) in thermodynamics from Fig. 7. The actual starting temperature is 1500-1550°C as statement, about 350°C higher than the former. The difference should be attributed to the activation energy of Re. (1). Using the data in Fig. 3 and according to the formula reported by Arrhenius ($k = A \exp(-E/RT)$),[10] the activation energy of Re. (1) was calculated as 358.0 kJ/mol.

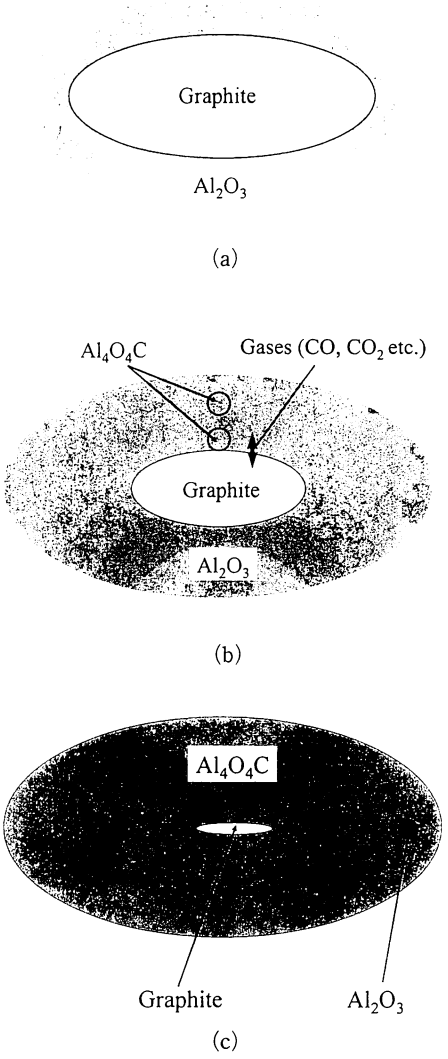

Fig. 8. Reaction models of Al_2O_3 with 0.1 μm grain size and graphite during heating ((a)→(b) →(c)).

2) Influence mechanism of change of Al_2O_3 grain size on Al_4O_4C synthesis

The change of Al_2O_3 grain size had obvious influence on composition of synthesized product as statement. The influence mechanism is discussed as the following.

The contents of phases in the heated specimens from Al_2O_3 with 0.1 μm in grain size and that from Al_2O_3 with 1 mm in grain size were extremely different (Fig. 4). The formation mechanisms of these products were emphatically discussed.

From SEM observation on the unheated mixtures, when Al_2O_3 was 0.1 μm and graphite was 30 μm, Al_2O_3 grains were adhering on the surface of graphite grains modeled in **Fig. 8** (a), and when Al_2O_3 was 1 mm and graphite was 30 μm, graphite grains were adhering on the surface of Al_2O_3 grains, modeled in **Fig. 9**(a).

As temperature was increased, Al_2O_3 reacted with graphite to form Al_4O_4C. When Al_2O_3 was 0.1 μm, Al_4O_4C would be formed in the contacting area of Al_2O_3 and graphite according to Re. (1) and in the Al_2O_3 grains area according to Res. (3) and (4) due to the diffusion of $CO(g)$ and $CO_2(g)$. Even if a part of formed Al_4O_4C reacted with C or $CO(g)$ to form Al_4C_3, the formed Al_4C_3 would react with Al_2O_3 again to form Al_4O_4C according to Re. (6).

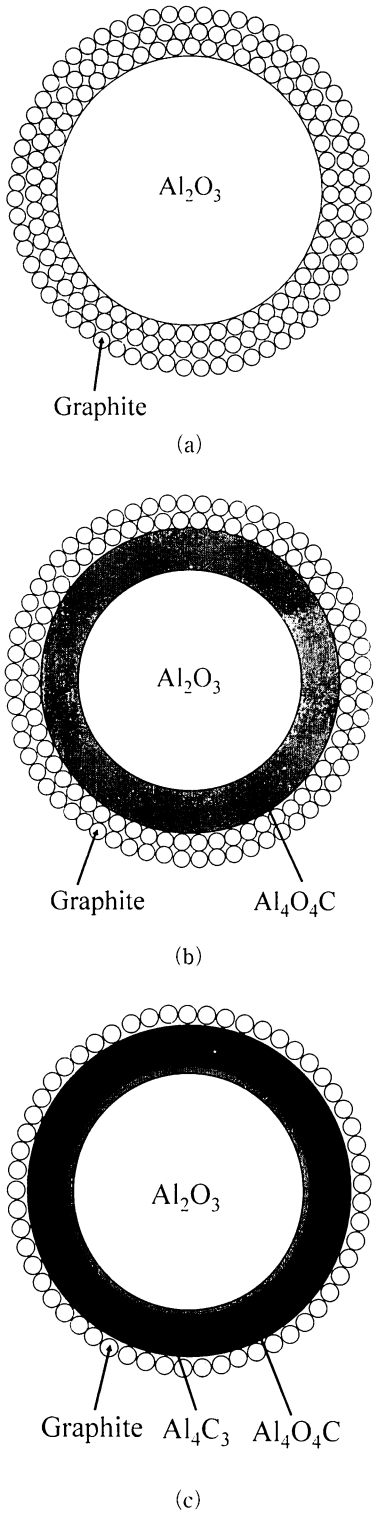

Fig. 9. Reaction models of Al_2O_3 with 1 mm grain size and graphite during heating ((a)→(b)→(c)).

$$4Al_2O_3(s) + Al_4C_3(s) \longrightarrow 3Al_4O_4C(s) \quad (6)$$

As long as C was not excessive ($C/Al_2O_3 \leq 1.5$), Al_4C_3 would not exist in the last product. This is the reason that the products shown in Fig. 3 included only Al_4O_4C, Al_2O_3 and C, no Al_4C_3. In these cases, overall reaction of Re. (2) and Re. (6) is same with Re. (1) ($0.5\times(2)+0.5\times(6)=(1)$), and overall reaction of Res. (4), (5) and (6) is also same with Re. (1) ($3\times(4)+0.5\times(5)+0.5\times(6)=(1)$). The reaction procedure was modeled in Fig. 8(b). The formed Al_4O_4C was dense grains as former statement. Since dense Al_4O_4C grains packed the residual graphite and so no gas was allowed to diffuse, the residual graphite could not further react with Al_4O_4C to form Al_4C_3. And because the formed Al_4O_4C estranged the residual graphite and the residual Al_2O_3, the residual graphite and Al_2O_3 also could not react with each other and so were remained in the last product, as modeled in Fig. 8(c).

When Al_2O_3 was 1 mm, the reduction of Al_2O_3 was slow and difficult and even a part of Al_2O_3 could not be reducted at last. Al_4O_4C would be formed on the surface of Al_2O_3 grains as modeled in Fig. 9(b). Since the formed Al_4O_4C and C or $CO(g)$ coexisted for a long time, C was excessive for the formed Al_4O_4C, the formed Al_4O_4C would further be reducted to form Al_4C_3 according to Res. (2), (5) and (4). The formed Al_4C_3 was packing the grains of Al_2O_3 from observation of the heated product. From Fig. 4, besides Al_2O_3 and Al_4C_3, there are a little of residual Al_4O_4C and C in the heated specimen. The residual Al_4O_4C is considered a part of the formed Al_4O_4C that was near the unreducted Al_2O_3 and was not reducted into Al_4C_3. Another probability is the residual Al_4O_4C is the result of the reaction between the formed Al_4C_3 and the unreducted Al_2O_3 according to Re. (6). The residual Al_4O_4C should locate between unreducted Al_2O_3 grain and formed Al_4C_3. The reason that residual C existed is considered that, because the formed Al_4C_3 had estranged C from Al_2O_3 and Al_4O_4C, C could not react with Al_2O_3 or Al_4O_4C and was remained on the surface of grains as modeled in Fig. 9(c). When Al_2O_3 was 30 μm and 60 μm, the reaction tendencies were between the two states as discussed above.

3) Oxidation mechanism of Al_4O_4C

When Al_4O_4C product was oxidized in air by using TG-DTA method, since the sample was little and the flowing rate of air was high, Al_4O_4C should be sufficiently oxidized from about 820°C by O_2 in air to form Al_2O_3 and CO_2 according to Re. (7).

$$Al_4O_4C(s) + 2O_2(g) \longrightarrow 2Al_2O_3(s) + CO_2(g) \quad (7)$$

From Fig. 5, it is also observed that the mass increase was turned into slow from about 1060°C to 1090°C for not only Al_4O_4C product but also the reheated powder. XRD patterns of the reheated powder and the specimens from reheated powder analyzed by using TG-DTA at 1060°C and 1250°C in air are shown in **Figs. 10**(a), (b) and (c), respectively. Contrasting Fig. 10(b) with Fig. 10(a) and (c), a higher degree of amorphous phase was found in the specimen analyzed at 1060°C. Probably this amorphous phase affected the mass variation from 1060°C to 1090°C.

When Al_4O_4C product buried in graphite powder was heated in air, Al_4O_4C should be oxidized according to Re. (8) to form Al_2O_3 and C, because the main gas is $CO(g)$ in carbon-containing refractories at high temperature.[11]

$$Al_4O_4C(s) + 2CO(g) \longrightarrow 2Al_2O_3(s) + 3C(s) \quad (8)$$
$$2C(s) + O_2(g) \longrightarrow 2CO(g) \quad (9)$$

Since CO was generated according to Re. (9), the overall reaction in this case is Re. (10) (= (8) + (9)).

$$Al_4O_4C(s) + O_2(g) \longrightarrow 2Al_2O_3(s) + C(s) \quad (10)$$

4) Advantage of Al_4O_4C as an additive for carbon-containing refractories

From Fig. 7, when partial pressure of $CO(g)$ is lower than the critical $CO(g)$ partial pressure of $Al_2O_3 \rightarrow Al_4O_4C$, Al_4O_4C (s) exists stably. It means that Re. (1) happens. When partial

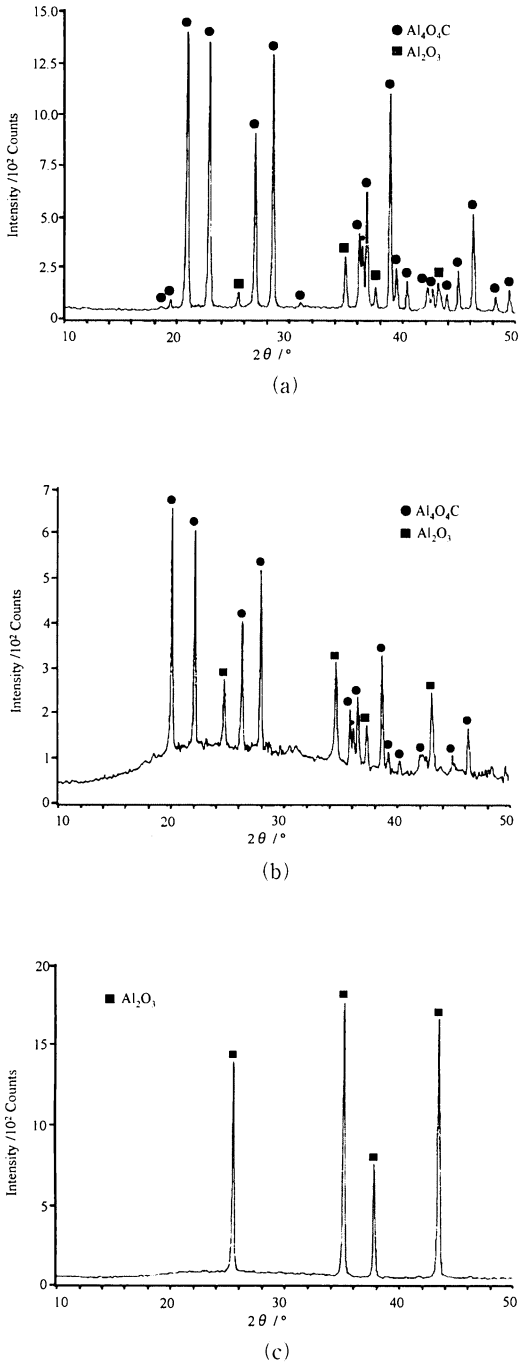

Fig. 10. XRD patterns. (a) Reheated powder, (b) Specimen from reheated powder analyzed in TG at 1060°C, (c) Specimen from reheated powder analyzed in TG at 1250°C.

pressure of $CO(g)$ is higher than the critical value, $Al_2O_3(s)$ exists stably. It means that Re. (8) happens. Because the main gas is $CO(g)$ in carbon-containing refractories at high temperature as statement, when Al_4O_4C, C and Al_2O_3 coexist in carbon-containing refractories and the refractories were used at working temperature in air, the main happening reaction will be Re. (8), but not Re. (1). Similarly, in carbon-containing refractories, Al_4O_4C as additive will not be reducted into Al_4C_3 according to Re. (2).

Since Al_4O_4C, added into carbon-containing refractories, will be oxidized into Al_2O_3 and C by CO. The formation of C will cause the fact that carbon raw material in the refractories is not reduced, even if the carbon raw material reacts with O_2 into CO. Al_4O_4C's role of oxidation resistance is concluded. The formed Al_2O_3 is a phase of enduring high temperature, it will not decrease the characteristic of erosion resistance of carbon-containing refractories. On the other hand, when Re. (8) is proceeded, the accompanying volume change is -2.1%. However, when Re. (11) is proceeded, the volume change is $+170.5\%$. The later great expansion can play a role of increasing density and decreasing porosity; however, this role is little because the porosity is already very low in carbon-containing refractories. At this time, the spalling caused by great expansion can not be neglected.

$$2Al(s) + 3CO(g) \longrightarrow Al_2O_3(s) + 3C(s) \qquad (11)$$

The spalling is one of the main factors of carbon-containing refractories damage. Particularly for MgO-C refractories, the formed Al_2O_3 will react with MgO into spinel with additional volume expansion, the combination of this expansion and the expansion of Re. (11) should greatly affect the spalling resistance of the MgO-C refractories. Al_4O_4C additive can slightly decrease the affection of expansion of spinel formation. So Al_4O_4C additive is considered better than Al additive on spalling resistance of refractories.

Furthermore, since Al_4O_4C will not be transformed into Al_4C_3, Al_4O_4C as an additive in carbon-containing refractories will not lead the refractories to collapse. Al_4O_4C also can be used in unshaped refractories containing water. When the used carbon-containing refractories with Al additive were recycled for using again, the formed Al_4C_3 in the refractories from reaction of Al and C was a serious problem. In general, these used refractories were especially dealt for removing the Al_4C_3. This process is complex and time-consuming. Using Al_4O_4C additive, this problem does not exist.

Moreover, Although Al_4O_4C started to be oxidized from about 820°C by O_2, later than graphite (from about 610°C by O_2), Al_4O_4C started to be oxidized at almost the same temperature with graphite when buried in graphite powder and heated in air. This indicates that Al_4O_4C can play a role of decreasing the oxidation of graphite in the carbon-containing refractories. Al_4O_4C, even if milled to very fine, has not combustible danger and so does not involve risks in utilization.

From the discussion above, Al_4O_4C is considered a promising additive for carbon-containing refractories.

5. Conclusions

Several dynamics factors influencing synthesis of Al_4O_4C and oxidation characteristics of Al_4O_4C were investigated and results are concluded as the following.

(1) The formed Al_4O_4C was increased with increase of heating temperature and extension of keeping time. Grain size of Al_2O_3 had obvious influence on synthesis of Al_4O_4C and enough fine Al_2O_3 should be used for synthesizing Al_4O_4C and avoiding Al_4C_3 formation.

(2) The activation energy of reaction of Al_2O_3 and graphite to form Al_4O_4C was calculated as 358.0 kJ/mol.

(3) Al_4O_4C started to be oxidized from about 820°C when heated in air.

(4) Al_4O_4C, buried in graphite powder and heated in air, started to be oxidized at almost the same temperature with graphite and was converted into Al_2O_3 and C. Al_4O_4C was considered a promising additive for carbon-containing refractories.

References

1) H. Kyoden, H. Nishio, K. Ito and S. Horita, *Taikabutsu*, 38, 242-250 (1986) [in Japanese].

2) A. Yamaguchi, *Taikabutsu*, 38, 506-512 (1986) [in Japanese].
3) A. Watanabe, H. Takahashi and S. Takanaga, *Taikabutsu*, 38, 740-746 (1986) [in Japanese].
4) S. Zhang and A. Yamaguchi, *J. Ceram. Soc. Japan*, 103, 235-239 (1995).
5) M. Heyrman and C. Chatillon, *J. Electrochem. Soc.*, 153, E119-E130 (2006).
6) S. Zhang and A. Yamaguchi, *J. Ceram. Soc. Japan*, 104, 393-398 (1996).
7) J. Zhao, W. Lin, A. Yamaguchi, J. Ommyoji and J. Sun, *Taikabutsu*, 59, 288-295(2007) [in Japanese].
8) J. M. Lihrmann, J. Tirlocq, P. Descamps and F. Cambier, *J. Eur. Ceram. Soc.*, 19, 2781-2787 (1999).
9) M. W. Chase, NIST-JANAF Thermo-chemical Tables, J. Phys. Chem. Ref. Data, Monograph No. 9, National Institute of Standards and Technology, Gaithersburg, MD 20899-0001, Fourth ed. (1998).
10) Y. Iwasawa, "Chemical Handbook (Initial Part, 2)," Chemical Society of Japan Fifth ed. (2004) pp. 377-378.
11) A. Yamaguchi, *Taikabutsu*, 38, 232-241 (1986) [in Japanese].

Journal of the Ceramic Society of Japan 115 [11] 761-766 (2007)

Paper

Synthesis of Al_4SiC_4 from Alumina, Silica and Graphite

Jianli ZHAO,*,** Wei LIN,*,† Akira YAMAGUCHI,* Junji OMMYOJI* and Jialin SUN**

*Okayama Ceramics Research Foundation, Nishikatakami 1406-18, Bizen, Okayama, 705-0021 Japan

**School of Material Science and Engineering, University of Science and Technology Beijing, 100083 China

Al_4SiC_4 has been reported to be a good additive for carbon-containing refractories. The present study investigated various factors influencing the synthesis of Al_4SiC_4 by heating mixtures of Al_2O_3, SiO_2 and graphite in an argon atmosphere. The formation of Al_4SiC_4 began from a temperature between 1450°C and 1500°C. The formed quantity of Al_4SiC_4 increased as the heating temperature was raised. As the heating time was extended, the Al_4SiC_4 increased to its greatest amount and then it hardly changed. SiC and Al_4O_4C were also formed as mediums and were decreased as the heating time was extended. The optimum molar ratio of C, Al_2O_3 and SiO_2 was 8:2:0.8 and at that time pure Al_4SiC_4 was formed. The formation mechanism of Al_4SiC_4 was also discussed.

[Receivd May 11, 2007; Accepted August 24, 2007]

Key-words : Al_4SiC_4, Synthesis, Al_2O_3, SiO_2, Graphite, Al_4O_4C, SiC, Carbon-containing refractories

1. Introduction

Metal Al, Si and SiC are frequently used in carbon-containing refractories as additives to improve the oxidation resistance and thermal properties, but they also cause some problems. For example, Al reacts with C in the refractories to form Al_4C_3, which may lead the refractories to collapse due to the poor hydration resistance of Al_4C_3.[1)-4)] Al can not be used in unshaped refractories containing water because it reacts with water.[5)] Fine Al powder is combustible, so its utilization involves risks. When Si or SiC is added into refractories, SiO_2 with a low melting point is formed due to oxidation.

In Al_4C_3-SiC system (**Fig. 1**[6)]), there is a compound, Al_4SiC_4, that is stable until 2080°C and has good hydration resistance. A protective film composed of Al_2O_3 and mullite will be formed on the surface when Al_4SiC_4 is oxidized, which prevents the further oxidation.[7)-10)] The Al_4SiC_4 added into MgO-C and Al_2O_3-C refractories will minimize the pores and improve the oxidation resistance and rupture modulus, because it reacts with CO gas to convert into Al_2O_3, $Al_6Si_2O_{13}$ and C.[4)-5)] So, Al_4SiC_4 has been considered to be a promising additive for carbon-containing refractories.

Several methods for synthesis of Al_4SiC_4 have been investigated by using metals (Al, Si) and carbides (Al_4C_3, SiC) as starting raw materials on a laboratory scale. Yamaguchi et al. obtained Al_4SiC_4 by heating a mixture of Al, Si and C in an argon atmosphere at 1700°C.[7),8),11)-14)] Yamamoto et al. synthesized Al_4SiC_4 at a low temperature of 1450°C by adding $N(CH_2CH_2OH)$ into the powder of Al, Si and C.[15)] Wills et al. used SiC and Al_4C_3 raw materials and hot-press process at 1750-1980°C in an argon atmosphere for the synthesis of Al_4SiC_4.[9)] Hasegawa et al. prepared Al_4SiC_4 at a low temperature of 1600°C utilizing superfine SiC and Al_4C_3 powders.[16)] Yamaguchi et al. gained Al_4SiC_4 by heating a mixture of Al, Si and C containing 3% Al_2O_3 at 1700°C,[7)] and Inoue et al. synthesized Al_4SiC_4 by heating a mixture of Al, kaolin and C at 1700°C in a vacuum.[17)]

In order to obtain some fundamental information on the development of an industrial scale synthesis process of Al_4SiC_4, Al_2O_3, SiO_2 and graphite were used as starting raw materials, without metals and carbides, and influence factors on the synthesis, such as the condition of the mixture (powder or pressed compact), heating temperature, heating time and ratios of the raw materials, were investigated in the present study.

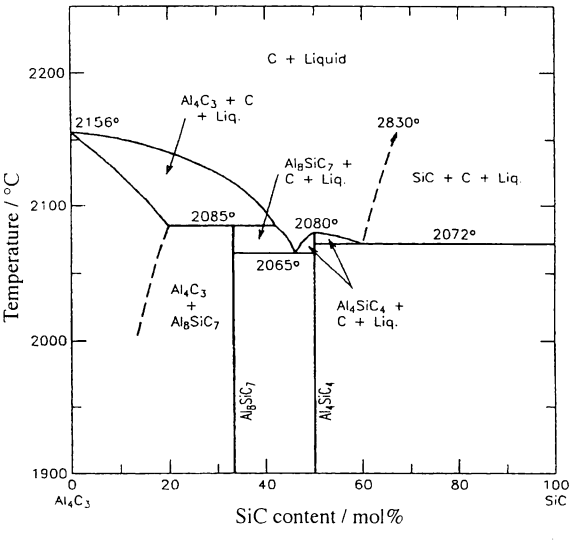

Fig. 1. Equilibrium diagram of Al_4C_3-SiC system.

2. Experimental procedure

Common Al_2O_3 (average grain size: 0.1 μm, purity: ≥99.99 mass%), SiO_2 (average grain size: 100 μm, purity: ≥99 mass%) and graphite (average grain size: 30 μm, purity: ≥99 mass%) were used as starting raw materials. They were weighted in proportions of $C:Al_2O_3:SiO_2 = 12:2:1$, 8:2:0.8, 8:2:0.85, 8:2:0.9, 8:2:1, 8:2:1.05, 8:2:1.1, 4:2:1 (molar ratio), mixed with alcohol and dried in a vacuum-rotary evaporator. 2 g of the mixture in a high purity graphite crucible was set into an electric furnace with a graphite heater (**Fig. 2**). Ar gas (purity: ≥99.9999 mass%) was poured into the furnace after the vacuum. The mixture was heated to a temperature of 1450-1700°C at a rate of 10°C/min and maintained for 3-9 h under flowing Ar (1 L/min). Finally, the specimens were cooled to room temperature within the furnace through shutting off the power supply, where the average cooling rate was 64°C/min from 1700 to 1000°C. Phases in the specimens were identified by using X-ray diffraction (XRD, RINT 2200, Rigaku, Japan), and the microstructure was observed using field emission scanning electron microscope (FE-SEM, JSM-6340F, JEOL, Japan).

† Present address; Shinagawa Refractories Co., Ltd.

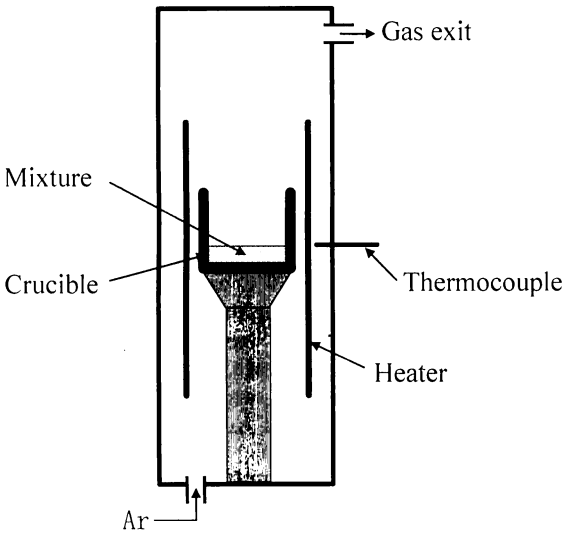

Fig. 2. Schematic diagram of experimental equipment.

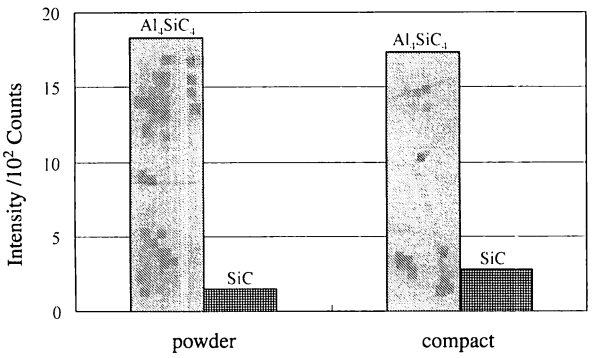

Fig. 3. Phases in powder specimen and compact specimen from the mixture with $C:Al_2O_3:SiO_2 = 8:2:1$ heated at 1700°C for 9 h.

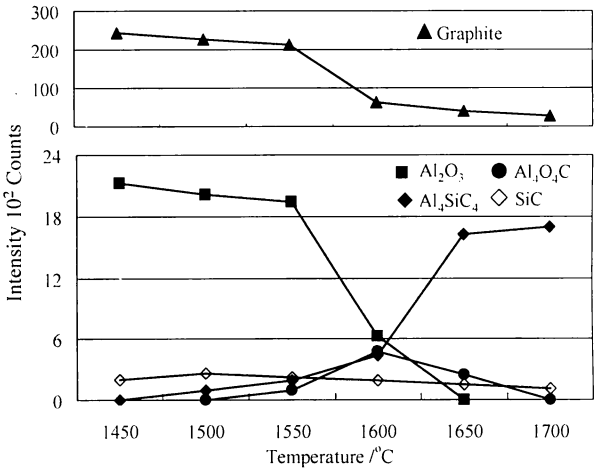

(a) $C:Al_2O_3:SiO_2 = 12:2:1$

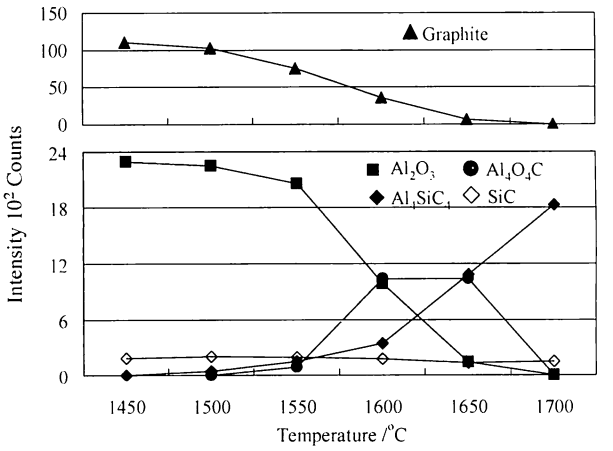

(b) $C:Al_2O_3:SiO_2 = 8:2:1$

Fig. 4. Phases in specimens heated at various temperatures for 9 h. (a) $C:Al_2O_3:SiO_2 = 12:2:1$, (b) $C:Al_2O_3:SiO_2 = 8:2:1$

3. Results

3.1 Influence of mixture's condition

A powder mixture with $C:Al_2O_3:SiO_2 = 8:2:1$ and pressed compact mixture with $C:Al_2O_3:SiO_2 = 8:2:1$ and 20 mm diameter pressed at 100 MPa were heated at 1700°C for 9 h. The voidage of the powder mixture was 78% and that of the pressed compact was 31% before heating. The intensity of the strongest XRD peak of each phase in the heated specimens is shown in **Fig. 3.** From Fig. 3, it is known that there are not significant differences on the formed phases when using the powder mixture or the pressed compact mixture. Considering the fact that the product from the pressed compact mixture is porous, similar with that from the powder mixture, the powder mixtures were used in the following tests for convenience.

3.2 Influence of heating temperature

The results of the powder mixtures with $C:Al_2O_3:SiO_2 = 12:2:1$ and 8:2:1 heated at 1450, 1500, 1550, 1600, 1650 and 1700°C for 9 h are shown in **Figs. 4**(a) and (b). Al_4SiC_4 was detected in the specimens heated at 1500°C and above, and the quantity of Al_4SiC_4 increased by increasing the temperature. All SiO_2 has been reducted into SiC at the lowest heating temperature, 1450°C, and the quantity of SiC slowly decreased as the temperature was raised from 1450 to 1700°C. The Al_4O_4C was observed from 1550°C and the quantity of Al_4O_4C increased by increasing the temperature up to 1600°C, but disappeared at 1700°C.

3.3 Influence of heating time

The results of the mixtures with $C:Al_2O_3:SiO_2 = 12:2:1$ and 8:2:1 heated at 1700°C for 3, 5, 7 and 9 h are shown in **Figs. 5** (a) and (b). In the former ratio, the quantity of Al_4SiC_4 increased until 5 h and hardly changed after 5 h. Al_4O_4C has been formed at 3 h and disappeared at 5 h. In the later ratio, the changing tendency of each phase was the same as that in the former case, but the change was slower. In the specimen from the mixture with $C:Al_2O_3:SiO_2 = 8:2:1$ heated at 1700°C for 9 h, the phases were only Al_4SiC_4 and SiC.

3.4 Influence of SiO_2 content in the mixture

The results of the mixtures with $C:Al_2O_3:SiO_2 = 8:2:x$ (x = 0.8, 0.85, 0.9, 1, 1.05, 1.1) heated at 1700°C for 9 h are shown in **Fig. 6.**

The quantity of SiC in the heated specimens dropped by decreasing the SiO_2 content in the mixtures. When $x = 0.8$, SiC disappeared and only Al_4SiC_4 existed in the specimen. XRD pattern and SEM micrograph of this specimen ($x = 0.8$) were shown in **Figs. 7** and **8**, respectively. The formed Al_4SiC_4 appeared to be powder consisting of plate-like crystals with about 1 μm thickness, 3-5 μm width and 6-8 μm in length.

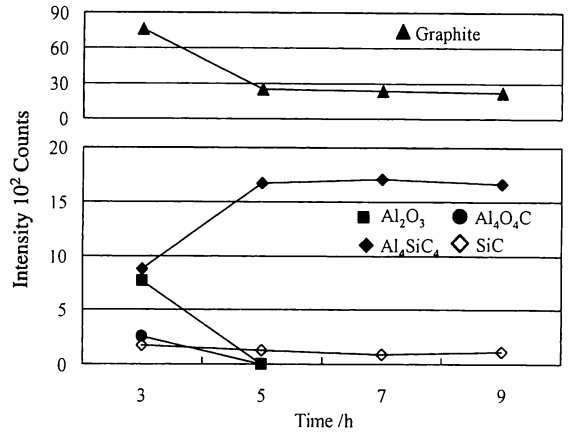

(a) $C:Al_2O_3:SiO_2$= 12:2:1

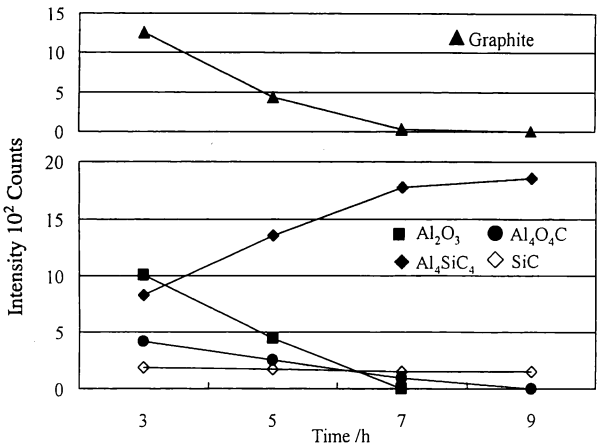

(b) $C:Al_2O_3:SiO_2$= 8:2:1

Fig. 5. Phases in specimens heated at 1700°C for different times. (a) $C:Al_2O_3:SiO_2$ = 12:2:1, (b) $C:Al_2O_3:SiO_2$ = 8:2:1

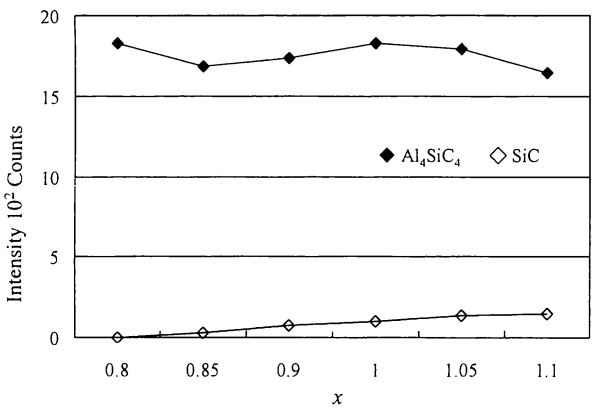

Fig. 6. Phases in specimens from the mixtures with various SiO_2 ratios heated at 1700°C for 9 h.

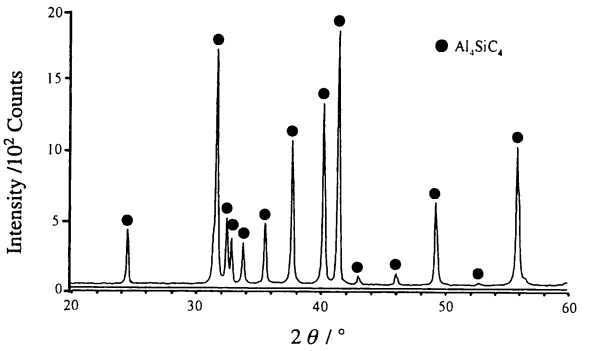

Fig. 7. XRD pattern of specimen from the mixture with $C:Al_2O_3:SiO_2$ = 8:2:0.8 heated at 1700°C for 9 h.

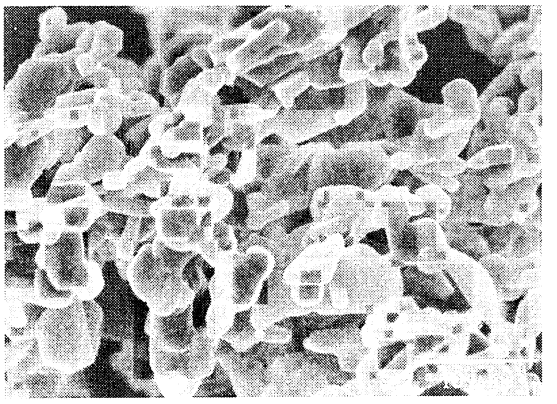

Fig. 8. SEM micrograph of specimen from the mixture with $C:Al_2O_3:SiO_2$ = 8:2:0.8 heated at 1700°C for 9 h.

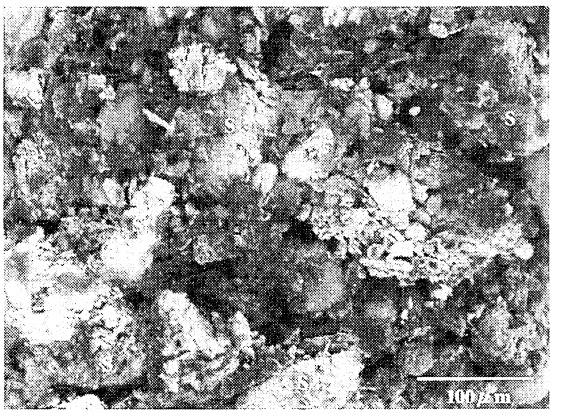

Fig. 9. SEM micrograph of the powder mixture with $C:Al_2O_3:SiO_2$ = 8:2:1.

4. Discussion

4.1 Formation mechanism of Al_4SiC_4

Figure 9 shows the SEM micrograph of the powder mixture with $C:Al_2O_3:SiO_2$ = 8:2:1. Since the starting raw materials are Al_2O_3 (average grain size: 0.1 μm), SiO_2 (average grain size: 100 μm) and graphite (average grain size: 30 μm), it was known that the great grains (Marked as S) with about 100 μm size are SiO_2 grains with fine Al_2O_3 on the surface and the flakes with about 30 μm size are graphite grains with fine Al_2O_3 on the surface. This condition of the unheated powder mixture was modeled as **Fig. 10**(a).

Figure 11 presents change of condensed phases for various partial pressures of CO(g) in the Al-Si-C-O system, calculated thermodynamically. The formation free energy of Al_4SiC_4 and Al_4O_4C reported by Yokokawa et al.[18] and Lihrmann et al.,[19] respectively, were used in the calculation. Those of Al_2O_3, SiO_2, SiC and CO were from NIST-JANAF Thermochemical Tables.[20] The standard pressure ($P°$) is 0.101325

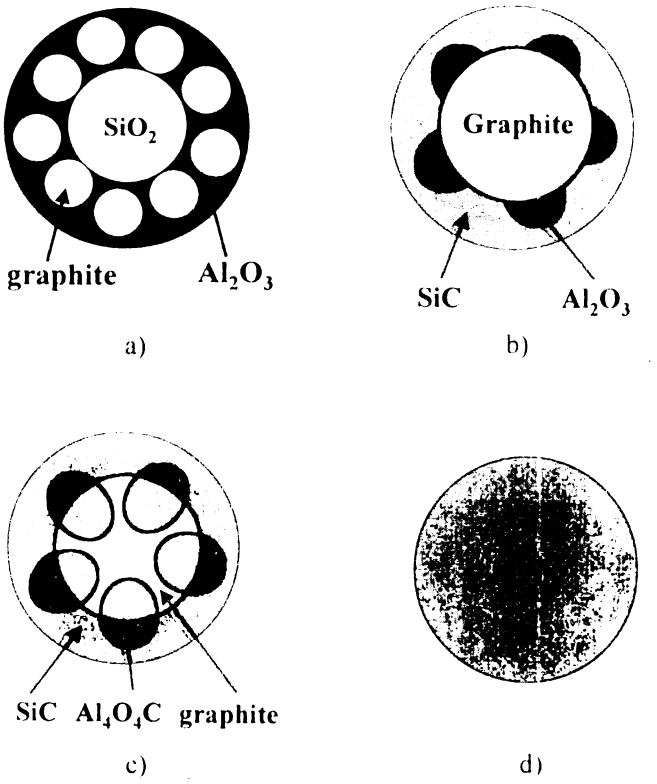

Fig. 10. Models of formation process of Al_4SiC_4 (a)→b)→c)→d)).

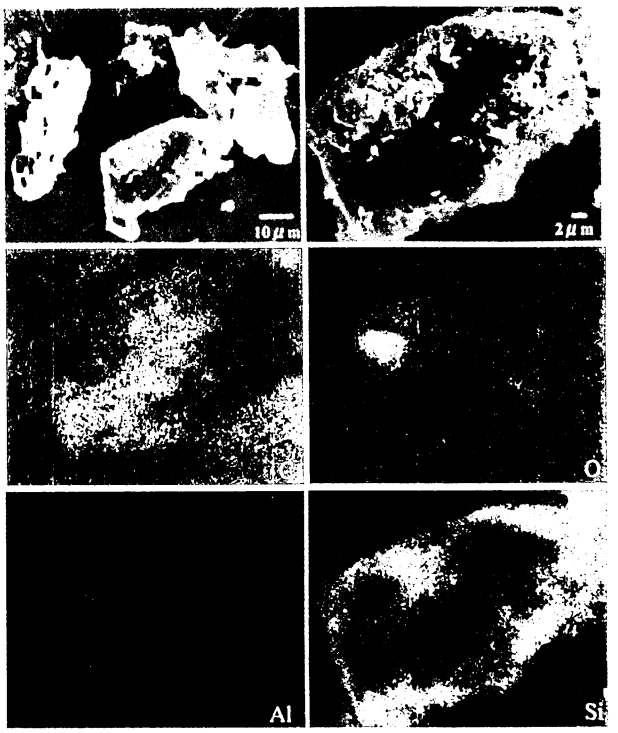

Fig. 12. SEM micrograph and EDAX analysis of specimen from mixture with $C:Al_2O_3:SiO_2 = 8:2:1$ heated at 1450°C for 9 h.

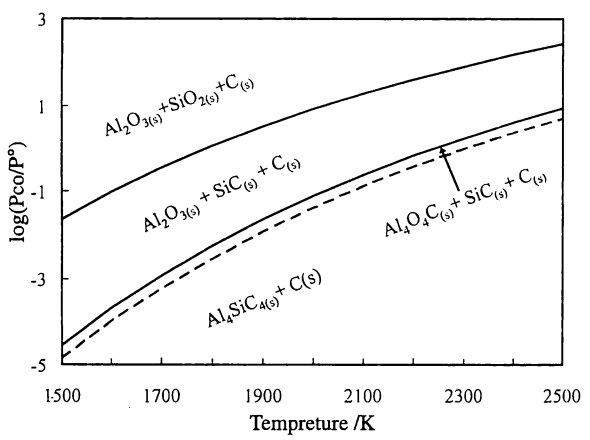

Fig. 11. Stable relation among the condensed phases in Al-Si-C-O system for temperature and partial pressure of CO(g).

MPa(=1 atm).

From Fig. 11, it can be known that the change of condensed phases is according to the following when coexisting with C(s) as decreasing partial pressure of CO(g).

$$(Al_2O_3 + SiO_2) \rightarrow (Al_2O_3 + SiC) \rightarrow (Al_4O_4C + SiC) \rightarrow (Al_4SiC_4)$$

Since the conversion starting temperature of $SiO_2 \rightarrow SiC$ is much lower than that of $Al_2O_3 \rightarrow Al_4O_4C$ and that of $Al_4O_4C \rightarrow Al_4SiC_4$ at a same partial pressure of CO from Fig. 11, SiC should be formed much earlier than Al_4O_4C and Al_4SiC_4. This was verified by the fact that all SiO_2 was converted to SiC at 1450°C, while Al_4O_4C and Al_4SiC_4 had not been observed at that temperature (Fig. 4(a)(b)).

Figure 12 presents the micrograph of the specimen from the mixture with $C:Al_2O_3:SiO_2 = 8:2:1$ heated at 1450°C for 9 h. It was observed that fine powders packed the grains. In the grains, grain A seems that its surface was partly damaged. The grain A was analyzed by using EDAX. Since the phases in this specimen are only graphite, Al_2O_3 and SiC (Fig. 4(b)), it can be assumed that grain A is graphite, the powders adhered on the surface of grain A were Al_2O_3 and SiC. The formed SiC was a fine powder and adhered on the surface of the graphite grains and the Al_2O_3 powder. This existing condition of SiC suggests that SiC was formed mainly by gas reactions. The probable reaction process was stated below.

As the temperature was raised, firstly, $SiO_2(s)$ would react with C(s) according to Re. (1).

$$SiO_2(s) + C(s) = SiO(g) + CO(g) \quad (1)$$

CO(g) would also reduct SiO_2 into SiO(g) according to Re. (2) and Re. (3).

$$SiO_2(s) + CO(g) = SiO(g) + CO2(g) \quad (2)$$
$$CO_2(g) + C(s) = 2CO(g) \quad (3)$$

Reaction. (1) is the same with the overall reaction of Re. (2) and Re. (3) ((2) + (3) = (1)).

SiC was considered formed by Re. (4) from SiO(g) and CO (g). The formed SiC powder accumulated on the surface of the graphite grains and the Al_2O_3 powder as modeled in Fig. 10(b) (The graphite grain was enlarged for easier looking.), which is advantageous to the next reactions to form Al_4SiC_4.

$$SiO(g) + 3CO(g) = SiC(s) + 2CO_2(g) \quad (4)$$

The overall reaction of SiO_2 and C translating into SiC is Re. (5) (= (1) + (4) + 2 × (3)).

$$SiO_2(s) + 3C(s) = SiC(s) + 2CO(g) \quad (5)$$

When the temperature was raised further, the Al_2O_3 would react with C to form Al_4O_4C according to Re. (6).

$$2Al_2O_3(s)+3C(s)=Al_4O_4C(s)+2CO(g) \quad (6)$$

Once the Al_2O_3 was separated from C by the formed Al_4O_4C, it should reacted with CO(g) following Res.(7) and (3) to form Al_4O_4C.

$$2Al_2O_3(s)+4CO(g)=Al_4O_4C(s)+3CO_2(g) \quad (7)$$

The overall reaction of Res. (7) and (3) is same with Re. (6). The formed Al_4O_4C contacted well with SiC powder as modeled in Fig. 10(c).

The stable area of Al_4O_4C is very narrow From Fig. 11, so the formed Al_4O_4C would be rapidly converted to Al_4SiC_4 during heating according to Re.(8) and Re.(9). Re. (8) is the same with the overall reaction of Re. (9) and Re. (3). The reaction result was modeled in Fig. 10(d). It was considered that Re.(8) was proceeded only in the starting period of the Al_4SiC_4 formation at the contacting points of Al_4O_4C, SiC and C. The main reaction for Al_4SiC_4 formation is Res. (9) and (3).

$$Al_4O_4C(s)+SiC(s)+6C(s)=Al_4SiC_4(s)+4CO(g) \quad (8)$$

$$Al_4O_4C(s)+SiC(s)+8CO(g)=Al_4SiC_4(s)+6CO_2(g) \quad (9)$$

The reason why Al_4SiC_4 was observed at 1500°C, but Al_4O_4C was not observed until 1550°C, is probably due to the rapid conversion from Al_4O_4C and SiC into Al_4SiC_4 after a little Al_4O_4C formed at 1500°C.

The overall reaction of Al_4SiC_4 formation from Al_2O_3, SiO_2 and C is Re. (10) (= (5) + (6) + (8)).

$$2Al_2O_3(s)+SiO_2(s)+12C(s)=Al_4SiC_4(s)+8CO(g) \quad (10)$$

4.2 Volatile gases in Al-Si-C-O system

Deposit was observed on the upper metal inwall of the furnace after heating. The deposit was collected after the furnace was cooled into room temperature and analyzed by using XRD. The result is shown in **Fig. 13**. It is seen that the main crystal phases are Al, Al_4C_3, Al_2O_3 and SiC and a amorphous phase also exists. These substances in the deposit are considered to be formed by the reactions of volatile gases of the Al-Si-C-O system.

Figure 14 shows the equilibrium partial pressure of gases formed in the Al-Si-C-O system at 1973K (1700°C) calculated thermodynamically. There are many kinds of gases in the system, while Al, Al_2O, SiO and CO gases have a relatively high partial pressure, being the main gases.

The formation reactions of the main gases are listed in Res. (1), (11) and (12) as examples.

$$Al_2O_3(s)+3C(s)=2Al(g)+3CO(g) \quad (11)$$

$$Al_2O_3(s)+2C(s)=Al_2O(g)+2CO(g) \quad (12)$$

The main gases may be also participating in the formation reactions of Al_4O_4C and Al_4SiC_4 in the powder mixtures. For example,

$$4Al(g)+4CO(g)=Al_4O_4C(s)+3C(s) \quad (13)$$

$$2Al_2O(g)+2CO(g)=Al_4O_4C(s)+C(s) \quad (14)$$

$$4Al(g)+SiO(g)+5C(s)=Al_4SiC_4(s)+CO(g) \quad (15)$$

$$2Al_2O(g)+SiO(g)+7C(s)=Al_4SiC_4(s)+3CO(g) \quad (16)$$

The overall reaction of ((11) + (13)) and ((12) + (14)) is the same as Re. (6). The overall reaction of ((1) + 2× (11) + (15)) and ((1) + 2× (12) + (16)) is Re. (10).

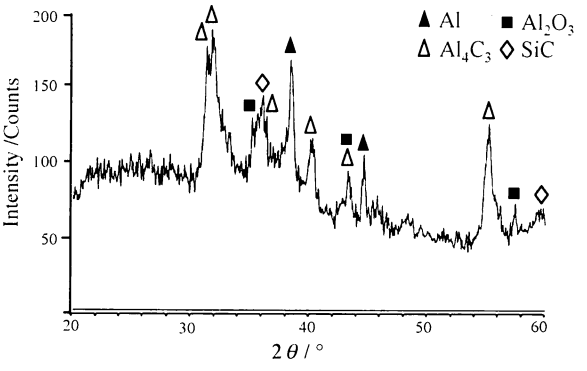

Fig. 13. XRD pattern of the deposit on the upper metal inwall of the furnace.

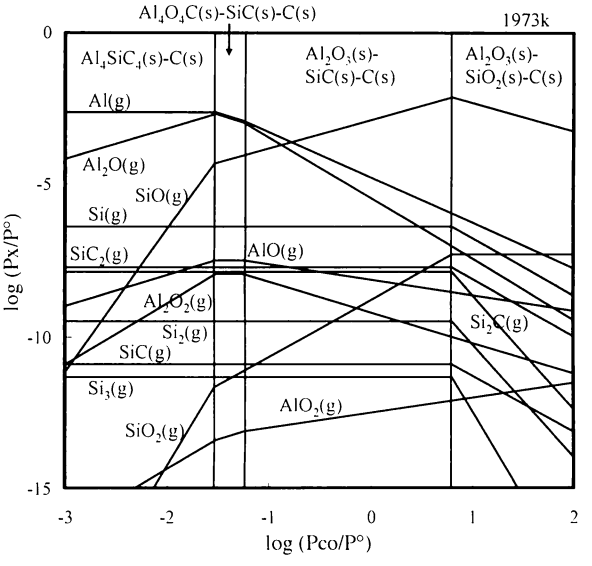

Fig. 14. Equilibrium partial pressures of gases formed in Al-Si-C-O system (1973 K).

The deposit was considered to be formed by the Al, Al_2O, SiO and CO gases according to Res.(17)-(20).

$$2Al(g)+3CO(g)=Al_2O_3(s)+3C(s) \quad (17)$$

$$Al_2O(g)+2CO(g)=Al_2O_3(s)+2C(s) \quad (18)$$

$$2Al_2O(g)+8CO(g)=Al_4C_3(s)+5CO_2(g) \quad (19)$$

$$SiO(g)+3CO(g)=SiC(s)+2CO_2(g) \quad (20)$$

No Al_4SiC_4 crystal was detected in the deposit. The reason may be that Al_4SiC_4 was not formed because the temperature was low on the upper metal inwall of the furnace (In the heating period, the temperature at this site was estimated as no higher than 1000°C, because the furnace was cooled by flowing water in the metal wall.) or that Al_4SiC_4 was formed, but was in an amorphous phase.

On the other hand, the best ratio for the synthesis of pure Al_4SiC_4 phase is 8:2:0.8, different with the ratio of 12:2:1 in theory (Re. (10)). This indicates that the volatilized quantities of Al_2O_3 and SiO_2 are comparatively more than that of C and the volatilized quantity of Al_2O_3 is comparatively more than that of SiO_2 in this research.

5. Conclusions

Synthesis of Al_4SiC_4 by heating the mixture of Al_2O_3, SiO_2 and graphite in an argon atmosphere was investigated. The following results were obtained.

(1) The formation of Al_4SiC_4 began from a temperature between 1450°C and 1500°C. The formed quantity of Al_4SiC_4 was increased as the heating temperature was raised.

(2) As the heating time was extended, Al_4SiC_4 increased into its greatest amount and then hardly changed. SiC and Al_4O_4C were also formed as mediums and were decreased as the heating time was extended.

(3) The optimum molar ratio of C, Al_2O_3 and SiO_2 was 8:2:0.8 and at that time the pure Al_4SiC_4 was formed.

(4) The formed Al_4SiC_4 was powder consisting of plate-like crystals with about 1 μm thickness, 3-5 μm width and 6-8 μm in length.

References

1) H. Kyoden, H. Nishio, K. Ito and S. Horita, *Taikabutsu*, 38, 242-250 (1986) [in Japanese].
2) A. Yamaguchi, *Taikabutsu*, 38, 506-512 (1986) [in Japanese].
3) A. Watanabe, H. Takahashi and S. Takanaga, *Taikabutsu*, 38, 740-746 (1986) [in Japanese].
4) S. Zhang and A. Yamaguchi, *J. Ceram. Soc. Japan*, 103, 235-239 (1995).
5) S. Zhang and A. Yamaguchi, Proceedings of Unified International Technical Conference on Refractories, Nov. 4-7, New Orleans, USA (1997) pp. 861-869.
6) L. L. Oden and R. A. McCune, *Metallur-gical Transactions A*, 18A, 2005-2014 (1987).
7) A. Yamaguchi and S. Zhang, *J. Ceram. Soc. Japan*, 103, 20-24 (1995).
8) K. Inoue, A. Yamaguchi and S. Hashimoto, *J. Ceram. Soc. Japan*, 110, 1010-1015 (2002).
9) R. Wills and S. Goodrich, Ceramic Engineering and Science Proceedings, 26, 181-188 (2005).
10) J. Schoennahl, B. Willer and M. Daire, Materials Science Monographs 4: Sintering-New Developments, Elsevier Science Publishing, Amsterdam, 4, 338-345 (1979).
11) K. Inoue, S. Mori and A. Yamaguchi, *J. Ceram. Soc. Japan*, 111, 126-132 (2003).
12) K. Inoue and A. Yamaguchi, *J. Ceram. Soc. Japan*, 111, 267-270 (2003).
13) K. Inoue, S. Mori and A. Yamaguchi, *J. Ceram. Soc. Japan*, 111, 348-351 (2003).
14) K. Inoue, S. Mori and A. Yamaguchi, *J. Ceram. Soc. Japan*, 111, 466-470 (2003).
15) O. Yamamoto, M. Ohtani and T. Sasamoto, *J. Mater. Res.*, 17, 774-778 (2002).
16) M. Hasegawa, K. Itatani, M. Aizawa, F. S. Howell and A. Kishioka, *J. Am. Ceram. Soc.*, 79, 275-278 (1996).
17) K. Inoue and A. Yamaguchi, *J. Am. Ceram. Soc.*, 86, 1028-1030 (2003).
18) H. Yokokawa, M. Fujishige, S. Ujiie and M. Dokiya, Metallurgical Transac-tions B, 18B, 433-444 (1987).
19) J. M. Lihrmann, J. Tirlocq, P. Descamps and F. Cambier, *J. Eur. Ceram. Soc.*, 19, 2781-2787 (1999).
20) M. W. Chase, NIST-JANAF Thermo- chemical Tables, J. Phys. Chem. Ref. Data, Monograph No. 9, National Institute of Standards and Technology, Gaithersburg, MD 20899-0001, (Fourth ed., 1998).

Available online at www.sciencedirect.com
ScienceDirect
Journal of the European Ceramic Society 27 (2007) 1953–1959
www.elsevier.com/locate/jeurceramsoc

Effect of porosity on carbonation and hydration resistance of CaO materials

Min Chen [a,*], Nan Wang [a], Jingkun Yu [a], Akira Yamaguchi [b]

[a] *School of Materials and Metallurgy, 312# Northeastern University, 3-11 Wen-Hua Road, Shenyang 110004, China*
[b] *Research Laboratory, Okayama Ceramics Research Foundation, 1406-18 Nishi Katakami, Bizen, Okayama 705-0021, Japan*

Received 23 March 2006; received in revised form 20 May 2006; accepted 31 May 2006
Available online 1 August 2006

Abstract

CaO pellets with different porosity were carbonated at 700 °C in CO_2 atmosphere. The carbonation rate was controlled by the diffusion of CO_2, regardless of the difference in porosities. For the low-porosity pellet, carbonation reaction only occurred on the surface, with a dense $CaCO_3$ film thus formed, which combined well with the substrate material; while for the pellet of high-porosity, the carbonation reaction occurred simultaneously both on surface and inside pores, and each CaO grain was surrounded by $CaCO_3$ film that contained microfissures. Hydration test results showed that carbonation treatment could effectively improve the hydration resistance of CaO materials regardless of porosity, but the carbonated high-porosity pellet was prone to breakage due to poor combination between the carbonated CaO grains. Therefore, for the purpose to improve the hydration resistance by carbonation treatment, it is recommended that the CaO materials should be either with less appreciable apparent porosity or with a limited carbonation ratio for the high-porosity CaO material.
© 2006 Elsevier Ltd. All rights reserved.

Keywords: A. CaO materials; B. Porosity; C. Carbonation treatment; D. $CaCO_3$ film; E. Hydration resistance

1. Introduction

Lime has the properties of high melting temperature, low vapor pressure, and thermodynamic stability in the presence of carbon as well as high alkality, thus it has long been considered to use as the raw materials for high temperature ceramics (such as crucible and ceramic filter), refractories and metallurgical accessories (such as refining slag and tundish covering powder).[1–6] With the development of clean steel production, free lime containing materials have been becoming more and more important for increasing the service life and removing inclusions from molten steel.[7–11] It is considered that application of CaO containing materials is an essential direction for the development of metallurgical industries and other high temperature field.[12] However, the application of CaO containing materials have been inhibited due to their drawback of poor hydration resistance, and many studies on this subject had been carried out from quite a long time ago.[13–15]

Among all of the methods to improve the hydration resistance of CaO materials, carbonation treatment is considered to be "green", since no impurities are added into CaO materials so that their advantages are kept after $CaCO_3$ decomposes at high temperature. Another reason for calling this method "green" is that carbonation process can consume CO_2 which is friendly to environment. Therefore, the studies on improving hydration resistance of CaO materials by carbonation treatment have been conducted since 1970s.[16–19] However, most of these works focused on the carbonation conditions by using deadburned CaO clinker as starting material, and it has been concluded that the optimum carbonation temperature is around 700 °C.[16,17] In fact, besides the deadburned CaO clinker with high compactness used for refractory materials, there are also porous CaO materials, such as CaO filter and lightburned CaO for tundish covering powder, and it is more difficult to prevent these porous CaO materials from hydrating.[5] It is necessary to confirm the feasibility to improve these CaO materials by carbonation treatment. Therefore, the present work investigated the carbonation of CaO materials with different porosities. The influence of porosity on carbonation behavior and microstructure of CaO pellets as well as their hydration properties were discussed.

* Corresponding author. Tel.: +86 24 6368 2241; fax: +86 24 8368 1576.
E-mail address: slakejp@163.com (M. Chen).

0955-2219/$ – see front matter © 2006 Elsevier Ltd. All rights reserved.
doi:10.1016/j.jeurceramsoc.2006.05.101

2. Experimental

Reagent $CaCO_3$ powder (99.5% purity and average size of 10 μm) and lightweight $CaCO_3$ powder were used as starting materials. The lightweight $CaCO_3$ powder was prepared from precipitation reaction by bubbling CO_2 gas to aqueous solution of CaO (that was derived from heating reagent $CaCO_3$ powder at 900 °C), with average size less than 1 μm. The two kinds of powders were pressed to pellet sized of 20 mm × 20 mm × ~5 mm by CIP under pressure of 100 MPa, and then fired at 1500 °C for 4 h in an electric furnace to obtain CaO pellets with low- and high-porosities. To obtain the sintered CaO pellets with different porosities, the pellets pressed from lightweight $CaCO_3$ powder were also fired at 1250–1400 °C (with the temperature interval of 50 °C) for 4 h.

Then the obtained CaO pellets were led into a vertical alumina tube furnace kept at 700 °C, with mass change recorded continuously. CO_2 gas flowed into the tube furnace at the bottom and exited at the top with a rate of 0.4 L/min during the whole heating and cooling process. The flow of CO_2 was so slow that it did not disturb the measurement of mass change in the present experiment conditions.

The samples were characterized by bulk density and apparent porosity, X-ray diffraction (XRD, Cu target, 20 kV and 20 mA), scanning electron microscopy (SEM), and hydration resistance. The bulk density and apparent porosity of samples before and after carbonation were measured by immersion method in kerosene under vacuum using Archimedes' principle and calculated according to Eqs. (1) and (2):

$$\text{Bulk density} = \frac{m_1 d}{m_3 - m_2}\ (\text{g/cm}^3) \quad (1)$$

$$\text{Apparent porosity} = \frac{m_3 - m_1}{m_3 - m_2} \times 100\% \quad (2)$$

where m_1 is the mass of dried sample in air (g), m_2 is the mass of a sample in kerosene (g), m_3 is the mass of a sample with free bubbles on the surface (g), and d is the density of kerosene (g/cm^3).

The hydration resistance of the sample was evaluated by measuring the mass gain after soaking the pellets in a chamber kept at 70 °C and 90% relative humidity.

3. Results

3.1. Carbonation properties

Table 1 shows the porosity and relative density of the CaO pellets before and after carbonation treatment. After firing at 1500 °C for 4 h, the relative density of CaO pellet sintered from reagent $CaCO_3$ was 70% and its apparent porosity was 27% (hereafter called high-porosity pellet). The relative density was calculated by comparing bulk density of the pellet as the fraction of its theoretical density that was calculated from a fractional summation of the theoretical densities of cubic CaO (3.346 g/cm^3) and hexagonal $CaCO_3$ (2.710 g/cm^3) according to Eq. (3):

$$\text{Theoretical density} = \frac{m_{CaO} + m_{CaCO_3}}{m_{CaO}/3.346 + m_{CaCO_3}/2.710} \quad (3)$$

where m_{CaO} and m_{CaCO_3} are the mass of CaO and $CaCO_3$ in the pellet, respectively.

After carbonation treatment, the relative density of the high-porosity sample increased obviously, and almost all of the open pores turned to the closed ones. The relative density increased to 86% and the apparent porosity decreased significantly to 0.5%. But for the pellet sintered from lightweight $CaCO_3$, its relative density was 95% and the apparent porosity was 0.2% (hereafter called low-porosity pellet). After carbonation treatment, there was little change in relative density and the apparent porosity disappeared.

Fig. 1 shows the mass change of the low- and high-porosity pellets against carbonation time. The mass change was expressed by the percentage of mass gain to the original mass. The mass gain increased gradually and reached a plateau indicating completion of the carbonation process. The mass gain was only 2% for the low-porosity pellet, whereas it was about 14% for the high-porosity one. For both samples, a parabolic relationship between mass gain and carbonation time is observed. This result indicates that for both the low- and high-porosity CaO pellets, the carbonation reactions were controlled by the diffusion process.[20]

Fig. 2 shows the changes of relative density and apparent porosity of CaO pellets sintered at 1250–1400 °C for 4 h and subsequently carbonated at 700 °C for 24 h. It is observed that the relative density increased and apparent porosity decreased with increase of firing temperature. After carbonation treatment, the relative density of all samples increased appreciably, with the disappearance of the apparent porosity.

Table 1
Relative density and apparent porosity of the low- and high-porosity CaO pellets before and after carbonation treatment

Sample	Relative density (%)		Apparent porosity (%)	
	Before	After	Before	After
High-porosity	70	86	27	0.5
Low-porosity	95	95	0.2	0

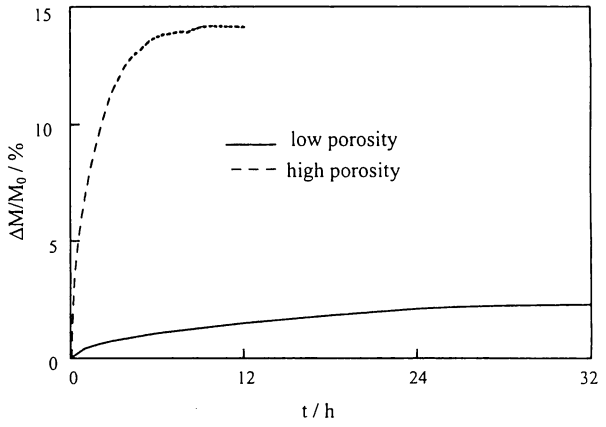

Fig. 1. Values of mass gain against carbonation time kept at 700 °C. M is the original mass of the sample and ΔM is the mass gain after carbonation treatment.

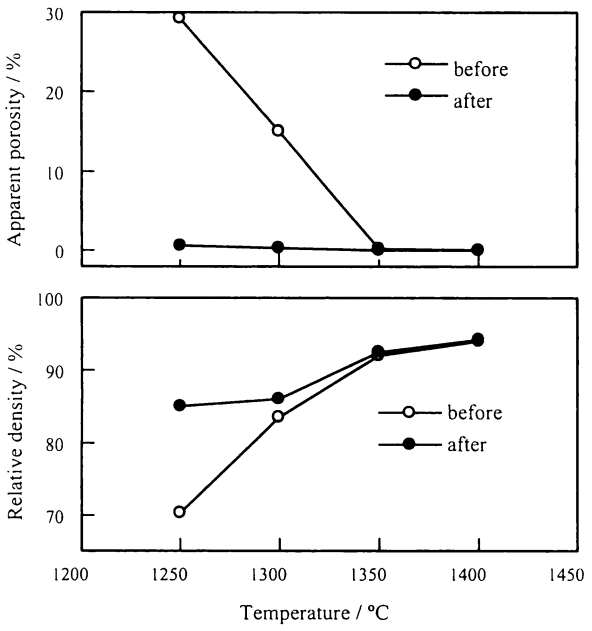

Fig. 2. Changes of relative density and apparent porosity of CaO pellets sintered under different temperatures and then carbonated at 700 °C for 24 h.

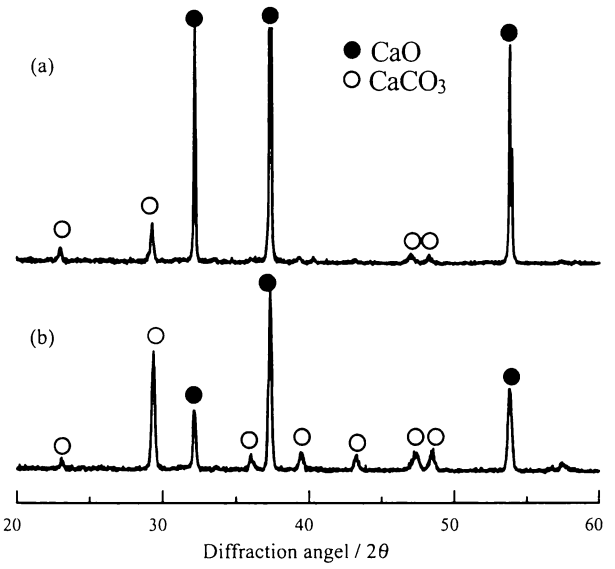

Fig. 3. X-ray surface diffraction patterns of the low- and the high-porosity pellets carbonated at 700 °C: (a) high-porosity and (b) low-porosity.

3.2. Phase composition and microstructure

Fig. 3 shows XRD patterns of the low- and high-porosity CaO pellets after carbonation treatment. $CaCO_3$ (calcite) was identified in both samples, indicating the formation of $CaCO_3$ after carbonation treatment. The intensity of the formed $CaCO_3$ in the high-porosity sample was much stronger than that in the low-porosity one, indicating the amount of the formed $CaCO_3$ in the high-porosity sample was more than that in the low-porosity one. For both the low- and high-porosity pellets, CaO was still the main phase after carbonation treatment.

Fig. 4 illustrates the microstructure of the low-porosity pellet before and after carbonation treatment. It is observed that the low-porosity pellet was only carbonated on the surface, with a dense $CaCO_3$ film about 2 μm in thickness formed. It is also observed that the $CaCO_3$ film combined well with the substrate CaO material. This result is correspondent to the previous works.[16,17] But different from the low-porosity sample, the high-porosity pellet was carbonated both on the surface and in the pores, with each CaO grain being encompassed by the formed $CaCO_3$ film. In addition, microfissures were observed in the formed $CaCO_3$ film (Fig. 5).

3.3. Hydration properties

Fig. 6 illustrates the relationship between mass change and hydration time kept at 70 °C and 90% relative humidity for both the low- and high-porosity pellets with and without carbonation treatment. The mass gain was expressed by the percentage of mass gain to the original mass of CaO pellets. The arrows represent the time when the pellets broke during hydration process. It shows that carbonation treatment significantly improved the hydration resistance of both the low- and high-porosity samples, with the formation of an induction period (during which there was no appreciable mass change).[18] For the low-porosity pellet, the hydration reaction proceeded from surface to inside gradu-

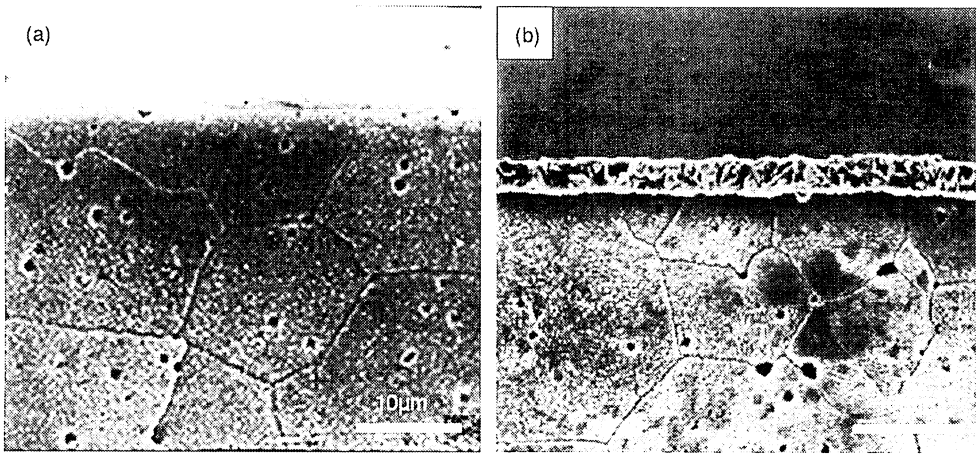

Fig. 4. Fractured surfaces of the low-porosity pellet: (a) before and (b) after carbonation treatment.

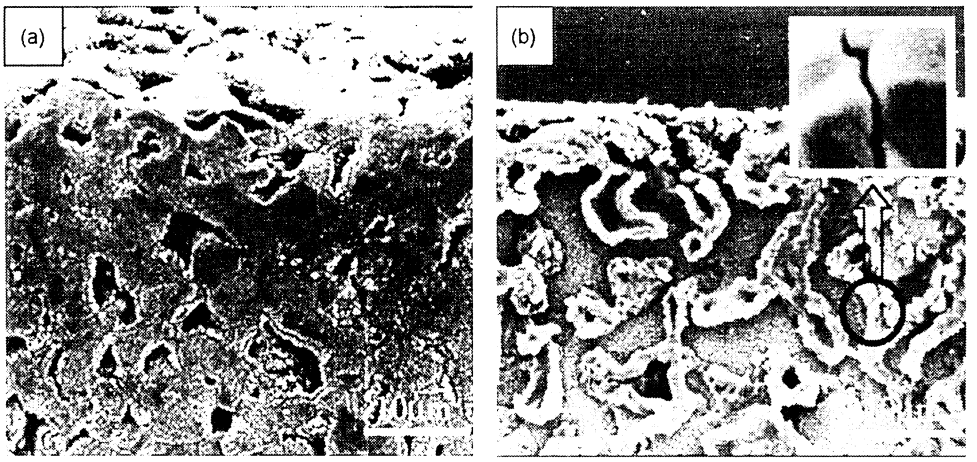

Fig. 5. Fractured surfaces of the high-porosity pellet: (a) before and (b) after carbonation treatment.

ally, with appreciable interface between the hydrated and unhydrated part. For the orientated growth of the formed $Ca(OH)_2$ and anisotropic volume expansion when CaO was hydrated,[21] cracks were observed at the corner (Fig. 7). After carbonation treatment, a long induction period of 7 days formed and the sample did not break after soaking for 21 days, with mass gain of about 22% that was a little more than that of the uncarbonated one (20%).

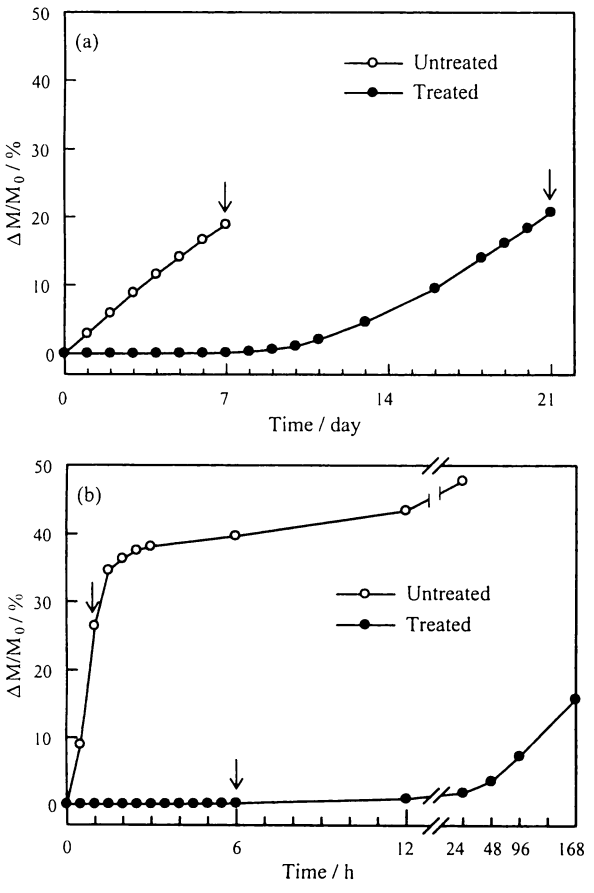

Fig. 6. Mass gains of: (a) the low- and (b) the high-porosity CaO pellets with time soaking at 70 °C and 90% RH. M is the original mass of the sample before hydration test and ΔM is the mass change after hydration test.

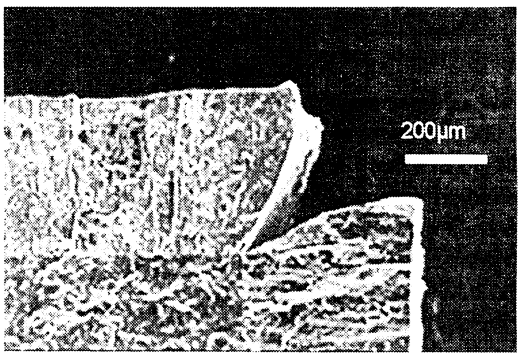

Fig. 7. Microstructures of CaO pellet after soaking at 70 °C and 90% humidity for 96 h.

But for the carbonated high-porosity pellet, there was only a short induction period of about 12 h. The interesting result was that the pellet broke to several pieces after hydration test for only 6 h. This time was within the induction period. Even after the induction period, the hydration reaction still proceeded at a low rate, and the mass gain was only about 2.5% after 24 h. Then with hydration time increasing, the broken pieces further turned to much smaller size gradually, and finally turned to fine powders. From these results, it is considered that the carbonated low- and high-porosity pellets were hydrated in different mechanisms.

Fig. 8 shows the hydration test result of the carbonated CaO pellets with different apparent porosity. It is found that although there was little apparent porosity for all the carbonated pellets, the time of the carbonated CaO pellet to break was abruptly decreased with increase of the apparent porosity of the original CaO pellet, even with a very limited mass gain. From this result, it is considered that the breakage of the carbonated CaO pellet was closely dependent to apparent porosity or compactness of the sintered original CaO pellet.

4. Discussion

4.1. Carbonation properties and microstructure

From the curves of mass gain and microstructure observation, it is considered that the CaO materials with different porosity

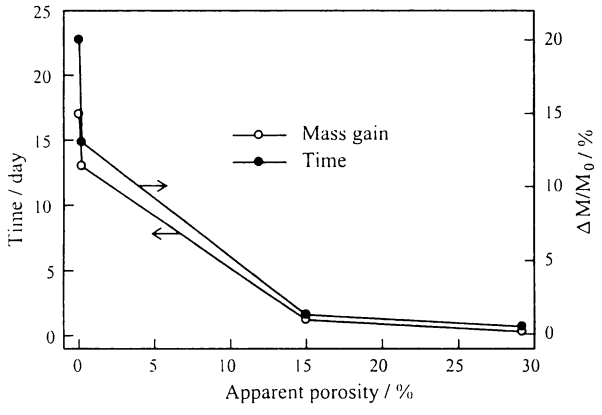

Fig. 8. The dependence of apparent porosity on the time of the carbonated CaO pellets to break and its mass gain during hydration process.

were carbonated in different mechanisms, as shown in Fig. 9. For the pellet without apparent porosity, CO_2 gas could not flow into the sample and thus the carbonation reaction only occurred on the surface, with a thin and dense $CaCO_3$ film formed on the surface. It is calculated that the molar volume of $CaCO_3$ (36.9 cm^3/mol) is larger than that of CaO (16.7 cm^3/mol), and there is a large volume expansion when CaO converts to $CaCO_3$, with the generation of stress between the formed $CaCO_3$ and the uncarbonated CaO grains. But for the amount of the formed $CaCO_3$ was limited when the low-porosity pellet was carbonated, the stress between the formed $CaCO_3$ and the substrate CaO grains was not so severe to form microfissures. Therefore, there was no microfissures were observed in the $CaCO_3$ film which combined well with the substrate CaO materials. It is unnecessary to concern for the formation of microfissure when the CaO materials of low-porosity were carbonated.

But for the pellet with apparent porosity, the CO_2 gas could easily flow to the inside of the sample, and thus carbonation reaction occurred in all open pores, with each CaO grain surrounded by $CaCO_3$ films. When the $CaCO_3$ films formed inside the pores, CO_2 gas had to pass through these films to maintain the reaction proceeding. Thus, though the carbonation reaction occurred inside all pores, the carbonation rate was still controlled by the diffusion of CO_2 through these formed $CaCO_3$

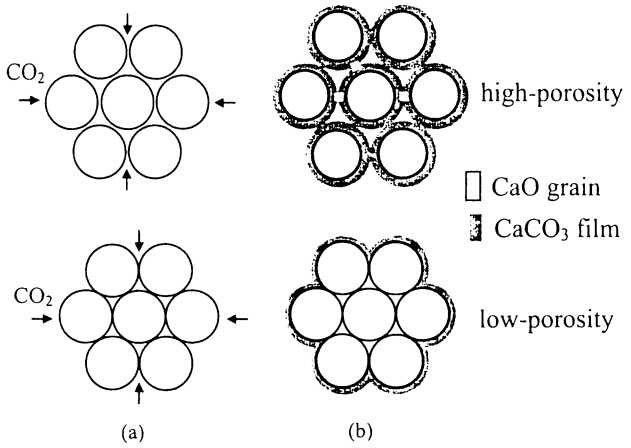

Fig. 9. Carbonation models of CaO pellets: (a) before and (b) after carbonation treatment.

films around CaO grains. With increase of the thickness of the formed $CaCO_3$ film and decrease of apparent porosity, the diffusion of CO_2 became so difficult that the carbonation reaction tended to cease. Since the reaction specific area of the high-porosity pellet was much larger than that of the low-porosity one, its carbonation rate was much fast than that of the low-porosity one, with a much more mass gain (Fig. 1). With the formation of the large amount $CaCO_3$ and the volume expansion, the stress between the formed $CaCO_3$ film and CaO grains was so severe that microfissures would form (Fig. 4). It is considered that the formation of these microfissures degraded the combining strength between the carbonated CaO grains.

Therefore, in order to prevent microfissure forming when the CaO materials is carbonated, the following two ways are recommended: one is that the pellet should be without appreciable apparent porosity and thus to ensure the carbonation reaction occurring on the surface; the other is to control the formed $CaCO_3$ amount, in another words, to control the carbonation ratio when the CaO materials with high-porosity is carbonated.

4.2. Hydration properties

Since the diameter of H_2O molecule (0.151 nm) is smaller than that of CO_2 molecule (0.232 nm), water vapor could still pass through $CaCO_3$ film although the carbonation reaction ceased owing to CO_2 diffusion. Therefore, carbonation treatment could effectively improve hydration resistance of CaO materials, but it could not inhibit CaO hydrating completely. For the low-porosity pellet, a long induction period of 7 days formed owing to the formation of dense $CaCO_3$ film after carbonation treatment. The time of the induction period is considered to be dependent to the thickness and the compactness of the formed $CaCO_3$ film. In fact, since the hydration reaction was conducted under the condition of 70 °C and 90% relative humidity, the hydration rate was several decade times to normal climate condition.[22] Thus an induction period of 7 days means that the carbonated CaO materials could be safely stored for more than 1 year. Therefore, it is considered that carbonation treatment could almost completely prevent CaO materials from hydrating during storage period. In addition, whether carbonated or not, the hydration process of the low-porosity pellet proceeded from surface to inside. The breakage of the pellet was due to the volume expansion with the hydration reaction proceeding, and thus the mass gains were equivalent when the carbonated and uncarbonated samples broke. Therefore, it is considered that carbonation treatment is suitable for improving hydration resistance of compact CaO materials, without concerning for the materials over carbonated.

For the uncarbonated CaO pellet with high apparent porosity, the water vapor easily flowed to the inside of the pellet, thus the hydration reaction occurred in the whole sample at the same time and a high hydration rate was obtained, which led to the pellet soon breaking to fine powder due to the abruptly volume expansion caused by hydration reaction. Similar to the low-porosity sample, the formation of dense $CaCO_3$ film after carbonation treatment effectively retarded occurrence of the hydration reaction, with the formation of an appreciable induction period.

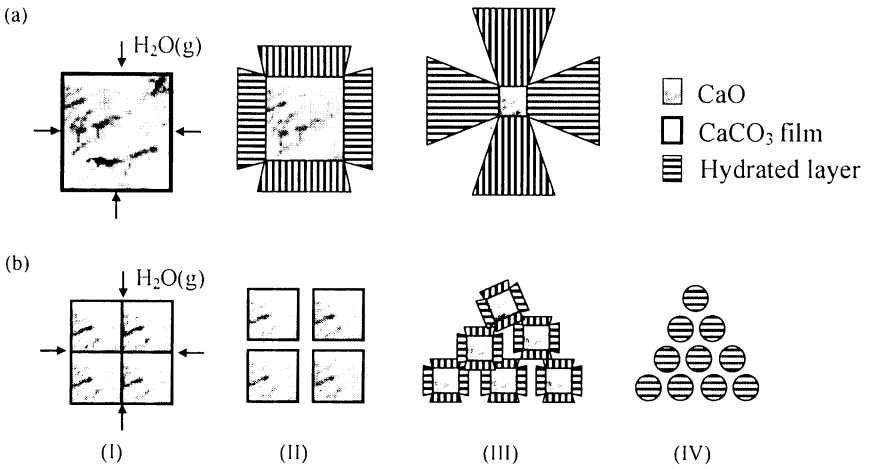

Fig. 10. Hydration models of the carbonated: (a) low- and (b) high-porosity CaO pellets.

As described above, the combination between the carbonated CaO grains was very weak due to the formation of microfissure when the carbonation ratio is too large, and it became much weaker when the pellet hydrated. Therefore, for the carbonated pellet of high-porosity, the breakage was so sensitive to the apparent porosity that the carbonated pellet would break even with a very small amount of CaO hydrated (Fig. 8). After the carbonated pellet broke, the $CaCO_3$ films around CaO grains still effectively inhibited the hydration reaction, so that the time of the pellet to break was shorter than the induction period (Fig. 6). Therefore, it is considered, for the carbonated high-porosity pellet, its breakage was not for the volume expansion with hydration proceeding, but mainly for the poor combination between the carbonated CaO grains. For this reason, compared with the low-porosity pellet, the carbonated high-porosity one was hydrated in a different mechanism, as shown in Fig. 10. A more stage formed during hydration process. It firstly broke to several pieces, and further turned to much smaller size gradually with hydration time increasing. Thus, it is considered, the following two ways to prevent the carbonated CaO materials easily breaking are recommended: one is that the original CaO pellet should be with less appreciable apparent porosity and thus to ensure the carbonation reaction occurring on the surface; the other is to control the formed $CaCO_3$ amount, in another words, to control the carbonation ratio to avoid "over carbonated" when the high-porosity CaO materials are carbonated.

5. Conclusion

Based on the above results, in order to improve the hydration resistance of CaO materials by carbonation treatment, the followings are concluded:

(1) The high-porosity CaO materials were carbonated with a higher rate compared to the low-porosity one. The carbonation processes were controlled by the diffusion of CO_2 through the formed $CaCO_3$ film, regardless of the porosity.
(2) The high-porosity CaO materials was carbonated both on the surface and in the pores, with each CaO grain being encompassed by $CaCO_3$ film containing microfissures; whereas the low-porosity one was only carbonated on the surface, with the formation of a dense $CaCO_3$ film that combined well with the uncarbonated CaO materials.
(3) The breakage of carbonated low-porosity pellet was due to the volume expansion caused by hydration reaction, whereas it was mainly due to the poor combination between the carbonated CaO grains for the high-porosity one.
(4) Carbonation treatment effectively improved the hydration resistance of CaO materials, with formation of appreciable induction period, regardless of porosity. For the low-porosity pellet, the induction period reached to 7 days. However, since the carbonated CaO materials of high-porosity would easily break due to the poor combination between the carbonated CaO grains caused by formation of microfissures, it is necessary to control the carbonation ratio to avoid "over carbonated".

References

1. Nadachowski, F., Lime refractories. *Interceram*, 1975, **24**, 42–45.
2. Brezny, B., Equilibrium partial pressure of Mg, SiO, Ca, and CO in carbon-containing doloma refractories. *J. Am. Ceram. Soc.*, 1976, **59**, 529–530.
3. Nadachowski, F., Refractories based on lime: development and perspectives. *Ceramurgia Internationa*, 1976, **2**(2), 55–61.
4. Degawa, T., Some properties and application of calcia ceramics. *Ceramics (Japan)*, 1988, **23**, 1052–1055.
5. Yuan, W. M. and Shang, B. L., Ways of improving the hydration resistance of CaO refractories for steel melt filtration. *Technol. Cast. (China)*, 1994, **79**(6/7), 31.
6. Kijac, J., Kovac, P., Steranka, E., Masek, V. and Marek, P., The current status of tundish covering slags in a slab caster plant. *Metalurgija*, 2004, **43**, 59–62.
7. Chen, Z. Y. and Tian, S. X., Relationship between clean steel and refractories. *Refractories/Naihuo Cailiao (China)*, 2004, **38**, 219–225.
8. Wei, Y. W., Li, N., Kuang, J. C. and Chen, F. Y., Desulfurization and dephosphorization of molten iron in basic refractories. *InterCeram: Int. Ceram. Rev.*, 2002, **51**, 200–205.
9. Feng, W. X., Niu, J. G., He, H. M., Su, S. H., Liu, Y., Chen, L. Y. *et al.*, Influence of MgO–CaO based spraying material and CaO based cover flux for tundish on steel cleanness. *Kang T'ieh/Iron and Steel (China)*, 2002, **37**, 25–27.
10. Wei, Y. W. and Li, N., Refractories for clean steelmaking. *Am. Ceram. Soc Bull.*, 2002, **81**, 32–35.

11. Wu, H. J., Cheng, Z. Q., Jin, S. T. and Wang, W. Z., Influences of magnesia–calcia and magnesia coatings for tundish on steel cleanness. *Refractories/Naihuo Cailiao (China)*, 2002, **36**, 145–147.
12. Zhong, X. C., Looking ahead-a new generation of high performance refractory ceramics. *Refractories/Naihuo Cailiao (China)*, 2003, **37**, 1–10.
13. Motoi, S., Reviews of lime refractories. *Gypsum Lime (Japan)*, 1978, **154**, 123–127.
14. Hamano, K., Lime refractories. *Gypsum Lime (Japan)*, 1978, **157**, 20–29.
15. Oda, Y., Preventive methods for hydration of calcia and dolomite clinkers. *Taikabutsu (Japan)*, 1989, **41**, 690–700.
16. Cutler, I. B., Felix, R. L. and Caywood Jr., L. P., Increasing hydration resistance of calcia. *Am. Ceram. Soc. Bull.*, 1970, **49**, 531–533.
17. Song, H. S. and Kim, C. H., Effect of surface carbonation on the hydration of CaO. *Cem. Con. Res*, 1990, **20**, 815–823.
18. Fukui, H., Tsugenu, S. and Nagaishi, T., Hydration properties of calcium oxide which is varied on it's surface by CO_2 gas flow. *Kayaku Gakkaishi (Japan)*, 1998, **59**, 246–253.
19. Dheilly, R. M., Tudo, J. and Queneudec, M., Influence of climatic conditions on the carbonation of quicklime. *J. Eng. Mater. Perfor.*, 1998, **7**, 789–795.
20. Oakeson, W. G. and Cutler, I. B., Effect of CO_2 pressure on the reaction with CaO. *J. Am. Ceram. Soc.*, 1979, **62**, 556–558.
21. Beruto, D., Barco, L., Belleri, G. and Searcy, A. W., Vapor-phase hydration of submicrometer CaO particles. *J. Am. Ceram. Soc.*, 1981, **64**, 74–80.
22. Shirogawa, A., Sintering and Hydration Properties of CaO Containing Composite. MD Thesis. Nagoya Institute of Technology, Japan, 1996.

BEHAVIOR OF Al_4SiC_4 ADDED TO THE CARBON CONTAINING REFRACTORIES

Yasuhiro Hoshiyama, Junji Ommyoji, Akira Yamaguchi
Okayama Ceramics Research Foundation, Okayama, Japan

INTRODUCTION

Authors are researching new materials in the Al-Si-C system for the refractories[1][2]. The Al-Si-C system includes five compounds of Al_4SiC_4, $Al_4Si_2C_5$, $Al_4Si_4C_7$, $Al_4Si_3C_6$ and Al_8SiC_7. In these compounds, Al_4SiC_4 is most expected to be a new material for refractories, because it is stable in a wide range of temperature and it has high melting point (2037°C[3]) and high slaking resistance[4]. In this study, in order to clarify the behavior and the effect of Al_4SiC_4 on the carbon containing refractories, the properties and phase changes of the MgO-C brick containing Al_4SiC_4 powder were investigated comparing with the MgO-C brick containing aluminum powder.

EXPERIMENTAL PROCEDURE

Al_4SiC_4 powder was prepared by the following methods. Aluminum powder, silicon powder and carbon black were weighted in a theoretical composition and dry-mixed by using a ball mill for 10 hours. The mixed powder were placed in a carbon crucible and heated at 1300°C for 3 hours in argon atmosphere. The composition of the heated powder was a single-phase of Al_4SiC_4, and its average particle diameter was 8μm after ball milling for 10 hours. Al_4SiC_4 powder prepared in this method was used for the following investigation.

Table 1 indicates the composition of the MgO-C brick samples. Electric fused magnesia of purity 99% and flake graphite of purity 99% were used. Al_4SiC_4 powder was added instead of aluminum powder. Sample number 4 and 5 had same molar ratio of aluminum and silicon. Novolac type phenol resin was used as a binder and hexamethylenetetramine were added as a hardening agent. Brick samples were prepared with heating at 200°C for 6 hours after mixing and pressing.

The brick samples were cut off to 25×25×25mm size and putted into the crucible which was filled by carbon powder, and then heated at various temperatures for 3 hours using an air atmosphere electric furnace. After heating, mass change, porosity, density and crushing strength of the samples were measured. The compositions of the heated samples were investigated by a powder X-ray diffraction method.

The samples with 25×25×25mm size were heated at 1400°C for 3 hours in air atmosphere in order to evaluate an oxidation resistance of the brick samples. The oxidation test was carried out with rapid heating and rapid cooling method. After heating, the decarbonized layer thickness of the samples was determined. In addition, in order to estimate a slaking resistance of the bricks after heating, the samples were heated at 1400°C for 3 hours in carbon powder using the air atmosphere furnace, and then the degree of their structure deterioration was monitored during putting them in the room.

Tab. 1. Composition of the MgO-C brick samples.

[mass%]

No.	1	2	3	4	5
Fused MgO (<1mm)	80	80	80	80	80
Flake graphite (<0.15mm)	20	20	20	20	20
Al powder (<75μm)		3		3	
Si powder (<45μm)				0.8	
Al_4SiC_4 powder			3		5.1
Phenol resin		4	4	4	4
Hexamethylenetetramine	0.4	0.4	0.4	0.4	0.4

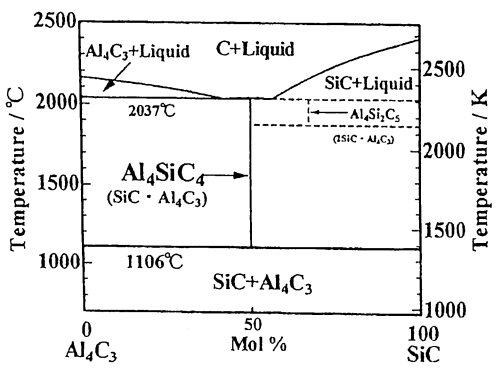

Fig. 1. Phase diagram for the pseudobinary Al_4C_3-SiC system.

RESULTS

The mass changes of the samples during heating at various temperatures in the reducing atmosphere are shown in **Figure 2**. The mass decrease at 800°C depends on the thermal decomposition of the phenol resin. Based on the data at 800°C, the rapidly mass gains are observed at 1000°C in the No.2 and No.4 samples which include the aluminum powder. The reaction with mass increase is considered to occur rapidly between 800°C and 1000°C. In the case of No.3 and No.5 which include Al_4SiC_4 powder, the mass gain is observed at 1200°C and continues to 1400°C. Therefore, the reaction with mass increase is considered

to occur gradually between 1000°C and 1400°C. After heating at 1400°C and 1500°C, the mass gain of No.3 and 5 is larger than that of No.2 and 4. It follows that Al_4SiC_4 causes large mass increase more than aluminum at high temperature.

Figure 3 shows the apparent porosity of the samples after heating at various temperatures in the reducing atmosphere. The porosity increase at 800°C depends on the thermal decomposition of the phenol resin. The porosity of No.1 sample which does not include any additives increases with rising of temperature. That of No.2 and No.4 which contain aluminum powder hardly increases above 800°C. In contrast, the porosity of No.3 and No.5 which contain Al_4SiC_4 powder decreases linearly above 800°C, then the porosity after heating at 1500°C is 2% lower than that after heating at 800°C. From this, it is understood that Al_4SiC_4 powder densifies the MgO-C brick texture efficiently with the mass increasing reaction shown in the Fig.2.

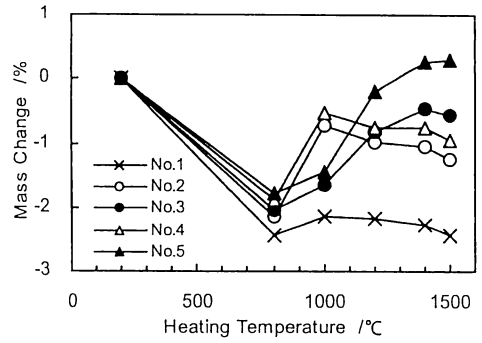

Fig. 2. Mass changes of the brick samples during heating in the reducing atmosphere.

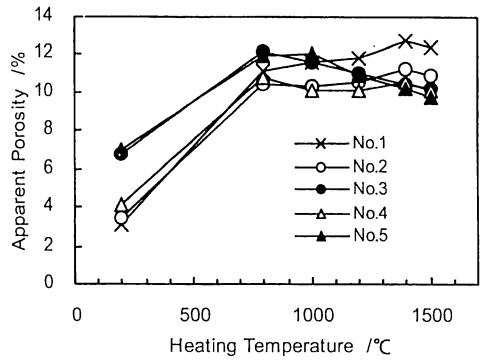

Fig. 3. Apparent porosities of the brick samples after heating in the reducing atmosphere.

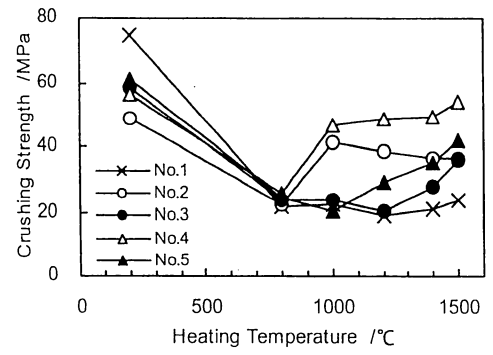

Fig. 4. Crushing strength of the brick samples after heating in the reducing atmosphere.

Figure 4 shows the cold crushing strength of the samples after heating at various temperatures in the reducing atmosphere. The strength decreases by the thermal decomposition of the phenol resin in the low temperature. The strength of No.2 and No.4 which include aluminum powder increases markedly between 800 and 1000°C. That of No.4 including silicon powder increases slightly above 1000°C. In contrast, the strength of the sample containing Al_4SiC_4 powder increases gradually with rising of temperature. In the case of No.3 which contains 3 mass% of Al_4SiC_4 powder, it occurs above 1200°C, and in the case of No.5 containing 5.1 mass% of Al_4SiC_4 powder, it occurs above 1000°C. The strength increase of No.3 and No.5 is characterized to be not rapid and be gradual. This phenomenon is interesting from the viewpoint of a spalling resistance improvement, because of the gradual change of the mechanical property with changing of temperature.

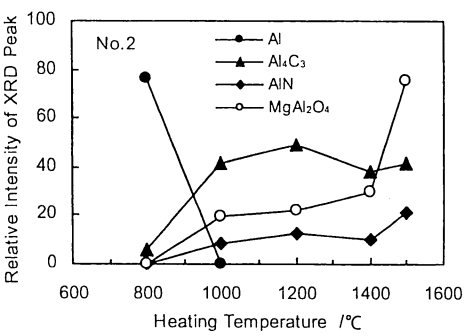

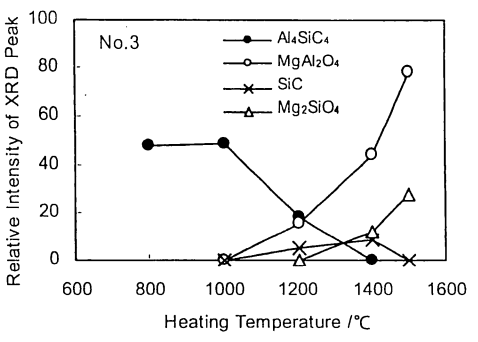

Fig. 5. Mineral phase of the brick samples after heating in the reducing atmosphere.

The mineral phase of the samples after heating in the reducing atmosphere is indicated in **Figure 5**. In the case of No.2, aluminum disappears and then Al_4C_3, AlN and $MgAl_2O_4$(spinel) are formed at 1000°C. In the case of No.3, Al_4SiC_4 does not change below 1000°C. The reaction products are observed above 1200°C. Spinel and SiC are formed at 1200°C and the spinel increases with increasing of temperature. In addition, Mg_2SiO_4(forsterite) is formed above 1400°C. Unlike No.2, the formation of Al_4C_3 and AlN are not observed. Al_4SiC_4 decreases at 1200°C and disappears at 1400°C. It follows that the reaction start temperature of Al_4SiC_4 powder in the MgO-C brick is understood to be high in comparison with aluminum powder. This tendency agrees with the results that the physical properties change gradually above 1200°C as shown in Fig.2 – Fig.4.

Figure 6 shows the results of the oxidation test. The bar in the figure indicates the decarbonized layer thickness of the sample after heating at 1400°C in the air. The oxidized layer thicknesses of the samples containing additives are thinner than that of the sample without additive. Comparing No.2 and No.3, the decarbonized layer thicknesses are almost same. In addition, comparing No.4 and No.5, they are almost same too. Therefore, the oxidation resistance of the MgO-C bricks is recognized to be improved by Al_4SiC_4 powder as well as by aluminum powder.

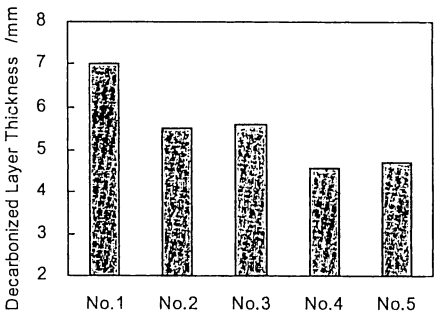

Fig. 6. Oxidation test results.

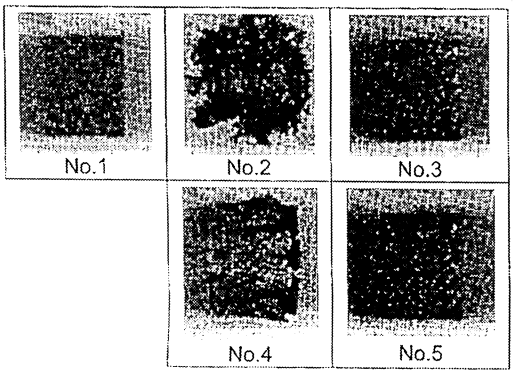

Fig. 7. Slaking test results.

The slaking test results are indicated in **Figure 7**. The photographs show the appearance of the samples which were kept in a room atmosphere for two weeks after the reducing atmosphere heating at 1400°C. No.2 sample added aluminum powder only is destroyed and became powder by the hydration reaction with the volume expansion. No.4 sample added aluminum and silicon powder has a smaller degree of deterioration than No.2. But many cracks are formed in the sample and its strength decreases by the hydration reaction. In comparison, in the case of No.3 and No.5 which were added Al_4SiC_4 powder, the crack is not observed at all. In the sample containing Al_4SiC_4 powder, Al_4C_3 and AlN which cause hydration reaction don't form during heating as indicated in Fig.5. That is thought to be a reason of the high slaking resistance.

DISCUSSION

The behavior of Al_4SiC_4 in the brick is discussed as follows. When the reactions of Al_4SiC_4 in the carbon containing refractories are considered, the gas phase existing in the pore of the texture is important. Since an actual furnace is usually used in the air atmosphere, the surface of the refractory is exposed to the air. In this case, if the temperature is above 1000°C, the inner pore of the carbon containing refractory is filled by CO gas, and then the partial pressure of CO gas is approximated to 1.013×10^5Pa (1atm, Pco=1). Al_4SiC_4 react mainly with CO gas under this condition, which means the solid–gas reaction occurs. The condition of the reducing atmosphere in this study is similar, the atmosphere in pores of the sample is considered to be near to Pco=1.

Al_4SiC_4 powder added to the MgO-C brick begins to change into $MgAl_2O_4$ and SiC at 1200°C as shown in Fig.5, that is, Al_4SiC_4 reacts with CO gas to form Al_2O_3 and SiC, and then Al_2O_3 react with MgO to form $MgAl_2O_4$. SiC react with CO gas and MgO to form Mg_2SiO_4 at 1400°C. These reactions are indicated as the following equations.

1st stage reaction;

$$Al_4SiC_4(s)+6CO(g)=2Al_2O_3(s)+SiC(s)+9C(s) \quad (1)$$

$$Al_2O_3(s)+MgO(s)=MgAl_2O_4(s) \quad (2)$$

$$(Al_4SiC_4(s)+2MgO(s)+6CO(g) =2MgAl_2O_4(s)+SiC(s)+9C(s)) \quad (3)$$

2nd stage reaction;

$$SiC(s)+2CO(g)=SiO_2(s)+3C(s) \quad (4)$$

$$SiO_2(s)+2MgO(s)=Mg_2SiO_4(s) \quad (5)$$

$$(SiC(s)+2MgO(s)+2CO(g)=Mg_2SiO_4(s)+3C(s)) \quad (6)$$

Table 2 indicates mass and volume change in the above reactions. It shows that these reactions (equation 3 and 6) involve the large increase of mass and volume.

In addition, the large increase is recognized to be mainly influenced by the reactions with CO gas (equation 1 and 4). The carbon precipitated in the equation 1 or 4 is considered to influences remarkably to the volume expansion and to causes the texture densification as shown in Fig.3.

Tab. 2. Culculated mass and volume increases.

Equation No.	Mass change /%	Volume change /%
1	+91.3	+199.2
2	0	+7.8
3	+63.5	+137.0
4	+139.7	+397.7
5	0	-3.4
6	+46.4	+136.8

*Following values were used as density [$\times 10^3$ kg·m^{-3}]
Al_4SiC_4(s):3.03 Al_2O_3(s):3.99 SiC(s):3.22 SiO_2(s):2.66
$MgAl_2O_4$(s):3.58 Mg_2SiO_4(s):3.22 C(s):1.60

Figure 8 shows the stable condensed phases and the equilibrium partial pressures of the gases in the Ai-Si-O-C system at 1700K under coexistence of the solid carbon[5]. It indicates that Al_4SiC_4(s), Al_2O_3(s)+SiC(s) and Al_2O_3(s)+$Al_6Si_2O_{13}$(s) are stable in the condition of $P_{CO}<10^{-3}$, $10^{-2}<P_{CO}<0.2$ and $P_{CO}>0.2$, respectively. Therefore, since the added Al_4SiC_4 is not stable in $P_{CO}=1$, Al_4SiC_4 first changes into Al_2O_3 and SiC, and next SiC changes into SiO_2. These relations agree with the results shown in Fig.5 and the equations described above. In addition, the equilibrium partial pressures of Al(g) and SiO(g) are elevated in the high temperature shown in Fig.8. Therefore, these gases are estimated to be involved in the reactions. From the figure, it is

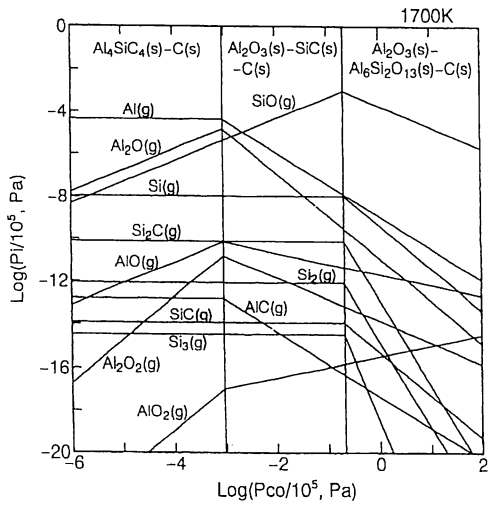

Fig. 8. Equilibrium partial pressures of the gases in the Al-Si-C-O system.

considered that Al(g) forms under existence of Al_4SiC_4(s), and SiO(g) forms under existence of SiC(s) (equation 7 and 10). These gases are assumed to disperse in the texture and condense in the pore according to equation 8 and 11 when the gases move to the high P_{CO} area.

$$Al_4SiC_4(s)=4Al(g)+SiC(s)+3C(s) \quad (7)$$

$$2Al(g)+3CO(g)=Al_2O_3(s)+3C(s) \quad (8)$$

$$(MgO(s)+2Al(g)+3CO(g)=MgAl_2O_4(s)+3C(s)) \quad (9)$$

$$SiC(s)+CO(g)=SiO(g)+2C(s) \quad (10)$$

$$SiO(g)+CO(g)=SiO_2(s)+C(s) \quad (11)$$

$$(2MgO(s)+SiO(g)+CO(g)=Mg_2SiO_4(s)+C(s)) \quad (12)$$

These condensed phases are considered to fill the pore, and that is assumed to be the reason of the more densification of the texture is provided.

CONCLUSIONS

The behavoir and effect of Al_4SiC_4 powder added to the MgO-C bricks have been investigated and discussed. The conclusions are as follows.

(1) The mass increases and the porosity decreases in the MgO-C brick which was added Al_4SiC_4 powder above 1000°C. The apparent porosity after heating at 1500°C is 2% lower than that after heating at 800°C.

(2) The brick strength increases gradually above 1000°C by the addition of Al_4SiC_4 powder.

(3) Al_4SiC_4 powder improves the oxidation resistance of the bricks as well as aluminum powder. The bricks containing Al_4SiC_4 has high slaking resistance after heating.

(4) Al_4SiC_4 reacts with CO gas to form spinel($MgAl_2O_4$) and SiC above 1200°C. The formed SiC also reacts with CO gas and MgO to form forsterite(Mg_2SiO_4) above 1400°C. Al_4C_3 and AlN are not formed in these reaction processes.

(5) The increase of mass and volume are caused by the reaction of Al_4SiC_4 and CO gas, the more densification of the texture is provided.

REFERENCES

[1] M.Fujita, J.Ommyoji, A.Yamaguchi, Taikabutsu, 57 [3] 142 (2005)
[2] M.Fujita, J.Ommyoji, A.Yamaguchi, Taikabutsu, 58 [3] 160 (2005)
[3] K.Inoue, S.Mori, A.Yamaguchi, J.Ceram.Soc. Japan., 111 [7] 466-470 (2003)
[4] S.Zang, A.Yamaguchi, J.Ceram.Soc.Japan, 103 [1] 20-24 (1995)
[5] S.Zang, A.Yamaguchi, J.Ceram.Soc.Japan, 103 [3] 235-239 (1995)